Metabolomics for Biomarker Discovery in Neurological Disorders

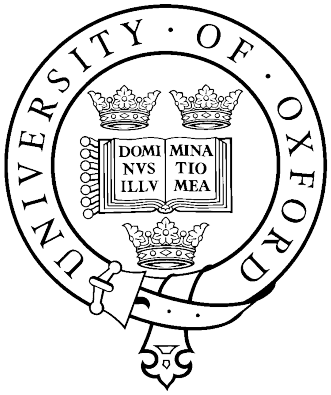

Wenzheng Xiong

Somerville College

University of Oxford

A thesis submitted for the degree of

Doctor of Philosophy

Department of Pharmacology

Trinity 2025

Abstract

Blood-borne metabolites can serve as readily accessible biomarkers reflecting biochemical alterations in neurological diseases, facilitating diagnostic, therapeutic and prognostic determination. In neurological disorders with overlapping symptoms, but with different aetiologies, timely diagnosis and appropriate treatment are crucial for optimal prognosis. This thesis employed nuclear magnetic resonance (NMR)-based metabolomics for biomarker discovery to improve diagnostics for antibody-mediated neurological disease.

^{1}H NMR is used for metabolite measurement due to its high reproducibility, instrument stability, minimal sample preparation requirements and ability to detect a wide range of biologically significant metabolites. Here, the effectiveness of NMR-based metabolomics to distinguish between disease classes was explored using orthogonal partial least squares-discriminant analysis (OPLS-DA), with 10-fold cross-validation with repetition and permutation testing. Plasma samples from a cohort comprising patients with autoimmune encephalitis (AE) and those with drug-resistant epilepsy (DRE) were analysed. NMR-based metabolomics effectively distinguished AE from DRE, achieving a high predictive accuracy of 87.0 ± 3.1%. This method also enabled the stratification of AE subtypes (NMDAR-Ab, LGI1-Ab, CASPR2-Ab AE), with subtype-specific metabolite signatures observed. Therefore, NMR-based blood tests are able to complement current autoantibody assays and could provide a faster, cost-effective, and highly accurate adjunct for AE diagnosis. The same methodology was then applied to serum samples from psychosis patients with and without the neuronal surface antibodies in common with those found in AE. A distinct metabolic signature, including decreased lipoprotein fatty acids and increased branched-chain amino acids and glucose, was identified in psychosis patients with voltage-gated potassium channel (VGKC) or glycine receptor (GlyR) antibodies. These patients have more severe psychotic presentations, suggesting a unique inflammatory subtype.

To facilitate clinical translation, this thesis work then addressed preanalytical variability

in blood samples by investigating the impact of pre-processing delays, post-processing delays, and different blood collection tubes on metabolite variability. A significant source of variability in blood was identified as the conversion of glucose to lactate owing to delays in blood pre-processing. However, it was discovered that the fluoride oxalate collection tubes effectively stabilise glucose and lactate levels for 24 hours at either 4 °C or room temperature, providing a viable alternative when rapid processing is not feasible.

Preanalytical variability can also arise in brain NMR metabolomics owing to suboptimal extractions. Investigations using rodent brain samples revealed that metabolites such as aspartate, acetate, N-acetyl aspartate, and glutamate exhibited instability as a consequence of inadequate protein precipitation with 50% acetonitrile or methanol. Conversely, a methanol/water/chloroform extraction method provides the necessary reproducibility and extraction efficiency while effectively preserving metabolite stability by sufficient protein precipitation. This method can, therefore, be recommended for untargeted brain NMR metabolomics, as it enables the reliable detection of metabolic alterations at the site of pathology, complementing histological analysis and enhancing diagnostic precision.

In conclusion, this thesis has demonstrated the potential of NMR-based metabolomics to be a powerful tool for distinguishing antibody-mediated neurological conditions, with the potential to enhance diagnostic precision, inform therapeutic strategies, and improve the understanding of disease mechanisms. By addressing preanalytical variability in both blood and brain metabolomics, this work has provided a blueprint to enhance the reliability and reproducibility of metabolomic analyses, leading to more accurate and consistent diagnostic and research outcomes.

Acknowledgements

I would like to express my deepest gratitude to my supervisors, Prof Daniel Anthony and Dr Fay Probert, for their guidance, support and supervision throughout my DPhil and the development of this thesis. I appreciate their care, patience, trust, and understanding.

Chapter 2 represents a collaborative effort with Prof Sarosh Irani's group. I am grateful to Dr Jeanne Tan May May, Dr Bryan Ceronie, Ms Archana Ramesh, Dr Ronan McGinty, Dr Sophia Michael, Dr Emma Torzillo, Dr Arjune Sen, Prof Sarosh Irani for their contribution to clinical data acquisition and interpretation. I also extend my thanks to Dr Tianrong Yeo, Dr Jeanne Tan May May, and Dr Fay Probert for their contributions in NMR acquisition.

Chapter 3 is collaborative work with Prof Belinda Lennox's group. I appreciate the contributions of Dr Alasdair Coles, Dr Peter Jones, Dr Ksenija Yeeles, and Prof Belinda Lennox in the collection of samples and clinical data within the PPiP cohorts. I am also thankful to Dr Patrick Waters for conducting antibody testing, and to Dr Tianrong Yeo, Dr Jeanne Tan May May, Dr Fay Probert for their contributions in NMR acquisition.

For Chapter 4, I would like to thank Dr Daniel Radford-Smith for his conceptualisation, supervision and assistance in NMR experiments, data analysis and interpretation. I am also grateful to Dr Suzie Anthony for blood collection, Ms Thi Bao Tien Ho for help in sample processing, and Prof Edouard Louis and Prof Jack Satsangi for the SPARE and STORI trials included in the analysis.

In Chapter 5, I would like to thank Dr Florian Zirpel and Prof Zam Cader for their help in brain tissue collection and animal resources.

Furthermore, I am grateful to everyone in the lab for their kindness, support, guidance, and care. I would like to thank Jaezah, Dan, and Abi for introducing me to the lab. Thank you to Izzy, Ross, and Tereza for their help, support, and the experiments we worked on together. I am also deeply thankful to my wonderful friends, Hanxiao, Pinqi, Listi, Tien,

Qiuhan, Tingwei, and Lianhan, whose companionship has been invaluable throughout my PhD, and for the unforgettable memories we have created together. Moreover, I suppose I should also thank myself for the hard work and persistence that carried me through this journey. Additionally, I am grateful to receive the Chinese Government Award for Outstanding Self-financed Students Abroad. Finally, my deepest gratitude goes to my parents for their unwavering support, as always.

Publications

Lennox B*, **Xiong W***, Waters *P*, Coles A, Jones PB, Yeo T, May JTM, Yeeles K, Anthony D, Probert F. The serum metabolomic profile of a distinct, inflammatory subtype of acute psychosis. *Mol Psychiatry*. 2022 Nov;27(11):4722-4730.

Xiong W, Anthony DC, Anthony S, Ho TBT, Louis E, Satsangi J, Radford-Smith DE. Sodium fluoride preserves blood metabolite integrity for biomarker discovery in large-scale, multi-site metabolomics investigations. *Analyst. 2024 Feb 12;149(4):1238-1249.*

Xiong W, Yeo T, May JTM, Demmers T, Ceronie B, Ramesh A, McGinty RN, Michael S, Torzillo E, Sen A, Anthony DC, Irani SR, Probert F. Distinct plasma metabolomic signatures differentiate autoimmune encephalitis from drug-resistant epilepsy. *Ann Clin Transl Neurol*. 2024 Jul;11(7):1897-1908.

Xiong, W.; Zirpel, F.; Cader, M.Z.; Anthony, D.C.; Probert, F. Extraction Methods for Brain Biopsy NMR Metabolomics: Balancing Metabolite Stability and Protein Precipitation. *Metabolites* **2024**, *14*, 609.

Table of Contents

List of Figures

List of Tables

List of Abbreviations

1D	one-dimensional
^{1}H	hydrogen-1
2D	two-dimensional
Ab	antibody
ACD	Acid citrate dextrose
AD	Alzheimer's disease
ADP	adenosine diphosphate
AE	autoimmune encephalitis
AMPAR	α-amino-3-hydroxy-5-methyl-4-isoxazolepropionic acid receptor
ANN	artificial neural networks
ANOVA	analysis of variance
ASM	anti-seizure medications
ASPA	aspartoacylase
AST	aspartate transaminase
ATP	adenosine triphosphate
AUC	area under curve
BBB	blood-brain barrier
BCAA	branched chain amino acids
BCSFB	blood-CSF barrier
BMI	body mass index
cAMP	cyclic adenosine monophosphate
CASPR2	contactin associated protein-like 2
CBA	cell-based assay
CFTR	cystic fibrosis transmembrane regulator
CI	confidence interval

CNS	central nervous system
CPMG	Carr-Purcell-Meiboom-Gill
CRP	C-reactive protein
CSF	cerebrospinal fluid
CSN	constant sum normalisation
CT	computed tomography
CV	cross validation
DNA	deoxyribonucleic acid
DRE	drug-resistant epilepsy
EDTA	ethylenediaminetetraacetic acid
EEG	electroencephalogram
ESI	electrospray ionisation
FBDS	faciobrachial dystonic seizures
FBTCS	bilateral tonic clonic seizures
FDR	false discovery rate
FID	free induction decay
FN	false negatives
FP	false positives
FT	Fourier transformation
FWER	family-wise error rate
FX	sodium fluoride/potassium oxalate
GABA	gamma-aminobutyric acid
GABAbR	gamma-aminobutyric acid type B receptor
GAD	glutamic acid decarboxylase
GC	gas chromatography
GFAP	glial fibrillary acid protein
GlyR	glycine receptor

GSH	glutathione
GSSG	glutathione disulfide
GTCS	generalised tonic-clonic seizure
HbA1c	haemoglobin A1c
HCV	hepatitis C virus
HDL	high-density lipoprotein
HIV	human immunodeficiency virus
HRMAS	high-resolution magic angle spinning
IBD	inflammatory bowel disease
IFX	infliximab
IQR	interquartile range
IVIg	intravenous immunoglobulin
JRES	J-resolved
KEGG	Kyoto Encyclopedia of Genes and Genomes
KO	potassium oxalate
LC	liquid chromatography
LDL	low-density lipoprotein
LDL-c	low-density lipoprotein cholesterol
LGI1	leucine-rich glioma-inactivated 1
LH	lithium heparin
MALDI	matrix-assisted laser desorption/ionisation
MHC	major histocompatibility complex
ML	machine learning
MOG	myelin oligodendrocyte glycoprotein
MRI	magnetic resonance imaging
MS	mass spectrometry
MWCO	molecular weight cut-off

NAA	N-acetyl aspartate
NaF/KO	sodium fluoride/potassium oxalate
NfL	neurofilament light chain
NIPALS	non-linear iterative partial least squares
NMDAR	N-methyl-D-aspartate receptor
NMOSD	neuromyelitis optica spectrum disorder
NMR	nuclear magnetic resonance
NOESY	nuclear overhauser effect spectroscopy
NPV	negative predictive value
NSAb	neuronal surface antibodies
OPLS-DA	orthogonal partial least squares discriminant analysis
OR	odds ratio
PANSS	positive and negative syndrome scale
PARP	poly(ADP-ribose) polymerase
PCA	principal component analysis
PEP	phosphoenolpyruvate
PERM	progressive encephalopathy with rigidity and myoclonus
PET	positron emission tomography
PFK	phosphofructokinase
PG	phosphoglycerate
PLEX	plasma exchange
PLS	partial least squares
PLS-DA	Partial least squares-discriminant analysis
PN	predictive negative
PP	predictive positive
PPV	positive predictive value
PQN	probabilistic quotient normalisation

PRESS	predicted residual sum of squares
PROJECT	periodic refocusing of J evolution by coherence transfer
p-tau	phosphorylated tau
PUFA	polyunsaturated fatty acids
RF	random forest
RIA	radioimmunoassay
RNA	ribonucleic acid
ROC	receiver operating curve
RSD	relative standard deviation
RSS	residual sum of squares
RT	room temperature
SD	standard deviation
SE	standard error
SEM	standard error of mean
SHAP	Shapley additive explanations
SOP	standard operating procedures
SST	serum separator tube
SVM	support vector machine
TBI	traumatic brain injury
TMS	tetramethylsilane
TN	true negatives
TOCSY	total correlation spectroscopy
TOF	time-of-flight
TP	true positives
TSP	3-(trimethylsilyl) propionic acid-2,2,3,3-d4
TSS	total sum of squares
UF	ultrafiltration

UFA	unsaturated fatty acids
VGKC	voltage-gated potassium channel
VIP	variable importance in projection
VLDL	very-low-density lipoprotein
XGBoost	extreme gradient boosting
α-DTX	I^{125}-α-dendrotoxin

Chapter 1: Introduction

1.1 Biomarkers

1.1.1 Definition

Biomarkers, or biological markers, are widely used in environmental studies as "indicators signalling events in biological systems or samples" to assess the effects of pollution on organisms, and ecosystem health (Committee on Biological Markers of the National Research Council, 1987). For example, the activity of acetylcholinesterase in organisms is used to monitor environmental contamination by organophosphate pesticides (Sarkar et al., 2006). Concurrently, the term "biomarker" has been used commonly in basic, clinical research and clinical practice. The concept of biomarker has evolved over time. The updated and commonly accepted definition of biomarker, according to the National Institutes of Health Biomarkers Definitions Working Group, is "a characteristic that is objectively measured and evaluated as an indicator of normal biological processes, pathogenic processes, or pharmacologic responses to a therapeutic intervention" (Biomarkers Definitions Working Group, 2001).

1.1.2 Classification

The classification by Frank and Hargreaves divides biomarkers into Type 0, Type I and Type II, based on their relationship to disease progression and clinical utility (Frank & Hargreaves, 2003). Type 0 biomarkers are natural history markers of a disease, serving as inherent indicators of a disease's natural course, and longitudinally correlate with known clinical indications. One such example is the measurement of serum creatinine to assess kidney function or monitor renal injury (van Veldhuisen et al., 2016). Type I biomarkers are drug activity markers which measure responses to therapeutic interventions. For instance, in antiviral therapy for diseases like hepatitis or human immunodeficiency virus (HIV), measuring viral load in response to medication serves as a Type I biomarker. Type II biomarkers are surrogate markers (or surrogate endpoints) that act as a substitute for a clinical outcome of a disease and predict clinical effect.

Consequently, they are relevant to both the disease pathophysiology and drug mechanism. Such markers may correlate with clinical endpoints but may not have a guaranteed relationship. For example, low-density lipoprotein cholesterol (LDL-c) is a Type II biomarker for cardiovascular diseases. Studies have established a correlation between LDL-c levels and the incidence of cardiovascular diseases, as well as the reduction in cardiovascular disease incidence associated with cholesterol lowering (Silverman et al., 2016). However, exceptions exist, such as cases of heart disease with low cholesterol levels, and instances where patients with high cholesterol levels do not develop heart disease.

Based on their characteristics, biomarkers can be classified as imaging biomarkers or molecular biomarkers. Imaging biomarkers include techniques like computed tomography (CT), positron emission tomography (PET), and magnetic resonance imaging (MRI). Molecular biomarkers are measurable in biological samples, including nucleic acids, peptides, proteins, lipids, metabolites and other small molecules (Laterza et al., 2007).

Biomarkers can also be categorised by their application, including diagnostic biomarkers, monitoring biomarkers, response biomarkers, predictive biomarkers, prognostic biomarkers (FDA-NIH Biomarker Working Group, 2016). The definitions and examples of each type of these biomarkers are listed in Table 1-1. The applications also reveal the importance of biomarkers in medicine and research, helping to improve diagnosis, treatment and patient outcomes.

Table 1-1 Classification of biomarkers based on their applications.

Classification	Definition	Example	Type (0, I, II)
Diagnostic biomarker	A biomarker used to identify individuals with a disease or a subtype of the disease.	Blood sugar or haemoglobin A1c (HbA1c) to identify Type 2 diabetes mellitus (American Diabetes Association, 2011).	Type 0

Classification	Definition	Example	Type (0, I, II)
Monitoring biomarker	A biomarker measured repeatedly to assess the status of a disease or to detect the effect of a medical product.	Hepatitis C virus ribonucleic acid (HCV-RNA) level to assess treatment response in patients with chronic hepatitis C (Terrault et al., 2018).	Type I
Response biomarker – Pharmacodynamic biomarker	A response biomarker that indicates the biologic activity of a medical product or environmental agent without necessarily linking to efficacy, disease outcome, or established mechanism of action.	Sweat chloride to assess response to cystic fibrosis transmembrane regulator (CFTR) potentiating agents in patients with cystic fibrosis (Durmowicz et al., 2013).	Type I
Response biomarker - Surrogate endpoint biomarker	A response biomarker that is an endpoint used in clinical trials as a substitute for a direct measure of how a patient feels, functions, or survives.	Blood pressure reduction as a validated surrogate endpoint for reduction in rates of stroke, myocardial infarction, and mortality (James et al., 2014).	Type II
Predictive biomarker	A biomarker that identifies individuals who are more likely to experience either a beneficial or adverse effect from exposure to a medical product or environmental agent.	BRCA1/2 genes mutations to identify responders to poly (ADP-ribose) polymerase (PARP) inhibitors in women with platinum-sensitive ovarian cancer (Ledermann et al., 2012).	Type I
Prognostic biomarker	A biomarker used to identify likelihood of a clinical event, disease recurrence or progression in patients who have the disease or medical	Mutations in the BRCA1/2 genes to indicate the likelihood of a second breast cancer in women with breast	Type 0

Classification	Definition	Example	Type (0, I, II)
	condition of interest.	cancer (Basu et al., 2015).	

Table content summarised from (FDA-NIH Biomarker Working Group, 2016).

1.1.3 Application in Neurological Disorders

Neurological disorders are one of the leading causes of disability globally, affecting millions of people (Feigin et al., 2019). However, timely and effective treatment for neurological disorders is a public health challenge. The complexity of the nervous system, along with the diverse aetiologies underlying these disorders and the variability in individual symptoms and treatment response, makes it challenging to prescribe precise medications (Pankevich et al., 2014). Biomarkers play a crucial role in enhancing our understanding of neurological diseases and have the potential to aid in diagnosis, monitor disease progression, guide treatment decisions. Many biomarkers can be measured using non-invasive or minimally invasive methods, such as blood tests, urine tests, or imaging techniques such as MRI or PET scans. Furthermore, biofluid biomarkers offer the advantage of accessibility in neurological diseases where accessing the nervous system is difficult.

Established biomarkers for assessing neurodegeneration include neurofilament light chain (NfL), glial fibrillary acid protein (GFAP), S100B and phosphorylated tau (*p*-tau). NfL is a structural component in neurons, and elevated NfL in cerebrospinal fluid (CSF) and blood are associated with neuroaxonal damage in many neurological diseases (Gaetani et al., 2019), including multiple sclerosis (Disanto et al., 2017), dementia, movement disorders (Olsson et al., 2019). GFAP, an intermediate filament assembly within astrocytes, serves as a biomarker of astrocyte injury, and elevated levels can be found in serum and CSF in a number of neurological diseases (Abdelhak et al., 2022). For example, applications include evaluation of traumatic brain injury (TBI) (Yue et al., 2019), multiple sclerosis (Abdelhak et al., 2018), stroke (Foerch et al., 2006). S100B is a calcium-binding protein predominantly expressed in the brain, particularly by astrocytes (T. Abboud et al., 2023). Elevated levels of S100B in biofluids are recognised

as reliable indicators of neural stress (Michetti et al., 2019). In particular, serum S100B has been clinically validated as a biomarker for mild traumatic brain injury (Faisal et al., 2023; Rogan et al., 2022). Lastly, plasma *p*-tau can predict tau and amyloid β pathologies, and differentiate Alzheimer's disease from other neurodegenerative disorders (Gonzalez-Ortiz et al., 2023; Karikari et al., 2020).

1.1.4 Evaluation of Biomarkers

The effectiveness of biomarkers can be evaluated and quantified using various statistical metrics. One fundamental tool for assessing classifiers is the confusion matrix. The confusion matrix summarises prediction outcomes over the test set by categorising them into true positives (TP), false positives (FP), true negatives (TN) and false negatives (FN) (Ng et al., 2023) (Figure 1-1A). These values are essential for calculating key performance metrics, including sensitivity, specificity, accuracy, positive predictive value (PPV), and negative predictive value (NPV) (Figure 1-1B).

Sensitivity and specificity are metrics that assess the performance of the test to detect a true positive or true negative, respectively (Trevethan, 2017). For example, an 80% sensitivity means that the diagnostic test correctly identifies 80% of all individuals with the condition being tested for as positive; while an 80% specificity means that the diagnostic test correctly identifies 80% of all individuals without the condition being tested for as negative. Accuracy describes the overall ability of a test to differentiate the patient and healthy cases correctly.

Positive predictive value (PPV) and negative predictive value (NPV), on the other hand, gives a probability that a particular person has the disease based on a positive or negative test result (Monaghan et al., 2021). For example, an 80% PPV means that 80% of all individuals with a positive test result have the condition being tested for, while an 80% NPV means that 80% of all individuals with a negative result do not have the condition being tested for.

The receiver operating characteristic (ROC) curve is commonly used to evaluate the

trade-off between sensitivity and specificity for different threshold values of a diagnostic test (Florkowski, 2008). The area under the curve (AUC) is used to summarise the overall performance of a diagnostic test based on the ROC curve (Figure 1-1C). The AUC ranges from 0.5 to 1.0, where 0.5 indicates no discrimination and 1.0 indicates perfect discrimination. AUCs below 0.6 are generally not considered medically useful, while values of 0.75 or higher are considered useful for clinical purposes (Taylor et al., 2008).

An ideal biomarker should possess several key characteristics to be effective in clinical and research settings (Bennett & Devarajan, 2011; Bodaghi et al., 2023; Verma et al., 2011). Firstly, it should demonstrate high specificity, accurately distinguishing the target condition from other conditions to minimise false positives. Similarly, it should boast high sensitivity, reducing the risk of false negatives. It should be easy to measure, rapid and reproducible. Accessibility and cost-effectiveness are also crucial for widespread clinical use, making the biomarker feasible for routine testing. Furthermore, it should have biological relevance, linked to the underlying disease mechanisms, thereby offering insights into pathophysiology, progression, and response to treatment. Ultimately, a biomarker with strong clinical utility not only aids in diagnosis but also supports treatment decisions, monitoring, and prognosis, enhancing patient outcomes and guiding precision medicine.

In many clinical contexts, particularly those involving diseases with heterogeneous presentations or multifactorial aetiologies, a single biomarker may not be sufficient to capture the complexity of the condition (Kang et al., 2022; Zemans et al., 2017). In such cases, combining multiple biomarkers into a panel can improve diagnostic or prognostic accuracy by providing a more comprehensive picture of the disease state (J. Yang et al., 2024). However, the integration of multiple biomarkers also presents challenges. These include increased analytical complexity, higher costs, and the necessity for rigorous statistical validation to ensure clinical utility. Standardised, reproducible analyses are essential to maintain reliability across different clinical settings (McDermott et al., 2013).

To mitigate the risk of overfitting, robust statistical approaches such as cross-validation, regularisation techniques, and validation in independent cohorts are essential. When appropriately modelled and validated, multivariate biomarker panels can provide substantial advantages, enhancing disease stratification and supporting personalised treatment strategies.

(A)

		Predicted condition	
	Total population	Positive (PP)	Negative (PN)
Actual condition	Positive (P)	True positive (TP)	False negative (FN)
	Negative (N)	False positive (FP)	True negative (TN)

(B)

Sensitivity = TP/P
Specificity = TN/N
Accuracy = (TP + TN)/(P + N)
Positive predictive value (PPV) = TP/PP
Negative predictive value (NPV) = TN/PN

(C)

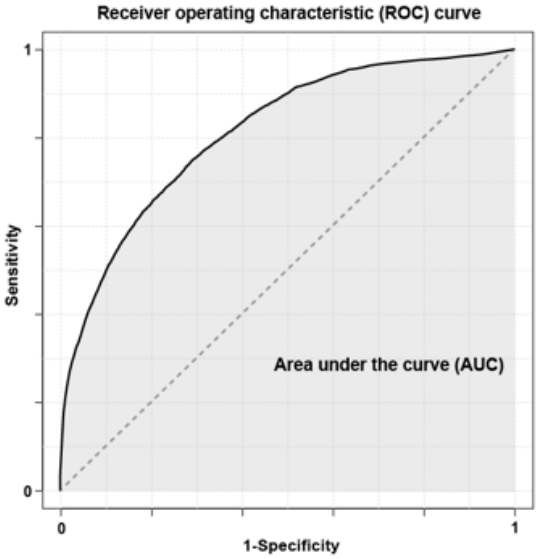

Figure 1-1 Metrics of validation. (A) Confusion matrix. (B) Formula of statistical metrics. (C) Receiver operating characteristics (ROC) curve and area under the curve (AUC). A ROC curve plots the true positive rate (sensitivity) against the false positive rate (1 - specificity) at various threshold settings. P, positive. N, negative. PP, predictive positive. PN, predictive negative. TP, true positive. FP, false positive. FN, false negative. TN, true negative.

1.2 Metabolomics

1.2.1 Definition

Omics technologies are high-throughput methods that enable the collection of vast amounts of data on specific molecular types within a single experiment (Quezada et al., 2017). They have emerged as powerful tools for biomarker discovery, capturing different levels of biological information, from genes (genomics) and transcripts (transcriptomics) to proteins (proteomics) and metabolites (metabolomics). This thesis focuses on metabolomics, the most downstream level of omics in an organism (Patti et al., 2012), for biomarker discovery.

Metabolomics is the study of the global collection of low molecular weight metabolites (< 1,500 Da) present in biological specimens, collectively known as the metabolome (Wishart et al., 2007). These small molecules, known as metabolites, play crucial roles in biological systems, such as energy production, synthesis of biomolecules, signal transduction, and metabolic regulation (Johnson et al., 2016). In energy production, specific metabolites can generate energy needed for cellular activities. For instance, glucose and fatty acids are broken down through glycolysis and beta oxidation to produce adenosine triphosphate (ATP), the primary energy currency for cellular functions. Additionally, metabolites act as building blocks for the synthesis of complex biomolecules; for example, amino acids contribute to protein synthesis, while nucleotides are integral to DNA/RNA synthesis. Apart from structural and energetic roles, metabolites facilitate signal transduction, where they function as signalling molecules that regulate cellular processes and intercellular communications. Cyclic adenosine monophosphate (cAMP), for example, mediates various intracellular signalling pathways involved in processes like cell growth, differentiation and apoptosis (YAN et al., 2016). Furthermore, metabolites contribute to the regulation of metabolism by acting as allosteric regulators or substrates for enzymes, thereby modulating enzyme activity and controlling metabolic flux. For instance, the glucose metabolite fructose-6-phosphate (F6P) acts as an allosteric regulator of the enzyme phosphofructokinase-1

(PFK-1) in glycolysis (Webb et al., 2015).

Metabolites originate from both endogenous sources and external factors such as diet, microbes, and xenobiotics. Thus, the metabolome reflects the physiological status of an organism in response to both genetic and environmental factors (Rattray et al., 2018). It provides direct signatures of biochemical activity, closely linked to the phenotype, representing a valuable reservoir for biomarker discovery and pathological investigation of diseases (A.-H. Emwas et al., 2019; Patti et al., 2012; A. Zhang et al., 2013).

Metabolites can be categorised into several major classes based on their chemical structure, including amino acids, carbohydrates, lipids, nucleotides, organic acids, amines (Wishart et al., 2021). Each metabolite class has specific roles that contribute to different biological processes. For example, Amino acids are primarily involved in protein synthesis but also participate in signalling and metabolic regulation (G. Wu, 2009). Carbohydrates serve as a major energy source and are involved in structural roles and cellular recognition (Chandel, 2021a). Lipids play key roles in energy storage, cellular membrane structure, and signalling (Segatto & Pallottini, 2020). Nucleotides are essential for genetic information storage and energy transfer (e.g., ATP) (Chandel, 2021b). Organic acids act as intermediates in metabolic cycles, such as the citric acid cycle, which is central to energy production (I. Goldberg & Rokem, 2009).

Currently, over 200,000 metabolites have been annotated in the human metabolome database (Wishart et al., 2021). As research progresses, this number continues to grow, driven by advancements in analytical methods and data repositories. However, despite these advancements, only a fraction of these metabolites can be accurately measured in practice.

1.2.2 Rationale for Using Metabolomics to Study Neurological Diseases

Diagnosing neurological diseases accurately and early is challenging, particularly in cases where symptoms overlap, such as between autoimmune encephalitis and psychotic

disorders (Funayama et al., 2022). Additionally, these diseases often have diverse underlying mechanisms, including, inflammation (Skaper et al., 2018), oxidative stress (Uttara et al., 2009), mitochondrial dysfunction (Norat et al., 2020), and altered neurotransmitter levels (Teleanu et al., 2022). Conventional diagnostic methods, such as neuroimaging, electrophysiological tests and neuropsychological tests, may lack sensitivity, can be invasive or costly, and do not always capture the biochemical changes associated with early disease onset or progression. This highlights a critical need for reliable biomarkers with robust diagnostic capabilities, convenient testing methods, and predictive value for treatment responses.

Metabolomics holds significant promise for meeting these needs. Given that metabolites are downstream of genomic, transcriptomic, and proteomic alterations, they can provide a more immediate reflection of physiological conditions. This biochemical snapshot can reveal subtle metabolic shifts that occur even before clinical symptoms appear, making metabolomics a powerful tool for identifying biomarkers (Skene et al., 2017).

The robustness of metabolomics lies largely in its foundational techniques, nuclear magnetic resonance (NMR) and mass spectrometry (MS), both of which are known for their high-throughput, sensitivity, and reproducible detection capabilities. These techniques are capable of the quantitative analysis of hundreds of metabolites in a sample in a single run.

Metabolomics also holds promise for predicting treatment responses. Many treatments for neurological diseases work by altering biochemical pathways, such as those involved in neurotransmitter synthesis or inflammation. By identifying metabolites associated with specific pathways and treatment responses, metabolomics can help predict how a patient will respond to a particular therapy (McGrath & Young, 2019; Muranaka et al., 2023, 2023; Teitsma et al., 2018; Zheng et al., 2024). For instance, distinct metabolomic profiles could indicate sensitivity or resistance to a given drug, allowing clinicians to tailor treatments. Additionally, monitoring changes in metabolomic profiles over time

can provide insights into treatment efficacy, helping to optimise therapeutic strategies and adjust interventions based on biochemical feedback.

The application of metabolomics spans various sample types, including biofluids (blood, urine, cerebrospinal fluids), and tissues (post extraction), providing flexibility in both research and clinical settings. While the invasive nature of tissue sampling limits its routine use in human studies, tissue metabolomics remains valuable in specific contexts. For example, tumour biopsies are increasingly analysed to characterise metabolic heterogeneity within cancers, offering insights into tumour biology, progression, and treatment response (H. A. Miller et al., 2022). In contrast, biofluids offer a less invasive way to obtain metabolic information and offer the advantage of repeated collection at multiple time points, making them more favoured for human studies. Among biofluids, cerebrospinal fluid (CSF) stands out as a prime candidate for studying neurological disorders due to its close proximity to the brain, as evidenced by the use of CSF metabolomics in detecting neuroinflammation (Yan et al., 2021). However, the invasive nature of CSF collection procedures limits its utility in large-scale studies. As a result, blood samples, collected as serum or plasma, have become the primary biofluid used in metabolomic analyses of neurological diseases (Quinones & Kaddurah-Daouk, 2009).

Metabolite exchanges between blood and the brain are thought to be tightly regulated by the blood-brain barrier (BBB) and the blood-CSF barrier (BCSFB), where aquaporins and membrane-bound carrier proteins regulate influx and efflux via passive and active transport processes (Carstens et al., 2024). BBB dysfunction is observed as an early critical feature of many inflammatory CNS diseases (Archie et al., 2021). In response to inflammation, the BBB undergoes an increase in solute permeability and facilitates lymphocyte trafficking into the brain (Sonar & Lal, 2018). This increased permeability of the BBB leads to an increase of blood-derived metabolites in the CSF and brain parenchyma. The inflammatory disruption of the BBB has showed to lead to metabolic consequences (Brown et al., 2016). The disruption of the BBB not only affects brain metabolic profiles but may also lead to alterations in the blood metabolome. While

blood metabolites are less directly associated with the brain than CSF, there is evidence linking blood metabolite changes with central metabolic alterations. For example, plasma tryptophan levels reflect CSF tryptophan and 5-hydroxyindoleacetic acid concentrations, thereby serving as an index of 5-hydroxytryptamine turnover in the CNS (Curzon, 1979). Additionally, blood metabolites have been shown to correlate with neuroimaging parameters in schizophrenia (Krzyściak et al., 2024) and with MRI measures and CSF biomarkers associated with Alzheimer's disease pathology (Varma et al., 2018).

The brain is metabolically active and relies heavily on systemic metabolism for energy and nutrient supply. Consequently, metabolic dysregulation in the brain, such as alterations in energy metabolism, neurotransmitter levels, or oxidative stress, can lead to changes in circulating metabolite levels (Donatti et al., 2020; Korczowska-Łącka et al., 2023). Additionally, brain alterations can evoke systemic responses in peripheral tissues and organs. Neuroinflammation, oxidative stress, or neuronal damage in the brain can stimulate immune cells, modulate metabolic pathways, or release inflammatory mediators systemically (Solleiro-Villavicencio & Rivas-Arancibia, 2018; H. Wang et al., 2023; Q. Yang et al., 2020). These peripheral responses may be detected as indirect indicators of CNS dysfunction.

1.2.3 Applications in Neurological Disorders

There is a growing number of metabolomics studies in biomarker discovery in neurological diseases, including Alzheimer's disease (AD), epilepsy, multiple sclerosis, and Parkinson's disease, which are among the most prevalent neurological diseases. Metabolomics identifies potential metabolic biomarkers that might facilitate diagnostic, therapeutic and prognostic determination in neurological diseases. By revealing altered metabolic pathways, metabolomics provides insights into disease mechanisms and uncovers potential therapeutic targets (Qiu et al., 2023).

For example, metabolomic studies have identified several metabolic pathways associated with AD pathogenesis and progression, including lipid metabolism, fatty acid

metabolism, energy metabolism, arginine and glutamate metabolism (Wilkins & Trushina, 2018; C. Yin et al., 2023). In epilepsy, metabolomic studies on patients with epilepsy and epileptic animal models have suggested glutamate, lactate and citrate as potential biomarkers for epilepsy, and have highlighted metabolic pathways involving alanine, aspartate, and glutamate metabolism (W. Lai et al., 2022). In multiple sclerosis, metabolomic analysis has been used to distinguish patients from healthy controls and other demyelinating disorders, and discriminate patients according to their disease stage, and monitor treatment effects (Rispoli et al., 2021).

Previous work in our group has demonstrated the value of NMR metabolomics in detecting and differentiating various autoimmune CNS diseases with overlapping symptoms. For instance, NMR plasma metabolomics has been shown to differentiate between relapsing-remitting and secondary progressive multiple sclerosis (Dickens et al., 2014, *p.* 2). Furthermore, NMR metabolomics has revealed plasma signatures for multiple sclerosis, aquaporin-4 (AQP4)-antibody and myelin oligodendrocyte glycoprotein (MOG)-antibody disease (Jurynczyk et al., 2017). It has also been used to subclassify within antibody-negative neuromyelitis optica spectrum disorder (NMOSD) patients, and distinguish between relapsing-remitting multiple sclerosis and Ab-NMOSD (Yeo et al., 2019). Additionally, combining biochemical, proteomic, and metabolomic analysis of CSF has been shown to predict clinical conversion to multiple sclerosis (Probert et al., 2021). Serum metabolite biomarkers indicative of relapses in multiple sclerosis have been identified by the use of NMR metabolomics (Yeo et al., 2021).

Through these advancements, metabolomics not only enhances our understanding of the molecular underpinnings of neurological diseases, but also drives the development of more effective, personalised treatment strategies.

1.2.4 Analytical Methods in Metabolomics

Mass spectroscopy (MS) and NMR are the primary analytical platforms for metabolic profiling. MS is typically coupled with chromatographic separation techniques, such as

liquid chromatography (LC-MS), and gas chromatography (GC-MS). Chromatography provides a means to separate the metabolites based on their chemical properties such as polarity, size, or volatility (Xiao et al., 2012). This separation reduces sample complexity and helps to resolve individual metabolites from interfering compounds, enhancing the sensitivity and specificity of detection by MS.

MS detects metabolites by first ionizing them, typically using techniques such as electrospray ionisation (ESI) or matrix-assisted laser desorption/ionisation (MALDI), which generate charged ions from the analyte molecules (Pitt, 2009). These ions are then accelerated through an electric field and passed into a mass analyser, such as a quadrupole or a time-of-flight (TOF) analyser. The mass analyser separates ions based on their mass-to-charge ratio (m/z), allowing ions of different masses to be detected separately. Finally, the ions are detected by a detector, which measures their abundance at specific m/z values. The resulting LC/GC-MS data typically consists of m/z, retention time, and intensity for every detected ion mass.

NMR spectroscopy, typically ^{1}H NMR spectroscopy is used for measure metabolites in a biological sample. NMR spectroscopy detects metabolites by subjecting a sample to a strong magnetic field and radiofrequency pulses (Lane, 2012). Nuclei within the sample absorb and emit energy at characteristic frequencies, known as chemical shifts, based on their chemical environment. These shifts provide information about the molecular structure of the metabolites and enable their quantification.

The strengths and weaknesses for each technique are listed in Table 1-2 (Emwas et al., 2019; Wishart, 2019). MS is more widely used, likely due to its high sensitivity, capability of detecting metabolites in nanomolar (nM) levels, and its extensive metabolite coverage, usually detecting thousands of metabolites in a biological sample. NMR accounts for about 20% of metabolomics studies, with the number of publications growing every year. NMR offers several unique strengths over MS: it boasts high reproducibility, good instrument stability, and minimal sample preparation requirements. These characteristics make it a popular automated platform for large-scale clinical or

epidemiological studies. Furthermore, ^{1}H NMR detects all protons in a sample, making it a universal, unbiased detector for metabolites above the limit of detection (See Table 1-2). In contrast, MS requires different instruments and ionisation methods to identify metabolites in different classes. Despite the lower sensitivity of NMR, detecting only metabolites above micromolar (μM) levels, the metabolome portion detectable by NMR often holds significant biological relevance. Moreover, NMR is capable of detecting compounds that are challenging for LC-MS, such as sugars, organic acids, alcohols, polyols, and other highly polar or low molecular weight compounds (Wishart et al., 2023). Additionally, NMR has also become the clinically approved method for measuring plasma lipoprotein and cholesterol classes (Jiménez et al., 2018). One limitation of NMR-based metabolomics is spectral peak overlap, where multiple metabolites share similar chemical shifts, leading to peak congestion in crowded regions of the spectrum. This can hinder accurate identification and quantification, especially in complex biological samples such as plasma or tissue extracts. While techniques such as two-dimensional NMR and spectral deconvolution software can alleviate some of these challenges, they often come at the cost of longer acquisition times and increased computational demands. In contrast, mass spectrometry, particularly when coupled with chromatography, generally provides superior resolution and separation of compounds, reducing issues related to signal overlap.

Table 1-2 Pros and cons of mass spectrometry and nuclear magnetic resonance spectroscopy in metabolomics.

	NMR	MS
Reproducibility	Excellent	Moderate
Sensitivity	Low (μM)	High (nM)
Selectivity	Generally used for non-selective (untargeted) analysis	Can be used for both targeted and untargeted analysis. Both GC-MS and LC-MS are superior for targeted analyses.
Metabolite coverage	Modest (usually 30-100)	Extensive (usually thousands detected, and hundreds

	NMR	MS
		identified)
Sample preparation	Minimal (usually transferring the sample to an NMR tube and adding deuterated locking solvent)	More demanding (requires chromatography; requires sample derivatization for gas chromatography)
Sample measurement	Relatively fast (average analytical time 5-10 minutes)	Relatively slow (usually 10-40 minutes; new methods can be as fast as 2-3 minutes)
Sample recovery	Non-destructive	Destructive
Quantification	Inherently quantitative	The intensity of the MS line is often not correlated with metabolite concentrations; not fully quantitative without standard curves.
Instrumentation	Robust instrumentation.	Frail instrumentation.
	Minimal instrument downtime.	Frequent instrument downtime.
	Very expensive instrumentation.	Moderately expensive instrumentation.
Overlapping peaks	May experience signal overlap, especially in crowded regions; complicates identification and quantification	Chromatography and high mass resolution reduce overlap

Adapted from (A.-H. M. Emwas et al., 2013; Wishart, 2019) with permission from the publishers.

1.3 Nuclear magnetic resonance-based metabolomics

1.3.1 NMR Principles

This thesis uses NMR spectroscopy for the metabolomics studies. To elucidate the principles underlying NMR's detection and quantification of metabolites in biological samples, key concepts were summarised from "Introduction to Spectroscopy", "High-resolution NMR Techniques in Organic Chemistry", and "Understanding NMR spectroscopy" (Claridge, 2009; Keeler, 2016; Pavia et al., 2014).

1.3.1.1 Spin States

Nuclei with an odd number of protons and/or an odd number of neutrons possess a property called spin, making them detectable through NMR. Commonly observed nuclei with spin are ^{1}H, ^{2}H, ^{13}C, ^{14}N, ^{17}O, and ^{19}F, while ^{12}C and ^{16}O lack this property. As moving electric charges generate magnetic fields, nuclei with spin generate their own tiny magnetic fields, resulting in a magnetic moment μ. In the absence of an external magnetic field, the spins are disordered, with no energy difference among different orientations. However, when an external magnetic field is applied, the nuclei align their spins in specific ways termed spin states. The number of available spin states for a nucleus in an external magnetic field is determined by its nuclear spin quantum number *(I)*, calculated using the formula $2I + 1$. For example, ^{1}H and ^{13}C nuclei (both with $I = 1/2$) have two spin states. The two spin states for a spin ½ nucleus are either aligned with the field (lower energy) or aligned against the field (higher energy). These states are referred to as parallel (α) and antiparallel (β), respectively.

1.3.1.2 Resonance

By convention, the applied magnetic field, denoted as B_0, is always aligned along the z-axis. Upon application of the magnetic field, the nucleus begins to precess around its own axis of spin at the Larmor frequency of the nucleus (Figure 1-2). The Larmor frequency, ω, is given by

$$\omega = -\gamma B_0 \text{ rad s}^{-1} \text{ or } \nu = \frac{\gamma}{2\pi} B_0 \text{ Hz} \qquad \text{Equation 1-1}$$

Where ω is the is the angular frequency in radians per second, ν is the frequency in hertz, and γ is the gyromagnetic ratio, a constant that depends on the specific type of

nucleus.

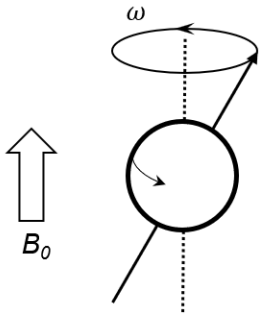

Figure 1-2 Precession of a spinning nucleus upon application of the magnetic field. B_0, the applied magnetic field. ω, angular frequency.

The precession of the nucleus generates an oscillating electric field of the same frequency as the Larmour frequency of the precessing nucleus. When radiofrequency pulses of Larmour frequency are applied to the precessing nucleus, the frequency of oscillating electric field component of the incoming radiofrequency matches that of the electric field generated by the precessing nucleus, leading to coupling of the two fields. This coupling can cause the nucleus to absorb energy from the radiofrequency pulse, transitioning from a low-energy spin state to a high-energy spin state. This phenomenon, termed resonance, indicates that the nucleus resonates with the incoming electromagnetic wave (Figure 1-3).

The energy gap (ΔE) between the two spin states is given by the equation:

$$\Delta E = h\upsilon = \frac{h\gamma B_0}{2\pi} \qquad \text{Equation 1-2}$$

where h is Planck's constant, and γ is gyromagnetic ratio (specific to each type of nucleus). Thus, as the applied field strength increases, ΔE increases. Nuclei can only absorb energy that matches ΔE.

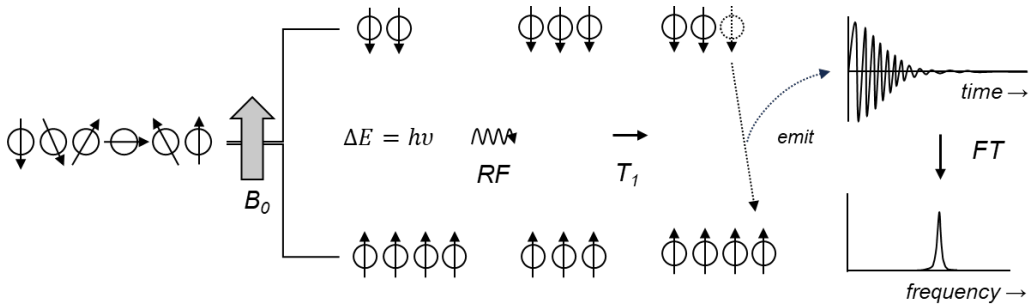

Figure 1-3 The process of nuclear magnetic resonance. Upon the application of an external magnetic field, the nuclei align their spins in their spin states and start precession. The precessing nuclei absorb energy, resonating with radiofrequency pulses at their Larmor frequency. Once the pulse stops, the excited magnetic nuclei return to equilibrium (relaxation). During this process, the oscillating magnetic fields generated by the relaxing spins produce an electrical signal that gradually diminishes over time, known as Free Induction Decay (FID). This signal is then processed through Fourier Transformation (FT), converting the time-domain signal into a frequency-domain spectrum, which reveals information about the chemical environment of the nuclei. T_1, the longitudinal relaxation time. FT, Fourier transformation.

1.3.1.3 Population excess

At thermal equilibrium, there will always be more nuclei in the low-energy state than the high-energy state, given by a Boltzmann distribution:

$$\frac{N_{high}}{N_{low}} = e^{\left(\frac{-\Delta E}{kT}\right)} \qquad \text{Equation 1-3}$$

where k is the Boltzmann constant and T is the absolute temperature in Kelvin. For an NMR instrument operating at 700 MHz (16.4 T) at 298 K, for every 1 million nuclei in the higher energy state, there are approximately 1,000,106 nuclei in the lower energy state — a population excess of 106 nuclei. This population excess (N_{low} – N_{high}) allows resonance to be observed.. Therefore, the small population excess explains the inherent insensitivity of NMR relative to alternative analytical techniques. The population excess gives rise to a resultant bulk magnetisation vector M along z-axis (Figure 1-4).

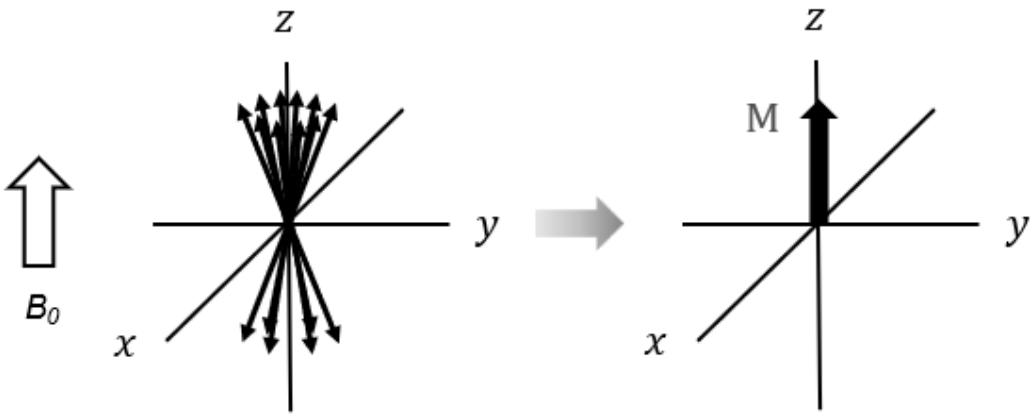

Figure 1-4 bulk magnetisation. The excess population of nuclei in the lower energy state results in a net bulk magnetization vector M oriented along the z-axis. This bulk magnetization arises from the alignment of nuclear spins in the presence of the applied magnetic field B_0.

1.3.1.4 Chemical shift

Protons in a molecule do not resonate at the same frequency, because the magnetic field they experience differs slightly from the applied external magnetic field B_0. This discrepancy arises from the influence of surrounding electrons, which generate tiny magnetic fields that oppose B_0. The density of electrons surrounding the protons varies subject to their chemical environments. Protons in regions with a higher electron density will resonate at higher frequencies, appearing further to the right on the NMR spectrum (Figure 1-5).

Chemical shift (δ) is a field-independent measure, typically reported in parts per million (ppm). It represents the resonant frequency of a nucleus relative to a standard in a magnetic field. The reference standard for ^{1}H and ^{13}C NMR is tetramethylsilane (TMS), $(CH_3)_4Si$, where its resonance frequency is defined as $\delta = 0$.

$$\delta = \frac{(shift\ in\ Hz)}{(spectrometer\ frequency\ in\ MHz)} \qquad \text{Equation 1-4}$$

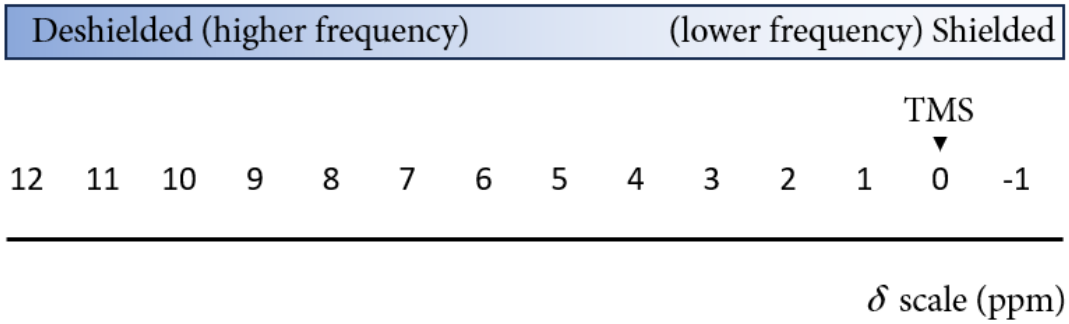

Figure 1-5 δ scale of chemical shift used in NMR spectroscopy.

1.3.1.5 Pulse, relaxation, and free induction decay

The bulk magnetisation vector M, resultant from the population excess, is used in the vector model of NMR to understand the behaviour of spins in NMR experiments. As M precesses at its Larmour frequency, a rotating frame of reference (coordinate system, $x'y'z'$) that rotates in the same direction and at the same speed as M, is introduced to simplify the study.

Modern Fourier Transform NMR instruments use pulses to excite all the magnetic nuclei present in the samples simultaneously. The pulse contains a wide range of frequencies, effectively exciting all magnetic nuclei in the sample with a single burst of energy. When the pulse is applied perpendicular to the M, all magnetic vectors begin to precess about the pulse axis and to tip towards the x-y plane, achieving phase coherence. The tipping angle is dependent on the duration of the pulse (pulse width). If a pulse applied along the x-axis, causing the M to tip 90° to the y-axis when the pulse ceases, it is referred as a $90°_x$ pulse.

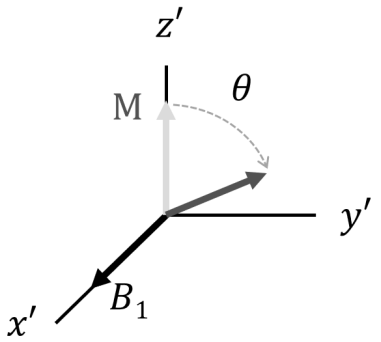

Figure 1-6 The radiofrequency pulse. Applying a B_1 pulse along the *x*-axis causes the bulk

magnetisation M to tip θ degrees towards the *y*-axis.

Subsequently, once the pulse stops, the excited magnetic vector returns to their equilibrium distribution. The magnitude of the M gradually diminishes along the y-axis and increases along the z-axis over time, due to both spin inversion restoring the Boltzmann distribution and the loss of phase coherence. This process is termed relaxation. The recovery of the magnetisation along z-axis or re-establishment of Boltzmann distribution is termed longitudinal relaxation (spin–lattice relaxation, Figure 1-7), given by:

$$M_z(t) = M_{z,eq}(1 - 2e^{-\frac{t}{T_1}}) \qquad \text{Equation 1-5}$$

where the longitudinal relaxation time T_1 is the decay constant for the recovery of the z component of the nuclear spin magnetisation.

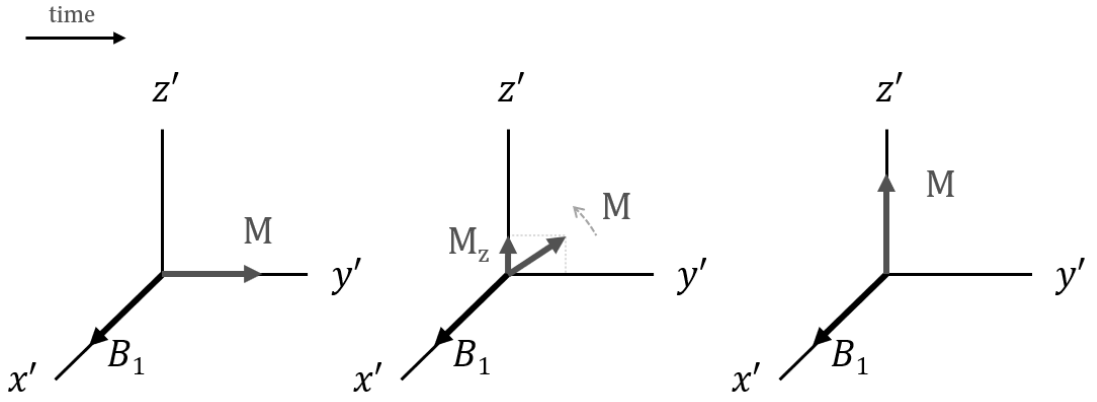

Figure 1-7 Longitudinal relaxation. Longitudinal component of the bulk magnetisation vector (M_z) exponentially relaxes to thermodynamic equilibrium.

The diminishment of the magnetisation in the x-y plane, or the complete loss of phase coherence, is termed transverse relaxation (spin–spin relaxation, Figure 1-8), given by:

$$M_{xy}(t) = M_{xy}(0)e^{-\frac{t}{T_2}} \qquad \text{Equation 1-6}$$

where the transverse relaxation time T_2 is the decay constant for the component of M perpendicular to B_0.

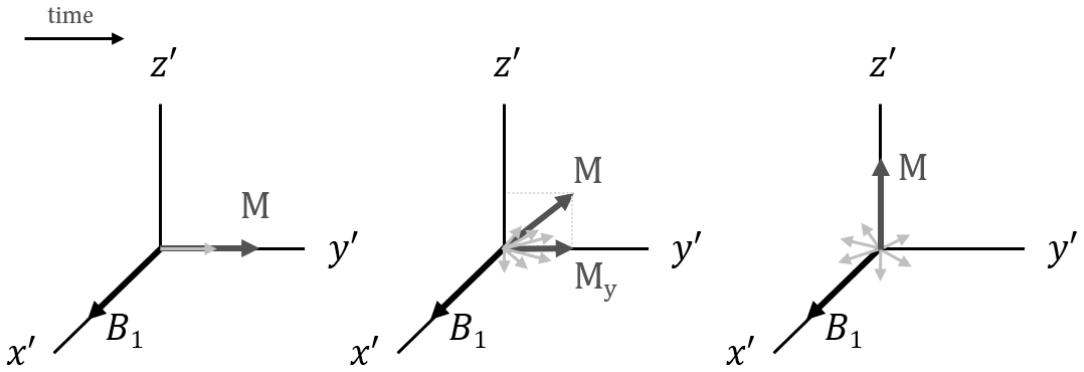

Figure 1-8 Transverse relaxation. The transverse component of the bulk magnetisation vector (M_y) exponentially decays to its equilibrium state, resulting in a loss of phase coherence.

For complete relaxation after a 90° pulse, a delay of at least $5T_1$ is necessary, allowing magnetisation to recover by 99.33%. T_2 correlates with the linewidth at half-height of the NMR signal.

In the NMR instrument, a receiver coil situated in the x-y plane detects the oscillating electronic magnetic field from transverse magnetisation. When the magnetisation relaxes back to the z-axis, the oscillating electronic magnetic field decays and becomes zero. This basic form of signal detected is called the free-induction decay (FID). The FID includes all the frequencies emitted and can be quite complex. Fourier Transform, a mathematical method, is used to separate the individual components from the FID signal and convert them into distinct frequencies. Spins that relax rapidly produce fast-decaying FIDs and broad resonances, while spins that relax more slowly result in longer FIDs and narrower resonances.

1.3.1.6 Spin-spin splitting

NMR proton signals can appear as multiplets, such as doublets, triplets, and quartets. This phenomenon, known as spin-spin splitting or J coupling, arises from the neighbouring spins. When a proton experiences spin-spin splitting with n equivalent neighbouring protons on adjacent carbon atoms, the NMR signal for this proton will be split into n + 1 peaks. Each peak corresponds to a different spin state combination of the neighbouring protons, and the spacing between these peaks is determined by the coupling constant J. The coupling constant, measured in Hertz (Hz), quantifies the

strength of the interaction between the spins of the coupled nuclei. For example, the ^{1}H NMR spectrum of lactate has two resonances, featuring a quartet derived from the -CH group and a doublet derived from the $–CH_3$ group (Figure 1-9).

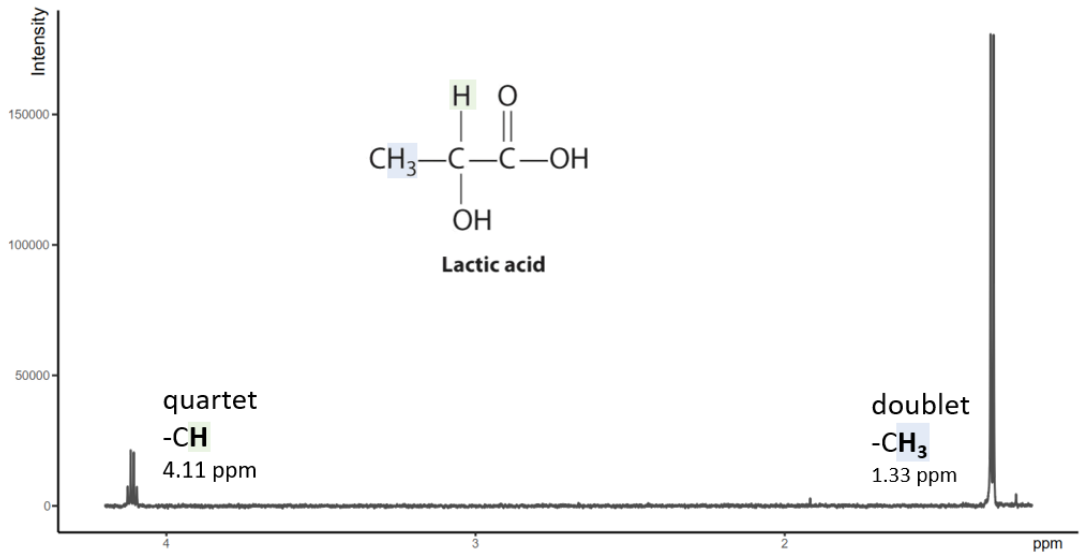

Figure 1-9 ^{1}H NMR spectrum of lactic acid.

1.3.1.7 Quantification

NMR has a quantitative capability, as it detects nuclear spins within the molecules. In principle, the NMR signal of an analyte should be proportional to the number of nuclei present. However, to acquire truly quantitative spectra, it is essential for spins to have full relaxation, necessitating a relaxation delay of at least $5T_1$ of the slowest relaxing nuclei. For example, the T_1 of maleic acid in D_2O phosphate buffered saline with a pH of 7.4, a commonly used internal standard, is about 6.2 s (Rundlöf et al., 2010). If this represents the longest T_1 among sample resonances, the inter-scan relaxation delay should exceed 30 seconds. However, such prolonged acquisition times are often impractical, particularly for high-throughput NMR metabolomics studies. In practice, shorter relaxation delays of 2-4 seconds are commonly used in most NMR metabolomics studies (Beckonert et al., 2007; A.-H. Emwas et al., 2016; Kostidis et al., 2017). While this may not achieve absolute quantification, it allows for relative quantitative comparisons between spectra collected under identical conditions. To achieve absolute quantification in such scenarios, one estimated approach is to apply a

T_1 correction factor to each quantified resonance (Bharti et al., 2008). Alternatively, calibration curves can be established for the resonances of interest by acquiring reference spectra of standards with known concentrations under identical conditions (Maes et al., 2012).

1.3.2 Workflow of NMR-based Metabolomics

Typically, the workflow for NMR-based metabolomics consists of four stages: sample preparation, data acquisition, data analysis, and biological interpretation (Figure 1-10). One of the advantages of NMR spectroscopy over mass spectrometry is its minimal sample preparation requirements. For example, biofluids such as serum, plasma and urine can be directly prepared into NMR samples by mixing with NMR buffer, while cells and tissues require extraction of metabolites for liquid-state NMR spectroscopy. Careful sample handling and storage conditions should be maintained throughout the preparation process to minimise sample degradation and ensure data integrity. This topic is further discussed in Section 1.5.1.

NMR spectroscopy utilises various NMR-active nuclei, with ^{1}H being the most widely used due to its presence in all metabolites and its higher NMR sensitivity (Gowda & Raftery, 2021). Popular experiments for metabolomics include one-dimensional (1D) Nuclear Overhauser effect spectroscopy (NOESY) experiments and Carr–Purcell–Meiboom–Gill (CPMG) experiments, which are further introduced in Section 1.3.3.

NMR data pre-processing involves a series of computational steps applied to raw NMR spectra to enhance data quality, correct for systematic errors and prepare the data for subsequent analysis. These steps are elaborated in Section 1.3.4

Data analysis aims to identify difference in both overall metabolite levels and individual metabolites across groups. It includes multivariate analysis to explore underlying patterns, identify clusters and build predictive models, as well as univariate analysis to assess the differences in metabolite abundance across groups and relationships among the metabolites. Further details are provided in Section 1.3.5.

Biological interpretation involves elucidating the biological relevance and meaning of the observed changes in metabolite levels or patterns. This begins with metabolite identification or assignment by matching spectral data to known metabolites in the literature or databases (Wishart et al., 2021). Pathway analysis is then used to identify biological pathways associated with observed metabolic alterations by integrating experimental data with pathway databases, such as the Kyoto Encyclopedia of Genes and Genomes (KEGG) (Kanehisa & Goto, 2000; Pang et al., 2021). Integrating metabolomic data with other omics datasets and clinical information further enhances biological context, allowing correlations between metabolite levels and biological variables such as gene expression levels or clinical parameters. Finally, experimental validation through targeted metabolite quantification or functional assays confirms the biological relevance and significance of key findings.

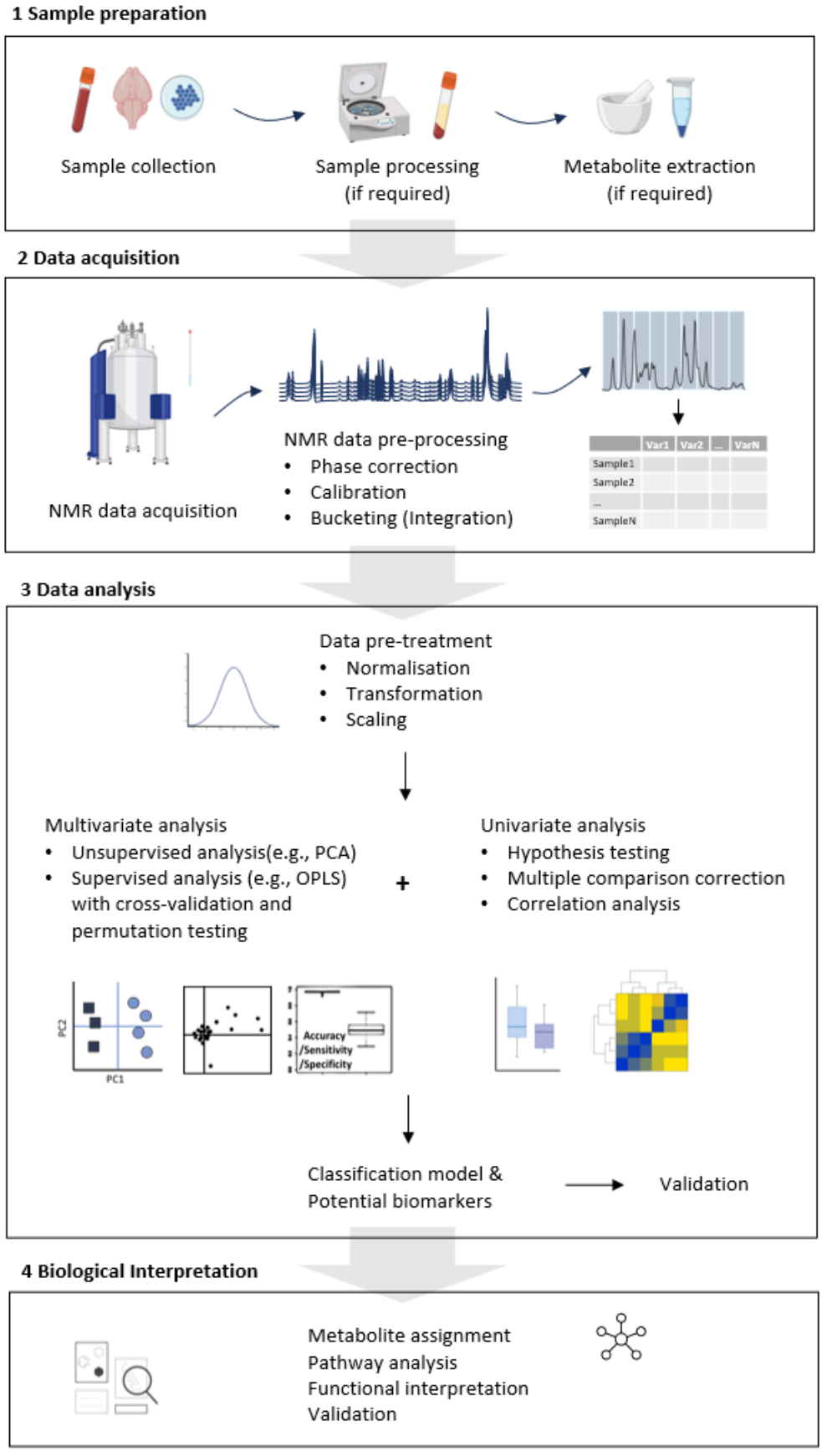

Figure 1-10 NMR-based metabolomics workflow.

1.3.3 NMR Experiments

One-dimensional (1D) ^{1}H NOESY experiments and 1D ^{1}H CPMG experiments are commonly used for NMR-based metabolomics. Additionally, 1D and two-dimensional (2D) total correlation spectroscopy (TOCSY) experiments can be used to aid in metabolite assignment.

1.3.3.1 Solvent Suppression

Solvent suppression is a common practice in NMR metabolomics, aimed at improving the detection of lower abundance metabolites and providing a smoother baseline for quantification (A.-H. Emwas et al., 2019). Water is ubiquitous in NMR metabolomics samples, such as serum/plasma metabolomics, where it is often mixed with phosphate buffer, or in brain metabolomics, where lyophilised brain extract is rehydrated in phosphate buffer. Deuterated solvents (99.9% D) and water suppression techniques are employed to suppress the water signal.

One of the simplest and most robust techniques for eliminating solvent signals is through presaturation of the solvent (Claridge, 2009; Hoult, 1976). This method involves the continuous application of weak radiofrequency irradiation at the solvent frequency before excitation and acquisition (Figure 1-11). It effectively saturates the solvent spins, making them undetectable during subsequent signal acquisition. Presaturation is straightforward to integrate into pulse sequences, such as NOESY and CPMG.

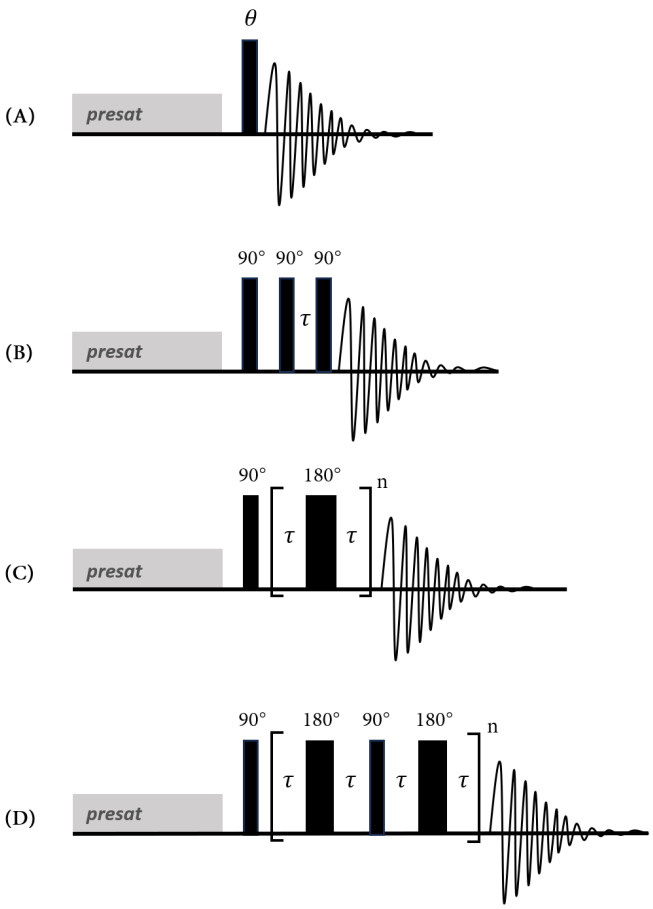

Figure 1-11 Pulse sequences commonly employed in metabolomics. (A) solvent presaturation. (B) 1D nuclear Overhauser effect spectroscopy (NOESY). (C) the Carr–Purcell–Meiboom–Gill (CPMG) sequence. (D) A CPMG variant called periodic refocusing of J evolution by coherence transfer (CPMG-PROJECT).

1.3.3.2 1D ^{1}H NOESY experiment

1D ^{1}H nuclear Overhauser effect spectroscopy (NOESY) coupled with water presaturation stands out as a widely adopted technique in NMR-based metabolomics investigations, renowned for its efficacy in suppressing the water signal while preserving other distal water signals within the spectra (Mckay, 2011). This method uses three 90° pulses alongside a long presaturation pulse for water suppression (Figure 1-11). Additionally, gradient pulses are integrated in the sequence to purge residual water signals.

1.3.3.3 1D ^{1}H CPMG-PROJECT experiment

Serum and plasma are rich in proteins and lipids. These macromolecules have broad NMR resonances that can overlap with and obscure the signals of small molecules, making quantification inaccurate. To address this issue, the Carr–Purcell–Meiboom–Gill (CPMG) sequence is frequently employed, leveraging the substantial discrepancy in T_2 relaxation times between small molecules and macromolecules to selectively filter out NMR signals originating from proteins and other biomolecules (Claridge, 2009). This sequence comprises a 90° pulse followed by a series of 180° pulses, generating spin echoes. Notably, signals originating from molecules with shorter T_2 relaxation times (such as large molecules like proteins) decay more rapidly, and are consequently suppressed in the NMR spectra. Typically, this pulse sequence is complemented by presaturation to further suppress signals arising from water.

A CPMG variant called periodic refocusing of J evolution by coherence transfer (PROJECT) has been introduced (Aguilar et al., 2011). This method uses perfect echoes to eliminate J modulation distortions (Aguilar et al., 2011), enabling more accurate integration and analysis of NMR signals.

1.3.3.4 TOCSY experiment

Total correlation spectroscopy (TOCSY) can aid in the identification and assignment of metabolites in NMR metabolomics. TOCSY relies on through-bond J-coupling, where magnetisation is transferred between coupled nuclei via J coupling interactions. This allows for the correlation of resonances belonging to the same spin system or molecule. In complex mixtures such as those encountered in metabolomics, NMR spectra can often have overlapping signals, making it difficult to distinguish between different metabolites. TOCSY can help resolve these overlapping signals by revealing which resonances are correlated with each other. This correlation allows for the grouping of signals belonging to the same metabolite, aiding in their identification and assignment.

Both 2D TOCSY and 1D selective TOCSY experiments are usually used for the above-

mentioned purposes. 2D TOCSY provides detailed connectivity information for all the spin systems in the sample but requires longer acquisition times and may miss small signals. On the other hand, 1D selective TOCSY selectively excite the frequency of interest and identifies the resonances from the same spin system. It enables targeted investigation and can improve signal resolution by selectively exciting the desired protons.

1.3.4 NMR Data Pre-processing

Pre-processing is the transformation of raw data to make it appropriate for subsequent data analysis.

1.3.4.1 Apodisation

In the FID of NMR, the signal intensity gradually diminishes over the acquisition time, while the noise amplitude remains consistent. Emphasising the early part of the FID and de-emphasising the later part can improve the signal-to-noise ratio and reduce undesirable artifacts. This process, known as apodisation or line broadening, involves multiplying the FID by a mathematical function, commonly a decaying exponential function. For ^{1}H NMR, a 0.3-0.5 Hz line broadening is typically used to enhance sensitivity without significantly compromising the line width (resolution).

1.3.4.2 Zero-filling

Zero-filling in NMR data processing involves appending zeros to the end of the FID signal. As the signal decays while noise remains constant, acquiring more data beyond a certain point adds little useful information. Zero-filling artificially enhances digital resolution by increasing the number of data points before Fourier transformation. Consequently, this results in more data points in the frequency domain, thereby improving spectral resolution and line shape definition without extra experimental time.

1.3.4.3 Fourier Transformation

The Fourier transform is a mathematical function which converts the time domain data (FID) into a frequency domain spectrum, given by:

$$f(\omega) = \int_{-\infty}^{+\infty} f(t)e^{i\omega t}\mathrm{dt} \qquad \text{Equation 1-7}$$

It decomposes the complex time-domain signal into its component frequencies, revealing the underlying frequency components present in the signal (Figure 1-12). The resulting spectrum represents the distribution of resonant frequencies within the sample.

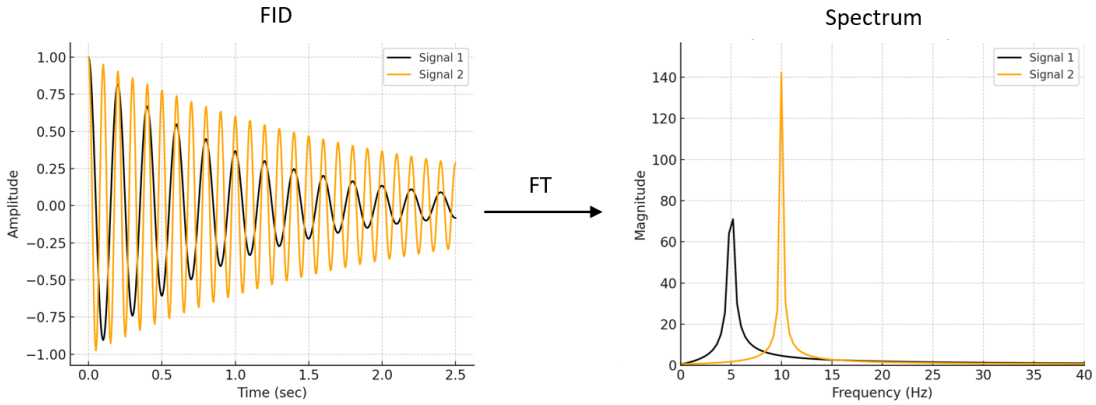

Figure 1-12 Fourier transform converts time domain data (FID) to a frequency domain spectrum.

1.3.4.4 Phase Correction

Following Fourier transformation, spectral peaks often show distortion owing to phase inconsistencies. To rectify these errors or variations and ensure accurate positioning and shapes of spectral peaks, phase correction (or phasing) is employed. Common phase correction methods include zero-order and first-order phase correction, which apply uniform or frequency-dependent phase adjustments to the spectrum, respectively (A.-H. Emwas et al., 2018). Phase correction is typically performed visually, with adjustments made by eye to ensure that spectral peaks display symmetric, well-defined shapes with minimal distortion and baseline artifacts.

1.3.4.5 Baseline Correction

Baseline correction refers to the process of removing or adjusting the baseline distortions present in the NMR spectrum to improve spectral quality and facilitate accurate peak integration and analysis. These distortions can stem from diverse sources such as instrumental noise, solvent signals, imperfect shimming, and phase

inconsistencies. Numerous baseline correction methods have been developed (A.-H. Emwas et al., 2018). One widely used technique is polynomial fitting, which involves fitting a polynomial function (usually a low-order polynomial) to the baseline regions of the spectrum and subtracting the fitted curve from the original spectrum.

1.3.4.6 Axis Calibration

Axis calibration in NMR data preprocessing refers to the adjustment or alignment of the spectral axes to ensure accurate representation of chemical shifts or frequencies. This process typically involves referencing spectral peaks to known chemical standards or internal reference compounds with well-defined resonances. For example, plasma spectral peaks can be referenced to the lactate -CH_3 doublet resonance at $\delta = 1.33$ ppm. This ensures consistency and accuracy in the chemical shift measurements across different spectra.

1.3.4.7 Bucketing

Bucketing, or binning, refers to the process of dividing the spectral region into discrete intervals or "buckets" and integrating the area under the curve within each bucket. Bucketing can be performed in an automated manner or in a manual manner. Automated bucketing divides the spectra into fixed-width buckets. While this method automates the bucketing process, it risks splitting one peak into more than one bucket or more than one peak in one bucket. In contrast, manual bucketing allows tailoring the bucket boundaries to match the specific peaks and separate overlapping peaks that might be merged together using automated bucketing methods. This approach helps to enhance the signal-to-noise ratio for some regions, potentially improving the quality of subsequent analysis.

1.3.5 Data Analysis

1.3.5.1 Data Normalisation

The primary objective of data normalisation in metabolomics is to minimise undesired technical and biological variance across samples (J. Sun & Xia, 2024; Zacharias et al.,

2018). These can arise from unspecific fluctuations in overall sample concentrations, differences in the number of scans or spectrometer performance. To address these variations, constant sum normalisation (CSN) and probabilistic quotient normalisation (PQN) are two commonly used normalisation methods.

CSN, also referred to as integral normalisation, normalises each spectral integral (area under the curve in each spectral bucket) by the total sum of all spectral integrals within a sample. The underlying assumption of CSN is that the total spectral integrals or total metabolite concentrations remain constant across all samples in the dataset (J. Sun & Xia, 2024). However, CSN may not be optimal in situations where this assumption is strongly violated. For example, differences can be overlooked when there are substantial differences in overall metabolite levels between sample classes; quantification of other integrals may be biased in the presence of strong changes in large signals (Dieterle et al., 2006).

PQN operates under the assumption that the majority of signal intensities are influenced by dilution only, while some parts of the spectra reflect both biological factors and dilution (Dieterle et al., 2006). This method calculates a probable dilution factor between the sample spectrum and the reference spectrum, which is then applied to adjust the sample's overall concentration. The algorithm of PQN starts with a CSN step, followed by the use of the median spectrum calculated from control samples as the reference spectrum. Quotients between the sample spectrum and the reference spectrum are then computed for all variables. The median quotient is identified as the most probable dilution factor for the sample. Subsequently, all variables in the sample are divided by this dilution factor. PQN is considered a more robust method compared to CSN, effectively minimising the impact of outliers (Dieterle et al., 2006).

1.3.5.2 Data Transformation

Data transformation might be necessary when data display characteristics such as skewness, heteroscedasticity, or nonlinearity (Zacharias et al., 2018). This need arises because numerous statistical tests and modelling techniques rely on the assumption of

normality or approximate normality in the data distribution. Log transformation is the most commonly used method to achieve these assumptions.

1.3.5.3 Data Scaling

NMR spectra often contain signals of varying intensities. Scaling each variable by a scaling factor standardises the magnitude and accommodates for differences in fold change across variables, addressing heteroscedasticity (J. Sun & Xia, 2024). In metabolomic analysis, many statistical methods, such as principal component analysis (PCA) or partial least squares-discriminant analysis (PLS-DA), require variables to be on a similar scale to avoid biases where those with the largest variance dominate the results. Two commonly used scaling methods in metabolomics are autoscaling and Pareto scaling (Table 1-3).

Table 1-3 Overview of autoscaling and pareto scaling.

Method	Definition	Advantages	Disadvantages
Autoscaling (unit variance scaling)	$y_i = \frac{x_i - \bar{x}}{\sigma}$	Equally weighting of all variables	Tends to inflate the importance of small metabolites, which may contain measurement errors.
Pareto scaling	$y_i = \frac{x_i - \bar{x}}{\sqrt{\sigma}}$	Closer to the original measurement	Sensitive to large fold changes.

Summarised from (J. Sun & Xia, 2024; van den Berg et al., 2006). y_i: data after centring. σ: the estimated standard deviation.

1.3.5.4 Unsupervised Multivariate Technique: Principal Component Analysis

The size and complexity of metabolomic data necessitates the use of multivariate analysis. Unlike univariate analysis, which deals with a single variable (mean and variance) at a time, multivariate analysis considers also the relationships among variables simultaneously (Saccenti et al., 2014). This approach helps to uncover patterns, correlations, and groupings within the data (Figure 1-13). Multivariate analysis can be categorised into unsupervised methods and supervised methods, depending on whether the response variables (sample classification information) are used in the

statistic model building.

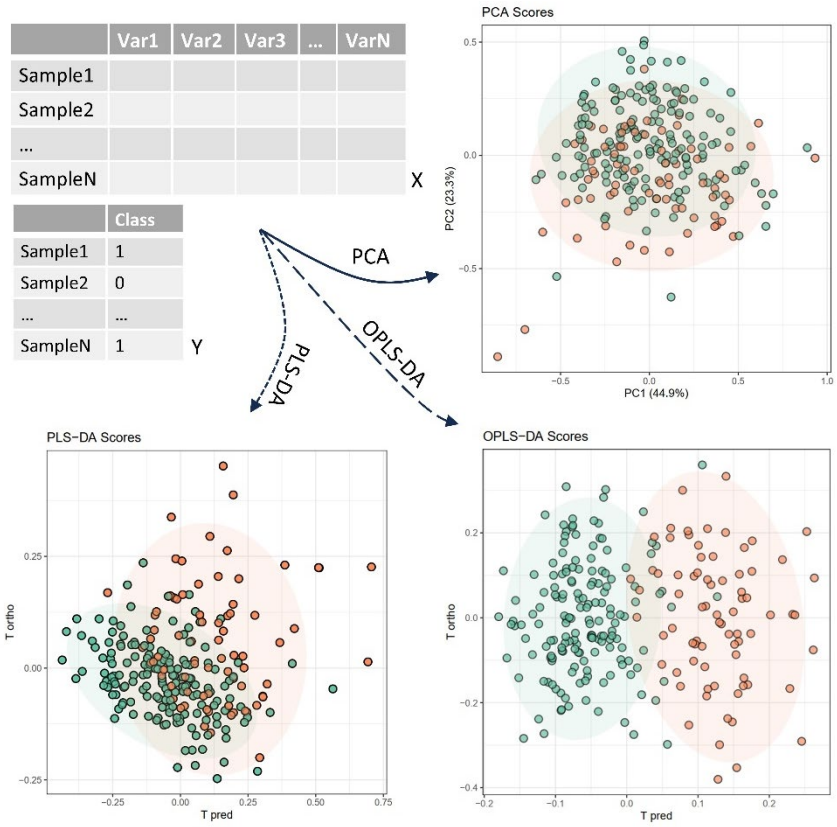

Figure 1-13 Representative scores plot for PCA, PLS-DA and OPLS-DA from the same dataset.

Unsupervised methods are typically used to explore and understand the inherent structure of the data, as they do not rely on sample classification information. PCA is probably the most widely used unsupervised method in metabolomics. It is a powerful technique used for dimensionality reduction and data visualisation. PCA works by transforming the original variables into a lower-dimensional space defined by orthogonal principal components, capturing the maximum variance in the data (Jolliffe, 2005).

The structure of a PCA model can be expressed as

$$X = TP^T + E \qquad \text{Equation 1-8}$$

where X is the metabolite variable matrix, T is the principal component scores matrix, P^T is the transpose of the loading matrix, and E is the residual matrix containing the

unexplained variance (Wold et al., 1987).

PCA can operate via eigenvalue decomposition (Figure 1-14). First, the dataset is pre-processed by centring or scaling to ensure that it is mean-centred. Next, PCA calculates the covariance matrix of the mean-centred data, which provides information about the relationships and variability between variables. Eigenvalue decomposition (or singular value decomposition) is then performed on the covariance matrix, yielding a set of eigenvalues and eigenvectors. The eigenvalues represent the amount of variance explained by each principal component, while eigenvectors define the directions or axes of maximum variance in the data. PCA extracts a set of orthogonal principal components from the sorted eigenvectors sorted in descending order of their corresponding eigenvalues. Finally, the original data is projected onto the principal components to obtain new coordinates or scores for each observation in the lower-dimensional space defined by principal components. The scores plot enables the identification of naturally occurring clusters and the detection of outliers within the data, while the corresponding loadings elucidate the significance of each variable in shaping the principal components.

In practice, the non-linear iterative partial least squares (NIPALS) algorithm is commonly used for calculating the PCA model due to its computational efficiency, particularly when dealing with large metabolomic datasets. Compared to the eigenvalue decomposition method, NIPALS is a more efficient approach, allowing for early termination when the user determines that a sufficient number of components have been computed (Dunn, 2023). Typically, in metabolomic analysis, computing the initial principal components is adequate for extracting meaningful information from the data.

Other unsupervised methods include K-means clustering, hierarchical clustering. These are also valuable for exploring and understanding the inherent structure of the data.

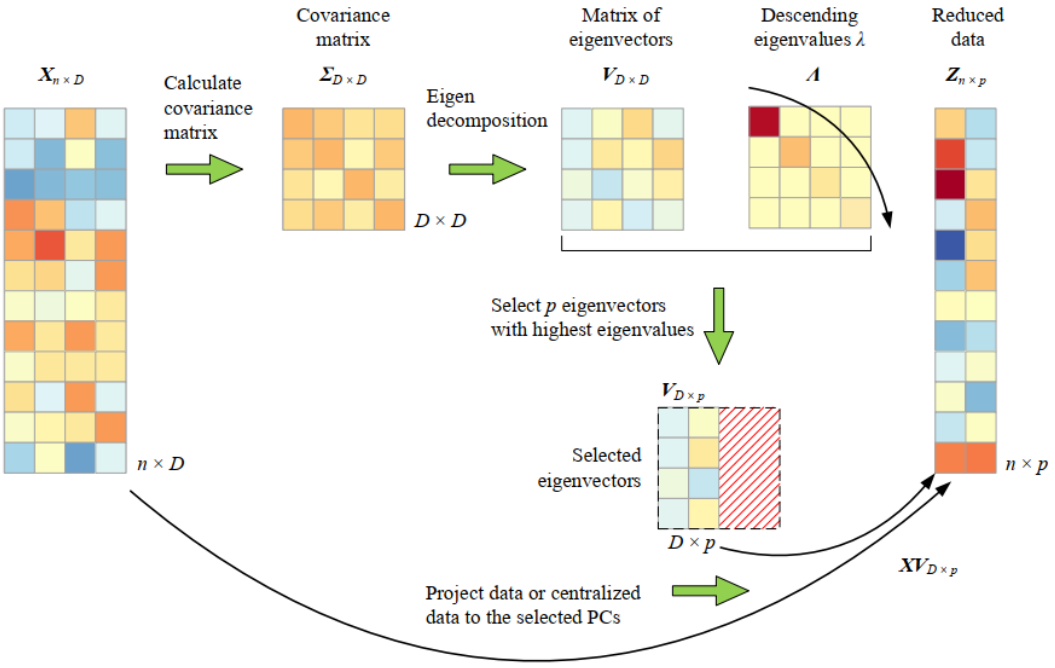

Figure 1-14 Principal component analysis via eigenvalue decomposition. Figure reproduced from (Jiang, 2024) with kind permission from the author.

1.3.5.5 Supervised Multivariate Technique: Orthogonal Partial Least Square Discriminant Analysis

While unsupervised methods reduce dimensionality to enable better visualisation of the data structure in its natural state, supervised methods investigate deeper into differences between groups by leveraging labelled data to guide the analysis and identify features associated with specific outcomes or classes (Ren et al., 2015). This makes supervised methods widely applied in classification, predication, and biomarker discovery. Depending on whether the response variables are continuous or categorical, supervised methods can be adapted for regression or discriminant analysis.

Partial least square discriminant analysis (PLS-DA), also known as projection to latent structures discriminant analysis, is a widely employed classification method in metabolomics (Wold et al., 2001). While PCA aims to retain as much variation by decomposing the X variable matrix into orthogonal latent components, PLS emphasises the relationship between Y response and X variable. PLS decomposes both the variable

X matrix and the response Y matrix in a way that the scores matrices T and U share maximum covariance while most effectively summarises X and Y (Worley & Powers, 2013)(Figure 1-13):

$$\begin{cases} \mathrm{X} = \mathrm{T}P^{\mathrm{T}} + \mathrm{E} \\ \mathrm{Y} = \mathrm{U}\mathrm{C}^{\mathrm{T}} + \mathrm{G} \end{cases} \qquad \text{Equation 1-9}$$

where T and U are scores matrices, P and C are loading matrices, E and G are residual matrices. A common approach to calculate the PLS model is through the NIPALS algorithm, which iteratively decomposes both the variable X and response Y matrices into a smaller set of latent variables, updating them until capturing the maximum covariance between X and Y (Dunn, 2023).

The importance of variables can be assessed through the loadings and variable importance in projection (VIP) scores (Debik, Sangermani, et al., 2022). Loadings represent the correlation coefficients between the original variables (X) and the components extracted by the PLS-DA model. VIP values quantify the importance of each variable in the PLS-DA model for class discrimination, with higher VIP values indicating greater contribution in classification. VIP values are commonly used for variable selection and feature ranking, allowing identification of the discriminatory variables for classification.

Orthogonal partial least square (OPLS), or orthogonal projections to latent structures, is a modification of PLS (Trygg & Wold, 2002). Compared to PLS, OPLS separates an orthogonal part from X where the variation is uncorrelated to Y (i.e., orthogonal to Y):

$$\mathrm{X} = \mathrm{T}_{\mathrm{o}}P_{\mathrm{o}}^{\mathrm{T}} + \mathrm{T}_{p}P_{p}^{\mathrm{T}} + \mathrm{E} \qquad \text{Equation 1-10}$$

where the subscript o denotes orthogonal, and the subscript p denotes predictive (Galindo-Prieto et al., 2015). OPLS reduces model complexity and improves model interpretability while preserving prediction ability (Trygg & Wold, 2002)(Figure 1-13). It is commonly used for binary classification tasks (e.g. control versus disease).

Other widely used methods in metabolomics include random forest, and support vector

machine. While (O)PLS is favoured for its capability in handling data with high collinearity, random forest and support vector machine can capture non-linear relationships within the data (Debik, Sangermani, et al., 2022). However, Mendez et al found that non-linear machine learning methods do not, in general, improve the predictability compared to linear methods in binary classification (Mendez, Reinke, et al., 2019). They also highlighted that the size of the dataset and the choice of performance metrics have a greater impact on overall predictive performance than the specific choice of machine learning algorithm (Mendez, Reinke, et al., 2019). Similarly, Vu et al evaluated the performance of five common classification algorithms (PLS, OPLS, principal component-linear discriminant analysis, support vector machine, and random forest), and reported comparable performance across these methods when applied to robust datasets (Vu et al., 2019). Notably, when the data contained subtle differences between classes, OPLS outperformed other methods, demonstrating its ability to identify key discriminant features with high classification accuracy (Vu et al., 2019). Conversely, Trainor et al reported better performance of support vector machine and random forest in both stimulated and real metabolomics datasets (Trainor et al., 2017).

1.3.5.6 Model Assessment: Diagnostic Statistics, Cross Validation and Permutation Testing.

Supervised methods are prone to overfitting, where the model captures noise in the training data, resulting in excellent performance on the training data but poor generalisability to new, unseen data. Therefore, robust validation needs to be employed to assess the validity of the model, such as cross validation and permutation testing.

Cross validation assesses how well a model will generalise to new, unseen data. It involves partitioning the available dataset into multiple subsets, where the model is trained on a subset of the data and evaluated on the remaining data. In one of the commonly used techniques, k-fold cross-validation, the dataset is first divided into k equal-sized folds. The model is then trained k times, with each iteration using k-1 folds for training and the remaining fold for validation. Performance metrics such as accuracy

or error rate are computed for each fold, and the average performance across all folds provides a robust estimate of model performance.

For (O)PLS models or those involving parameter tuning, a double cross-validation approach is recommended (Debik, Sangermani, et al., 2022; Westerhuis et al., 2008) (Figure 1-15). This approach consists of an inner loop to optimise the number of latent variables (or orthogonal components) for PLS (or OPLS), and an outer loop to validate the final model's performance and assess its generalisability.

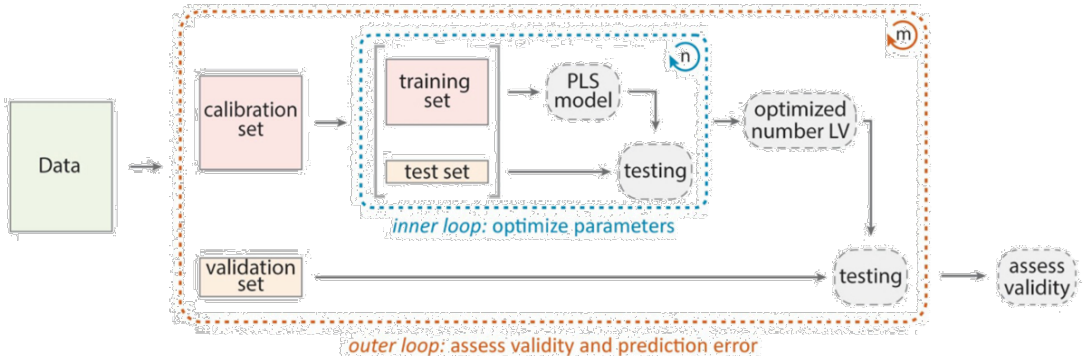

Figure 1-15 Double cross validation for the (O)PLS model. Figure reused from (Debik, Sangermani, et al., 2022) with permission, published under CC-BY-NC.

Several diagnostic metrics are used to assess the validity of (O)PLS models (Table 1-4). R^2 and Q^2 are commonly used during model optimisation, while more robust evaluation statistics for final model assessment include AUC, sensitivity, specificity, and accuracy calculated from external validation. However, it is important to note that a high Q^2 value alone may not suffice to deem a model predictive (Golbraikh & Tropsha, 2002; Triba et al., 2014).

Table 1-4 Diagnostic metrics for (O)PLS models.

Metric	Definition	Formula
R_X^2	Proportion of variation in the predictor variables (X-variables) explained by the model.	$R_X^2 = 1 - \frac{RSS}{TSS} = 1 - \frac{\sum_i (x_i - \hat{x}_i)^2}{\sum_i (x_i - \bar{x}_i)^2}$
R_Y^2	Proportion of variation in the response variable (Y-variable) explained by the model.	$R_Y^2 = 1 - \frac{RSS}{TSS} = 1 - \frac{\sum_i (y_i - \hat{y}_i)^2}{\sum_i (y_i - \bar{y}_i)^2}$

Metric	Definition	Formula
Q^2	Proportion of variation in the response variable that can be predicted by the model (calculated from the held-out data).	$Q^2 = 1 - \frac{PRESS}{TSS}$ $= 1 - \frac{\sum_i (y_i - \hat{y}_i)^2}{\sum_i (y_i - \bar{y}_i)^2}$
Sensitivity	The ability of a test to detect a true positive.	$\frac{TP}{TP + FN}$
Specificity	The ability of a test to detect a true negative.	$\frac{TN}{TN + FP}$
Accuracy	The ability of a test to differentiate the patient and healthy cases correctly.	$\frac{TP + TN}{P + N}$
Area under the curve (AUC)	Measure of the discriminative power of the model in binary classification tasks.	/

RSS, residual sum of squares (calculated from the training set). PRESS, Predicted Residual Sum of Squares (calculated from the test set). TSS, total sum of squares. TP, true positives. TN, true negatives. FP, false positives. FN, false negatives. P, positives. N, negatives.

Permutation testing is often performed complementary to cross validation to assess the significance of model performance under null conditions (random classification) (Westerhuis et al., 2008). The process involves permuting the class labels in the dataset, building models, recalculating the relevant metrics, and repeating this process typically thousands of times to create a null distribution. The observed metrics are then compared with the distribution of metrics obtained from the permuted data. If the observed value significantly differs from the values obtained by chance, it suggests a statistically significant relationship between the metabolite features and the outcome.

Moreover, it is advisable for these models to undergo further validation using independent datasets acquired from other cohorts or different labs to assess their robustness and generalisability (Debik, Sangermani, et al., 2022; Taylor et al., 2008).

1.3.5.7 Univariate Analysis

Univariate analysis techniques, such as t test and analysis of variance (ANOVA), are complementary parts of metabolomic analysis alongside multivariate analysis. They are

used to assess the statistical differences in metabolite abundance across groups, often following multivariate model building to further investigate key contributors identified in the model. Additionally, univariate analysis can serve as a preliminary screening step for identifying variables possibly relevant to classification, using methods like fold change analysis, t-tests, and volcano plots for feature selection before building multivariate models, thus reducing computational burdens (Y. Chen et al., 2022).

Given the typically large number of variables in metabolomic datasets, addressing Type I errors (false positives) is necessary during extensive hypothesis tests. Common methods for multiple comparison correction include the Benjamini and Hochberg method (also known as the false discovery rate or FDR method) (Benjamini & Hochberg, 1995) and the Bonferroni method (Abdi, 2007). While the FDR method controls FDR by controlling the expected proportion of false discoveries among rejected hypotheses, the Bonferroni method adjusts the significance threshold (alpha level) by dividing it by the number of comparisons to control the family-wise error rate (FWER) but often considered overly conservative and less powerful. Therefore, the FDR method is preferred in many scenarios due to its greater power in detecting true positives while controlling the rate of false discoveries. Nonetheless, despite correction for multiple comparisons being necessary in metabolomics studies to reduce the risk of false positives, it is noteworthy that it also increases the risk of false negatives (Saccenti et al., 2014).

1.4 Unmet Need for Biomarkers in Neurological Diseases

1.4.1 Autoimmune Encephalitis

Our lab has successfully used metabolomics to generate diagnostic and prognostic tests for several autoimmune diseases of the CNS, including NMOSD, MS and MOG antibody disease (Dickens et al., 2014; Jurynczyk et al., 2017; Probert et al., 2021; Yeo et al., 2019, 2021), as described in Section 1.2.3. Based on this work, this thesis investigates the potential of blood NMR metabolomics tests as a diagnostic tool for other autoimmune CNS diseases, including autoimmune encephalitis.

1.4.1.1 General

Encephalitis, defined as brain inflammation associated with neurological dysfunction (Tunkel et al., 2008), presents diverse clinical manifestations due to its various aetiologies. These symptoms include fever, changes in behaviour, personality, cognition and consciousness, as well as local neurological deficits, seizures, movement disorders, and autonomic instability (Alam et al., 2023).

The estimated incidence of encephalitis in England is around 5-9 cases/100,000/year (Granerod et al., 2013), and a US study reports an inpatient mortality rate around 6% in a US study (Vora et al., 2014, pp. 1998–2010). Notably, the aetiology remains unspecified in 40-50% of cases. Encephalitis can arise from either infectious or autoimmune causes. Historically, infections were the primary known causes until the discovery of neuroglial surface autoantibodies (Uy et al., 2021). With increasing awareness and improved diagnostic capabilities, the detection of autoimmune encephalitis (AE) has risen, and its prevalence is now comparable to that of infectious encephalitis (Dubey et al., 2018; Gable et al., 2012).

AE is defined as encephalitis associated with autoantibodies targeting self-antigens expressed in the central nervous system (Uy et al., 2021). These autoantibodies fall into two categories: neuronal surface antibodies (NSAb) and intracellular antibodies. NSAb target extracellular epitopes of surface proteins, ion channels and receptors such as N-methyl-D-aspartate receptor (NMDAR), contactin-associated protein-like 2 (CASPR2), leucine-rich glioma-inactivated 1 (LGI1), α-amino-3-hydroxy-5-methyl-4-isoxazolepropionic acid receptor (AMPAR), and gamma-aminobutyric acid type B receptor (GABAbR), etc. In contrast, Intracellular antibodies are autoantibodies targeting intracellular antigens such as Hu (ANNA-1), glutamic acid decarboxylase (GAD), and Ma2, and are less prevalent in AE compared to NSAb (Lancaster, 2016). This classification holds clinical significance as it implies a difference in pathogenesis, treatment response, association with tumours, and prognoses (Bien et al., 2012; Kelley et al., 2017).

1.4.1.2 AE Associated with Intracellular Autoantibodies.

Most subtypes of AE associated with intracellular autoantibodies are associated with tumours, often termed paraneoplastic. For example, the study by Gultekin et al shows that 94% of anti-Hu AE patients have small-cell lung cancer and all anti-Ma2 AE patients have testicular tumours (Gultekin et al., 2000). Paraneoplastic AE arises when a robust immune response develops against the intracellular neuronal antigens ectopically expressed by tumour cells. Dendritic cells capture tumour-derived antigens, presenting them to activate $CD4^+$ and $CD8^+$ T cells. This activation allows the production of autoantibodies and T cells to target and partially control tumour growth. Furthermore, activated T cells gain the ability to cross the blood-brain barrier (Goverman, 2009).

Neurons, particularly under inflammatory conditions, express major histocompatibility complex (MHC) class I molecules and can present intracellular peptides, making them susceptible to $CD8^+$ (cytotoxic) T cell attack and causing neuronal damage and related AE manifestations (Pignolet et al., 2013). Cytotoxic T cell mechanisms are believed to underlie the pathogenesis of this type of AE (Bien et al., 2012). The presence of intracellular autoantibodies is incidental to the autoimmune response and are not considered pathogenic since they cannot access intracellular antigens. However, they can serve as reliable biomarkers for the paraneoplastic neurological syndromes and cancer (Graus & Dalmau, 2019). This explains why this type of AE often carries a poor prognosis, as it is linked to irreversible neuronal damage, concurrent cancers, and the difficulty of managing such immune responses (Lancaster, 2016).

1.4.1.3 AE Associated with NSAb

Many of most common subtypes of AE involves NSAb. These antibodies often target key synaptic proteins, ion channels or receptors. NSAb are considered pathogenic because they can bind directly to exposed, extracellular targeted antigens. This binding can lead to decreased receptor density due to receptor internalisation, inhibition of receptor signalling by blocking ligand binding sites, disruption of protein-protein binding, and

neuronal injury from complement activation and inflammation (Gill & Venkatesan, 2022). The neuronal dysfunction in AE associated with NSAb is less severe and often reversible, compared to the neuronal damage caused by the cytotoxic T cell mechanism in AE associated with intracellular antibodies. This type of AE responds well to immunotherapies, and are less commonly associated with cancer (H. Abboud et al., 2021b).

Neuronal surface autoantibodies can arise in tumour-associated (paraneoplastic) or infectious contexts, particularly after viral encephalitis. (Gill & Venkatesan, 2022). The tumour-associated scenario has been described in the previous section. Viral infection can induce the generation of neuronal self-antigens through direct neuronal injury and subsequent release of the antigen or molecular mimicry where similarities between viral and self-antigens results in cross-activation of autoreactive T or B cells (Oldstone, 2014). Specifically, antigens are trafficked to regional lymph nodes via antigen presenting cells, where the processed antigen and $CD4^+$ T cells stimulate B cells to differentiate into antibody-producing plasma cells and memory B cells. Peripherally produced autoantibodies can, in some instances, cross the BBB, particularly during BBB dysfunction caused by factors such as stress, trauma, infection and inflammation (Diamond et al., 2013). Though it is not known whether antibodies are produced in the CNS as well, memory B cells may infiltrate the CNS (Jain & Yong, 2022), where they can undergo restimulation with neuronal antigens and subsequent differentiation into CNS-resident plasma cells. This could result in local CNS production of high-affinity autoantibodies targeting self-neuronal antigens. Once within the CNS, these autoantibodies can bind their antigen targets on the surface neurons, resulting in neuronal dysfunction (Dalmau, 2016; Gill & Venkatesan, 2022). Additionally, emerging data suggests the involvement of defective B cell tolerance in autoantibody production in NSAb-mediated diseases (Prüss, 2021; B. Sun et al., 2020).

1.4.1.3.1 NMDAR

Anti-NMDAR encephalitis is the most common type of AE, surpassing even the

prevalence of viral encephalitis among young individuals (Gable et al., 2012). It was first reported by in 2007, sparking extensive studies in this field (Dalmau et al., 2007). Anti-NMDAR encephalitis predominantly affects young women, with a median age of 22 years, and 80% of cases occur in women (Titulaer et al., 2013). Around 50% of young female patients have an underlying ovarian teratoma, while this association with tumours is much less frequent (6%) in men and children (Titulaer et al., 2013). Tumours and herpes simplex encephalitis are two identified triggers for anti-NMDAR encephalitis, although in half of the cases no specific triggers are identified (Dalmau et al., 2017).

The NMDAR is a multi-subunit glutamate (and glycine) receptor, primarily functioning as a calcium channel crucial for regulating fast excitatory glutamatergic neurotransmission. IgG antibodies against NMDAR's GluN1 subunit lead to the crosslinking of NMDARs and disruption of their interaction with the EphB2 receptor, resulting in receptor internalisation and subsequent lysosomal degradation (Ladépêche et al., 2018).

Anti-NMDAR encephalitis has a characterised progression of symptoms, beginning with viral-like prodrome such as fever, headaches. This is followed by psychiatric symptoms such as psychosis, agitation, hallucinations, and mania (Al-Diwani et al., 2019). As the condition advances, temporal lobe dysfunction emerges, leading to symptoms like amnesia and seizures. Eventually, the disease progresses to severe neurological impairments, including autonomic dysfunction, abnormal muscle movements, and profound cognitive decline (Dalmau et al., 2011). Nonetheless, early diagnosis and treatment of anti-NMDAR encephalitis often lead to a favourable prognosis, restoring patients to their baseline functional status (Dalmau et al., 2011).

1.4.1.3.2 VGKC, LGI1 and CASPR2

The voltage-gated potassium channel (VGKC) is a transmembrane channel specific for potassium, crucial for restoring neuronal resting potential. Antibodies against VGKC were firstly described in patients with neuromyotonia, then Morvan's syndrome, and

limbic encephalitis, where patients tested positive for VGKC antibodies using radioimmunoassay (RIA) (Shillito et al., 1995; Barber et al., 2000; Buckley et al., 2001). However, subsequent studies have demonstrated that these antibodies targeted associated proteins in the complex, notably leucine-rich glioma-inactivated1 (LGI1) and contactin-associated protein-like 2 (Caspr2), rather than VGKCs themselves (Figure 1-16) (Irani, Alexander, et al., 2010a; M. Lai et al., 2010). This distinction led to the identification of three VGKC-positive subgroups: anti-LGI1 patients, anti-CASPR2 patients, and VGKC-positive patients lacking both antibodies (van Sonderen, Schreurs, Wirtz, et al., 2016).

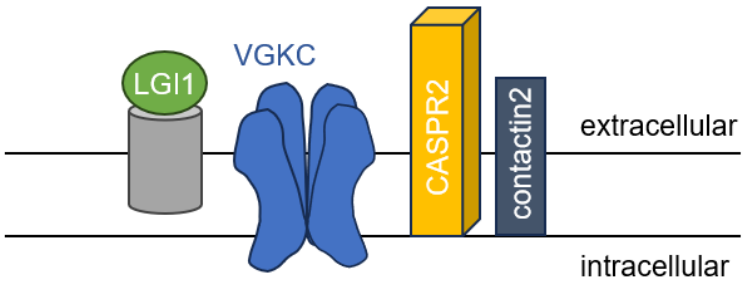

Figure 1-16 schematic of VGKC complex proteins.

LGI1 plays an important role in synaptic regulation through interacting with both presynaptic and postsynaptic proteins (Fels et al., 2021). Mutations in LGI1 have been found to cause autosomal-dominant partial epilepsy with auditory features in humans (Kalachikov et al., 2002). Anti-LGI1 encephalitis typically affects elder males, with a median age of onset around 60 years and around 67% of cases occurring in males (Irani, Alexander, et al., 2010a). Most patients present with limbic encephalitis, characterised by cognitive impairment, seizures, sleep disturbance, psychiatric and behavioural disorders. Around 60% of cases have faciobrachial dystonic seizures (FBDS), which are highly characteristic of anti-LGI1 encephalitis. Tumours are rarely associated with LGI1 encephalitis (Irani, Alexander, et al., 2010a).

CASPR2 facilitates the clustering and development of potassium channels, contributing to axon formation (L. Wu et al., 2023). Mutations in its encoded gene CNTNAP2 are

associated with schizophrenia and epilepsy (Friedman et al., 2008). Around 90% of patients are male, with a median age at onset around 65 years (van Sonderen, Ariño, et al., 2016). 42% patients developed limbic encephalitis, 29% patients had Morvan's syndrome, 13% patients had peripheral nerve hyperexcitability (van Sonderen, Ariño, et al., 2016). Common symptoms include cognitive decline, seizures, neuropathic pain. 19% cases have associated tumour such as thymomas (van Sonderen, Ariño, et al., 2016).

VGKC antibodies double negative to LGI1 and CASPR2 comprise around 85% of VGKC-positive results, and are considered to be non-pathogenic (Michael et al., 2020). It is shown that double-negative serum IgG did not bind to surface determinants on live hippocampal neurons or the extracellular domain of HEK293T cell surface-expressed VGKC (B. Lang et al., 2017). On the other hand, around 1/3 of these antibodies bound to intracellular aspects of the VGKC subunits, and some bind to the I^{125}-α-dendrotoxin (α-DTX) used in the VGKC radioimmunoassay (Michael et al., 2020).

The clinical significance of double-negative VGKC positivity is uncertain. Patients with double-negative VGKC antibodies have heterogeneous clinical syndromes and poor response to immunotherapy. Syndromes include epilepsy, pain, cognitive decline, peripheral neuropathy, etc (B. Lang et al., 2017; Olberg et al., 2013; van Sonderen, Schreurs, de Bruijn, et al., 2016). The immunotherapy response observed in 27% of double-negative patients is considered similar to the placebo response rates observed in other neurological diseases, and is much lower than those reported in LGI1 or CASPR2 AE (B. Lang et al., 2017). Furthermore, VGKC antibodies are relatively frequently detected in healthy controls and well-selected disease controls, with a prevalence of about 5%, whereas the average prevalence of most NSAb is much lower, at 0.23% (K. Lang & Prüss, 2017).

1.4.1.4 Diagnosis

The diagnosis of AE relies on clinical symptoms, MRI, electroencephalogram (EEG), CSF studies and autoantibody testing. Suspicions of AE are based on clinical syndromes, such as subacute onset of cognitive, epileptic, and/or psychiatric symptoms (Graus et al.,

2016). Suspected cases undergo further evaluation through neuroimaging, EEG, CSF analysis and autoantibody testing to confirm the diagnosis (Hébert et al., 2022).

MRI can reveal hyperintensities or abnormal signals in specific brain regions, aiding in the differentiation of AE from other conditions. For instance, the mesial temporal lobes are characteristic of limbic encephalitis, which is also a common AE presentation. 75% of cases of anti-LGI1 encephalitis show mesial temporal lobe abnormalities (Muñiz-Castrillo et al., 2021), whereas neuroimaging can be normal in about 80% of cases of anti-NMDAR encephalitis (Kelley et al., 2017). Moreover, distinctive MRI scans have been identified for AE with autoantibodies to GABAAR (Deng et al., 2022).

EEG provides real-time information about brain electrical activity. Over 90% of anti-NMDAR encephalitis show abnormal EEG results, with some patients having a unique electrographic pattern called "extreme delta brush" (Schmitt et al., 2012; Sonderen et al., 2018). Additionally, two EEG patterns unique to anti-LGI1 encephalitis can be diagnostic (Steriade et al., 2016; Wennberg et al., 2018).

CSF analysis can reveal elevated levels of inflammatory markers such as CSF leukocyte count, protein concentration, and the presence oligoclonal bands (indicative of intrathecal IgG synthesis). CSF findings vary among different AE subtypes. AE associated with NMDAR, GABAbR and AMPAR show more frequent inflammatory CSF changes, whereas these can be absent in AE subtypes such as anti-CASPR2, LGI1, GABAAR, and GlyR AE (Blinder & Lewerenz, 2019).

Autoantibody detection provides a definite diagnosis of AE by identifying the specific subtype of disease-associated autoantibodies. In clinical practice, two principles guide autoantibody testing for AE: prompt initiation of treatment before receiving test results, and comprehensive testing for all autoantibodies in both serum and CSF (Hébert et al., 2022). For undifferentiated AE presentations, using multiple assays to test both serum and CSF is recommended, as discrepancies between serum and CSF autoantibody positivity have been observed in some subtypes. For example, patients of anti-NMDAR encephalitis are more likely to have anti-NMDAR autoantibody detected in their CSF,

with 15% of cases showing negative serum results (Titulaer et al., 2013). In contrast, 22% of patients with anti-LGI1 encephalitis show serum positivity exclusively (Muñiz-Castrillo et al., 2021).

Immunohistochemistry and cell-based assay (CBA) are commonly used for antibody testing in AE. Immunohistochemistry involves staining rat brain section incubated with patient serum or CSF to detect binding of autoantibodies to their target antigens within the tissue. It can be used as an initial screening method due to its ability to detect all possible antigens available. Additionally, immunohistochemistry assesses different brain regions and provides specific staining patterns, which may be unique to a specific AE subtype. CBA can be used to further confirm the specific target of autoantibodies. CBA involves incubating patient serum or CSF on transfected cells expressing a recombinant antigen, and detecting the binding of autoantibodies using indirect immunofluorescence (van Coevorden-Hameete et al., 2016). Live CBA has been found to be more sensitive as the recombinant antigen mimic the *in vivo* status, while fixed CBA may alter the conformation of the antigen. Studies have shown that despite being commercially available and quick to perform, fixed CBAs tend to yield false negative results, especially for LGI1 and CASPR2 (McCracken et al., 2017; Ruiz-García et al., 2021). Commercial fixed CBA missed 12% of true positives, including around 30% LGI1 and CASPR2 positives (McCracken et al., 2017). Additional in-house CBA and brain immunohistochemistry should be performed when evaluating negative results from commercial CBA with a strong suspicion of AE. Immunohistochemistry and CBA should be performed in parallel to achieve the highest sensitivity and specificity (van Coevorden-Hameete et al., 2016).

1.4.1.5 Treatment

Treatment for AE is often initiated prior to receiving antibody test results due to the time required for testing and the benefits associated with early intervention. Early treatment has been linked to improved long-term functional and cognitive outcomes (Balu et al., 2019; Hébert et al., 2018). Primary treatments include immunotherapies

and, when applicable, the removal of the immunologic trigger such as tumour resection (Dalmau & Graus, 2018).

First-line immunotherapies typically involve the use of steroids, intravenous immunoglobulin (IVIg), and/or plasma exchange (PLEX) (H. Abboud et al., 2021a). If symptoms persist or worsen, second-line immunotherapies such as rituximab and cyclophosphamide may be administered. Cyclophosphamide functions by inhibiting the proliferation of immune cells, including T cells and B cells, while rituximab targets CD20 antigens on B cells, leading to B cell depletion. However, for AE associated with intracellular autoantibodies, response to immunotherapies is often suboptimal due to involvement of cytotoxic T cell responses and paraneoplastic mechanisms.

In AE cases linked to tumours, prompt tumour treatment is essential for achieving favourable short-term and long-term outcomes (Dai et al., 2019; Hébert et al., 2018; Titulaer et al., 2013). Furthermore, cancer screening can be performed in long-term management, guided by the antibody test results, to detect and monitor for the presence of associated tumours. This allows for early intervention and improved patient outcomes. (Hébert et al., 2022).

1.4.1.6 Unmet Need for Biomarkers in AE

Timely diagnosis and initiation of immunotherapies are crucial for optimal prognosis in AE (Nosadini et al., 2021; Thompson et al., 2018). The diagnosis of AE typically involves a combination of clinical features, laboratory antibody tests and imaging (Dalmau & Graus, 2018; Flanagan et al., 2023; Nosadini et al., 2021; Smith et al., 2021; Steriade et al., 2020a; Thompson et al., 2018; Van Steenhoven et al., 2023). While the detection of NSAb is a valuable tool, it can be expensive, laborious, and time-sensitive, potentially delaying treatment initiation. Moreover, false positive antibody test results can harm patient care (Flanagan et al., 2023), and many seronegative cases exist, meaning negative test results do not exclude AE (Lee & Lee, 2016). Therefore, further adjunctive diagnostics are valuable for AE patients, as they can also guide therapy and prognosis. Currently, no robust stratifying biomarkers exist for AE.

1.4.2 Autoimmune Psychosis

It has become clear that some individuals with psychosis may have an autoimmune signature (Pouget et al., 2019; Ripke et al., 2014), and, surprisingly, autoantibodies against the same neuronal cell surface targets have been found in some patients with psychosis, which are common to those found in AE (Lennox et al., 2017). Thus, in the context of psychosis, adjunct diagnostic tools to differentiate psychosis with an autoimmune bases are also needed to enable timely and targeted interventions for improved outcomes. For this reason, this thesis also examines the potential of blood NMR metabolomics to identify psychosis patients with NSAb.

1.4.2.1 Psychosis

Psychosis is a mental disorder characterised by a disconnection from reality, leading to symptoms such as hallucinations, delusions, and impaired thought processes (Arciniegas, 2015). Psychosis can manifest in primary psychotic disorders, such as schizophrenia spectrum disorders, and secondary psychotic disorders, which can result from neurological conditions like Alzheimer disease, traumatic brain injury, or anti-NMDAR encephalitis (Arciniegas, 2015).

1.4.2.2 Autoimmune Psychosis: Distinct, Mild Form of Autoimmune Encephalitis

Patients with AE typically develop clear neurological symptoms such as seizures, movement disorders, and cognitive dysfunction, in addition to psychiatric symptoms (Dalmau & Graus, 2018). However, there is growing recognition of cases with isolated psychotic presentations (with no or minimal neurological features), testing positive for neuronal antibodies and responsive to immunotherapy. This phenomenon is predominantly observed with anti-NMDAR encephalitis due to its strong association with psychiatric features (Al-Diwani et al., 2019). In fact, 77% (395/515) of patients with anti-NMDAR encephalitis initially present with psychiatric symptoms (Sarkis et al., 2019). Another study shows that 4% (23/571) of patients with anti-NMDAR encephalitis have isolated psychiatric symptoms on initial presentation or relapse (Kayser et al.,

2013). These psychiatric symptoms at the onset of anti-NMDAR encephalitis can resemble those seen in primary psychiatric disorders like schizophrenia, leading to potential misdiagnosis. A study in the Netherlands found that 80% (12/15) of patients with anti-NMDAR encephalitis presented with prominent psychiatric symptoms and 53% (8/15) were initially referred to a psychiatric service (Maat et al., 2013). In such cases, psychotropic medications are often ineffective, whereas early intervention or tumour removal has shown better outcomes.

The prevalence of NMDAR antibodies varies across studies, influenced by differences in IgG subclasses included, testing methods, and threshold for antibody positivity (Cullen et al., 2021). Nonetheless, when limited to studies using live cell-based assay (which are more sensitive than fixed cell-based assay), NMDAR seropositivity is found to be more common in psychosis patients compared to controls (OR of 4.43 [95% CI 1.7 to 11.36]) (Cullen et al., 2021). When considering NSAb in psychotic disorders, about 9% of first-episode psychosis patients have serum NSAb, compared to 4% in healthy controls (Lennox et al., 2017). Another study in Australia identified NSAb in 5% (6 out 113) of first-episode psychosis patients, all of whom responded to immunotherapy, highlighting the importance of early diagnosis and treatment for optimal recovery (Scott et al., 2018).

Cases with isolated psychotic presentations, NSAb positivity, and responsiveness to immunotherapy are considered possibly incomplete or forme fruste cases of AE with dominant psychotic features, sometimes referred to as mild encephalitis or autoimmune psychosis (Najjar et al., 2018). Leading international psychiatrists have reached a consensus advocating for the term “autoimmune psychosis” for this subtype, arguing that it is sufficiently distinct from typical AE (Pollak et al., 2020).

By establishing guidelines for identifying psychosis of autoimmune origin in psychiatric practice, the consensus aims to assist psychiatrists in better distinguishing between classic psychosis and autoimmune psychosis. Furthermore, it seeks to raise awareness among psychiatrist regarding autoimmune psychosis, emphasising the importance of conducting appropriate neurological workups, such as neuroimaging, EEG and CSF

analysis to avoid delays in diagnosis and appropriate treatment in psychiatric clinics (Najjar et al., 2018; Pollak et al., 2020). With increasing awareness of autoimmune psychosis, the consensus also aims to prevent overdiagnosis and inappropriate immunotherapy. According to the criteria, a positive serum autoantibody alone is insufficient for diagnosing probable autoimmune psychosis. Patients with acute psychosis and a positive serum autoantibody must also have at least one red flag symptom and additional paraclinical evidence, such as EEG or CSF indications of CNS inflammation, to meet this relatively conservative diagnostic criteria and minimise the risk of misdiagnosis (Pollak et al., 2020).

1.4.2.3 Positive and Negative Syndrome Scale

The Positive and Negative Syndrome Scale (PANSS) is a widely used clinical tool for measuring symptom severity in individuals with schizophrenia and other psychotic disorders (Kay et al., 1987). Developed by Kay, Fiszbein, and Opler in 1987, PANSS provides a detailed assessment of a broad range of symptoms through a structured interview process, resulting in a comprehensive profile of the patient's psychopathology. The scale consists of 30 items categorised into three subscales: positive symptoms, negative symptoms, and general psychopathology. Positive symptoms, such as delusions and hallucinations, represent an excess or distortion of normal functions. Negative symptoms, such as blunted affect and social withdrawal, indicate a reduction or loss of normal functions. The general psychopathology subscale encompasses a variety of symptoms including anxiety, depression, and cognitive impairment. Each item is rated on a scale from 1 (absent) to 7 (extreme), allowing clinicians to quantify the severity of symptoms and track changes over time. PANSS is considered a gold standard in psychosis research and clinical practice due to its reliability, validity, and sensitivity to treatment effects, making it an essential tool for both diagnosis and longitudinal assessment (Furukawa et al., 2015; Kay et al., 1988).

1.4.2.4 Unmet Need for biomarkers in Autoimmune Psychosis

Distinguishing autoimmune psychosis from primary psychotic disorders may help to

expedite immunotherapies in these patients. However, this task poses a significant challenge due to the symptomatic overlap between autoimmune psychosis and primary psychosis. Similar to diagnosing AE, diagnosing autoimmune psychosis requires a comprehensive assessment including clinical evaluation, serum and CSF antibody tests, EEG, MRI, and CSF analysis (Pollak et al., 2020). Unfortunately, access to these diagnostic tools may be limited in some psychiatric settings, leading to potential delays in diagnosis and treatment initiation.

Currently, there is no biochemical test capable of accurately identifying psychosis stemming from an underlying inflammatory cause or autoimmune cause. Developing such a test would be an important step towards identifying who might require different treatments and have improved outcomes. Addressing this unmet need for reliable biomarkers in autoimmune psychosis is imperative for optimising patient care and management strategies in psychiatric practice.

1.5 Unmet Need for Method Development in Metabolomics

To enable the translation of NMR metabolomics into clinical practice, a key challenge lies in preserving metabolite integrity in samples, which can be compromised by preanalytical factors such as variations in blood collection tubes, delays in erythrocyte separation, and delays in NMR measurement. These preanalytical variations can obscure true metabolic differences between groups, potentially undermining diagnostic accuracy. Therefore, it is crucial to systematically analyse and mitigate these variations to ensure reliable metabolomics results. This thesis addresses this challenge by investigating the impact of these preanalytical factors on NMR blood metabolomics and optimising protocols to minimise their effects.

1.5.1 Preanalytical Factors Affecting Serum Metabolite Integrity.

Metabolomic analysis provides a snapshot of the metabolites present in a sample at a given time, ideally reflecting the *in vivo* levels closely. However, metabolic profiles can be significantly altered from the point of sample collection to metabolite measurement.

For instance, a blood sample undergoes several stages, including blood collection, blood processing, serum or plasma storage, and sample preparation (Figure 1-17). During these processes, various factors can affect metabolic profiles. The type of blood collection tube used can introduce specific additives. Pre-processing delays, i.e. the time between blood collection and centrifugation, can alter metabolite profile due to ongoing cellular metabolism. Post-processing delays, occurring between centrifugation and sample storage or between sample preparation and metabolite measurement, can also result in changes due to enzymatic activity or chemical instability.

It is important to understand the impact of these factors on metabolic profiles and control them to minimise their effects, ensuring the measured metabolites accurately reflect the *in vivo* state. By minimising alterations due to preanalytical factors, more reliable metabolomic data can be obtained, leading to more accurate interpretations.

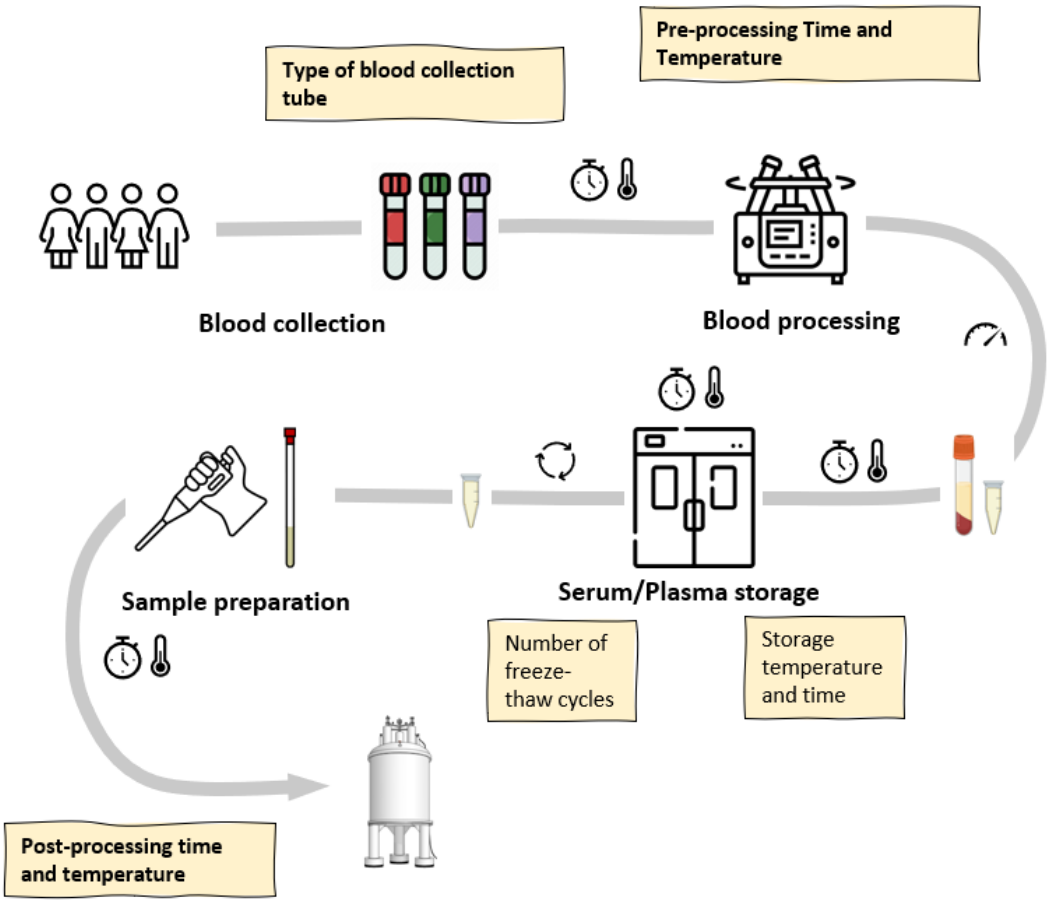

Figure 1-17 Pre-analytical factors in serum/plasma metabolomics.

1.5.1.1 Type of Blood Collection Tubes

Both plasma and serum are commonly collected in clinical research and used in metabolomics studies. Plasma is obtained by adding anticoagulants to prevent clotting, followed by centrifugation to separate it from the cellular components. On the other hand, serum is the clear fluid that remains after blood has been allowed to clot and then centrifuged to remove the clot and cellular components. They are collected from different types of blood tubes. Table 1-5 lists the most commonly used blood collection tubes.

The most frequently used anticoagulants in plasma tubes are heparin, citrate, ethylenediaminetetraacetic acid (EDTA), and fluoride oxalate, each with specific properties and applications. These anticoagulants prevent clotting through different mechanisms: heparin inhibits thrombin formation, while citrate, EDTA, and oxalate bind calcium ions to prevent coagulation. EDTA, which preserves cell morphology and inhibits platelet aggregation, is commonly used in haematology tests. Citrate tubes are primarily used for coagulation studies because the binding between citrate and calcium is reversible, allowing for the study of coagulation under controlled conditions. Sodium fluoride in fluoride oxalate tubes acts as an antiglycolytic agent, inhibiting enolase in the glycolytic pathway, preserving the stability of glucose and lactate for accurate measurement.

Several MS-based studies have found that many metabolites with higher concentrations in serum compared to plasma. (Nishiumi et al., 2018; Paglia et al., 2018; Yu et al., 2011). This could be explained by the volume displacement effect, where the coagulation causes a reduction in volume, leading to the concentration of metabolites (Ball & Sadusk, 1936; Kronenberg et al., 1998). Therefore, serum may provide higher sensitivity for biomarker discovery studies than plasma (Paglia et al., 2018). On the other hand, plasma offers quicker and simpler processing as it does not require exposure to room temperature for clotting, keeping platelets in a quiescent state and avoiding potentially variable clotting processes (Lehmann, 2015).

Generally, the different additives or the use of different blood tubes were found to have a minor effect on metabolites (Bervoets et al., 2015; Denery et al., 2011; Pinto et al., 2014a). Metabolite differences between serum and plasma samples were mainly related to small peptides reflecting the presence or absence of coagulation (Barri & Dragsted, 2013; Pinto et al., 2014a). Small metabolite differences across plasma tubes were noticed, primarily caused by ion suppression or enhancement caused by citrate and EDTA (Barri & Dragsted, 2013).

EDTA, citrate, and acid citrate dextrose (ACD) generates prominent peaks in ^{1}H NMR spectra. They can interfere with the detection of certain metabolites when their signals overlap with the metabolite signals. However, some metabolites may have other unobscured peaks allowing for quantification, so the use of these anticoagulants does not forbid the samples being used for metabolic profiling with NMR (Barton et al., 2009). The differences across these plasma samples are mainly due to the interfering peaks from the anticoagulant rather than endogenous metabolites being altered by the anticoagulants (Sotelo-Orozco et al., 2021a).

Currently, there is no definitive conclusion on the best type of blood collection tube for metabolomics. The choice of blood tube should be based on the aim and design of the study. An appropriate selection should be compatible with the analytical techniques used, avoid introducing contaminants that could interfere with metabolite detection, and best preserve the metabolites. Consistent use of the same type of blood tube from the same manufacturer throughout the study is important to minimise variability.

Table 1-5 Common types of blood collection tubes

Tube Cap Colour	Additive	Function of Additive	Use
Red	Spray-coated silica	Activates and accelerates clotting of the specimen	Serum determinations in chemistry, serology, and immunohematology
Gold	Spray-coated silica and a polymer gel	Silica activates and accelerates clotting; gel forms a barrier between clot and	Serum determinations in chemistry

Tube Cap Colour	Additive	Function of Additive	Use
		serum after centrifugation	
Light Green	Spray-coated lithium heparin and gel	Prevents clotting by inhibiting thrombin and thromboplastin	Plasma determinations in chemistry
Dark Green	Spray-coated lithium heparin	Prevents clotting by inhibiting thrombin and thromboplastin	Plasma determinations in chemistry
Purple	Spray-coated K_2EDTA	Prevents clotting by binding calcium	Whole blood haematology determinations and immunohematology testing
Gray	Fluoride oxalate	Fluoride inhibits glycolysis; oxalate prevents clotting by precipitating calcium	Glucose, lactate determinations
Blue	3.2% buffered sodium citrate solution	Prevents blood from clotting by binding calcium	Routine coagulation studies

Table summarised from the BD Vacutainer Tube Guide.

1.5.1.2 Pre-processing

After blood collection, blood samples need to be spun to obtain the serum or plasma. However, delays are common in clinical situations, and large-scale studies. During these delays, the cellular activity of blood cells can continue to alter the metabolome. When mature erythrocytes are removed from circulation, they experience disruptions in glycolytic flow, leading to accumulation of lactate, and upstream metabolic intermediates, including fructose-1,6-diphosphate, glyceraldehyde-3-phosphate, and dihydroxyacetone phosphate (Tilton et al., 1991).

Many studies have found that glycolysis-related metabolites were among the most labile and affected by prolonged pre-processing delays (Bervoets et al., 2015; Fliniaux et al., 2011a; Kamlage et al., 2014, 2018a; Santos Ferreira et al., 2019a; Teahan et al., 2006) For

example, a MS-based study found that prolonged delays in blood pre-processing at room temperature (6 hours versus 30 minutes) affect 24% of serum metabolites (54/225) with large alterations in taurine, glucose, and lactate (Kamlage et al., 2018a). Fewer metabolites were affected when using NMR analysis, with alterations observed in glucose, lactate, pyruvate, acetate, histidine and diacylglycerol (Santos Ferreira et al., 2019b). These metabolic alterations are slowed down at cold temperatures (Kamlage et al., 2014; Nishiumi et al., 2018; Teahan et al., 2006).

Glycolysis related metabolites are important biomarkers in some diseases, particularly in cancer, where low glucose and high lactate levels indicate enhanced glycolysis due to Warburg effect (Larkin et al., 2022a; Vander Heiden et al., 2009). Ideally, metabolite concentrations measured by metabolomic platforms should closely reflect their *in vivo* level. Therefore, it is important to minimise the alterations caused by delays in blood pre-processing. In multi-site, large-scale studies where immediate centrifugation may be challenging, it is essential to strictly control the time interval between blood collection and centrifugation to reduce variability derived from pre-processing. When plausible, storage of blood samples at cold temperatures (4 °C) should be implemented.

1.5.1.3 Post-processing

Studies have found that ongoing metabolic changes still occur after erythrocyte separation, likely due to enzymes secreted or released upon cell damage before centrifugation (D. Chen et al., 2023). However, the alterations caused by prolonged post-processing delays are less pronounced than those occurring during pre-processing delays (Santos Ferreira et al., 2019b). The number of metabolites affected by the post-processing and the extent of their alteration depend on the length of the delay and the temperature. (Anton et al., 2015a; Kamlage et al., 2014; Moriya et al., 2016; Santos Ferreira et al., 2019a).

Short post-processing delays of up to 2 hours at room temperature resulted in minimal changes to metabolite concentrations (Kamlage et al., 2014; Moriya et al., 2016). A 12-hour delay at room temperature leads to more profound alterations than a 1-week delay

at 4 °C (Moriya et al., 2016). A MS-based metabolomics study has found that 19% (24/127) metabolites show significant linear alterations over time due to post-processing delays, mostly involving amino acids and phosphatidylcholines (Anton et al., 2015a). The increase in amino acids is inferred to be derived from protein degradation processes, while the decrease in phosphatidylcholines can be attributed to hydrolysis by phospholipase A2, which can be present in serum either as secreted enzyme or released upon cell rupture before centrifugation (Anton et al., 2015a). An NMR study shows that a 24-hour post-processing delay at room temperature, with or without the addition of phosphate NMR buffer, affects histidine, phenylalanine, diacylglycerol, and low-density lipoprotein particle size (Santos Ferreira et al., 2019b). Similar to alterations due to pre-processing delays, these changes are found to be less pronounced when storing at cold temperature.

Ideally, serum or plasma should be collected immediately after centrifugation, aliquoted, and promptly stored at −80 °C. However, delays can happen due to logistical reasons, especially in large-scale studies. Additionally, post-processing delays can occur before the metabolite measurement, when serum or plasma samples are thawed, prepared, and queued for NMR analysis. Samples are usually prepared in batches, leading to waiting times for the data acquisition. The time between sample preparation and measurement should be limited to avoid significant alterations. When the delays are unavoidable, samples are recommended to be stored at 4 °C to minimise alterations, such as during queuing for data acquisition when an autosampler with a cooling system is advised.

1.5.1.4 Other Factors

Other preanalytical factors include haemolysis, freeze-thaw cycles, and storage time. Haemolysis has been found to significantly impact MS-based metabolic profiles (Kamlage et al., 2014; *P.* Yin et al., 2013), whereas it does not affect NMR metabolic profile, likely due to the limited sensitivity of NMR (Bervoets et al., 2015). Multiple freeze-thaw cycles can also alter metabolic profiles, with most variations observed after three cycles (Pinto et al., 2014a). Minor accumulated changes in 32 lipoprotein

parameters and acetate were observed from NMR analysis after five repeated freeze-thaw cycles (F. Wang et al., 2019). Additionally, the freeze-thaw effect was found to be sample dependent, with a larger impact for samples rich in lipids (Barton et al., 2009). Regarding storage time, NMR-derived metabolites were unaffected after 30-month storage at -80 °C (Pinto et al., 2014a), while MS-based profiles were altered after a 5-year storage at -80 °C (Haid et al., 2018).

1.5.1.5 Unmet Need in Large-scale Metabolomic Studies

In large-scale metabolomic studies, such as UK Biobank, both pre-processing delays and post-processing delays commonly occur due to practical logistical requirements. Typically, blood samples are collected into blood tubes in clinics throughout the day, maintained at specified temperatures, and transported together overnight (Elliott et al., 2008; Peakman & Elliott, 2008a). Upon arrival at the processing lab the following morning, the samples are processed and aliquoted. During processing, aliquots are held at 4°C before being transferred to long-term storage at -80°C (Elliott et al., 2008).

Pre-processing delays can significantly alter glycolysis-related metabolites, while prolonged post-processing can affect levels of amino acids and phosphatidylcholine. However, the impact of the type of blood collection tube on metabolite integrity, given delays in centrifugation and/or sample measurement, has not been thoroughly investigated. Sodium fluoride/potassium oxalate (NaF/KO) blood tubes are known for its ability to inhibit glycolysis thus preserve the stability of relevant metabolites (Dibbasey et al., 2024). Despite this, the use of NaF/KO blood tubes in metabolomics is scarce and the stability of metabolites derived from this type of tube remains unexplored (Sotelo-Orozco et al., 2021a).

Addressing these unmet needs is crucial for improving the accuracy and reliability of large-scale metabolomic studies. Understanding and mitigating the effects of pre- and post-processing delays, as well as evaluating the impact of different blood collection tubes, will enhance the robustness of metabolomic data and its application in clinical and epidemiological research.

1.5.2 Metabolite Extraction Methods for Brain Metabolomics

Metabolomics offers a versatile approach that is applicable to various biological sample types, including cells, tissues, biofluids. When applied to tissue specimens relevant to a particular disease, metabolomics allows for direct detection of metabolic processes associated with organ dysfunction or disease pathology (Saoi & Britz-McKibbin, 2021). This approach, for example, is particularly valuable for studying brain tissues or specific brain regions affected by neurological diseases, offering insights into the metabolic alterations underlying these conditions. However, the invasive collection procedures limit the applicability of tissue metabolomics, often restricting studies to animal models. Nevertheless, it can also be applied to human brain biopsies, which are routinely used in clinical practice to establish the type and grade of tumour, to exclude infectious diseases, and for autoimmune or inflammatory diseases where other methods have proved equivocal. While histological analysis alone may not always yield definitive conclusions, metabolomics offers complementary insights that enhance diagnostic precision. To support such applications, this thesis investigates brain extraction methods that optimise extraction efficiency and reproducibility while preserving metabolite stability.

1.5.2.1 Metabolic Profiling in Brain Tissue

The field of metabolomics, particularly in examining brain tissues, has evolved, allowing researchers to interrogate the biochemical shifts associated with varying physiological states and to understand better the downstream molecular mechanisms that contribute to the outcome of individual disease pathologies (Gonzalez-Riano et al., 2016).

NMR, particularly liquid-state NMR, accounts for about 20% of all brain metabolomics research, as indicated by PubMed data showing 427 references for “metabolomics AND brain AND nuclear magnetic resonance NOT MRI” and 403 references when high-resolution magic angle spinning (HRMAS) NMR—which involves semi-solid samples rather than liquid-state analysis—is also excluded. In comparison, the equivalent search for mass spectrometry (“metabolomics AND brain AND mass spectrometry NOT MSI”)

returned around 1760 references.

1.5.2.2 Brain Metabolite Extraction

Metabolic profiling via liquid-state NMR requires the extraction of biological tissue samples, the concentration of metabolites to levels compatible with NMR detection, and the simultaneous removal of macromolecules in a manner that preserves metabolite stability. The selection of the extraction method, including the choice of extraction solvent, depends on factors such as the type of biological sample studied, and the molecules of interest. Methanol/water and acetonitrile/water are commonly favoured for their efficient extraction of polar metabolites, precipitation of proteins, analytical compatibility and ease of handling (Álvarez-Sánchez et al., 2010). Additionally, methanol/water/chloroform is commonly used for simultaneous biphasic extraction of polar and non-polar metabolites, and for improved protein precipitation, despite being more time-consuming (Lin et al., 2007).

The choice of extraction solvent can significantly impact reproducibility, metabolite recovery, and protein removal. For instance, methanol has emerged as the preferred extractant for plasma samples due to its superior performance in these areas compared to acetonitrile (Cai & Li, 2016; Gowda & Raftery, 2014; Lepoittevin et al., 2023; Nagana Gowda et al., 2015; Want et al., 2006). Similarly, different extraction methods have been evaluated in liver tissues, where acetonitrile/water demonstrated the highest metabolite yield but also recovered some macromolecules and lipids, whereas methanol/water/chloroform provides excellent deproteinisation while maintaining high yield and reproducibility (Lin et al., 2007). In NMR analysis of brain extracts, acetonitrile/water also showed better yield compared to methanol/water and methanol/dichloromethane/water, while methanol/water showed lower reproducibility (Diémé et al., 2017).

1.5.2.3 Unmet Need in Brain Metabolite Extraction Methods

Due to the reduced sensitivity of NMR relative to MS along with the routine use of pulse

programs, such as the CPMG sequence, which filters out macromolecule signals, extraction methods which prioritise metabolite recovery over deproteinisation are often favoured in NMR metabolomics studies. However, residual proteins in samples may still alter metabolic profiles either through enzymatic activity or binding to free metabolites. Indeed, it has been shown that brain homogenates, containing residual protein, undergo significant metabolic changes with prolonged incubation, whereas minimal changes occur in the aqueous phase of brain extracts subjected to the methanol/chloroform/water method after incubation (Fomenko et al., 2022a). Furthermore, Paskevich et al. discovered that after NMR sample preparation, the alpha carbon hydrogen (αH) of aspartate was replaced by deuterium from the NMR buffer, whereas deproteinated samples extracted with a methanol/water/chloroform mixture could prevent this replacement (Paskevich et al., 2013).

This observation gives rise to the hypothesis that residual proteins in brain NMR samples can continue to alter the metabolome. While residual enzymatic activity is a well-documented issue in metabolomics, particularly for biofluids such as serum, plasma, and urine, where it has been extensively studied (Ghini et al., 2019, 2022; Kamlage et al., 2014, 2018b), these biofluids can often be analysed directly by NMR after being mixed with an appropriate buffer, without the need for an extraction step. In contrast, brain tissue samples require a more complex preparation process, including an extraction step, to obtain a liquid-state NMR spectrum. Prior to NMR analysis, mixing the lyophilised brain tissue extracts with the NMR buffer (e.g., deuterated phosphate buffer, pH 7.4) can potentially reactivate residual enzymes, leading to metabolite conversions. Despite the critical role of extraction in preparing brain tissues for NMR analysis, no research has systematically investigated the relationship between metabolite stability and residual protein levels across different extraction methods in rodent brain extracts. Therefore, it is important to bridge this gap in knowledge by evaluating whether such alterations exist with commonly used extraction methods, understanding their impact, and identifying ways to control them. By minimising the effects of

preanalytical variability, the metabolites measured can more accurately reflect the *in vivo* state, leading to improved interpretation.

1.6 Overview of the Thesis

The overarching aim of my DPhil thesis was to use NMR-based metabolomics for biomarker discovery to improve diagnostics for antibody-mediated pathology in neurological diseases.

Specifically, this thesis investigated the following hypotheses:

(1) That plasma NMR-based metabolomics, in combination with multivariate statistical techniques and machine learning, can distinguish patients with AE from those with drug-resistant epilepsy (DRE).
(2) That psychosis patients with defined neuronal cell surface antibodies (in common with AE) will have a different serum metabolomic profile compared to those without these autoantibodies.
(3) For translation purposes, that sodium fluoride/potassium oxalate blood tubes, which inhibit glycolysis, are more effective at preserving metabolite integrity than the widely used lithium heparin or serum blood tubes during preanalytical delays.
(4) For metabolomics in brain tissue biopsy, that extractant with superior protein precipitation capabilities better maintain metabolite stability during NMR analysis.

Chapter 2: Distinct Plasma Metabolomic Signatures Differentiate Autoimmune Encephalitis from Drug-Resistant Epilepsy.

The data in this chapter has been published as: Xiong, W., Yeo, T., May, J.T.M., Demmers, T., Ceronie, B., Ramesh, A., McGinty, R.N., Michael, S., Torzillo, E., Sen, A., Anthony, D.C., Irani, S.R. and Probert, F. (2024), Distinct plasma metabolomic signatures differentiate autoimmune encephalitis from drug-resistant epilepsy. *Ann Clin Transl Neurol*. https://doi.org/10.1002/acn3.52112

2.1 Introduction

Epilepsy is a heterogeneous neurological disorder affecting approximately 50 million people worldwide (World Health Organization, 2019), with 30% of cases being drug-resistant epilepsy (DRE) (Ngugi et al., 2010). AE often refractory to anti-seizure medications (ASMs) (Ramanathan et al., 2021; B. Sun et al., 2020), is another significant cause of seizures, sometimes misdiagnosed as non-autoimmune epilepsy, especially in patients with LGI1 antibodies (Flanagan et al., 2023; Smith et al., 2021; Steriade et al., 2020b; Thompson et al., 2018; Van Steenhoven et al., 2023).

Timely diagnosis and initiation of immunotherapies are crucial for optimal prognosis in AE (Nosadini et al., 2021; Thompson et al., 2018). Further adjunctive diagnostics, such as an NMR blood test that is fast, affordable, and minimally invasive, could prove valuable in guiding both therapy and prognosis. Currently, no robust stratifying biomarkers exist.

Previous studies from our group have highlighted the potential of NMR metabolomics in detecting systemic inflammation and autoantibody-mediated pathology in CNS diseases with overlapping symptoms (Dickens et al., 2014; Jurynczyk et al., 2017; Probert et al., 2021; Yeo et al., 2019, 2021). Building on these findings, this chapter

explores the hypothesis that NMR metabolomics, combined with robust multivariate analysis, can distinguish AE from DRE and, further, differentiate three of the commonest AE subtypes associated with autoantibodies against LGI1, NMDAR and CASPR2.

2.2 Methods

2.2.1 Human Subjects

AE and DRE patients were recruited from the John Radcliffe Hospital, Oxford, UK. The study was approved by the Research Ethics Committee (REC16/YH/0013) and all participants gave written informed consent. Matched clinical information was retrieved from the electronic patient record (Cerner Millenium). AE patients were diagnosed based on their clinical syndrome in association with serum and CSF antibody positivity at the peak of their disease determined by fixed and live cell-based assays for CASPR2 and NMDAR-antibodies, and serum positivity alone for LGI1-antibodies, as described previously (Irani, Alexander, et al., 2010b, *p.* 1; Irani, Bera, et al., 2010). Inclusion criteria for DRE patients were stipulated such that: (1) DRE patients with known positive antibody results were excluded from the analysis, and (2) Patient records of the DRE patients were reviewed to further exclude cases potentially associated with autoimmune etiologies.

2.2.2 Blood Samples

Blood was collected in BD™ Vacutainer™ Lithium Heparin tubes (BD 367886) and plasma was isolated by centrifugation at 500 x g for 10 minutes at room temperature prior to storage at -80 °C.

2.2.3 NMR Sample Preparation

On the day of NMR data acquisition, plasma samples were defrosted at room temperature before being centrifuged at 100000 x g for 30 mins at 4 °C. 150 µL of the plasma samples were then mixed with 400 µL NMR buffer (75 mM phosphate buffer in

D_2O, pH = 7.4) and transferred to a 5 mm borosilicate NMR tube (Norell).

2.2.4 NMR Experiments

NMR spectroscopy was performed using a 700-MHz Bruker AVIII spectrometer (Department of Chemistry, University of Oxford) operating at 16.4 T equipped with a ^{1}H [$^{13}C/^{15}N$] TCI cryoprobe at 298 K. Each plasma sample was subjected to both a 1D ^{1}H NOESY experiment and a CPMG-PROJECT experiment, with the CPMG-PROJECT spectra used for downstream analysis.

The 90-degree pulse length (P1) was determined by measuring a null spectrum with an approximate 360-degree pulse using the Bruker zg pulse sequence. P1 was optimised using one representative sample from the cohort and applied consistently to all plasma samples throughout the study.

The 1D ^{1}H NOESY experiment was conducted with relaxation delay of 2 s, an acquisition time of 1.5 s, 8 data collections and a fixed receiver gain. 1D ^{1}H CPMG-PROJECT spectra were collected with a τ interval of 400 μs, 80 loops, a total filter time of 40 ms, 32 data collections, an acquisition time of 1.5 s, relaxation delay of 2 s, and a fixed receiver gain.

For quality control, pooled samples were spread throughout the run to monitor technical variation. Additionally, 2D TOCSY spectra were acquired for representative samples to aid in the assignment of metabolites, collected with a time domain of 2048 complex points in the direct dimension (t_2) and 512 increments in the indirect dimension (t_1), using a relaxation delay (d_1) of 2 s, a mixing time (d_9) of 100 ms, and 24 scans per increment (ns = 24). The total acquisition time for each TOCSY spectrum was approximately 6 hours.

2.2.5 NMR Data Pre-processing

Resulting free induction decays were zero-filled by a factor of 2 and multiplied by an exponential function corresponding to 0.30 Hz line broadening prior to Fourier transformation. All spectra were phased, baseline corrected and referenced to the lactate

-CH_3 doublet resonance at $\delta = 1.33$ ppm, followed by visual inspection for errors and contaminations (Topspin 4.1, Bruker, Germany). Plasma NMR spectra were rationally divided into 122 spectral bins in a manual manner to avoid overlapping signals, excluding noise and water signals (ACD/Labs Spectrus Processor Academic Edition 12.01, Advanced Chemistry Development, Inc.). Each spectral integral was normalised by the total sum of all spectral integrals within a sample (constant sum normalisation), accounting for any variations in sample dilution.

2.2.6 Metabolite Assignments

Metabolite assignments for NMR signals was performed by referencing to literature values (Nicholson et al., 1995; Oostendorp et al., 2006; Soininen et al., 2009; Tynkkynen et al., 2012), the Human Metabolome Database (Wishart et al., 2007), and via 2D total correlation spectroscopy (TOCSY) experiments. Approximately 50 metabolites, including a range of lipoprotein and lipid species, amino acids, glucose, organic acids, nucleotides, and amides were identified.

2.2.7 Statistical Analysis

2.2.7.1 Multivariate Analysis

Multivariate analyses were performed in R software 4.1.2 (R Foundation for Statistical Computing, Vienna, Austria) using in-house R scripts and the 'ropls' package (Thévenot et al., 2015a). Multivariate analysis of NMR metabolomics data included PCA and OPLS-DA. Sum-normalised integral values were pareto scaled for the multivariate analysis. PCA was used to reduce data dimensionality and identify any spontaneous clusters and important variables accounting for the clustering. OPLS-DA was used to generate diagnostic models and identify significant differences in metabolite levels between groups. The number of orthogonal components in OPLS-DA was optimised through repetitions of the default 7-fold internal cross-validation, with the final number determined by the median value obtained from the repetitions. For the full dataset, the optimal number of orthogonal components was determined by 50 repetitions, while for

the training set in the cross-validation loop, 10 repetitions were used (**Figure 2-1**). These repetitions were introduced because the number of orthogonal components determined by the built-in function in the ropls package was variable for this dataset and tended to underfit the dataset.

The OPLS-DA models underwent rigorous validation using a 10-fold external cross-validation with 100 repetitions and permutation testing (Figure 2-1). To correct for unequal class sizes, samples from the larger class were randomly selected to match the number of samples in the smaller class. The equalised dataset was then randomly shuffled and split into a training set (90% of data) and a test set (10% of data). The OPLS-DA model was trained exclusively on the training set with model optimisation and evaluated on the test set to measure accuracy, sensitivity, and specificity. The process of splitting the dataset was repeated 10 times, ensuring each sample appeared in a test set exactly once. The entire process, from randomly selecting samples to 10-fold external cross-validation, were repeated 100 times, producing a total of 1000 models.

The cross-validation described above assessed how well the model performed on independent data, while permutation testing was used in parallel to assess whether the model performed significantly better than random chance. The null distribution was generated by randomly permuting class assignments and building OPLS-DA models with the same 10-fold cross-validation with repetition scheme. The accuracy of the true models was compared to the null distribution using the Kolmogorov-Smirnov test. Models were considered significant only if their accuracies were significantly better than random chance (~50%). Discriminatory variables were identified by calculating the average of the variable importance in projection (VIP) scores of the ensemble of models, which indicated the contribution of a variable to the model. An inflection point was picked manually in the curve of VIP scores and was used as a cut-off for picking discriminatory metabolites in multivariate.

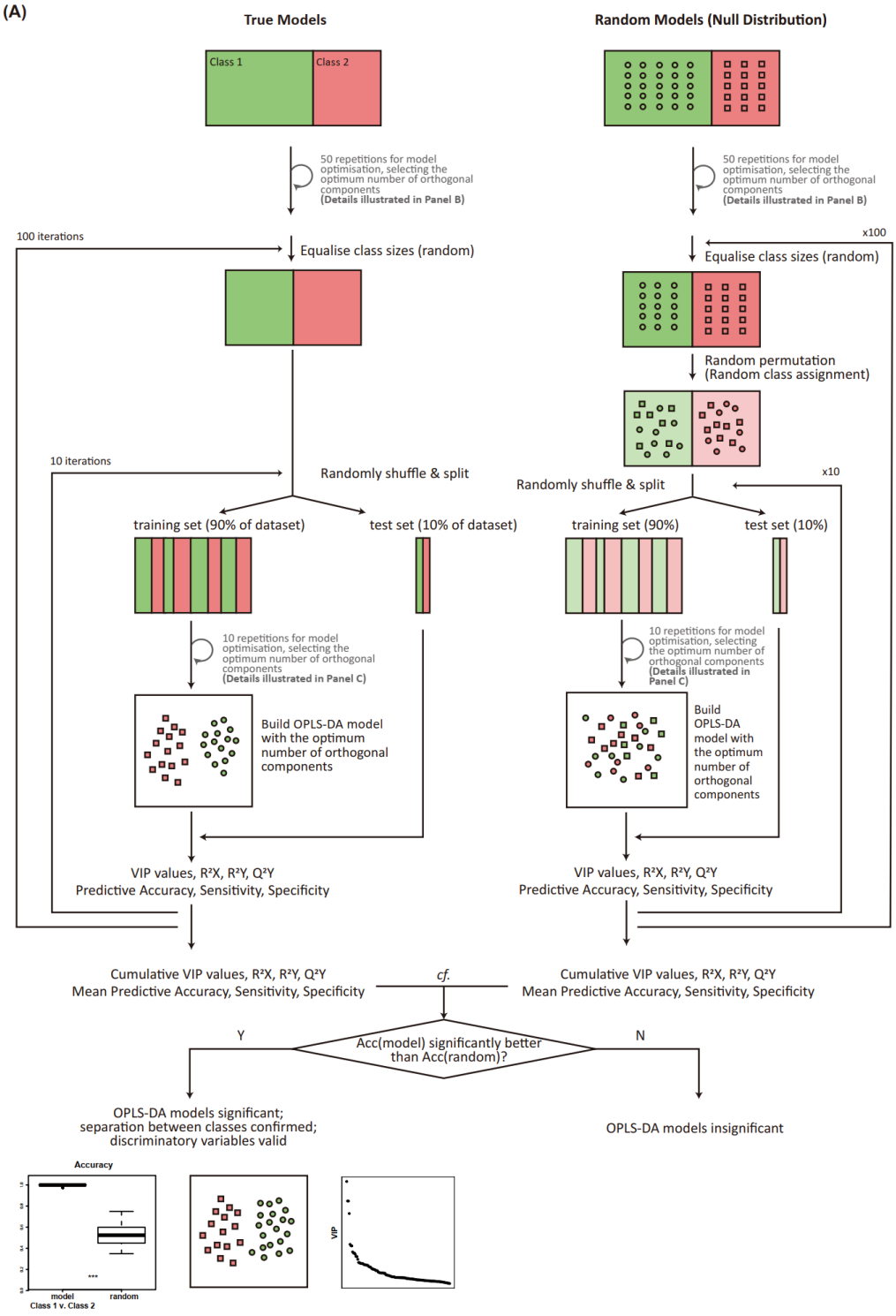
(A)
True Models
Random Models (Null Distribution)
Class 1
Class 2
50 repetitions for model optimisation, selecting the optimum number of orthogonal components
(Details illustrated in Panel B)
100 iterations
Equalise class sizes (random)
x100
Random permutation
(Random class assignment)
10 iterations
Randomly shuffle & split
x10
training set (90% of dataset)
test set (10% of dataset)
training set (90%)
test set (10%)
10 repetitions for model optimisation, selecting the optimum number of orthogonal components
(Details illustrated in Panel C)
Build OPLS-DA model with the optimum number of orthogonal components
VIP values, R²X, R²Y, Q²Y
Predictive Accuracy, Sensitivity, Specificity
Cumulative VIP values, R²X, R²Y, Q²Y
Mean Predictive Accuracy, Sensitivity, Specificity
cf.
Y
N
Acc(model) significantly better than Acc(random)?
OPLS-DA models significant; separation between classes confirmed; discriminatory variables valid
OPLS-DA models insignificant
Accuracy
model
random
Class 1 v. Class 2
VIP

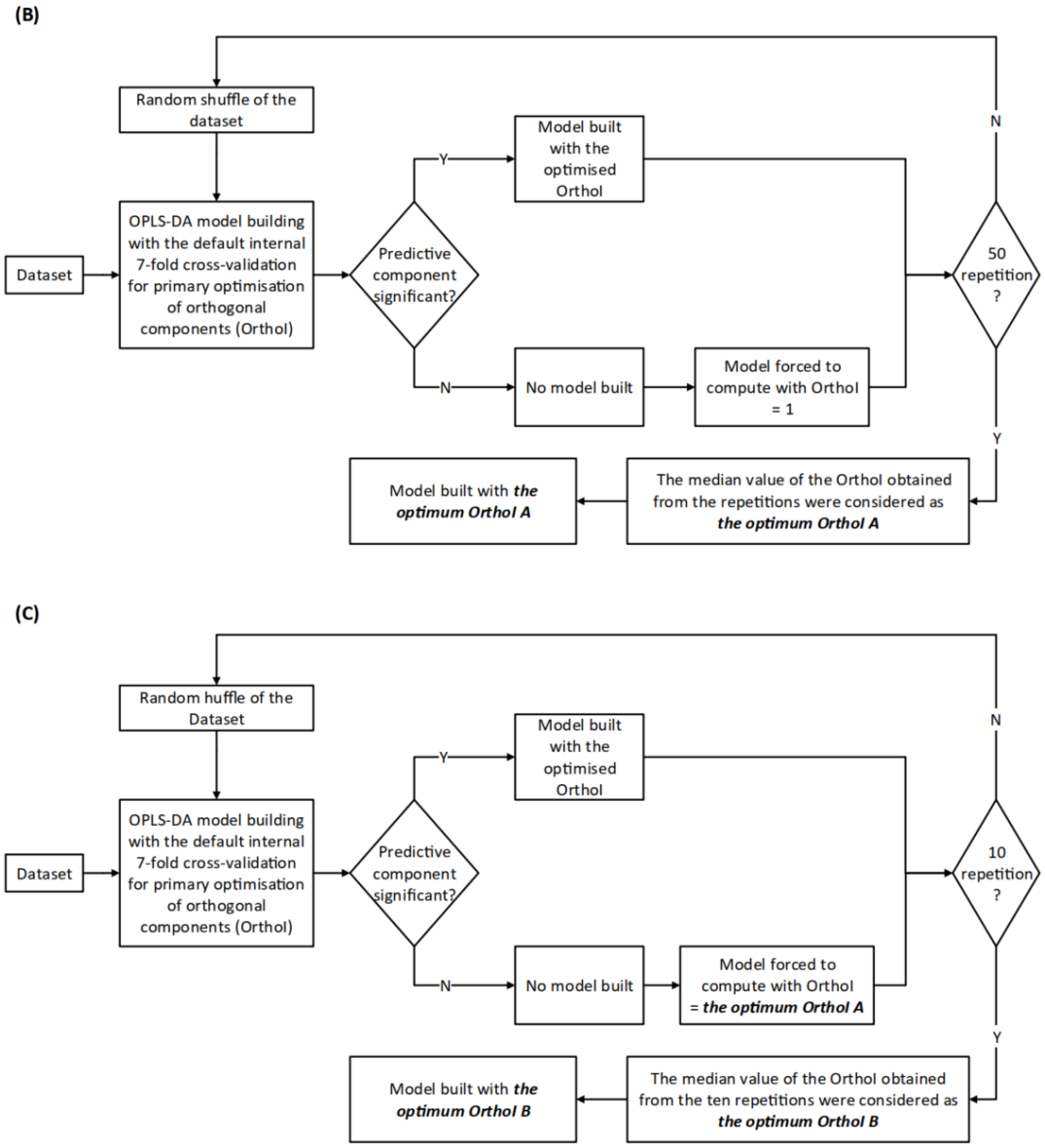

Figure 2-1 Schematic representation of model optimisation, cross-validation and permutation strategy.(A) Steps for the OPLS-DA model building and cross-validation (B) OPLS-DA model optimisation for the full dataset. (C) OPLS-DA model optimisation for the training set in the cross-validation.

2.2.7.2 Univariate Analysis

Univariate statistical analyses, such as Student's *t* test or one-way ANOVA, were performed to identify significant differences in the mean for each discriminatory metabolite. Benjamini-Hochberg method was used to control the false discovery rate at 0.05. Univariate ROC analyses based on individual metabolite concentrations and multivariate ROC analyses using a combination of features using logistic regression

were performed using MetaboAnalyst 5.0 (Pang et al., 2021). For patient demographic and clinical information, normality was tested by Anderson-Darling test. Kruskal-Wallis test with Dunn's multiple comparisons test was used to identify significant differences for non-normal continuous variables. Chi-Square test with Bonferroni correction for multiple comparisons was used for categorical variables. Adjusted two-tailed *p*-values ≤ 0.05 were considered statistically significant.

2.3 Results

2.3.1 Clinical Features

The patient cohort ($n = 238$) comprised 162 DRE patients, and 76 AE patients including 27 with CASPR2-, 29 with LGI1-, and 20 with NMDAR-antibody encephalitis. Baseline demographic and treatment details are summarised in Table 1-1. The median age of the DRE patients was 37 years old and 62% were female. As expected, CASPR2 and LGI1 patients were older (72 and 74 years old, median age) compared to DRE and more were males (89% and 79%, respectively), whereas NMDAR-antibody encephalitis patients had a median age of 30 and were predominantly female (95%) (Irani, Alexander, et al., 2010b; Irani, Bera, et al., 2010; Thompson et al., 2018). While all DRE patients were receiving ASMs (100%), the percentage was lower in AE patients (54%) who frequently received immunotherapies. Again, as expected, more AE patients (19% CASPR2-, 24% LGI1-, 40% NMDAR-antibody patients) had systemic tumours, also focal and generalised seizures contrasted across the cohorts. DRE patients were relatively stable and provided their blood samples during routine outpatient clinics, while AE patients were potentially sampled both during acute in-patient stays and at outpatient clinics.

Table 2-1 Patient demographic and clinical information.

	DRE	AE-CASPR2	AE-LGI1	AE-NMDAR	*p* value (adjusted *p* value)
	N = 162	N = 27	N = 29	N = 20	
Age, Median (IQR)	37 (27, 48) [C L]	74 (66, 78) [D N]	72 (57, 73) [D N]	30 (23, 58) [C L]	< 0.001 (< 0.001)

	DRE	AE-CASPR2	AE-LGI1	AE-NMDAR	*p* value (adjusted *p* value)
Sex, *n* (%)					
Female	100 (62%) [CLN]	3 (11%) [DN]	6 (21%) [DN]	19 (95%) [CDL]	< 0.001 (< 0.001)
BMI, Median (IQR)	27 (24, 31)	27 (23, 28)	26 (20, 31)	28 (21, 32)	0.7 (> 0.9)
Unknown	60 (37%)	20 (74%)	21 (72%)	10 (50%)	
Use of ASMs, *n* (%)					< 0.001 (< 0.001)
Yes	162 (100%) [CLN]	17 (63%) [DN]	20 (69%) [DN]	4 (20%) [CDL]	
Unknown	0	3 (11%)	2 (7%)	0	
Use of Steroids, *n* (%)					< 0.001 (< 0.001)
Yes	1 (1%) [CLN‖]	6 (22%) [DL]	17 (59%) [CD]	7 (35%) [D]	
Unknown	0	1 (4%)	2 (7%)	1 (5%)	
Use of Other Immunotherapies, *n* (%)					< 0.001 (< 0.001)
Yes	2 (1%) [CLN]	9 (33%) [D]	11 (38%) [D]	9 (45%) [D]	
Unknown	0	1 (4%)	2 (7%)	0	
Identified tumour(s), *n* (%) [#]					0.0013 (0.010)
Yes	21 (13%) [LN]	5 (19%)	7 (24%) [D]	8 (40%) [D]	
Unknown	0	7 (26%)	12 (41%)	0	
Seizure Semiology, *n* (%)					< 0.001 (< 0.001)
Focal seizures	121 (75%) [LN]	19 (70%)	24 (83%) [D]	1 (5%) [D]	
Focal †	65	19	20	1	
Focal + FBTCS ‡	56	0	4	0	
Generalised	39 (24%) [LN]	1 (4%)	1 (3%) [D]	5 (25%) [D]	
GTCS	36	1	1	5	
Other §	3	0	0	0	
Unknown	2 (1%)	7 (26%)	4 (14%)	14 (70%)	

	DRE	AE-CASPR2	AE-LGI1	AE-NMDAR	p value (adjusted p value)
Disease Duration (from onset to sampling date, months), median (IQR)	160 (180) [C L N]	38 (38) [D]	25 (46) [D]	16 (24) [D]	<0.001 (<0.001)
Unknown	1 (1%)	0	0	0	
Seizure-free days (from last seizure to sampling date), median (IQR)	16 (143) [C L N]	646 (1369) [D]	272 (726) [D]	814 (761) [D]	<0.001 (<0.001)
Never had seizures	0	7 (26%)	2 (7%)	12 (60%)	
Unknown	0	2 (7%)	3 (10%)	2 (10%)	

Kruskal-Wallis test with Dunn's multiple comparisons test was used to identify significant differences of each class in age, BMI, disease duration and seizure-free days. Pairwise Chi-Square test with Bonferroni correction for multiple comparisons were used for categorical variables. Omnibus p values and adjusted omnibus p values with Bonferroni correction across demographic variables were reported. D, C, L, and N indicate a significant difference ($p < 0.05$) exists with DRE, CASPR2, LGI1, NMDAR, respectively, in the corresponding post-hoc multiple comparisons. # identified tumours encompass any tumour (including cancer) detected anywhere in the whole body (including brain), as documented in the electronic patient records at the time of blood sampling. † includes focal aware seizures and focal impaired awareness seizures. ‡ Focal seizures and focal to bilateral tonic clonic seizures (FBTCS). § absence seizures, myoclonus. IQR, interquartile range. GTCS, generalised tonic-clonic seizure. ‖The patient was on lifelong hydrocortisone replacement due to childhood-onset hypopituitarism, unrelated to autoimmune pathology.

2.3.2 NMR Plasma Metabolomics Coupled with OPLS-DA Models Discriminate Autoimmune Encephalitis Patients from Those with Drug-Resistant Epilepsy.

To compare plasma metabolomic signatures between DRE ($n = 162$) and AE patients ($n = 76$), ^{1}H NMR spectroscopy was performed with predictive models of OPLS-DA using 10-fold external cross validation. Cross validation and permutation testing showed that the model was able to identify AE patients in the test set from DRE patients with 87.0 ± 3.1% accuracy, 87.9 ± 3.4% sensitivity and 86.3 ± 3.6% specificity and the model performed significantly better than random chance (50.0 ± 5.3% accuracy, 50.0 ± 6.9% sensitivity, 49.8 ± 7.4% specificity, p <0.001, Kolmogorov–Smirnov test), indicating it is both robust and not a result of overfitting (Figure 2-2 and Table 2-2). In addition, NMR spectra were also obtained for three subjects selected to have post-AE

epilepsy who had AE for 2–3 years before being treated as epilepsy with only ASMs. Notably, when applying this OPLS-DA model to predict these three patients using their plasma metabolome, all three patients were classified as epilepsy, clustered with the DRE group (Figure 2-3).

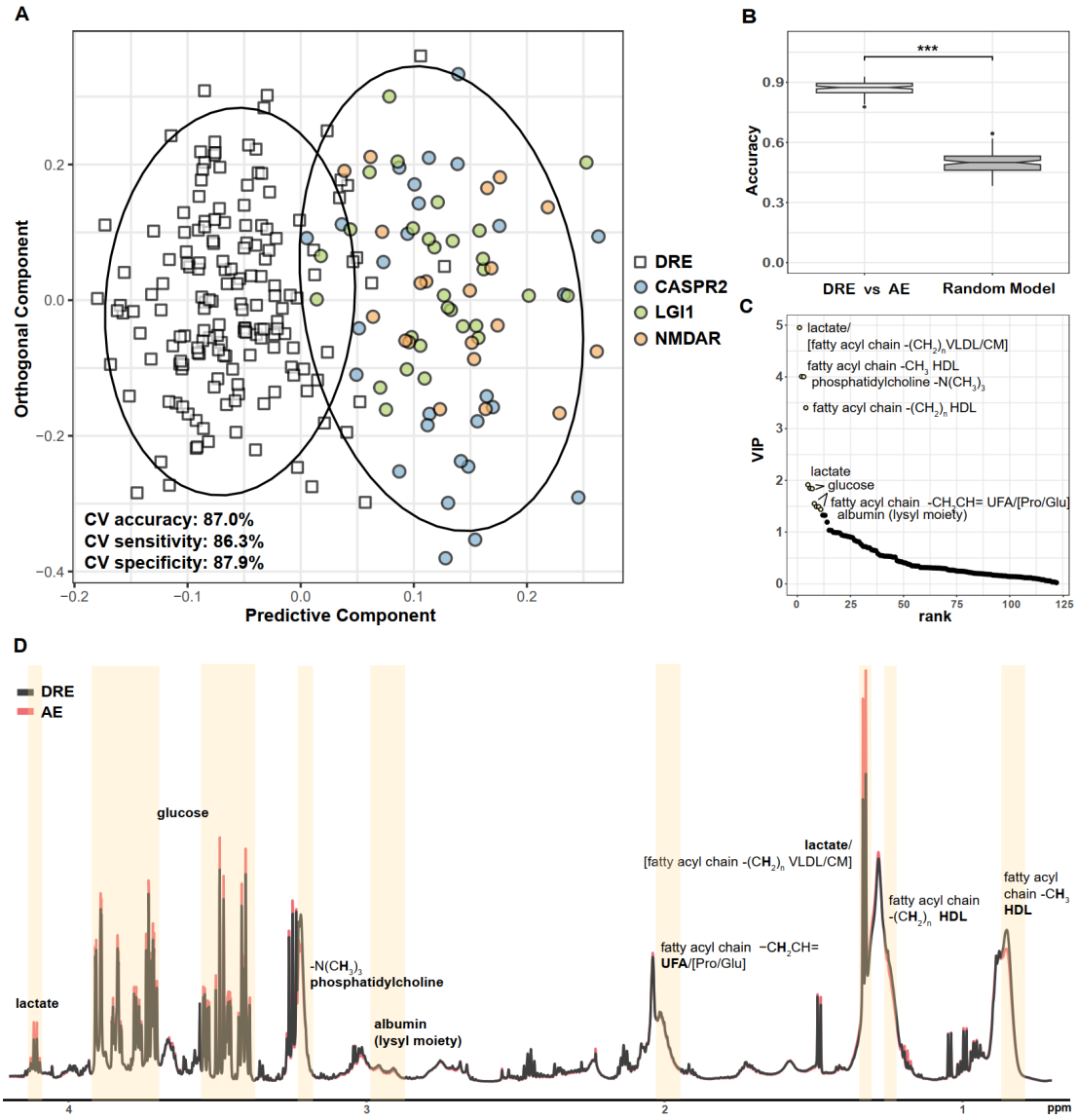

Figure 2-2 Altered plasma metabolome between AE patients and DRE patients.(A) Representative OPLS-DA scores plot showing separation of AE (circle, n = 76) from DRE (square, n = 162) patient plasma samples. AE plasma samples are coloured according to the subtype (autoantibody specificity, CASPR2/LGI1/NMDAR, blue/green/orange). The ellipses indicate 95% confidence interval. The OPLS-DA model was generated with 1 predictive component and 7 orthogonal components. CV, cross validation. (B) Predictive accuracy of the ensemble of the OPLS-DA models compared with that of the randomly permutated null distribution. Kolmogorov-Smirnov test. *** $p < 0.001$. (C) Discriminatory metabolites driving the separation of the OPLS-DA models, ranked by VIP scores. The top 11 resonances, identified

with the inflection point with a VIP score cut-off of 1.4, were labelled. "/" indicates the mentioned metabolites are overlapped in the spectral region. Metabolite names in square brackets refers to non-dominant overlapping metabolites also found in that spectral region. VLDL, very-low-density lipoproteins. CM, chylomicrons. (D) Mean NMR spectra of plasma samples from AE (red, $n = 76$) and DRE patients (black, $n = 162$) highlighted and labelled with discriminatory metabolites derived from the OPLS-DA models.

Table 2-2 Statistical metrics of the OPLS-DA models.

comparison	model accuracy	model sensitivity	model specificity	accuracy (random)	R^2Y	R^2Y (random)	Q^2	Q^2 (random)
AE vs DRE	87.0 ± 3.1%	87.9 ± 3.4%	86.3 ± 3.6%	50.0 ± 5.3%	0.70 ± 0.06	0.29 ± 0.04	0.53 ± 0.05	-0.44 ± 0.15
CASPR2 vs DRE	80.0 ± 5.1%	83.5 ± 6.8%	78.2 ± 5.8%	50.4 ± 8.6%	0.82 ± 0.03	0.56 ± 0.06	0.34 ± 0.11	-0.84 ± 0.42
LGI1 vs DRE	82.3 ± 5.0%	82.8 ± 6.9%	82.7 ± 6.2%	50.9 ± 9.0%	0.72 ± 0.10	0.57 ± 0.06	0.46 ± 0.10	-0.84 ± 0.40
NMDAR vs DRE	80.4 ± 7.3%	80.5 ± 7.8%	82.0 ± 9.0%	50.9 ± 9.8%	0.85 ± 0.10	0.83 ± 0.06	0.42 ± 0.11	-1.32 ± 0.73
CASPR2 vs LGI1	69.2 ± 3.0%	66.7 ± 4.4%	73.3 ± 5.8%	49.4 ± 8.5%	0.34 ± 0.01	0.22 ± 0.05	0.11 ± 0.03	-0.28 ± 0.16
CASPR2 vs NMDAR	68.9 ± 5.4%	68.8 ± 7.8%	66.5 ± 7.8%	51.4 ± 10.7%	0.60 ± 0.03	0.44 ± 0.06	0.09 ± 0.10	-0.56 ± 0.32
LGI1 vs NMDAR	77.5 ± 5.0%	79.4 ± 7.8%	76.1 ± 6.8%	50.2 ± 10.2%	0.85 ± 0.02	0.64 ± 0.06	0.24 ± 0.11	-0.86 ± 0.50

Values were presented in mean ± SD. OPLS-DA models were validated on independent test data (10%) using an external 10-fold cross-validation strategy with repetition coupled with permutation testing. Accuracy, sensitivity, and specificity were calculated from the external test set to assess the robustness and predictive ability of the models. Accuracy/Sensitivity/Specificity (random) indicated the metrics calculated using the permutated dataset. R^2 and Q^2 were calculated from the OPLS-DA model built using the full data set, where R^2 provides a measure for how much variation is represented by the model and Q^2 for the goodness of prediction.

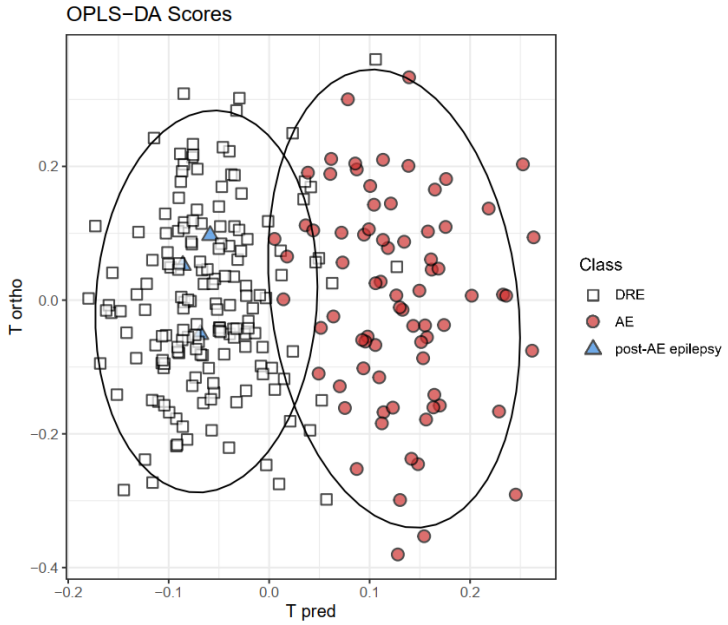

Figure 2-3 Prediction of subjects with post-AE epilepsy. The OPLS-DA scores plot illustrates the application of the OPLS-DA model, differentiating AE from DRE, for the prediction of three individuals with post-AE epilepsy. The plot includes the projection of these three subjects with post-AE epilepsy onto the DRE vs AE separation. Patients situated to the left of the dashed vertical line are anticipated to have DRE.

Mean spectra from DRE patients and AE patients (Figure 2-2) show discriminatory metabolites derived from the model. Compared to DRE patients, AE patients had increased plasma lactate, glucose and decreased high-density lipoprotein (HDL, fatty acyl chain -(CH_2)$_n$-, -CH_3 in lipoproteins, the spectral integral predominated by HDL), phosphatidylcholine ($N^+(CH_3)_3$, choline-containing phospholipids, predominantly phosphatidylcholine), unsaturated fatty acids (UFAs, -CH_2CH= from the unsaturated fatty acyl components) and albumin (lysyl moiety of albumin) (Nicholson et al., 1995) .

Univariate ROC analysis was conducted for each of the most discriminatory metabolites, indicating their individual potential to classify AE and DRE patients with an AUC ranging from 0.59 to 0.72 (Figure 2-4 A-F). Multivariate ROC analysis coupled with logistic regression on all the 11 most discriminatory resonances yielded an AUC of 0.820 (95% CI: 0.744-0.907). Notably, when selecting lactate, HDL (-CH_3), the albumin lysyl moiety, and glucose, four features with lower covariation that are routinely measurable in the clinical setting, the ROC analysis showed a comparable AUC of 0.820 (95% CI: 0.742-0.892) (Figure 2-4G).

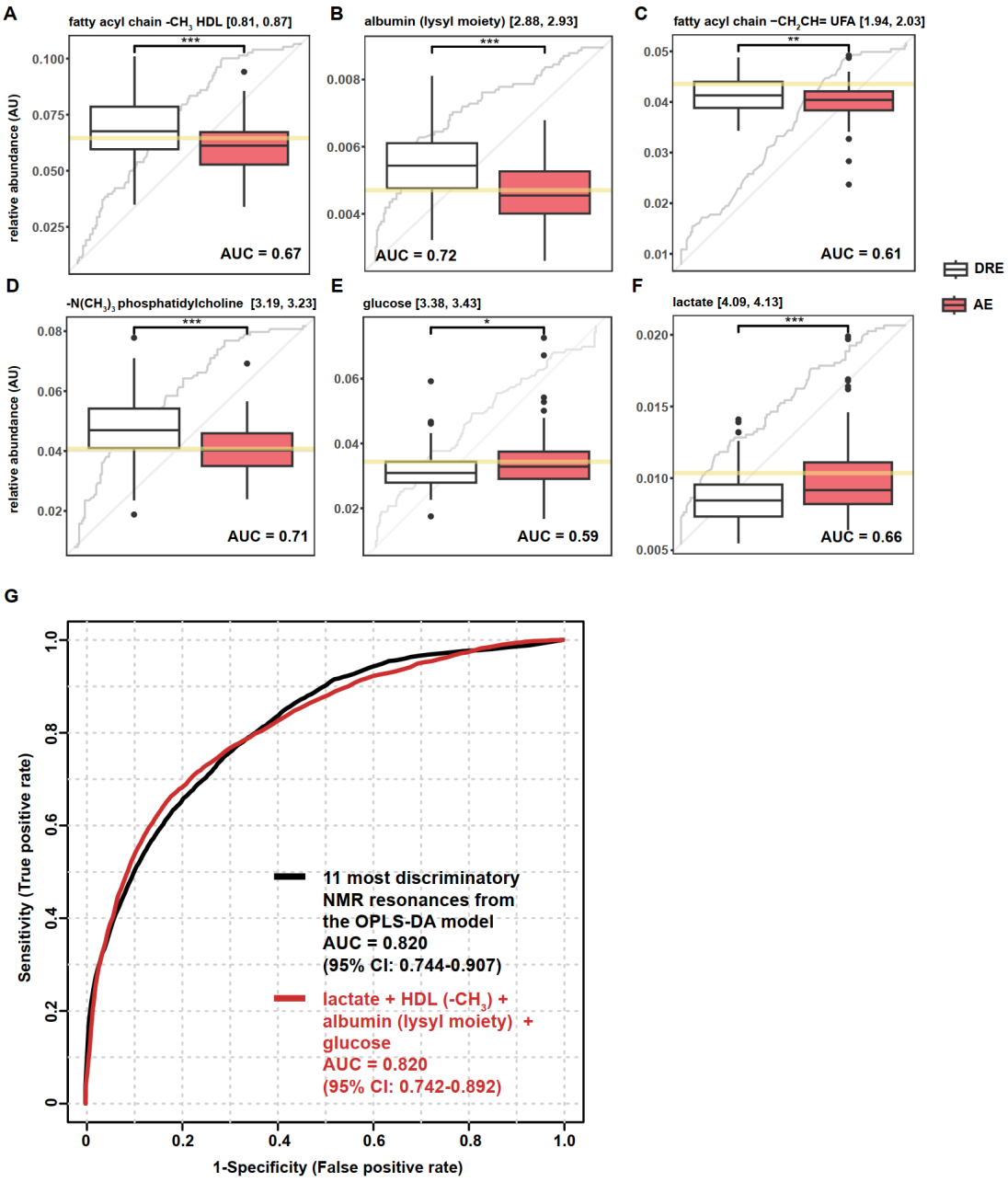

Figure 2-4 ROC analysis for discriminatory metabolites. (A-F) boxplots of the highest ranked discriminatory metabolites identified by the OPLS-DA model in AE vs DRE. Grey lines were ROC curves of each metabolite. Yellow lines indicate optimal cutoff (closest to top-left corner) from univariate ROC analyses. Univariate ROC analyses were based on individual metabolite concentration differences, while multivariate ROC analyses used logistic regression on combined features. (G) Multivariate ROC analysis on a combination of 11 most discriminatory NMR resonances from the OPLS-DA model (black) and on 4 selected features (red).

2.3.3 Distinct Metabolomic Signatures Identified for Each AE Subtype.

Upon further examination of the discriminatory metabolites, each AE subtype appeared to have its own unique metabolic signature apart from the shared metabolomic

perturbation in HDL –$(C\mathbf{H}_2)_n$–, HDL –$C\mathbf{H}_3$, phosphatidylcholine and the albumin lysyl moiety (Figure 2-5A). Plasma lactate levels were increased in LGI1-antibody encephalitis patients, and, even more so, in CASPR2-antibody encephalitis patients. Elevated plasma glucose and decreased UFA were only observed in the plasma of LGI1-antibody patients. Individual OPLS-DA models were developed for each AE subtype, compared to the DRE group. These models achieved cross-validation accuracies of 80.0 ± 5.1%, 82.3 ± 5%, and 80.4 ± 7.3% for distinguishing CASPR2-, LGI1- and NMDAR-antibody encephalitis, respectively, from DRE (Table 2-2). Notably, distinct metabolite signatures were identified for each subtype, including lactate, HDL (-$C\mathbf{H}_3$, -$(C\mathbf{H}_2)_n$-), and phosphatidylcholine for CASPR2; HDL (-$C\mathbf{H}_3$, -$(C\mathbf{H}_2)_n$-), lactate, phosphatidylcholine, glucose and UFA for LGI1; and phosphatidylcholine, HDL (-$C\mathbf{H}_3$, -$(C\mathbf{H}_2)_n$-), and glycoprotein A (GlycA) for NMDAR (Figure 2-5A, Figure 2-6, Figure 2-8).

Pairwise OPLS-DA models were built within the three AE subtypes to further study if each subtype can be stratified based on the differences in the metabolomic alteration. The accuracies of the models (CASPR2 vs LGI1, CASPR2 vs NMDAR, LGI1 vs NMDAR) were 69.2 ± 3.0%, 68.9 ± 5.4%, and 77.5 ± 5.0%, respectively (Table 2-2). The significantly superior performance of the models than random chance ($p < 0.001$, Kolmogorov-Smirnov test) indicated distinct metabolomic alterations exist within the three AE subtypes (Figure 2-7**,** Figure 2-8). Specific alterations in plasma metabolome in each AE subtype relative to DRE and each other are summarised in the Venn diagram (Figure 2-5B).

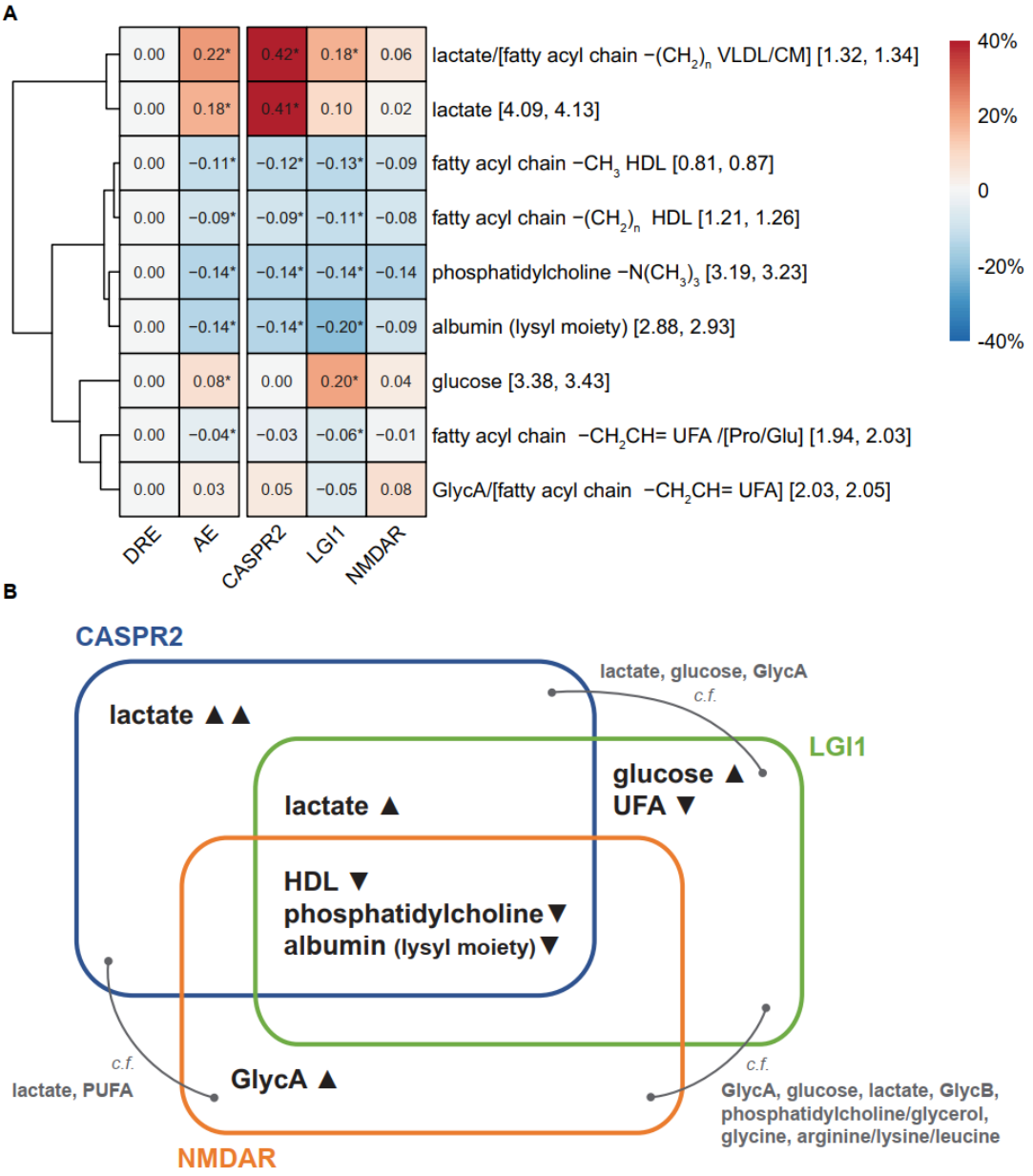

Figure 2-5 Specific alteration in plasma metabolome in each AE subtype. (A) Heatmap of percentage changes in key metabolites identified by the OPLS-DA models of AE vs DRE, and in each AE subtype relative to the DRE group. Numbers in the square brackets represent the boundary of corresponding spectral region in ppm. "/" indicates the mentioned metabolites are overlapped in the spectral region. Metabolite names in square brackets refers to non-dominant overlapping metabolites also found in that spectral region. * Significance in mean compared to DRE group ($q < 0.05$ in univariate analysis). (B) Venn diagram illustrating metabolic signatures of AE subtypes. Metabolites in black were identified from OPLS-DA models of AE vs DRE, and each AE subtype vs DRE, while metabolites in grey were identified from OPLS-DA models of pairwise AE subtype comparisons. HDL, high density lipoprotein. UFA, unsaturated fatty acids. PUFA, polyunsaturated fatty acids. GlycA/B, Glycoprotein A/B.

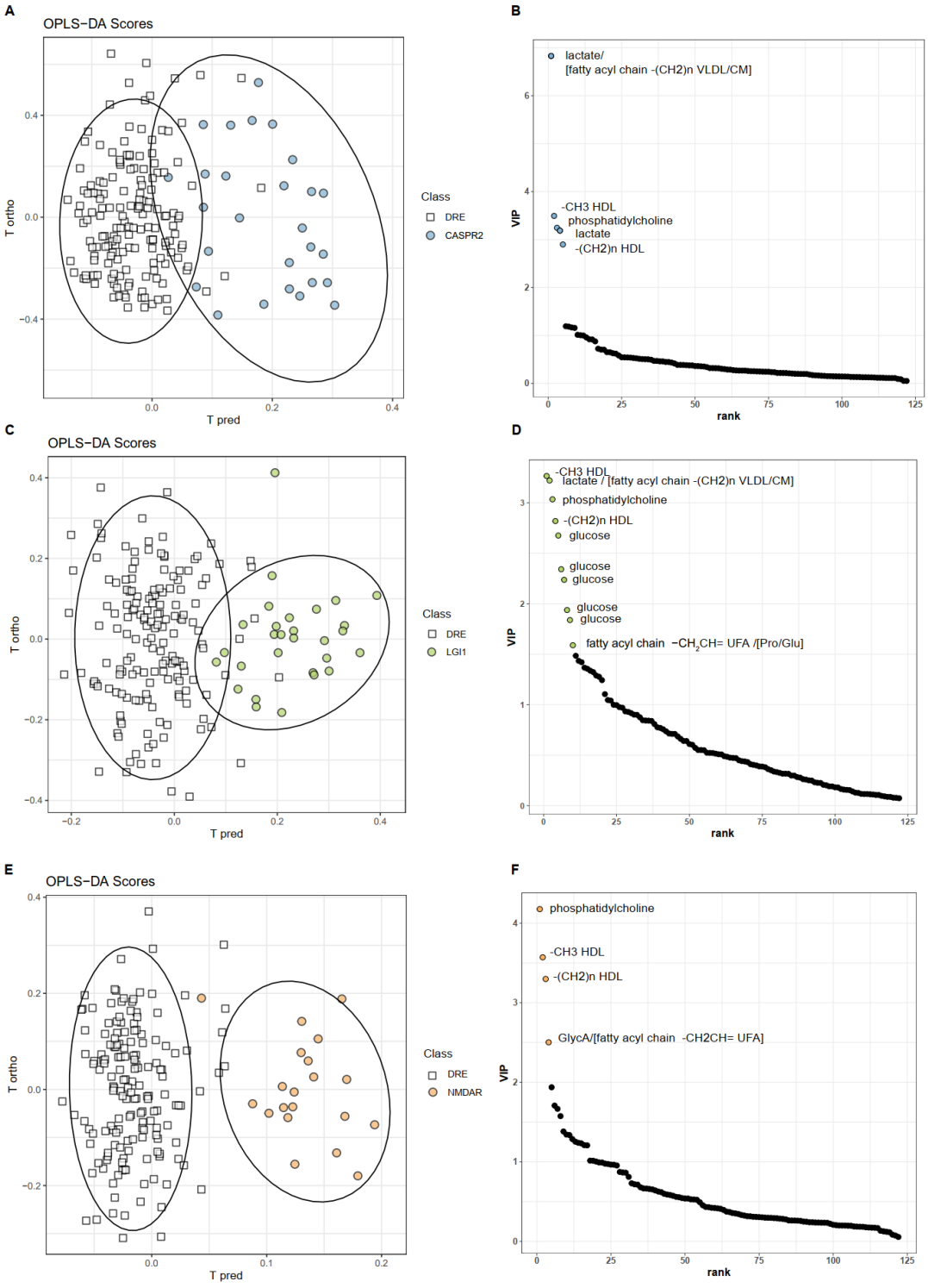

Figure 2-6 OPLS-DA models discriminating DRE and each AE subtype.(A, C, E) OPLS-DA scores plot differentiating between DRE and each AE subtype (CASPR2, LGI1, NMDAR). (B, D, F) Corresponding discriminatory metabolites responsible for the separation of the OPLS-DA models, ranked by VIP scores.

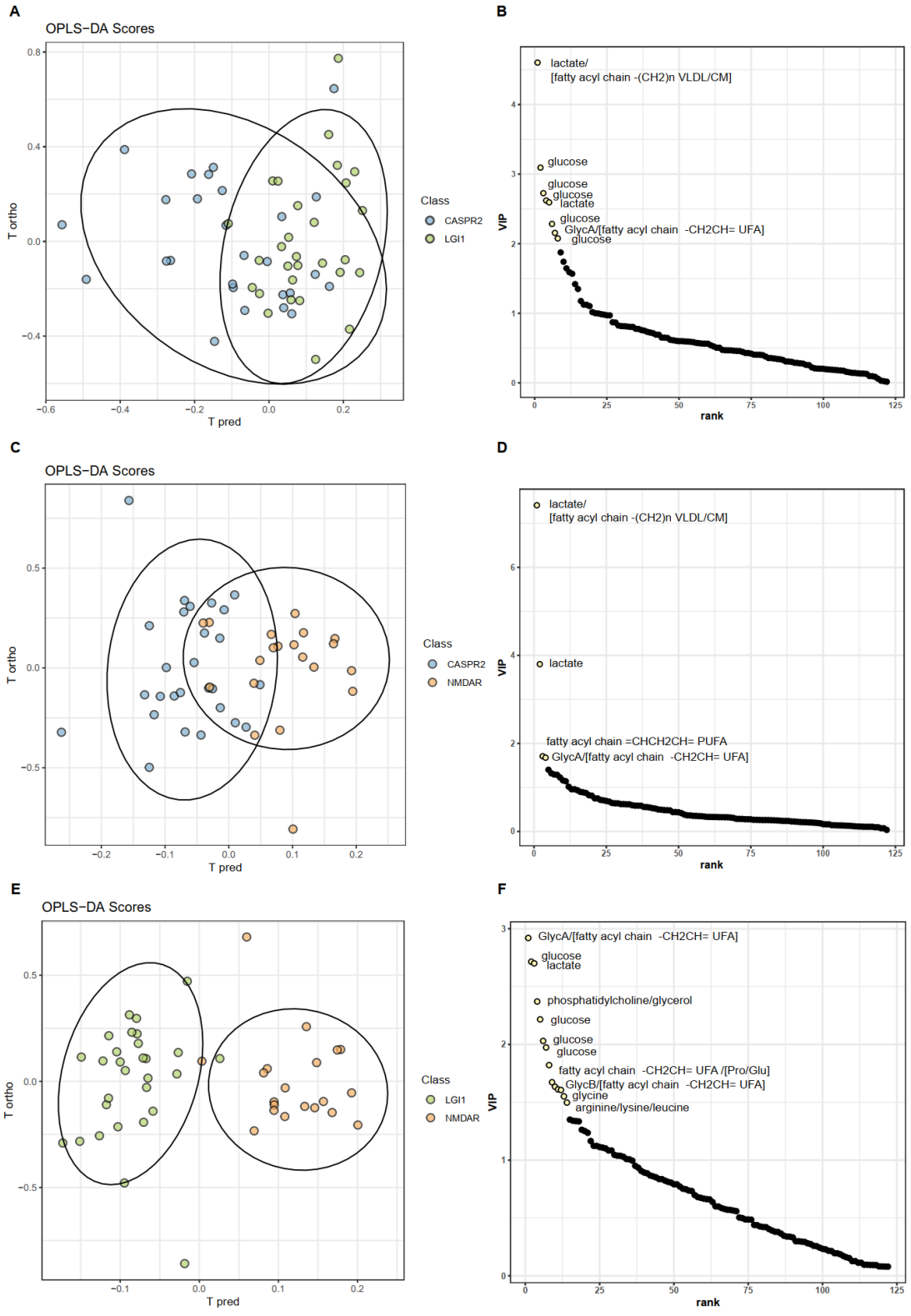

Figure 2-7 OPLS-DA models discriminating between AE subtypes. (A, C, E) OPLS-DA scores plot differentiating between AE subtypes (CASPR2 vs LGI1, CASPR2 vs NMDAR, LGI1 vs NMDAR). (B, D, F) Corresponding discriminatory metabolites responsible for the separation of the OPLS-DA models, ranked by VIP scores.

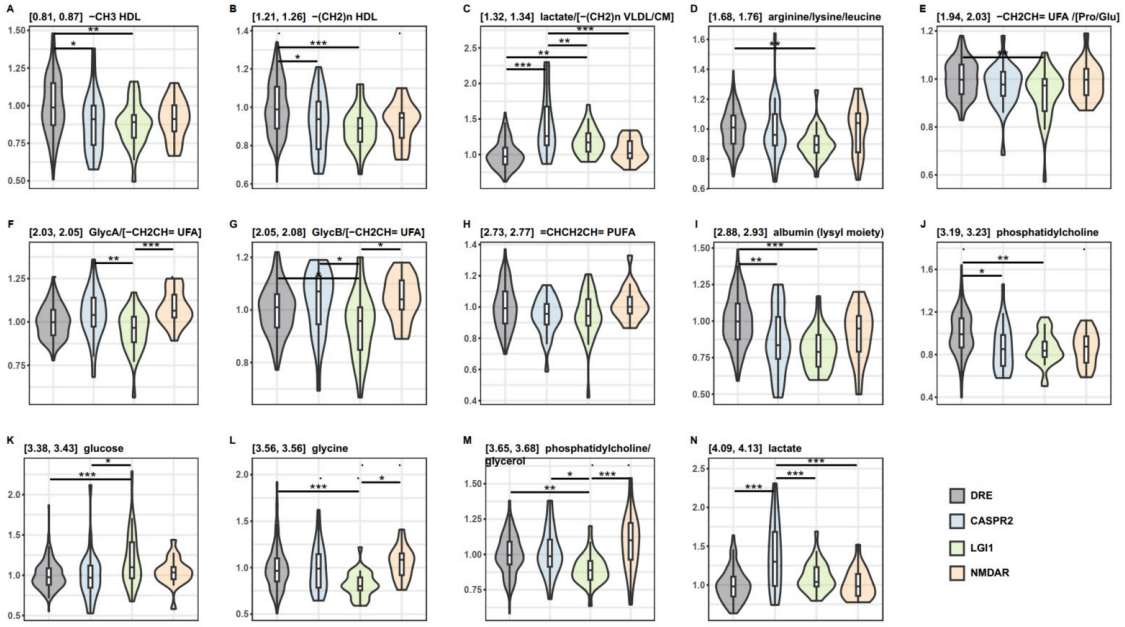

Figure 2-8 Violin plots of the discriminatory metabolites derived from the OPLS-DA models(AE vs DRE, CASPR2 vs LGI1, CASPR2 vs NMDAR, LGI1 vs NMDAR) in DRE (grey, n = 169), CASPR2 (blue, n = 27), LGI1 (green, n = 30), NMDAR (orange, n = 23). Significance was determined using one-way ANOVA with post hoc Tukey's HSD tests. Holm-Bonferroni method was applied for adjustment of p values due to multiple comparisons. * $q < 0.05$, ** $q < 0.01$, *** $q < 0.001$. HDL, high density lipoprotein. VLDL, very low-density lipoprotein. CM, chylomicrons. GlycA/B, glycoprotein A/B. UFA, unsaturated fatty acids. UFA, unsaturated fatty acids. PUFA, polyunsaturated fatty acids.

2.3.4 Potential Confounding Factors Including Seizure Semiologies.

To investigate whether different seizure semiologies or the seizure proximity (Table 2-1) were reflected in the plasma metabolome, OPLS-DA models were built to compare patients with focal seizures (n = 121) vs patients with generalised seizures (n = 39). However, the 10-fold cross-validation demonstrated a mean accuracy of 55.8 ± 5.9%, only marginally superior to random chance. Even when employing a subset of patients with focal aware/impaired awareness seizures (n = 20) matched with patients experiencing generalised tonic-clonic seizures (GTCS) (n = 20) in terms of age, gender, and seizure-free days, the model yielded a mean accuracy of 57.0 ± 4.7%. Similarly, when assessing the impact of seizure proximity by stratifying patients who had seizures in less than 15 days (n = 79) versus those without seizures for more than 300 days (n = 38), the model had a mean accuracy of 58.8 ± 6.0%. These results suggest that the impact of epilepsy on the blood metabolome is independent of the location, the type, and the

proximity of seizure.

Other potential confounders lie in the observation that DRE and AE cohorts have multiple differences, as outlined in Table 2-1. To examine the influence of these potential confounders in the model, scores plots demonstrating the separation of the two groups were coloured according to each variable to test for observable correlations (Figure 2-9). Among these, age, the use of steroids and other immunotherapies displayed notable correlations. Consequently, OPLS-DA models were constructed to compare younger (< 25, n = 34) vs older (> 50, n = 32) DRE patients, and the model was able to distinguish younger vs older DRE with a 71.9 ± 4.0% cross-validation accuracy. Nonetheless, the discriminatory metabolite resonances responsible for the age separation were mainly very-low-density lipoprotein -(C**H**$_2$)$_n$- (VLDL, 1.26-1.32 ppm) and unsaturated fatty acids -**H**C=C**H**- (5.25-5.38 ppm), different from those driving the separation between DRE and AE (Figure 2-10).

A substantial proportion of the AE cohort was undergoing treatment with steroids and/or other immunotherapies. The OPLS-DA model was able to distinguish between AE patients who were using steroids (n = 30) and those who were not (n = 42), with a cross-validation accuracy of 65.4±4.1%. AE patients on steroids exhibited elevated glucose and GlycA levels (Figure 2-11). However, the OPLS-DA model yielded only a 55.7 ± 4.5% cross-validation accuracy to identify AE patients receiving other immunotherapies (n = 44 + 25) (Figure 2-12). Therefore, while steroid administration may contribute marginally to the elevation of glucose levels in the AE vs DRE cohorts, the AE pathology remains the primary factor distinguishing their plasma metabolomics.

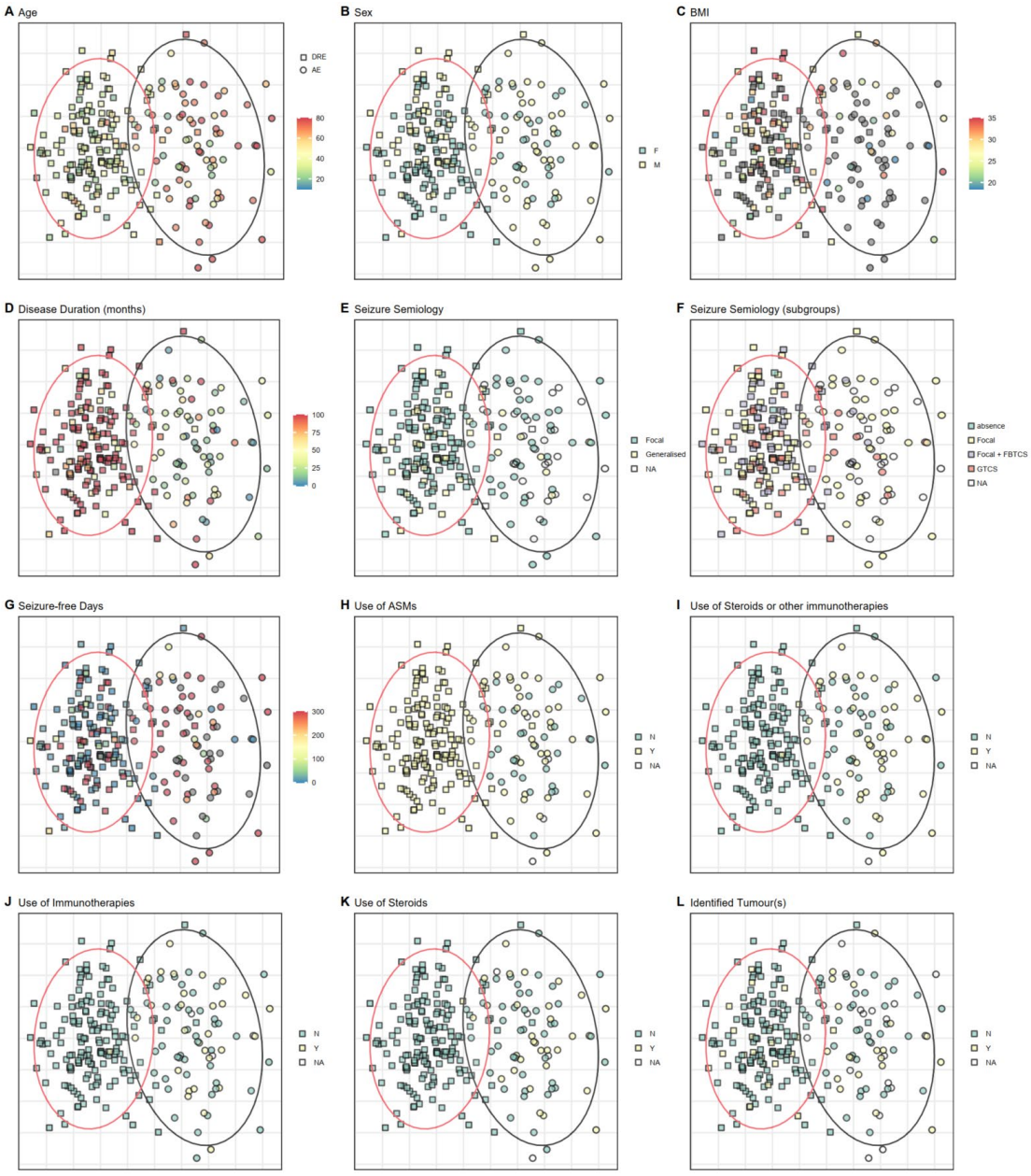

Figure 2-9 OPLS-DA scores plot of AE (circle) vs DRE (square) coloured by potential confounding factors.

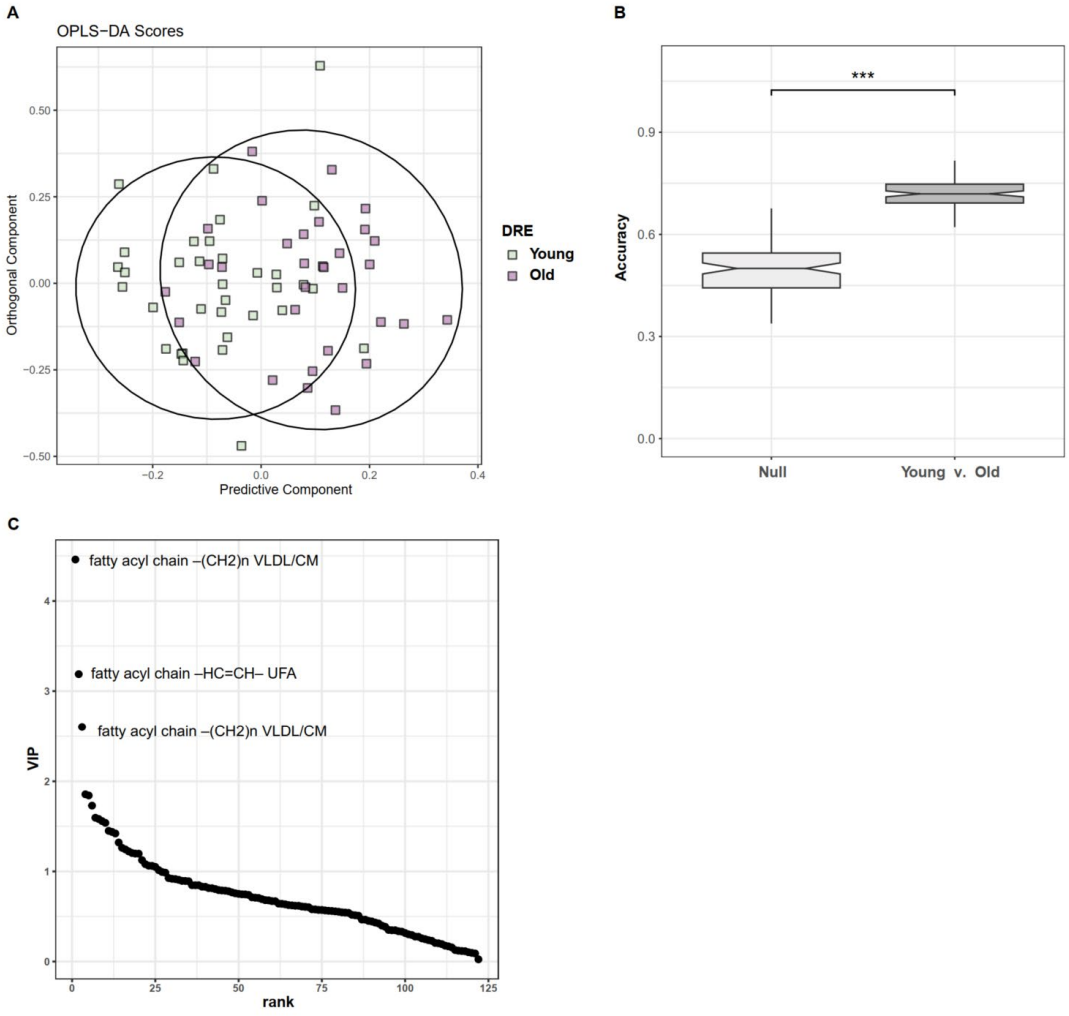

Figure 2-10 OPLS-DA was able to distinguish younger vs older DRE with a 71.9% cross-validation accuracy (A, B). VLDL and unsaturated fatty acids were responsible for driving the separation in age (C).

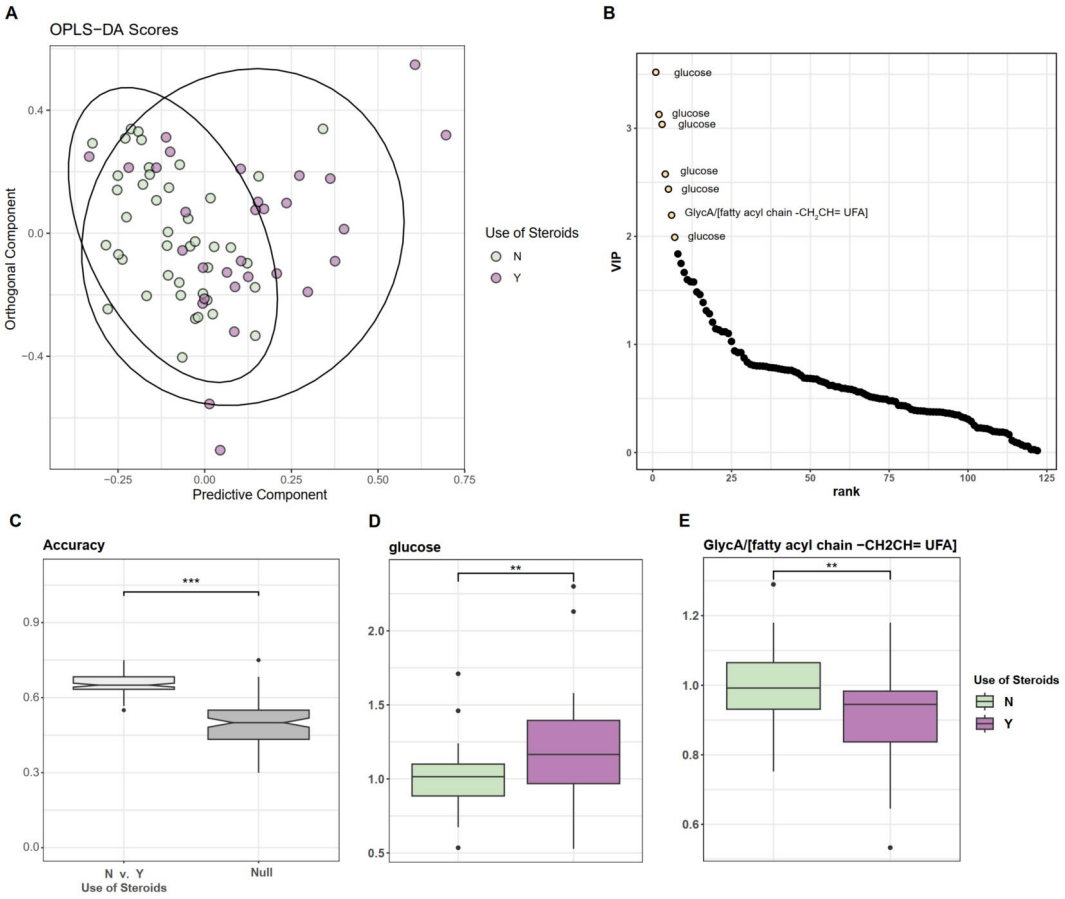

Figure 2-11 OPLS-DA was able to distinguish between AE patients who were using steroids and those who were not with a 65.1% cross-validation accuracy (A, C). Glucose and GlycA were responsible for driving the separation in Steroid usage (B, D, E).

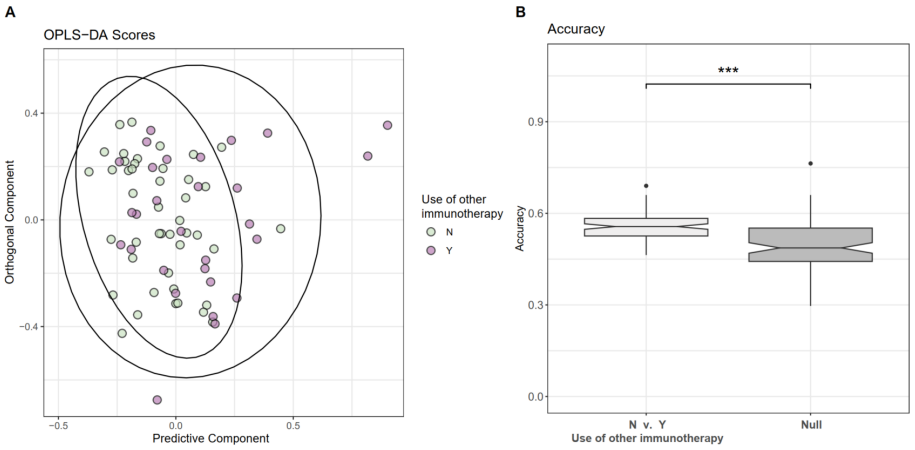

Figure 2-12 OPLS-DA yielded only a 55.7 ± 4.5% cross-validation accuracy to identify AE patients receiving immunotherapies (A, B).

2.4 Discussion

This chapter demonstrated the ability of metabolomics to differentiate patients with AE

from those with DRE, and to separate three common subtypes of autoantibody-mediated AE. This represents the first biomarker offering these discriminatory properties. While autoantibody assays will likely remain the gold standard, the NMR-based blood test offers a promising adjunct to facilitate the diagnosis of AE given the speed of testing, affordability, and high diagnostic accuracy. Metabolomic testing may be especially valuable when patients present with seizures in the absence of obvious causes such as traumatic brain injury, neoplasms, and infectious disease. Moreover, as autoantibody assays only detect known antibodies, it is conceivable that patients harbouring unknown NSAb may be detected with NMR approaches (McCracken et al., 2017; Woodhall et al., 2022). While prior research has explored non-antibody-based biomarkers such as neurofilament light chain (NfL) and cytokines (Brenner et al., 2023; Levraut et al., 2021; Wesselingh et al., 2023; F. Zhang et al., 2023), these have limitations, such as NfL's susceptibility to age and various confounding factors. Hence, the unique advantages offered by the NMR metabolomics methods in AE diagnosis and subtype differentiation may prove valuable for several applications.

This study has found that different AE subtypes (CASPR2, LGI1, NMDAR) have both overlapping and distinct metabolome perturbations, suggesting the existence of both shared and distinct pathogenic mechanisms. Here it shows that the common plasma metabolomic signatures shared by AE patients include decreased levels of HDL (fatty acyl chain -($C\mathbf{H}_2$)$_n$-, -CH_3 resonances), phosphatidylcholine and albumin (lysyl moiety). While the clinical signs in AE are largely associated with the interaction with their respective target antigens in the CNS, there is also some peripheral expression of these proteins (e.g. LGI1), where autoimmune response might have contributed to the altered blood chemistry profiles observed (Anderyas et al., 2022).

Lipid profiles, especially with decreased HDL levels, are implicated in inflammatory and autoimmune diseases. For example, low HDL cholesterol and high triglycerides levels have been associated with higher levels of multiple sclerosis disability, as well as poor recovery and relapse in NMOSD (Cho et al., 2020; Tettey et al., 2014, 2017; K. Wu et al.,

2019). Additionally, several studies have found lower HDL-cholesterol levels in individuals with NMDAR- antibody encephalitis compared to healthy controls, and associated with a poorer prognosis and increased likelihood of relapse (Liu et al., 2021, 2022; Shu et al., 2017).

Decreased levels of -N(CH_3)$_3$ resonances from phosphatidylcholine were found in AE plasma in the study at hand and were highly positively correlated with HDL -CH_3 levels (r = 0.95, p < 0.001, Figure 2-13). As phosphatidylcholine is the main phospholipid present in plasma and an integral component of lipoproteins (particularly HDL) the observed decrease in phosphatidylcholine levels may be attributed to the reduced levels of HDL. Additionally, the decreased levels of phosphatidylcholine may occur secondary to AE-induced inflammation, as cellular lipid profiles are modulated following inflammatory stress, including a decrease in phosphatidylcholines (Campos et al., 2016).

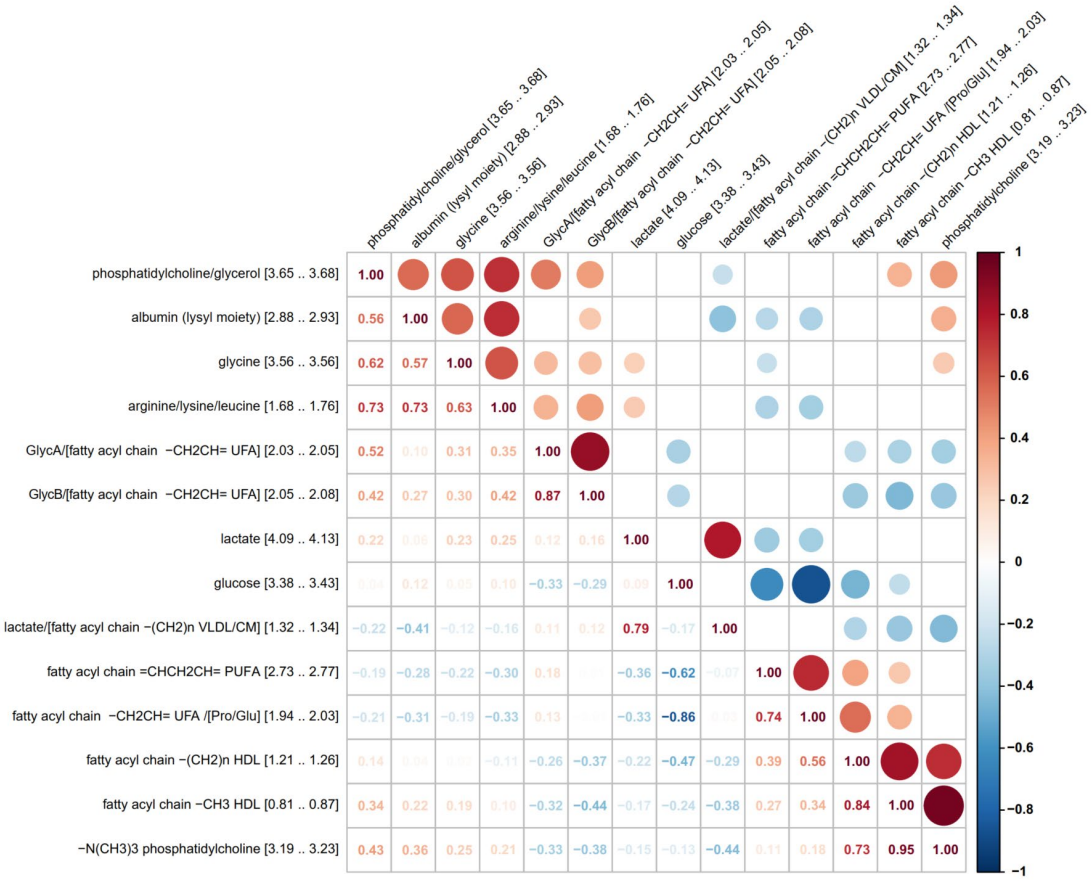

Figure 2-13 Correlation plot of discriminatory metabolites from the OPLS-DA models. The correlation plot encompasses all discriminatory metabolites extracted from the OPLS-DA

models involving different comparisons (AE vs DRE, CASPR2 vs LGI1, CASPR2 vs NMDAR, LGI1 vs NMDAR). Pearson correlation coefficient *r* is visualised with different sized circles in the upper triangular of the correlation matrix, and the original *r* values are shown in the lower triangular. Holm-Bonferroni method was applied for adjustment of *p* values due to multiple comparisons. The plot includes only significant correlations.

Consistent with these findings, significantly lower albumin levels have been reported in AE patients, with plasma albumin levels decreased in NMDAR-antibody encephalitis relative to healthy controls, and pre-treatment low plasma albumin associated with worse prognosis in AE (Jang et al., 2018; Shu et al., 2018). Albumin is a negative acute phase reactant and reduced serum albumin levels have been shown to correlate with systemic and central inflammatory disease, which could be due to increased albumin degradation caused by a high catabolic rate and elevated albumin transudation resulting from increased capillary permeability (Ishida et al., 2014; Lyons et al., 2010). Thus, taken together, the significant decreases observed in lipoprotein and albumin resonances of AE patients observed here, are consistent with an inflammatory metabolic signature.

This chapter has also demonstrated that various subtypes of AE exhibit distinct metabolic changes, aligning with the observation that different NSAb are often associated with distinct clinical syndromes and prognoses (Dalmau & Graus, 2018). Elevated lactate levels were observed in both CASPR2- and LGI1-antibody patients, especially for CASPR2-antibody patients, while elevated plasma glucose levels were found in CASPR2-antibody AE only. GlycA levels were higher in NMDAR- and CASPR2-antibody patients but lower in LGI1-antibody patients, while UFA levels were decreased in LGI1-antibody encephalitis only.

Lactate is one of the most enriched by-products of cellular metabolism in tissues with immune cell infiltration. Studies have indicated that the activation of inflammatory immune cells can cause a shift from oxidative phosphorylation to aerobic glycolysis, resulting in an increase in lactate (Manosalva et al., 2022). For example, elevated levels of serum lactate, have been reported in individuals with multiple sclerosis and the increases are positively correlated with increasing disability (Amorini et al., 2014; W. L. Miller & Auchus, 2011).

GlycA/B, NMR specific biomarkers of systemic inflammation, derive from the glycan moieties of acute-phase proteins (Mallagaray et al., 2023). Studies have reported elevated levels of GlycA in patients with autoimmune diseases like rheumatoid arthritis and systemic lupus erythematosus (Durcan et al., 2016; Ormseth et al., 2015). Therefore, the increased GlycA levels observed in NMDAR-antibody patients are potentially indicative of ongoing inflammatory processes in this patient population. However, alone, GlycA is a non-specific marker (Mallagaray et al., 2023).

The limitations of this study are acknowledged, as it did not include healthy controls nor patients with other antibody-mediated diseases. Consequently, it is challenging to assert whether the identified pattern is specific to AE. Nonetheless, a comparative analysis with our prior research was conducted, where NMR metabolomics enabled successful stratification of antibody-positive NMOSD and relapsing remitting multiple sclerosis patients (Jurynczyk et al., 2017). Notably, some common signatures in the autoantibody-positive NMOSD group, including reduced phosphatidylcholine and lactate levels, along with alterations in lipoprotein profiles (Jurynczyk et al., 2017). The shared metabolic signatures in these cohorts with antibody mediated diseases underscore the potential relevance of lipid metabolism and glucose regulation in various autoimmune and neurological conditions, warranting further exploration of these metabolic pathways for potential biomarkers or therapeutic targets.

In conclusion, this is the first study to use NMR-based metabolomics in distinguishing AE patients from DRE patients, highlighting the diagnostic potential of the NMR-based blood test for such differentiation. Furthermore, each AE subtype was found to exhibit a distinct biochemical signature, providing insights into the distinct metabolic impact of the different AE target antigens. Yet, no discriminatory metabolomic signatures were observed for different seizure semiologies or proximity in the DRE cohort. Future work needs to validate identified biomarkers externally in an independent cohort. It will also be important to explore the applicability of the NMR blood test in identifying other AE subtypes, seronegative AE patients and whether the AE metabolomic signature might

be used to predict the persistence of AE.

Chapter 3: The Serum Metabolomic Profile of a Distinct, Inflammatory Subtype of Acute Psychosis

The data in this chapter has been published as Lennox, B*., **Xiong, W.*,** Waters, *P.* et al. The serum metabolomic profile of a distinct, inflammatory subtype of acute psychosis. *Mol Psychiatry* 27, 4722–4730 (2022). https://doi.org/10.1038/s41380-022-01784-4 (* co-first authorship)

3.1 Introduction

Chapter 2 demonstrated the distinct blood metabolic profile of patients with AE compared to those with DRE, suggesting the diagnostic potential of NMR-based blood tests to identify antibody-mediated pathology in CNS diseases. The presence of NSAb causative for AE has also been observed in the blood of some patients with psychosis. The Lennox Group has been screening patients with psychosis for NSAb for the past nine years (Lennox et al., 2017). Over this time, the range of antibodies that has been recognised has expanded, and the evidence around the pathogenicity of some of these antibodies has grown. For instance, pre-clinical studies support the pathogenicity of the NMDAR antibody in patients with AE (Hughes et al., 2010), and the nature of the clinical syndrome is well characterised (Dalmau et al., 2011; Irani, Bera, et al., 2010). The clinical relevance of these antibodies in those with psychosis is less certain, even though there are clear overlaps in terms of symptoms seen (Al-Diwani et al., 2017). Studies that have directly examined NMDAR antibodies from patients with psychosis also demonstrate their functional effects on synaptic function (Gréa et al., 2019), and small case series of patients with psychosis and NMDAR antibodies demonstrate a comparable treatment response to immunotherapy (Lennox et al., 2019; Zandi et al., 2014). In contrast, the evidence around the pathogenicity of antibodies targeting VGKC is controversial across all clinical presentations. This was the first NSAb to be described in association with encephalitis in 2001 (Buckley et al., 2001). However, more recent

studies have specified the particular targets as being components of the VGKC – LGI1 and CASPR2 (Irani, Alexander, et al., 2010b), such that the value of testing for generic VGKC antibodies, using radioimmunoassay is now questioned in encephalitis (van Sonderen, Schreurs, de Bruijn, et al., 2016), and the clinical recommendation is to only test for LGI1 and CASPR2 (B. Lang et al., 2017). However, the utility of VGKC antibody testing in neurological diseases other than encephalitis remains to be seen. Indeed, other studies indicate that VGKC antibody assays do still have value, indicating an immunotherapy responsive illness in children for instance (Hacohen et al., 2015). There are further antibodies where clinical relevance in CNS disorders is more unclear, such as Glycine receptor (GlyR) antibodies, more associated with progressive encephalomyelitis with rigidity and myoclonus (Carvajal-González et al., 2014), and others that are so rare that there is little to guide clinical practice (GABA-A antibodies) (Spatola et al., 2017).

This highlights the need for adjunctive diagnostic tools to differentiate psychosis with an autoimmune basis, facilitating timely and targeted interventions for improved patient outcomes. In this chapter, NMR serum metabolomics analysis was applied to identify novel subgroups within a cohort of psychosis patients and relate the identified metabolic phenotypes to measures of disease severity at presentation, using PANSS, and the presence of a range of neuronal cell surface antibodies in the serum of these patients. To further investigate any distinct metabolic phenotypes identified in this psychosis cohort and investigate the possible relevance of these antibodies, a cohort of antibody negative patients (negative for all antibodies tested), matched for age, gender, and ethnicity to the antibody positive group, was included. The hypothesis was that those with defined NSAb would have a different metabolomic profile than those without.

3.2 Methods

3.2.1 Study Participants

Serum samples were collected from 1574 patients with acute psychosis across England as part of the Medical Research Council (MRC) Prevalence of Pathogenic Antibodies in Psychosis study (PPiP1 [2013-2014] and PPiP2 [2015-2018]) (Lennox et al., 2017). The inclusion criteria for the study were ages 16-35, first episode of psychotic illness, antipsychotic medication less than 6 weeks and at least one moderate or more severe symptom of psychosis. These criteria were then broadened in 2016 to widen the age range 16-70 and extend the length of illness to 24 months and included those at relapse as well as first episode.

Following informed consent, a serum sample was collected, alongside demographic details and a clinician rating of severity of selected positive and negative syndrome scale (PANSS) items at the same time point (P1 Delusions, P2 Conceptual disorganisation, P3 Hallucinatory behaviour, N1 Blunted Affect, N4 Passive/apathetic social withdrawal, N6 Lack of spontaneity and flow of conversation, G5 Mannerisms and posturing and G9 Unusual thought content) (Kay et al., 1987). The items mentioned above were rated on a 7-point scale: 1 = absent, 2 = minimal, 3 = mild, 4 = moderate, 5 = moderate severe, 6 = severe, and 7 = extreme (Kay et al., 1987). Clinicians were asked to only rate the symptoms that were moderate or more severe (≥ 4). Absent-mild symptoms did not have ratings by clinicians, and their item score was considered as 1 during statistical analyses. Total and subscales' scores were calculated with the eight items mentioned above. For the participants in PPiP1 a full PANSS rating was obtained. In these subjects, a P1 rating was given as a record of any delusional beliefs in participants. This includes those rated as having more specific ratings of delusions of suspiciousness or grandiosity in the full PANSS interview. As these items (P6 and P7) were not included in the brief PANSS ratings, the highest scoring item has been taken as the rating for P1 for these participants.

A total of 145 patients with sufficient serum sample volume for both antibody testing

and metabolomics analysis were included in this study; 75 patients who were antibody positive along with 70 antibody negative controls matched for age, gender, and ethnicity and illness course. Two patients were positive for more than one Ab and so were excluded from model training.

3.2.2 Standard Protocol Approvals, Registrations, and Patient Consents

Written informed consent was obtained from all patients according to the Declaration of Helsinki. Ethical approval was obtained by the local research ethics committee (12/EE/0307 PID 97740).

3.2.3 Serum Collection

Serum was collected in a serum separator tube (BD Vacutainer™ SST™ II Advance Tubes), supplied by the study team, and posted to Oxford. Samples were allowed to clot at room temperature before being centrifuged at 1300 × *g* for 10 minutes at room temperature. The serum supernatant was immediately stored at -80 °C.

3.2.4 Antibody Testing

Antibody testing for NMDAR, GlyR, GABAAR, LGI1, CASPR2 IgG antibodies was undertaken in the Nuffield Department of Clinical Neuroscience, according to published methods (Irani, Alexander, et al., 2010b; Irani, Bera, et al., 2010; Pettingill et al., 2015). VGKC Antibodies were measured by radioimmunoassay in a National Health Service (NHS) Clinical laboratory (Oxford University Hospitals NHS Trust). A threshold of 100 pM was taken as the cut off for a positive result. All samples collected were tested for all antibodies.

3.2.5 NMR Experiments

NMR sample preparation and NMR experiments were conducted as previously described in Section 2.2. Serum samples were thawed at room temperature and centrifuged at 100 000 × *g* for 30 minutes at 4 °C. 150 µL of supernatant was then diluted with 450 µL of 75 mM sodium phosphate buffer prepared in D_2O (pH 7.4). ^{1}H 1D NOESY and CPMG-PROJECT spectra were acquired for each sample using a 700-MHz

Bruker AVIII spectrometer. CPMG-PROJECT spectra were split into 213 0.02-ppm-wide bins for integration, excluding the water resonance and noise regions. Sum-normalised integral values were pareto scaled prior to multivariate analysis.

3.2.6 Statistical Analysis

3.2.6.1 Multivariate Analysis

Multivariate analysis was performed as described in Section 2.2, with the exception that the repetitions for optimising number of orthogonal components were not included, as such variability in number of orthogonal components determined by the *ropls* package was not observed in this dataset.

3.2.6.2 Univariate Analysis

Mann-Whitney U test was used for non-normal continuous variables in two-group comparisons. Ordinary one-way ANOVA (with post hoc Tukey's multiple comparisons test) was used for continuous variables in comparisons of more than two groups. When unequal variance was present amongst groups, Brown-Forsythe and Welch ANOVA tests (with Dunnett's T3 multiple comparisons test) were used instead. For variables with non-normal distribution or limited group sample size, Kruskal-Wallis test with Dunn's multiple comparisons test was used in comparisons of more than two groups. Fisher's exact tests were used for categorical variables as appropriate, while a Bonferroni correction was applied throughout to account for multiple comparisons. Two-tailed p values ≤ 0.05 were considered statistically significant.

3.3 Results

3.3.1 Patient Demographics and Antibody Status

The most prevalent serum antibodies detected in those with antibodies were NMDAR antibodies (47%, $n = 35$), followed by VGKC antibodies (19%, $n = 13$). Two double-positive patients were identified, one positive for both CASPR2 and VGKC antibodies and another positive for both CASPR2 and NMDAR antibodies and so these were excluded from model training. The groups were well matched for age, gender, ethnicity,

episode type, and illness duration. The VGKC antibody-positive group had higher PANSS total compared to the Control group ($n = 70$, $p < 0.01$, Kruskal-Wallis test), LGI1 antibody positive group ($n = 9$, $p < 0.05$, Kruskal-Wallis test) and NMDAR antibody positive group ($n = 35$, $p < 0.05$, Kruskal-Wallis test) (Table 3-1).

Table 3-1 Patient information, grouped by different neuronal cell surface antibodies.

	Ab negative (Ctrl)	Ab positive	GlyR-Ab	VGKC-Ab	CASPR2-Ab	LGI1-Ab	NMDAR-Ab
Number of patients	70	73	7	13	9	9	35
Age (years), median (IQR)	27 (15)	25 (13)	24 (10)	23 (8)	24 (11.5)	25 (15)	32 (18)
Gender, Female, no. (%)	31 (44.3)	30 (41.1)	4 (57.1)	5 (38.5)	3 (33.3)	1 (11.1)	17 (48.6)
Ethnicity (%)							
White	71.4	67.1	100	61.5	55.6	77.8	62.9
Asian	12.9	12.3	0	0	22.2	11.1	17.1
Black (African/Caribbean)	7.1	9.5	0	23.1	11.1	11.1	5.7
Mixed	4.3	6.8	0	7.7	11.1	0	8.6
Other	4.3	0	0	0	0	0	0
Unknown	0	4.1	0	7.7	0	0	5.7
Disease duration (duration from the episode date to the consent date, days), median (IQR)	86 (258.8)	103 (244.5)	267 (399)	37 (23)	230 (317)	132 (404)	113 (229)
Unknown, no.	0	4	2	1	0	1	0
Episode type, no. (%)							
First episode	45 (64.3)	50 (68.5)	7 (100)	13 (100) (adjusted p value =0.51)	6 (66.7)	7 (77.8)	17 (48.57)
Relapse	24 (34.3)	22 (30.1)	0 (0)	0 (0)	3 (33.3)	1 (11.1)	18 (51.4)
Unknown	1 (1.4)	1 (1.4)	0 (0)	0 (0)	0 (0)	1	0 (0)

	Ab negative (Ctrl)	Ab positive	GlyR-Ab	VGKC-Ab	CASPR2-Ab	LGI1-Ab	NMDAR-Ab
						(11.1)	
PANSS							
Total score, median (IQR)	12 (6)	14 (8.8)	19 (6)	23 (12.5)**	11 (8.5)	12 (4.5)	13 (7)
Unknown, no.	0	0	1	0	0	0	0

The Kruskal-Wallis test with Dunn's multiple comparisons test was used to identify significant differences of each class compared to Control for numerical variables (age, PANSS scores) while Fisher's exact test was used for categorical variables. Ethnicity data was analysed by comparing White vs Combined Asian/Black/Mixed/Other ethnic groups in Ctrl, combined VGKC/GlyR Group, combine NMDAR/LGI1/CASPR2 Group, as applicable to Chi-square test/Fisher's exact test. *$p < 0.05$, ** $p < 0.01$, ***$p < 0.001$

Ctrl: control, psychosis patients tested negative for the following neuronal cell surface antibodies. Ab: antibody, psychosis patients tested positive for one of the following neuronal cell surface antibodies. GlyR: glycine receptor. VGKC: voltage-gated potassium channel complex. CASPR2: contactin associated protein-like 2. LGI1: leucine-rich glioma inactivated 1. NMDAR: N-methyl-D-aspartate receptor. PANSS: Positive and Negative Syndrome Scale. IQR: Interquartile Range.

3.3.2 Two Distinct Serum Biochemical Signatures were Detected by Unsupervised analysis, which Correspond to VGKC antibody and GlyR Antibody Positivity

Unsupervised PCA (blinded to antibody status and all other demographic data) of the NMR metabolome alone, spontaneously separated the cohort into two distinct groups of $n = 18$ and $n = 125$ (Figure 3-1A). This suggests, that 18 of the patients in the cohort have distinct serum biochemical signatures when compared to all other samples. When demographic data was superimposed on to the unsupervised scores plot no association between this biochemically distinct group and age, gender, ethnicity, episode type, or disease duration was observed (Figure 3-2). However, a clear association with antibody status was observed (Figure 3-1B). All antibody negative, NMDAR, LGI1 and CASPR2 antibody patients were found to fall with the predominant biochemical signature group while all but two VGKC antibody positive patients (85%, $n = 11$) and all GlyR antibody positive patients (100%, $n = 7$) fell within the 'distinct biochemical signature' group.

This suggests that the serum biochemical signature of NMDAR, LGI1, and CASPR2 antibody psychosis patients is indistinguishable from antibody negative psychosis patients. In contrast, VGKC and GlyR antibody psychosis patients have a shared biochemical signature which is distinct.

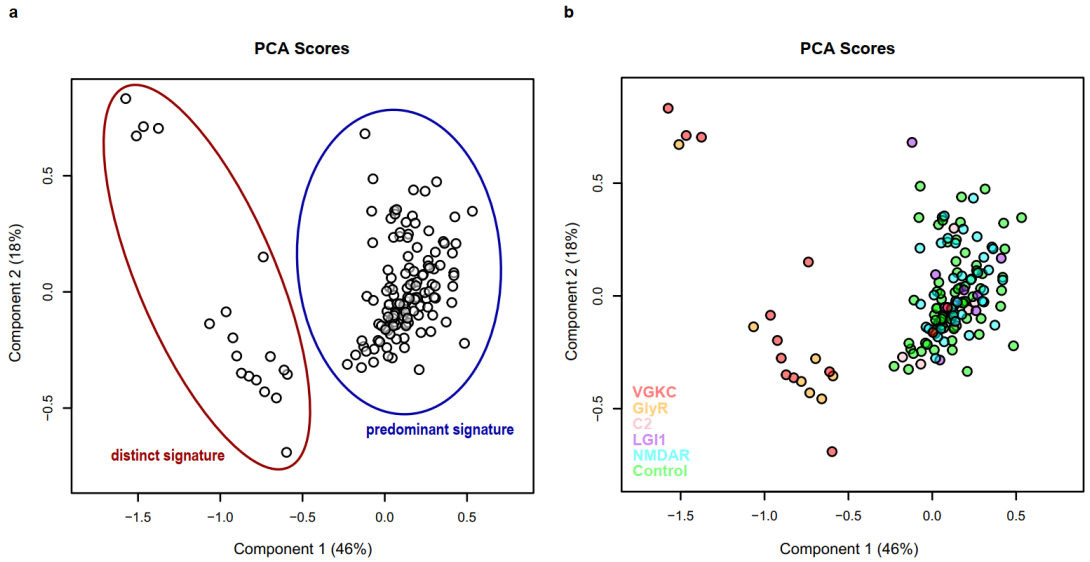

Figure 3-1 PCA scores plots of NMR serum metabolomics. (a) The NMR metabolite signature spontaneously separated the psychosis patient cohort into two groups: the 'predominant biochemical signature group' and the 'distinct biochemical signature group'. (b) Psychosis patients who tested positive for serum antibodies against VGKC (red, $n = 13$) or GlyR (orange, $n = 7$) spontaneously separated from those who tested positive for CASPR2 (pink, $n = 9$), LGI1 (purple, $n = 9$), or NMDAR (blue, $n = 35$) and antibody negative control (green, $n = 70$) samples.

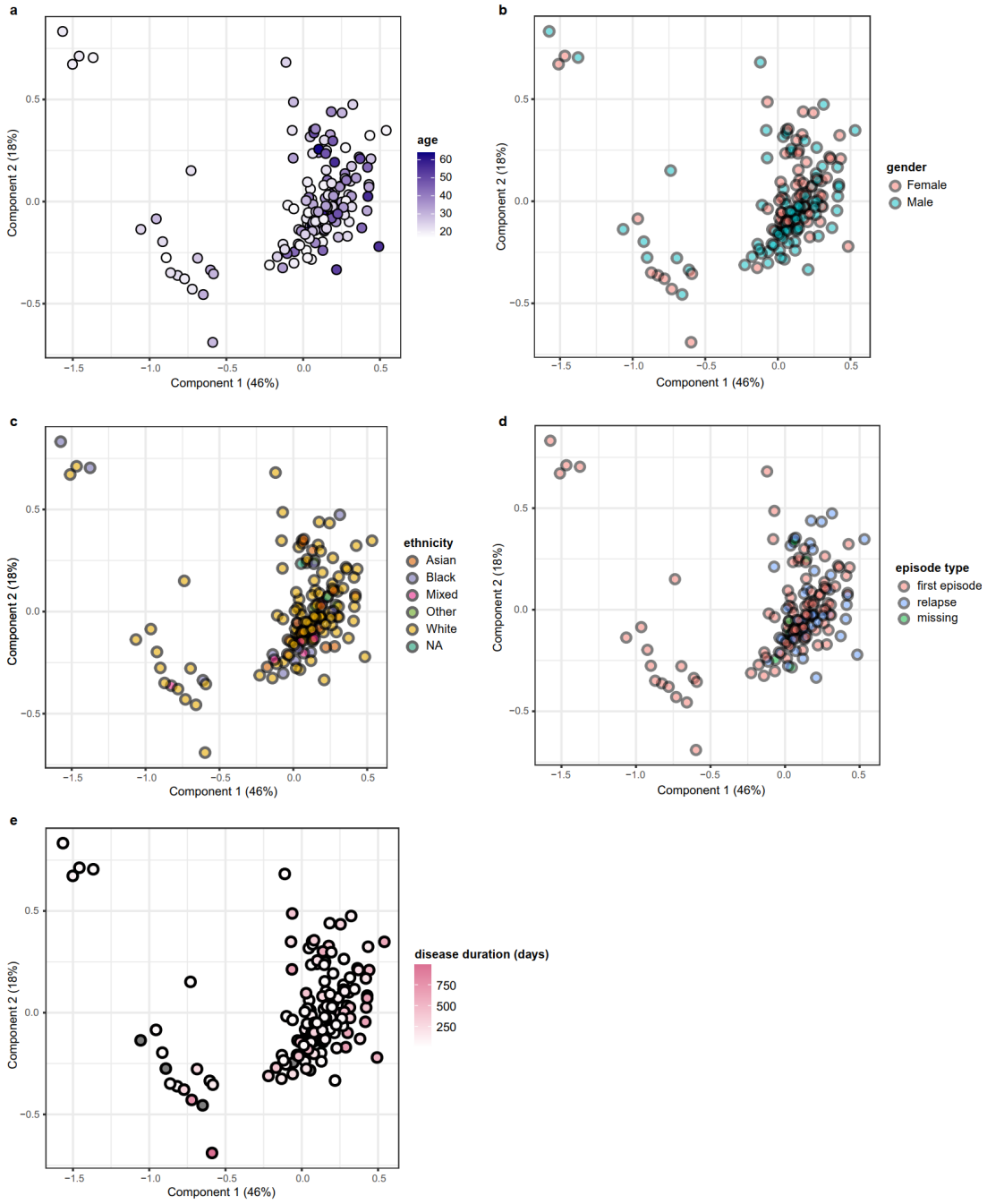

Figure 3-2 PCA scores plot of NMR serum metabolomics coloured by potential confounders. The spontaneous separation of NMR metabolomics was not associated with age (a), gender (b), ethnicity (c), episode type (d), and disease duration (e).

3.3.3 Significant Metabolic Imbalances Including Decreases in Serum Lipoproteins Along with Increased Amino Acid Concentrations were Observed in VGKC and GlyR Antibody Positive Psychosis Patients.

To further understand the biochemical perturbations associated with sub-groups identified above, the cohort was split into three groups: (1) a VGKC and GlyR antibody

combined group (VGKC/GlyR, $n = 20$), (2) a group consisting of patients with NMDAR, LGI1, or CASPR2 antibodies (NMDAR/LGI1/CASPR2, $n = 53$), and (3) a control group of patients negative for all antibodies tested (Control, $n = 70$). Supervised OPLS-DA analyses were performed to build predictive models and tested on independent data (data that was not used to train the model) by cross-validation.

No separation was observed between the control and NMDAR/LGI1/CASPR2 antibody groups in the OPLS-DA scores plot (Figure 3-3a) and the performance of the model, on independent test data, was not significantly better than that expected by random chance (Figure 3-3b, p value > 0.05, Kolmogorov-Smirnov test) confirming there are no detectable differences in biochemical signature between these groups in this cohort. In contrast, OPLS-DA was able to predict which patients, in the test data, belonged to the VGKC/GlyR group with 94.78 ± 0.80% accuracy, 99.76 ± 1.21% sensitivity, and 92.75 ± 2.21% specificity (p values all < 0.001, Kolmogorov-Smirnov) relative to controls (Figure 3-3c,d) and 94.75 ± 0.75% accuracy, 99.60 ± 1.39% sensitivity, and 93.11 ± 2.12% specificity (p values all < 0.001, Kolmogorov-Smirnov) relative to NMDAR/LGI1/CASPR2 positive patients (Figure 3-3e,f).

The metabolites perturbed in the VGKC and GlyR antibody psychosis patients were identified by inspection of the variable importance of projection (VIP) scores of the significant OPLS-DA models described above. Significant decreases were observed in several fatty acid resonances within serum lipoproteins ($-C\mathbf{H}_3$, $(-C\mathbf{H}_2\text{-})_n$, $\text{-N}(C\mathbf{H}_3)_3$, unsaturated fatty acid, $=C\mathbf{H}\text{-}CH_2\text{-}CH_2-$) while several amino acids (leucine, isoleucine, lysine, and valine) were increased in the VGKC and GlyR antibody patients (Figure 3-4, Table 3-2, p values all <0.001, one-way ANOVA with Tukey's post hoc test).

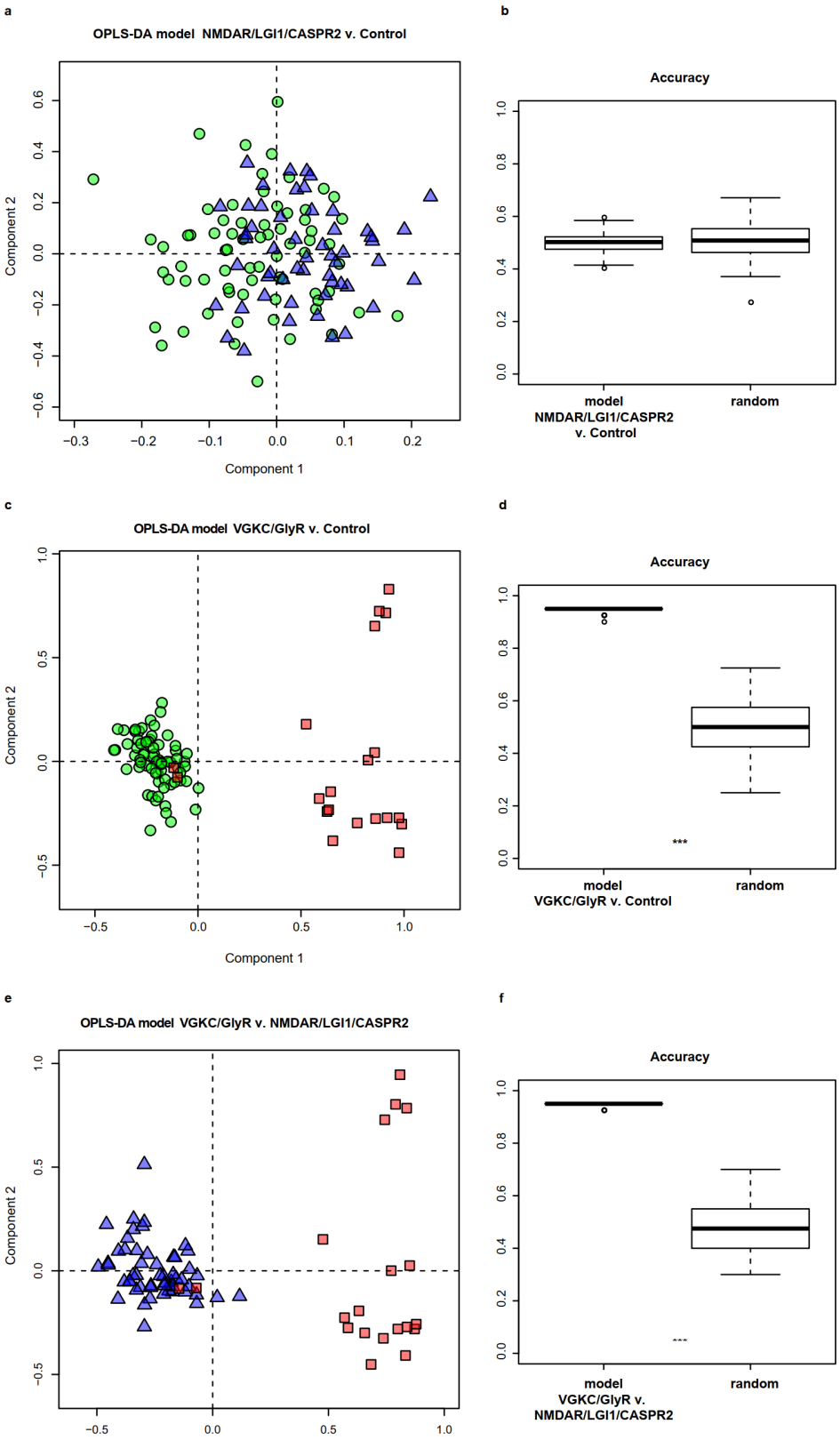

Figure 3-3 OPLS-DA models discriminating VGKC/GlyR (red square, *n* = 20) samples from NMDAR/LGI1/CASPR2 (blue triangle, *n* = 53) samples and Control (green circle, *n* = 70) samples using NMR serum metabolomic data.(a, c, e) OPLS-DA scores plots of NMDAR/LGI1/CASPR2 v. Control, VGKC&GlyR v. Control, VGKC/GlyR v. NMDAR/LGI1/CASPR2. (b, d, f) Predictive accuracy of the ensemble of the OPLS-DA models

compared with that of the randomly permutated null distribution. Kolmogorov-Smirnov test. ***$p < 0.001$

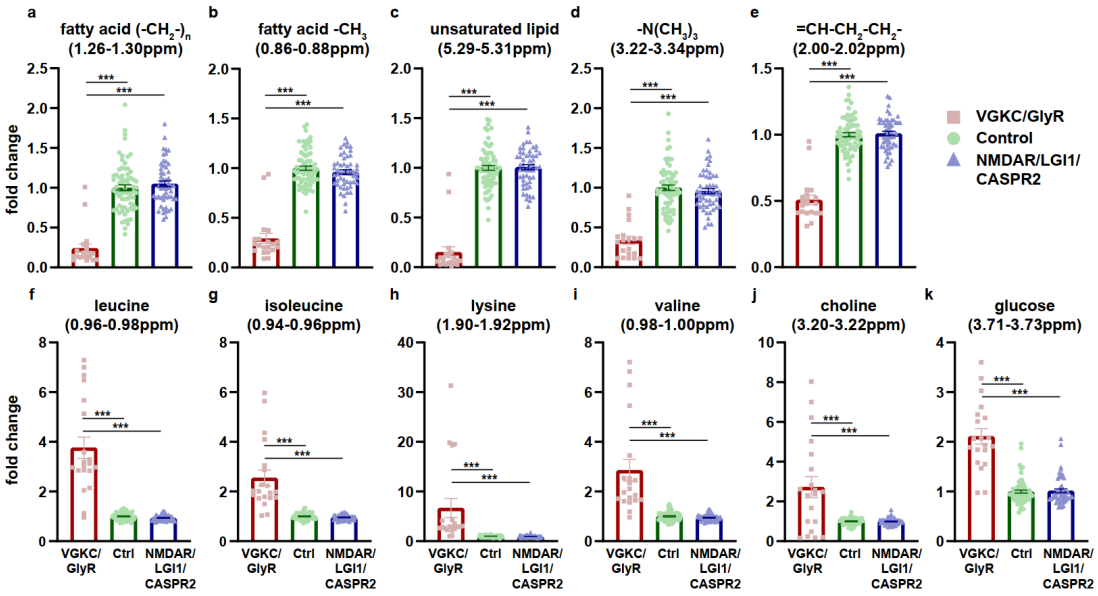

Figure 3-4 Levels of discriminatory serum metabolites selected by the OPLS-DA models in VGKC/GlyR (red, $n = 20$), control (green, $n = 70$), and NMDAR/LGI1/CASPR2(blue, $n = 53$) groups. (a–e) Decreased levels of several fatty acid resonances within serum lipoproteins (–CH3, (–CH2-)n, -N(CH3)3, unsaturated fatty acid, =CH-CH2-CH2–) in the VGKC/GlyR antibody group. (f–k) Increased levels of several amino acids (leucine, isoleucine, lysine, and valine), choline and glucose in the VGKC/GlyR antibody group. Error bars: ±SEM. One-way ANOVA with Tukey's post-hoc corrections. ***$p < 0.001$.

Table 3-2 Discriminatory metabolites selected from the OPLS-DA models of VGKC/GlyR vs Control and OPLS-DA models of VGKC/GlyR vs NMDAR/LGI1/CASPR2.

Discriminatory metabolites	Chemical shift of spectral bins (ppm)	VGKC/GlyR : Control (p value)	NMDAR/LGI1/CASPR2 : Control	VIP score (VGKC/GlyR vs Control)	VIP score (VGKC/GlyR vs NMDAR/LGI1/CASPR2)
fatty acid (-CH_2-)$_n$ Chyl/VLDL	[1.26, 1.30]	0.24 (<0.0001)	1.05	3.41	3.52
fatty acid -CH_3 HDL/LDL	[0.86, 0.88]	0.29 (<0.0001)	0.96	3.24	3.07
leucine	[0.96, 0.98]	3.76 (<0.0001)	0.94	3.00	2.99

Discriminatory metabolites	Chemical shift of spectral bins (ppm)	VGKC/GlyR : Control (p value)	NMDAR/LGI1/CASPR2 : Control	VIP score (VGKC/GlyR vs Control)	VIP score (VGKC/GlyR vs NMDAR/LGI1/CASPR2)
choline	[3.20, 3.22]	2.72 (< 0.0001)	0.99	2.83	2.84
-$N(CH_3)_3$	[3.22, 3.24]	0.34 (< 0.0001)	0.96	2.48	2.44
isoleucine	[0.94, 0.96]	2.55 (< 0.0001)	0.95	2.04	2.05
lysine	[1.90, 1.92]	6.68 (< 0.0001)	0.97	1.98	1.96
unsaturated lipid	[5.29, 5.31]	0.15 (< 0.0001)	1.01	1.90	1.89
valine	[0.98, 1.00]	2.86 (< 0.0001)	0.95	1.75	1.76
=CH-CH_2-CH_2-	[2.00, 2.02]	0.51 (< 0.0001)	1.01	1.70	1.69
glucose	[3.71, 3.73]	2.11 (< 0.0001)	1.01	0.65	0.44

The table shows fold changes of levels of metabolites selected from the OPLS-DA models and glucose. Metabolites shown above (except glucose) had a VIP score ≥ 1.7 (in the model of VGKC/GlyR vs Control) or ≥ 1.69 (in the model of VGKC/GlyR vs NMDAR/LGI1/CASPR2). The cut-off of VIP scores was decided based on the inflection point of the curve of VIP scores. The discriminatory metabolites in both models were identical, indicating they were metabolic signatures specific to VGKC/GlyR group.

Chyl, chylomicron. VLDL, very low-density lipoprotein. HDL, high density lipoprotein. LDL, low density lipoprotein. VIP, variable importance in projection. OPLS-DA, orthogonal partial-least square discriminant analysis.

3.3.4 Patients with Elevated Serum VGKC Antibody or GlyR Antibody Have Significantly Higher PANSS Ratings

To determine whether the metabolic disturbances identified in the VGKC and GlyR antibody patients were associated with a distinct clinical phenotype, the PANSS scores across these groups were investigated by comparing the median scores. VGKC and GlyR antibody patients had significantly higher PANSS totals than either the antibody negative or NMDAR, LGI1, CASPR2 antibody patients (both p values < 0.001, Kruskal-

Wallis test with Dunn's multiple comparisons test) (Table 3-3). In exploring the subscale scores, the VGKC/GlyR antibody had higher positive symptoms, negative symptoms, and general symptoms than the control patient groups (p values < 0.05, <0.05, and <0.001, respectively, Kruskal-Wallis test with Dunn's multiple comparisons test) (Table 3-3). In order to explore the possibility that the metabolic signature identified in the VGKC/GlyR group was a marker of severity of illness, a separate OPLS-DA model of high PANSS versus low PANSS (independent of antibody status) was built. This resulted in lower accuracy, sensitivity, and specificity of model, indicating that this metabolomic profile was not just a marker of illness severity (−30.82%, −28.91%, and −26.51% respectively).

Table 3-3 Comparison of PANSS scores of patients with VGKC/GlyR antibody, NMDAR/LGI1/CASPR2 antibody test, and antibody negative control groups.

	Ctrl	VGKC/GlyR	NMDAR/LGI1/CASPR2
Number of patients	70	19	53
Age (years), Median (IQR)	27 (15)	23 (8)	28 (15)
Gender, Female, no. (%)	31 (44.3)	8 (42.1)	21 (39.6)
PANSS, Median (IQR)			
Positive symptom score	6 (2.3)	9 (5)*	7 (3)
Negative symptom score	3 (3)	6 (6)*	3 (3)
General symptom score	2 (0)	5 (5)***	2 (0)†††
Total score	12 (6)	19 (8)***	12 (6)†††

The PANSS score for one VGKC/GlyR patient was not available and so was excluded from this table.

The Kruskal-Wallis test with Dunn's multiple comparisons test was used to identify significant differences of each class for numerical variables (age, PANSS scores) while Fisher's exact test was used for categorical variables. *indicates significant differences of each class compared to Ctrl. †indicates significant differences of each class compared to VGKC/GlyR. $^{*}p < 0.05$, $^{***}p < 0.001$. $^{\dagger\dagger\dagger}p < 0.001$.

Ctrl: control, psychosis patients tested negative for the following neuronal cell surface antibodies. VGKC/GlyR: voltage-gated potassium channel complex & glycine receptor; psychosis patients tested positive for either antigen. CASPR2, contactin associated protein-like 2; LGI1, leucine-rich glioma inactivated 1; NMDAR, N-methyl-D-aspartate receptor. NMDAR/LGI1/CASPR2: psychosis patients tested positive for CASPR2/LGI1/NMDAR. PANSS: Positive and Negative Syndrome Scale. IQR: Interquartile Range.

3.4 Discussion

Unsupervised and untargeted metabolomics analysis identified a biochemical signature of VGKC and GlyR antibody positive psychosis which consisted of decreased fatty acid lipoprotein levels along with increased leucine, isoleucine, valine, lysine, free choline, and glucose concentrations.

Serum lipoproteins are increasingly recognised to play a role in the immune system and active inflammation is commonly associated with decreased small lipoprotein particles such as high-density lipoproteins (HDL) and low density lipoproteins (LDL) coupled with an increase in triglyceride concentration and the larger, very low-density lipoprotein (VLDL) particles (Feingold & Grunfeld, 2000). In addition, pro-inflammatory cytokines have been shown to induce dyslipidaemia (Klingenberg et al., 2013) and lead to a reduction in HDL cholesterol (Haas & Mooradian, 2010). Finally, increasing LDL cholesterol concentration and improving HDL cholesterol efflux have been shown to improve C-reactive protein (CRP) associated inflammation in diseases such as rheumatoid arthritis (Liao et al., 2015; Robertson et al., 2017). Thus, the decrease in fatty acid lipoprotein signatures identified here are suggestive of increased inflammation in the VGKC and GlyR antibody-positive groups.

Elevated plasma concentrations of branched chain amino acids (BCAA) and lysine have been previously reported in people with schizophrenia (Meltzer, 1989) and elevated BCAA inhibit transport of dopamine and serotonin precursors (tyrosine and tryptophan, respectively) into the brain, which can lead to anxiety and mood disorders (Fernstrom, 1981; Koochakpoor et al., 2021). Elevated BCAA may also lead to insulin resistance (Lynch & Adams, 2014; Newgard, 2012) which is associated with first-episode psychosis (Fehsel & Löffler, 2017). The significant increase in glucose concentration observed here supports this and, along with the increased BCAA levels identified, may be associated with the increased PANSS scores observed in the VGKC and GlyR antibody positive patients.

Taken together, the metabolomics analysis suggests a distinct metabolomic phenotype

in VGKC and GlyR antibody positive patients which is associated with increased PANSS scores at presentation, and potentially increased inflammation, decreased neurotransmitter precursors and insulin resistance.

The finding of a distinct metabolomic and clinical phenotype associated with VGKC and GlyR antibodies was somewhat against the original hypothesis. The NSAb with the strongest evidence for pathogenicity are the NMDAR, LGI1, and CASPR2 antibodies, with substantial case report evidence that they have a direct effect on neuronal function and cause the expression of neuropsychiatric illness. Additionally, Chapter 2 has demonstrated the ability of metabolomics to differentiate AE patients associated with NMDAR, LGI1 and CASPR2 from DRE patients. Therefore, distinct metabolic profiles were expected in psychosis patients with these NSAb.

However, in spite of the accepted pathogenicity of these antibodies it has also been recognised, paradoxically, that classical measures of neuroinflammation may also be absent in these patients, whether that it in MRI scans, or in serum or CSF measures of inflammation (Dürr et al., 2021; Finke et al., 2013). The absence of a distinctive metabolomic profile in those with NMDAR/LGI1/CASPR2 serum antibodies in psychosis does not necessarily indicate that these antibodies are not having an effect in the brain in these patients.

VGKC and GlyR antibodies, by contrast, do not have such a strong literature to support their direct pathogenicity in neuropsychiatric disorders. A particularly influential paper, reviewing the presence of VGKC antibodies in the absence of LGI1 or CASPR2 antibodies in a clinical cohort at the Mayo clinic, found that the presence of the antibodies was not associated with an immunotherapy responsive illness (Klein et al., 2012; van Sonderen, Schreurs, Wirtz, et al., 2016). However, this clinical sample was of largely older people with a range of other degenerative diagnoses, and not comparable to a younger cohort of people without comorbidity. It is possible therefore, in these cases that the VGKC antibodies were a secondary, non-specific marker of neurodegeneration.

A further clinical study suggests that non-LGI1, non-CASPR2 VGKC antibodies are a

non-specific marker of an inflammatory brain condition in children. A series of patients were tested for antibodies, and separately rated according to clinical and paraclinical measures into having a likely inflammatory brain condition, or not. Of 39 patients with these VGKC antibodies, 30 were considered clinically to have an inflammatory condition. The probability of an inflammatory condition was raised with a higher titre of the antibody (Hacohen et al., 2015). There are further case reports of those with atypical dementia or pain syndromes and VGKC antibodies that are responsive to immunotherapy, suggesting that these antibodies may be a marker of an inflammatory condition (Prüss & Lennox, 2016). Further work is now required to investigate the biological function and relevance of titre level of these antibodies in psychosis.

GlyR is a glycine-gated chloride ion channel typically expressed on the surface of motor neurons in the brainstem and spinal cord, regulating neuronal excitability. GlyR is also found in the human hippocampus, but its role here is less clear (Xu & Gong, 2010). GlyR antibodies were first described in progressive encephalopathy with rigidity and myoclonus (PERM) (Hutchinson et al., 2008), and not previously described in association with psychiatric presentations (Swayne et al., 2018).

Taken together, it is likely therefore that these antibodies are acting as non-specific markers of a possible inflammatory aetiology in these patients, rather than indicating a more specific VGKC or GlyR pathology.

The association between the GlyR and VGKC antibodies and higher PANSS ratings overall indicates patients with these antibodies are less responsive to antipsychotic medication. The finding of greater negative symptoms in this group is in keeping with the notion that negative symptoms are the result of neuroinflammation, with inflammatory stimuli decreasing neural activity in the ventral striatum, decreasing connectivity in reward pathways, and resulting in a lack of motivation in patients (Feingold & Grunfeld, 2000).

There are limitations to this study. As this was a pilot study and a number of different antibodies were included, the numbers in each group were small. There was no

significant difference in any of the potential confounders investigated (age, gender, ethnicity, episode type). Nonetheless, the effect of each potential confounder on the multivariate model was investigated and it was further confirmed that neither age, gender, ethnicity, nor episode type were contributing factors to the models (Figure 3-2).

Prescribed medication was not recorded in participants recruited after 2016 and it is possible that this could affect the metabolomic profile seen. However, in the samples collected prior to 2017 almost all patients were prescribed atypical antipsychotics, in keeping with usual clinical practice in UK. It is a reasonable assumption that similarly the later patients were also all prescribed an atypical antipsychotic. There would be no reason why those with antibodies would systematically be given a different medication, although this cannot be definitely proven.

The samples were all collected in the same brand of serum separator tube that was supplied by the study team, and the samples were assessed by the same researcher for the presence of antibodies, reducing the chance of any systematic bias. The samples were sent at room temperature to the study team. This led to a delay of a day or two before the samples were processed. This delay likely led to a degradation of samples, and a consequent lack of sensitivity to detect some metabolites. Additionally, motor symptoms were not measured in the patients to know whether there were any correlates with the GlyR antibodies. Finally, as no other psychiatric or neurological groups were included in this study, it is not possible to say whether this pattern is distinct in psychosis, or not.

These limitations do not detract from the main finding of a biochemically distinct subgroup of patients with first episode psychosis that is associated with higher PANSS scores and VGKC and GlyR antibody positivity, which indicates a potential inflammatory aetiology for a proportion of patients and gives the potential for different treatment approaches for these patients. Further work is now required to validate the biomarkers identified in a larger, prospective cohort and assess the performance of the multivariate diagnostic model to other inflammatory diseases of the central nervous system and routinely used inflammatory markers.

In conclusion, this chapter has demonstrated a distinct metabolic profile of a subgroup of patients with acute psychosis who have a more severe illness. This is particularly exciting, because it is these patients, resistant to current antipsychotic medication, that are in particular need of new therapeutic approaches. If confirmed, these findings could therefore lead to the trial of novel targeted treatments on the basis of individuals' metabolomic profile.

Chapter 4: Sodium Fluoride Preserves Blood Metabolite Integrity for Biomarker Discovery in Large-scale, Multi-site Metabolomics Investigations.

The data in this chapter has been published as: Xiong W, Anthony DC, Anthony S, Ho TBT, Louis E, Satsangi J, Radford-Smith DE. Sodium fluoride preserves blood metabolite integrity for biomarker discovery in large-scale, multi-site metabolomics investigations. *Analyst*. 2024 Feb 12;149(4):1238-1249. doi: 10.1039/d3an01359f.

4.1 Introduction

Chapters 2 and 3 demonstrated the utility of blood NMR metabolomics to identify patients with AE and psychosis associated with VGKC or GlyR antibodies, showcasing its potential as a diagnostic tool. However, translating these findings into robust clinical biomarkers requires validation in large, multi-centre cohorts (Vuckovic, 2012). A significant challenge in such studies is preserving metabolite integrity in samples, which can be compromised by preanalytical variations. Factors such as centrifugation speed and time (Jobard et al., 2016), incubation temperature (Alexander et al., 2023; Santos Ferreira et al., 2019b; P. Yin et al., 2013), the type of collection tube (Sotelo-Orozco et al., 2021b; Vignoli et al., 2022), and the number of freeze-thaw cycles (Fliniaux et al., 2011b; Muti et al., 2023; Pinto et al., 2014b; P. Yin et al., 2013) are just some of the pre-analytical variables known to influence metabolite composition in blood. Among these, the time between blood collection and erythrocyte separation, as well as the delay to sample storage at -80 °C, presents unique challenges in large, multi-centre clinical trials, where logistical constraints often limit strict adherence to pre-defined protocols (Alexander et al., 2023; Anton et al., 2015b; Ellervik & Vaught, 2015). These two factors have been shown to drastically influence the relative abundance of metabolites involved in glycolysis (Bernini et al., 2011; Brunius et al., 2017; Debik, Isaksen, et al., 2022; Fliniaux et al., 2011b; Fomenko et al., 2022b; Jobard et al., 2016; McClain et al., 2021;

Peakman & Elliott, 2008b; Pinto et al., 2014b; Santos Ferreira et al., 2019b; *P.* Yin et al., 2013), as well as other metabolite classes such as lipoproteins, although evidence for the latter remains inconsistent (Debik, Isaksen, et al., 2022; Pinto et al., 2014b). Despite evidence highlighting the influence of these delays, the effect of blood tube type on metabolite stability under delayed centrifugation conditions has yet to be investigated.

Ideally, standard operating procedures (SOPs) are, prospectively, put in place in advance of longitudinal, multicentre research projects to reduce pre-analytical variability in metabolite levels within and between biobanks. In practice, this may be difficult to achieve depending on the scale and resources of individual collection sites. Previous studies have demonstrated conflicting efficacy of keeping blood tubes refrigerated at 4 °C prior to centrifugation, aliquoting, and freezing on the variability in metabolite levels (Alexander et al., 2023; Fliniaux et al., 2011b; Peakman & Elliott, 2008b). Moreover, a secure cold chain may not be feasible in all sites, and the level of compliance to SOPs is unclear and is often left unreported. Most importantly, all previous studies addressing these pre-analytical variables treated all samples identically when varying time to erythrocyte separation and time at room temperature (RT). Therefore, it is largely unsurprising that, in at least one analytical dimension, inter-individual differences are maintained. In practice, this identical treatment of individual differences does not occur; samples may be processed at any time between, for example, 0 and upwards of 24 hours.

Guidelines on how to prepare samples and observations on the effects of delayed erythrocyte separation are insufficient to advance methods of reducing biomarker variability for NMR. Similarly, *z*-scoring of metabolite concentrations to facilitate comparisons across cohorts (Barrios et al., 2018; Buergel et al., 2022) impedes the discovery of healthy and disease-associated metabolite ranges that may be clinically relevant. Practical solutions to stably preserve blood metabolite levels are required, and clear reporting guidelines are required to explain potential non-biological between-sample variability.

This chapter addresses these challenges by systematically evaluating the relative efficacy of sodium fluoride/potassium oxalate (FX), lithium heparin (LH), and additive-free serum blood tubes in preserving metabolite integrity under delayed processing conditions. Specifically, it investigates the impact of delays of up to 24 hours before centrifugation and up to 48 hours before sample measurement after NMR sample preparation, with the expectation that sodium fluoride/potassium oxalate tubes, which inhibit glycolysis, would better preserve the metabolic state at the time of blood collection compared to lithium heparin or serum vacutainers. To provide broader context, the chapter also examines global NMR-based metabolite variability across biobanks, including large-scale resources such as the UK Biobank and TwinsUK, as well as biobanks from multicentre clinical trials focused on inflammatory bowel disease (IBD). Finally, the blood metabolome of 12 healthy adult volunteers was analysed to compare the effects of different blood tube types and pre-processing parameters, aiming to determine the optimal tube type for preserving an individual's blood metabolomic fingerprint under significantly delayed processing conditions.

4.2 Methods

4.2.1 UK Biobank

The UK Biobank is a general population cohort recruited from 22 assessment centres across England, Scotland, and Wales between 2006 and 2010 (*UK Biobank*, 2024). It comprises 502,411 individuals of middle and old age (mean 56.5 years, range 37-73 years). Written, informed consent was provided by all participants. The UK Biobank has generic ethical approval from the Northwest Multi-centre Research Ethics Committee (ref 11/NW/03820). The current study is registered under the approved research ID 95409. At the time of this study, NMR metabolomic data was available on ~120,000 participants. Individuals were typically non-fasting prior to blood sampling (median fasting time 3 hours, standard deviation 2.4 hours). Whole blood was collected into spray-coated K_2EDTA tubes and immediately centrifuged at 2,500 × *g* for 10 minutes at 4 °C. Plasma was not aliquoted. Rather, tubes were transported to a central storage

facility at 4 °C for aliquoting and archiving at -80 °C (mean time from venepuncture to freezing 24 hours, standard deviation 2.5 hours) (Allen et al., 2021). Acquisition of NMR metabolite data was performed by Nightingale Health Ltd, with detailed methods described in (Julkunen et al., 2023).

4.2.2 TwinsUK

TwinsUK is a volunteer twins cohort in the United Kingdom (Moayyeri et al., 2013). Generic ethic approval was obtained from Guys & St Thomas' Trust ethics committee. At the time of this study, NMR metabolomic data was available on ~2,000 female individuals across up to three timepoints (total samples 4,830) collected between 1996 and 2014. The mean age at blood sampling was 59.4 years (range 34-88 years). Samples were collected after a minimum fast of 6 hours into serum separator blood tubes (BD Vacutainer® SST™). The tubes were then allowed to rest after 3-time inversions for 40 minutes at 4 °C. Samples were centrifuged for 10 minutes at 1,439 × *g*. Serum was collected immediately and stored at -45 °C (Yu et al., 2012). Acquisition of NMR metabolite data was performed by Nightingale Health Ltd, with detailed methods described in (Barrios et al., 2018).

4.2.3 STORI

The STORI trial (2006 - 2009) investigated the risk of relapse in Crohn's disease after cessation of infliximab in patients who had achieved prolonged remission on combination therapy: infliximab alongside antimetabolites (Louis et al., 2012). Patients with a baseline serum aliquot available for analysis were included in the study ($n = 97$).

4.2.4 SPARE

The SPARE trial (2015 - 2021) sought to evaluate three treatment approaches for Crohn's disease patients in steroid-free remission due to combined infliximab and immunosuppressant therapy: maintaining the combination, continuing only the immunosuppressant, or continuing only infliximab (Louis et al., 2023). A subgroup of patients from the SPARE trial who had been randomised to infliximab withdrawal and

had a baseline serum aliquot available were included for analysis ($n = 63$).

In both STORI and SPARE, biomarkers associated with relapse was a pre-defined secondary endpoint. Blood was collected into BD Vacutainer SST II Advance Tubes (BD 367958), allowed to clot, and centrifuged at room temperature for 10 minutes at 3,000 *g*. The target for clotting time at room temperature was between 0.5 and 2 h, and the target time-to-freezing of serum aliquots was within 4 hours of the blood draw. Serum aliquots were then stored at -80 °C. All patients provided informed consent and ethical approval was obtained. All patients had been treated with a combination therapy of infliximab (IFX) and anti-metabolite > 8 months and had been in sustained steroid-free remission > 6 months. Patients were not fasted prior to blood collection.

4.2.5 Healthy Volunteers and Controlled Variation of Pre-analytical Parameters

12 healthy volunteers were recruited from Oxford, UK (mean age 30.3 years, range 23-53 years). Blood was collected under informed written consent. Local ethical approval was obtained from the University of Oxford Medical Sciences Interdivisional Research Ethics Committee.

Blood was collected into BD Vacutainer blood tubes under the conditions described in Table 4-1. Vacutainer tubes were centrifuged initially at 300 × *g* for 10 minutes at 4 °C. After the supernatant (either serum or plasma) was carefully collected into a new tube, the sample was again centrifuged at 5,000 *g* for 10 minutes at 4 °C and the supernatant collected into a new tube and stored at -80 °C prior to sample preparation.

Table 4-1 Summary of pre-analytical parameters in the healthy volunteer cohort. n = 12 per condition.

Tube	Time to centrifugation, h (temperature)	Delay between sample preparation and measurement, h (temperature)
Serum (Red, BD 367837)	0.5 (RT)	0 (RT), 12 (4 °C), 24 (4 °C), 48 (4 °C)
	24 (RT)	0 (RT)
	24 (4 °C)	0 (RT)
Lithium Heparin Plasma	0.5 (RT)	0 (RT), 12 (4 °C), 24 (4 °C), 48 (4 °C)

(Green, BD 367885)	24 (RT)	0 (RT)
	24 (4 °C)	0 (RT)
Fluoride/Oxalate Plasma (Grey, BD 368921)	0.5 (RT)	0 (RT), 12 (4 °C), 24 (4 °C), 48 (4 °C)
	24 (RT)	0 (RT)
	24 (4 °C)	0 (RT)

4.2.6 NMR spectroscopy

NMR spectroscopy and global metabolite quantification from serum and plasma was performed in-house for the SPARE, STORI, and healthy volunteer cohorts. On the day of NMR spectroscopy, serum or plasma samples were thawed at room temperature, mixed by pipetting, and combined with 75 mM sodium phosphate buffer prepared in D_2O (pH 7.4) as a 1:5 ratio of serum to buffer (total volume 600 µL) in a 5 mm borosilicate glass NMR tube (Norell 502–7).

NMR experiments and spectral processing were conducted as previously described in Section 2.2. 1D NOESY and CPMG-PROJECT experiments were conducted on each sample, and CPMG-PROJECT spectra were used for downstream analysis.

The NMR spectra were segmented into 100 integral regions using a manual binning approach, with exclusion of noise and water signals. Metabolite peaks were integrated carefully to minimise overlapping and were aligned with literature assignments.

Resonances were assigned to metabolites using a combination of literature values and 2D spectra of human plasma and serum, leading to the confident identification of 39 metabolites. Spectral regions with overlapped metabolites were annotated in the assignment using a '/' and '[]' notation. The absolute integral values were subject to the main statistical analysis unless stated otherwise. Additional statistical analyses using probabilistic quotient normalisation (PQN) and sum normalisation were also performed. In the healthy control cohort, lactate and glucose levels were also calculated based on the absolute millimolar concentration using a standard curve.

4.2.7 Statistical Analysis

After pareto scaling of the absolute integral values, PCA was performed using the *ropls* package to visualise and compare individual metabolite profiles in an unsupervised fashion (Thévenot et al., 2015a). *Post-hoc* analysis of TwinsUK, STORI, and SPARE NMR data was limited to univariate *t*-testing of glucose and lactate metabolite levels, based on inspection of the corresponding PCA loadings plots. UK Biobank NMR metabolite data were further correlated against time of day of blood collection, fasting time, and delay in sample measurement using Pearson's correlation. In the healthy control cohort, individual metabolites (39 identified metabolites) were subject to repeated measures two-way ANOVA with Šidák *post hoc* test (Singmann et al., 2015), and Benjamini–Hochberg method was used for *p* value adjustment to control the false discovery rate across all metabolites. Adjusted two-tailed *p* values (*q* values) ≤ 0.05 were considered statistically significant. * $p \leq 0.05$, ** $p \leq 0.01$, *** $p \leq 0.001$.

4.3 Results

4.3.1 Lactate and Glucose Drive Metabolite Variation Between and Within Biobanks.

NMR metabolite data was collated between the UK Biobank and TwinsUK cohorts. As the TwinsUK cohort is predominately female sex, a female cohort from the UK Biobank (n = 4,830) was randomly sampled for comparison. Principal component analysis revealed greater variation in the metabolome within the UK Biobank cohort compared to the TwinsUK cohort along the first principal component, as well as systematic variation between the two biobanks along the same component (Figure 4-1A). Inspection of the corresponding loadings plot revealed the key role of lactate in driving this variation along the first principal component, and glucose in driving within-biobank variation along the second principal component (Figure 4-1B).

Lactate levels were increased in the UK Biobank cohort (mean 3.7) relative to the TwinsUK cohort (mean 1.37; mean difference 2.36 [Welch's *t*-test 95% CI 2.33-2.40], *p*

value < 0.0001, Figure 4-1C). Glucose levels were decreased in the UK Biobank cohort (mean 3.48) relative to the TwinsUK cohort (mean 3.76; mean difference 0.29 [Welch's *t*-test 95%CI 0.26-0.31], *p* value < 0.0001, Figure 4-1D). Analysis of available metadata from the UK Biobank revealed systematic linear variation in plasma lactate (Pearson's r = -0.26, n = 118,021, *p* value < 0.0001, Figure 4-1E) and glucose (Pearson's r = 0.16, n = 118,021, *p* value < 0.0001, Figure 4-1F) levels according to the time of sample collection. This may correspond to a systematic delay between sample collection and centrifugation according to queued collected samples. Samples collected earlier in the day likely had a delayed processing time as compared to samples collected later in the day.

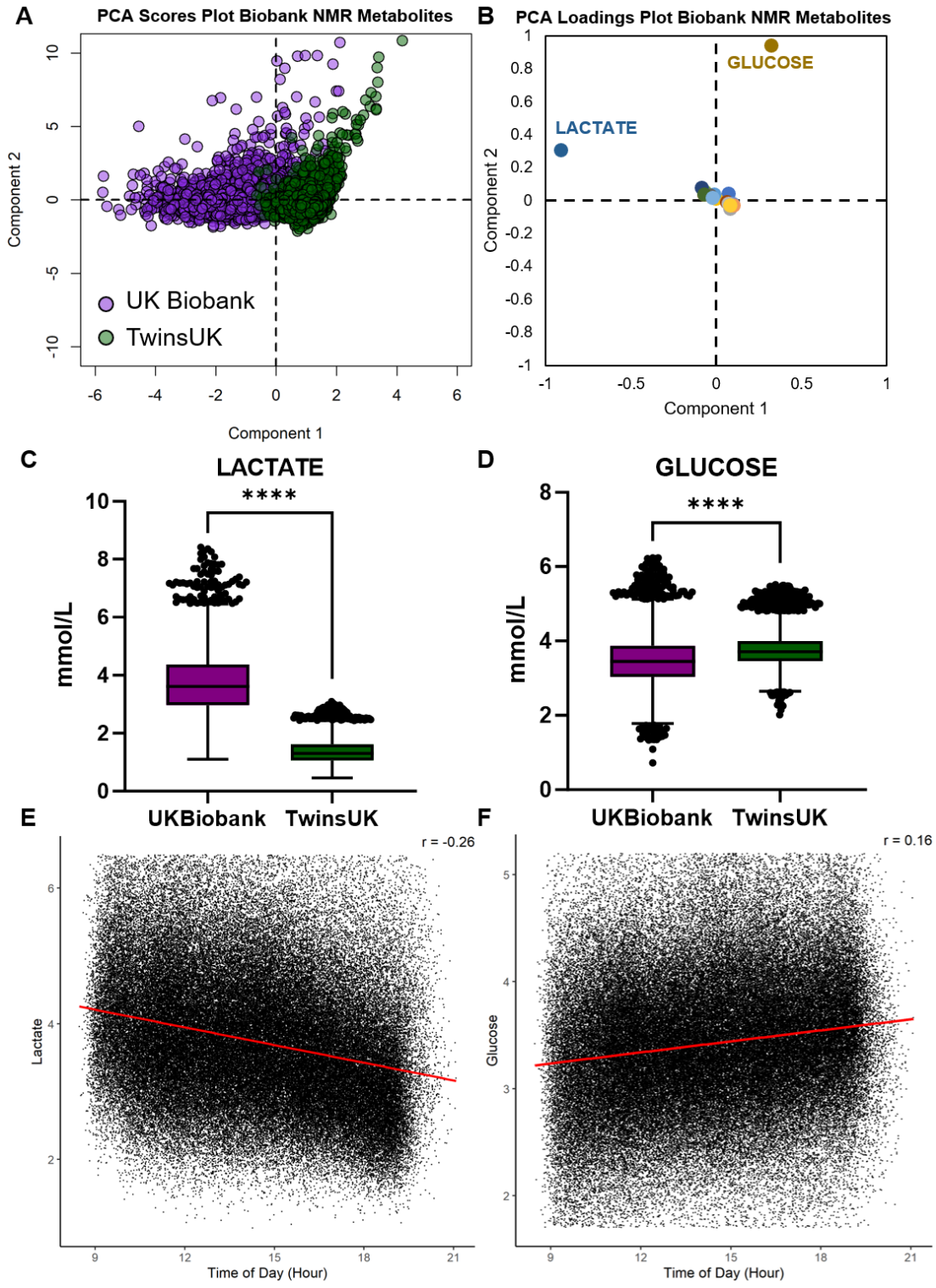

Figure 4-1 Lactate and glucose levels drive variation in the blood metabolome within and between biobanks. (A) PCA plot and (B) corresponding loadings plot of TwinsUK and sampled female UK Biobank participants with blood metabolomics data. (C, D) Boxplots comparing lactate (C) and glucose (D) levels in participants between the UK Biobank and TwinsUK study indicate systematically elevated lactate levels and decreased glucose levels in the UK Biobank, both $p < 0.0001$. (E, F) Pearson correlation between time of day of sample collection and lactate or glucose concentration in the UK Biobank samples, both $p < 0.0001$.

As a second example, and on a smaller scale, lactate and glucose were also found to drive serum metabolome variation between clinical biobank data pertaining to the SPARE and STORI cohorts (Figure 4-2). Here, data acquisition and relative metabolite quantification were performed in-house. The PCA scores plot (Figure 4-2A) and corresponding loadings plot (Figure 4-2B) illustrate systematic variation in lactate and glucose levels along the second principal component. Glucose levels were decreased in the STORI cohort (mean 0.0058) relative to the SPARE cohort (mean 0.011; mean difference 0.0055 [Welch's *t*-test 95%CI 0.0046-0.63], p value < 0.0001). Lactate levels were increased in the STORI cohort (mean 0.13) relative to the SPARE cohort (mean 0.053; mean difference 0.073 [Welch's *t*-test 95%CI 0.064-0.082], p value < 0.0001). These differences are visualised in the median NMR spectrum of each cohort (Figure 4-2E).

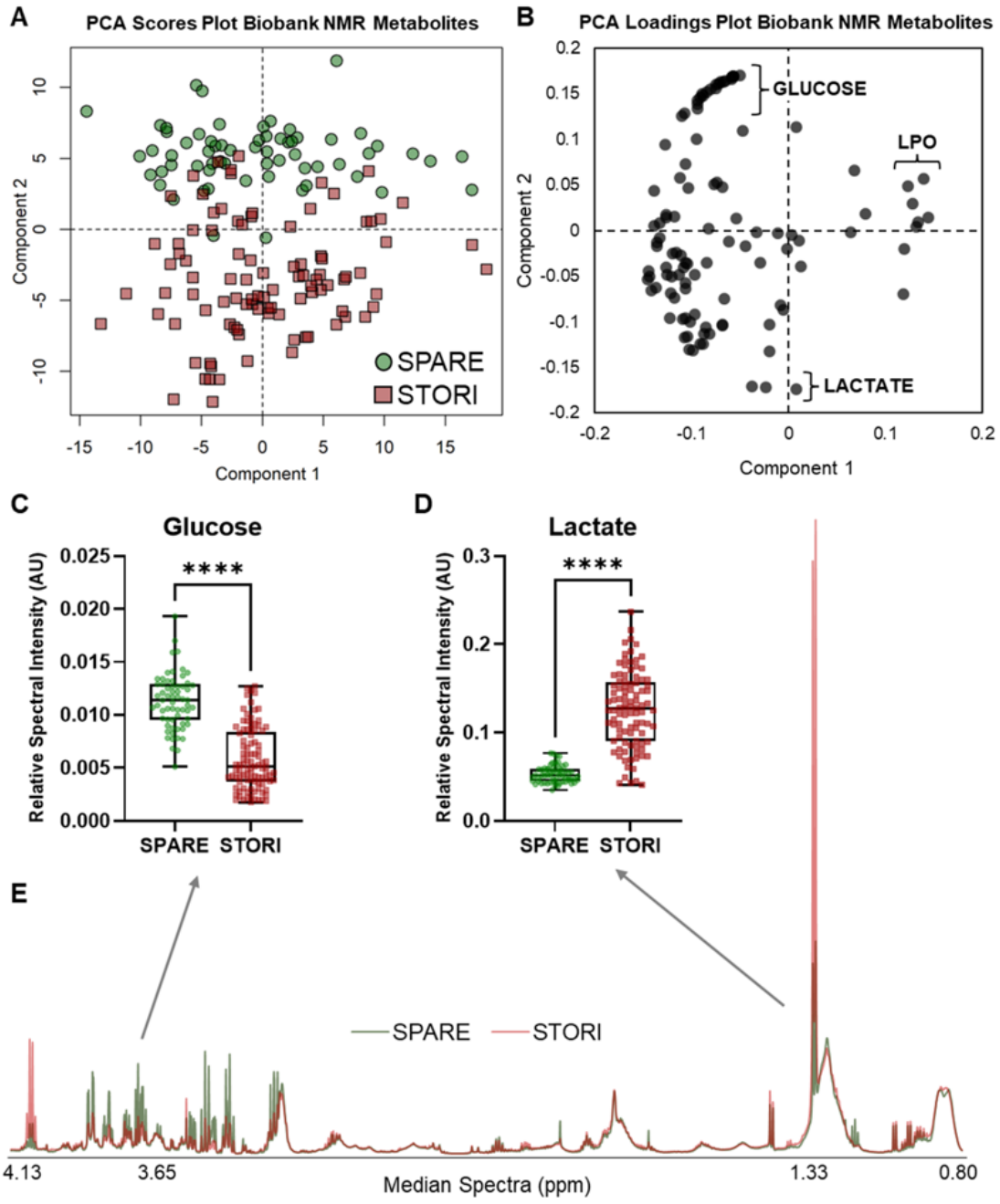

Figure 4-2 Lactate and glucose levels contribute to blood metabolite variation between discovery and validation cohorts in clinical trials. (A) PCA plot and (B) corresponding loadings plot of the SPARE and STORI participant baseline serum metabolomics data. (C, D) Variation between cohorts is driven by serum glucose and lactate resonances, both $p < 0.0001$. (E) Median NMR spectrum of SPARE and STORI samples.

4.3.2 Effects of Delayed Sample Measurement on Absolute Plasma and Serum Metabolite Concentrations.

UK Biobank metabolomic metadata was used to determine the effect of time between

sample preparation and measurement on plasma metabolite levels. Approximately 25% of samples were run within 12 hours of sample preparation, 63% within 24 hours, and 97% within 48 hours (Figure 4-3A). The top six metabolites had a Pearson correlation coefficient > 0.1 ($p < 0.0001$) and are shown in Figure 4-3B-G. Plasma histidine concentration showed a strong negative correlation with time to sample preparation (Pearson's $r = -0.36$, Figure 3B). Glycine ($r = -0.14$), glutamine ($r = -0.13$), phenylalanine ($r = -0.09$), citrate ($r = -0.10$) were also negative correlated with time to sample preparation, while free cholesterol in intermediate density lipoprotein ($r = 0.10$) was positive correlated (Figure 4-3C-G, respectively).

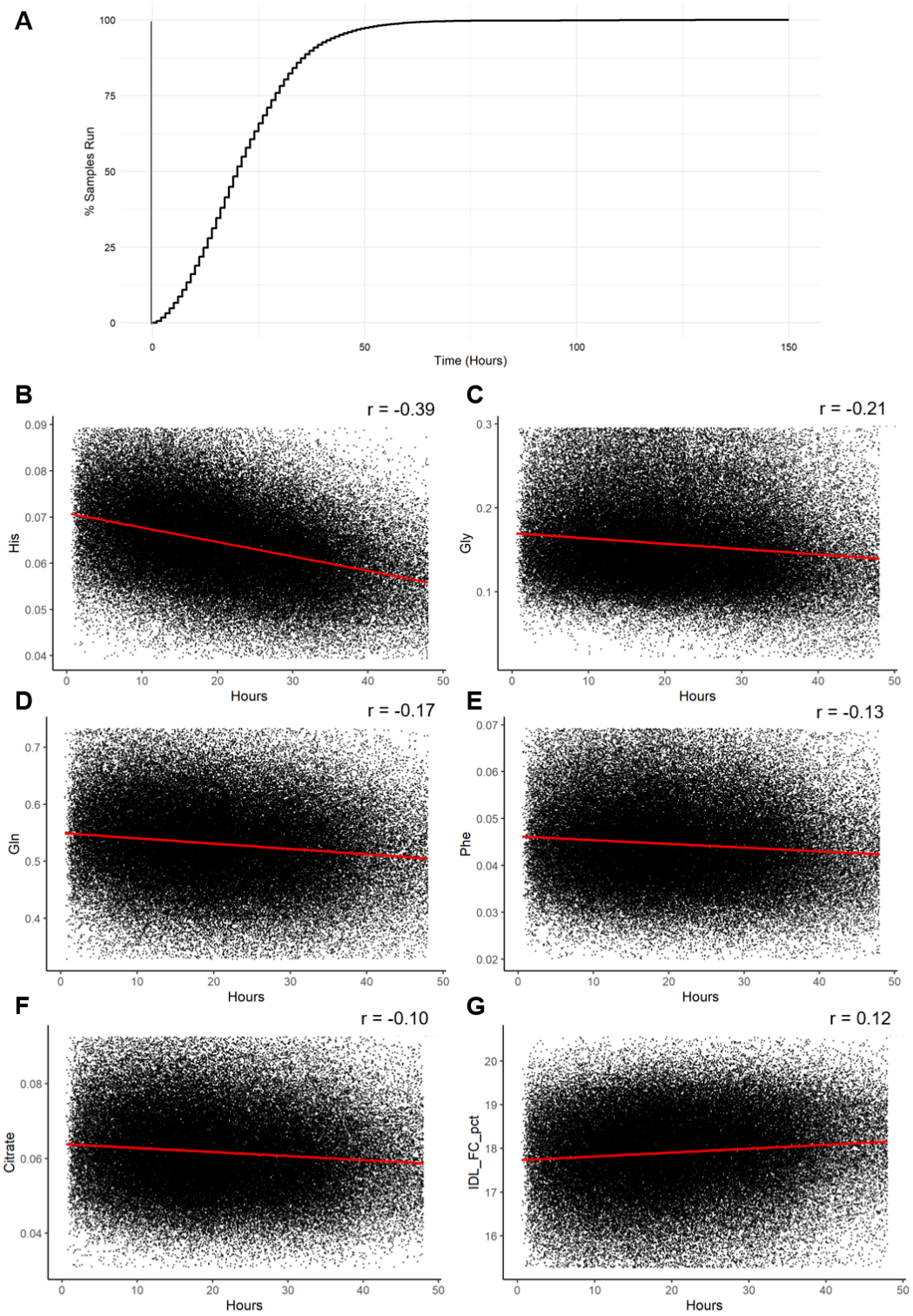

Figure 4-3 Histidine is the metabolite predominately affected by delayed sample measurement in the UK Biobank. Line graph indicating the percentage of plasma samples analysed by NMR once prepared for analysis, within a given timeframe (A). Pearson correlation between time to sample measurement by NMR and histidine (B), glycine (C), glutamine (D), phenylalanine (E), citrate (F), and IDL_FC_pct (Free cholesterol to total lipids ratio in intermediate density lipoproteins)(G), all $p < 0.0001$.

In the healthy control cohort (n = 12 per condition), delayed sample measurement

resulted in detectable changes in the metabolome (Figure 4-4). Consistent with data from the UK Biobank, the effect of delayed sample measurement was small relative to interindividual variation. Most samples shifted in the second component in the PCA scores plot, driven by decreased levels of glucose, high-density lipoprotein (HDL) and glycerophosocholine. The stability of the serum/plasma metabolome was maintained even after a 12-hour delay in NMR measurement, as demonstrated by minimal changes in metabolite levels (Figure 4-5). However, when LH Plasma samples were subjected to a 24-hour delay in measurement, a significant decrease was observed in 31 out of 39 metabolites (repeated measures two-way ANOVA with Šidák post hoc test). Notably, it was observed that LH Plasma samples started forming precipitates after 12 hours, and all samples exhibited precipitates after 24 hours. In contrast, Serum and FX Plasma demonstrated better stability than LH Plasma after a 24-hour and even 48-hour delay in measurement as indicated by changes in percentages of most metabolites below 10% and significant alterations observed in only a few metabolites. The majority of metabolites showed a decreasing trend resulting from the delay in measurement, except for glutamate, which tended to increase over time, particularly in FX Plasma (Figure 4-5). Albumin, phosphocholine, glycerophosphocholine and glucose levels significantly decrease after 24 hours in at least two types of plasma/serum samples. Aligning with the observations in the UK Biobank dataset, histidine and glutamine levels tend to decrease over time, especially after 24 hours in LH Plasma (Figure 4-5).

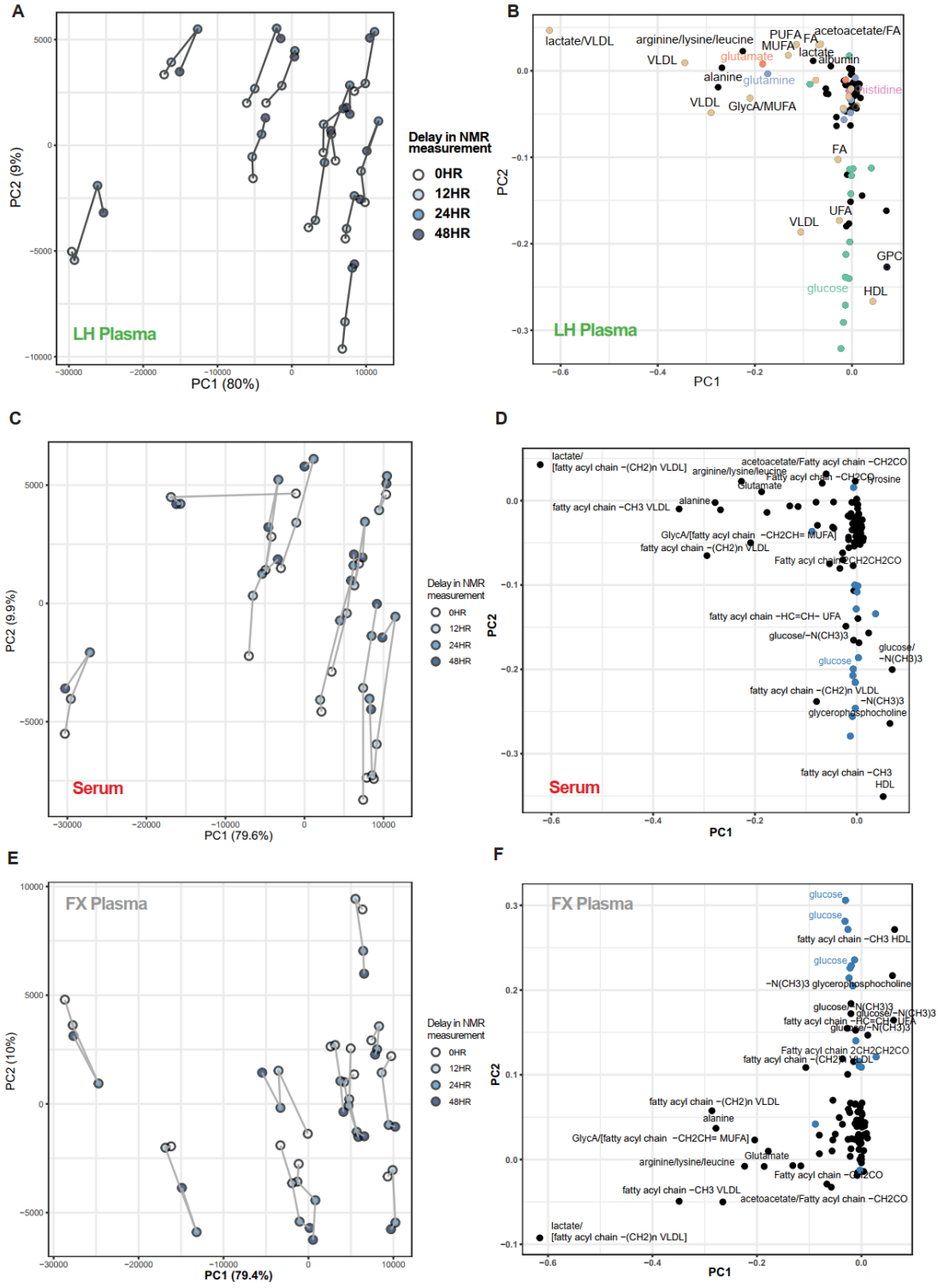

Figure 4-4 Variation in the metabolome due to delayed sample measurement is small compared to interindividual variation in the healthy control cohort. PCA scores plot (A) demonstrating the effect of delayed NMR measurement on LH plasma samples (A), serum (C), and FX (E). Each line connects samples from the same individual. Loadings plot (B, D, F) illustrating the metabolites that contribute to the variation observed in principal component 1 and 2.

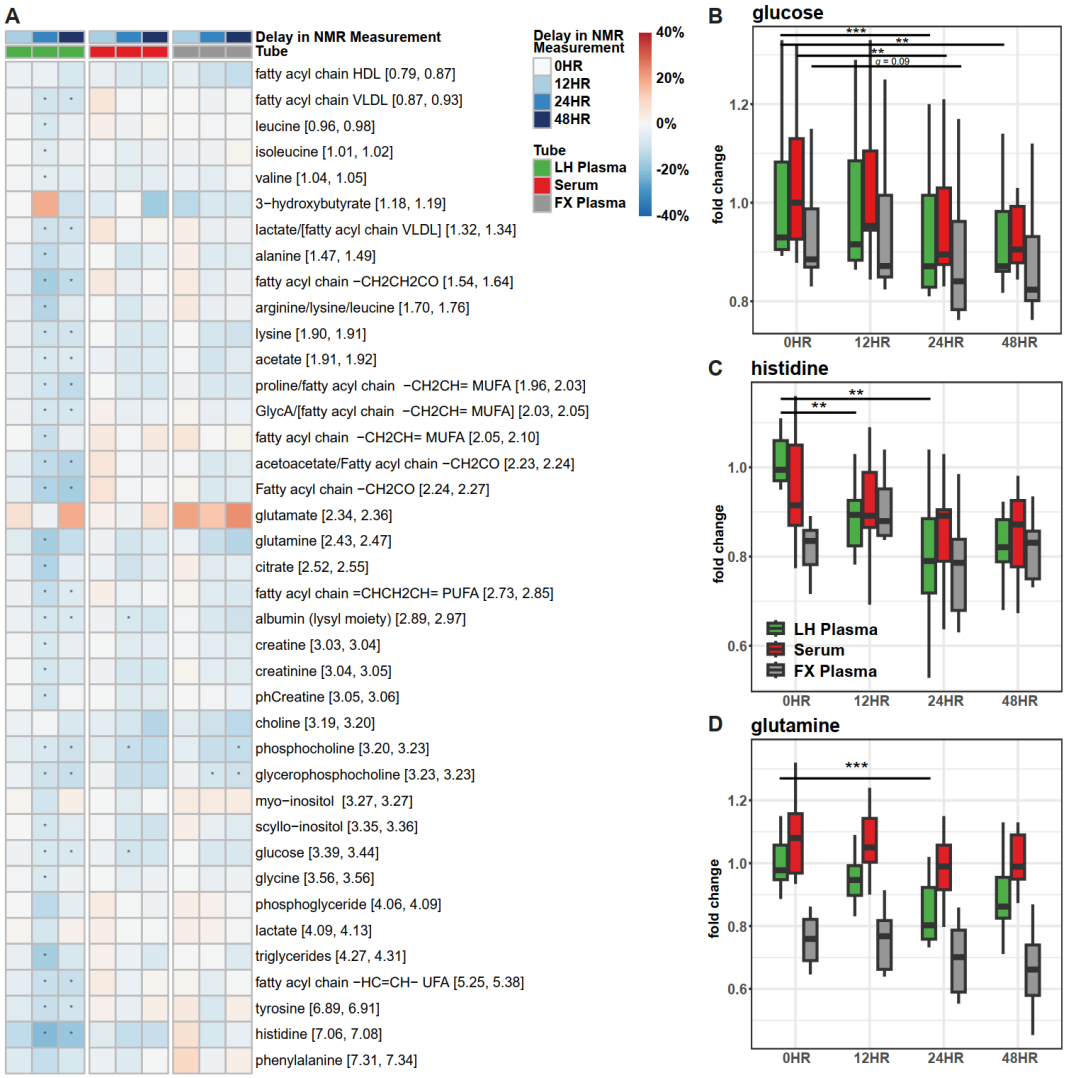

Figure 4-5 Effects of delayed sample measurement on metabolites. (A) Heatmap displaying percentage changes in metabolite levels resulting from varied delays in NMR measurement across three types of plasma/serum. The numbers in square brackets represent the corresponding spectral region boundaries in parts per million (ppm). Percentage changes calculated from absolute integral values and compared to the optimum processing condition. Significant differences in means of metabolites were represented by * ($q < 0.05$). (B-D) Boxplots presenting the effect of delayed NMR measurement on levels of histidine, glutamine, and glutamate. "/" indicates the mentioned metabolites are overlapped in the spectral region. Metabolite names in square brackets refers to non-dominant overlapping metabolites also found in that spectral region.

4.3.3 Metabolite Differences by Tube Type Using Optimal Processing Parameters in the Healthy Control Cohort.

The abundances of metabolites were then investigated to determine how they differed between BD Vacutainers under optimal processing conditions. Absolute metabolite concentrations of LH plasma (green) and serum (red) tubes were comparable (Figure

4-6). In contrast, the total integral of the spectra (spectral intensity) from FX plasma (grey) was reduced in both the NOESY and CPMG experiments due to the decline in albumin and lipoprotein levels in FX plasma (Figure 4-6). When using a PQN or sum-normalised approach to adjust for the total integral between samples and make FX plasma comparable, few differences remained between tube types. Branched chain amino acids (BCAAs, including leucine, isoleucine, valine) were increased in FX tubes relative to LH plasma and serum. And 3-hydroxybutyrate levels increased in FX plasma compared to LH plasma and serum, potentially influenced by variations in the lipoprotein line shape.

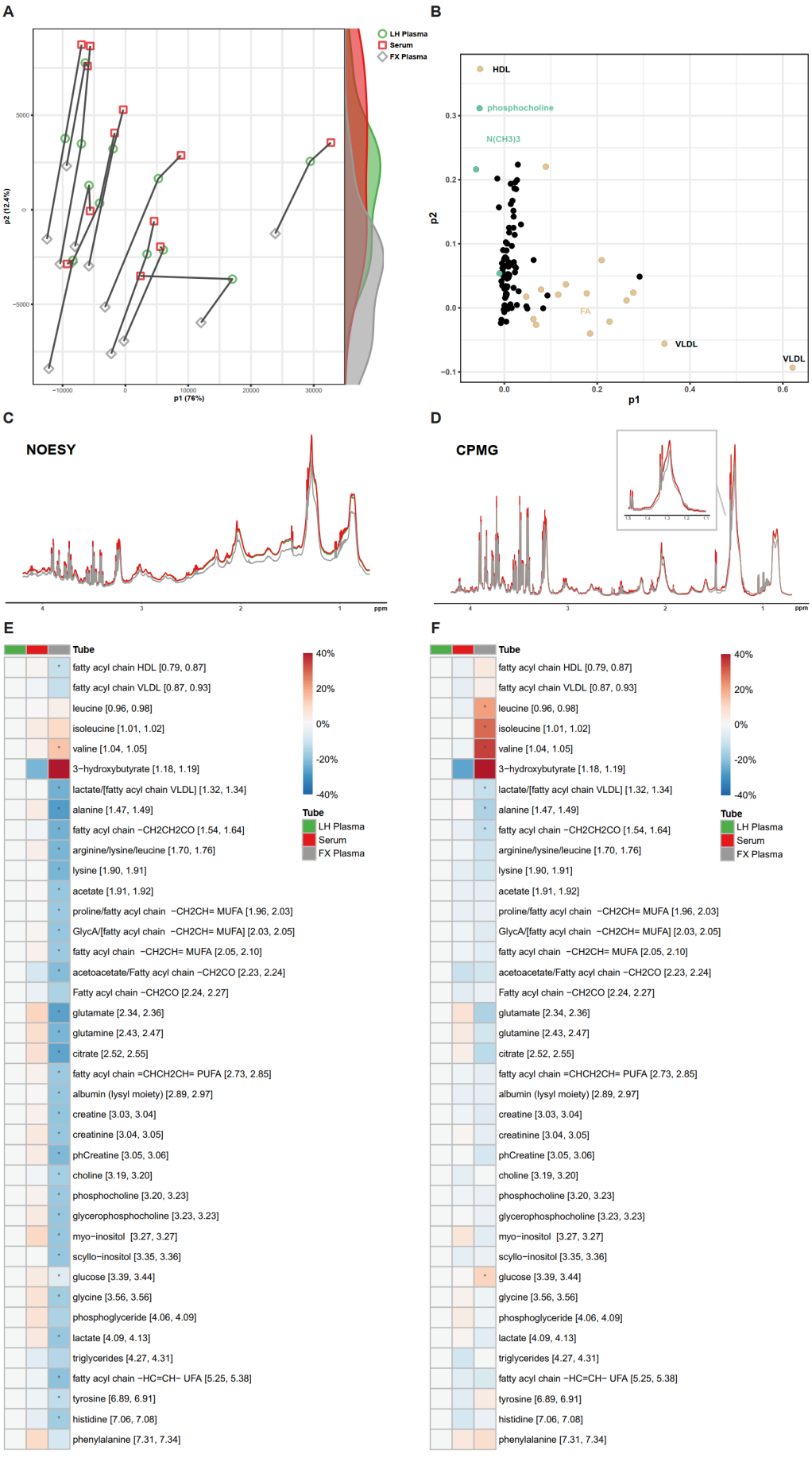
A
LH Plasma
Serum
FX Plasma
p2 (12.4%)
p1 (76%)
B
HDL
phosphocholine
N(CH3)3
FA
VLDL
VLDL
p2
p1
C
NOESY
ppm
D
CPMG
ppm
E
Tube
fatty acyl chain HDL [0.79, 0.87]
fatty acyl chain VLDL [0.87, 0.93]
leucine [0.96, 0.98]
isoleucine [1.01, 1.02]
valine [1.04, 1.05]
3−hydroxybutyrate [1.18, 1.19]
lactate/[fatty acyl chain VLDL] [1.32, 1.34]
alanine [1.47, 1.49]
fatty acyl chain −CH2CH2CO [1.54, 1.64]
arginine/lysine/leucine [1.70, 1.76]
lysine [1.90, 1.91]
acetate [1.91, 1.92]
proline/fatty acyl chain −CH2CH= MUFA [1.96, 2.03]
GlycA/[fatty acyl chain −CH2CH= MUFA] [2.03, 2.05]
fatty acyl chain −CH2CH= MUFA [2.05, 2.10]
acetoacetate/Fatty acyl chain −CH2CO [2.23, 2.24]
Fatty acyl chain −CH2CO [2.24, 2.27]
glutamate [2.34, 2.36]
glutamine [2.43, 2.47]
citrate [2.52, 2.55]
fatty acyl chain =CHCH2CH= PUFA [2.73, 2.85]
albumin (lysyl moiety) [2.89, 2.97]
creatine [3.03, 3.04]
creatinine [3.04, 3.05]
phCreatine [3.05, 3.06]
choline [3.19, 3.20]
phosphocholine [3.20, 3.23]
glycerophosphocholine [3.23, 3.23]
myo−inositol [3.27, 3.27]
scyllo−inositol [3.35, 3.36]
glucose [3.39, 3.44]
glycine [3.56, 3.56]
phosphoglyceride [4.06, 4.09]
lactate [4.09, 4.13]
triglycerides [4.27, 4.31]
fatty acyl chain −HC=CH− UFA [5.25, 5.38]
tyrosine [6.89, 6.91]
histidine [7.06, 7.08]
phenylalanine [7.31, 7.34]
40%
20%
0%
-20%
-40%
Tube
LH Plasma
Serum
FX Plasma
F
Tube
fatty acyl chain HDL [0.79, 0.87]
fatty acyl chain VLDL [0.87, 0.93]
leucine [0.96, 0.98]
isoleucine [1.01, 1.02]
valine [1.04, 1.05]
3−hydroxybutyrate [1.18, 1.19]
lactate/[fatty acyl chain VLDL] [1.32, 1.34]
alanine [1.47, 1.49]
fatty acyl chain −CH2CH2CO [1.54, 1.64]
arginine/lysine/leucine [1.70, 1.76]
lysine [1.90, 1.91]
acetate [1.91, 1.92]
proline/fatty acyl chain −CH2CH= MUFA [1.96, 2.03]
GlycA/[fatty acyl chain −CH2CH= MUFA] [2.03, 2.05]
fatty acyl chain −CH2CH= MUFA [2.05, 2.10]
acetoacetate/Fatty acyl chain −CH2CO [2.23, 2.24]
Fatty acyl chain −CH2CO [2.24, 2.27]
glutamate [2.34, 2.36]
glutamine [2.43, 2.47]
citrate [2.52, 2.55]
fatty acyl chain =CHCH2CH= PUFA [2.73, 2.85]
albumin (lysyl moiety) [2.89, 2.97]
creatine [3.03, 3.04]
creatinine [3.04, 3.05]
phCreatine [3.05, 3.06]
choline [3.19, 3.20]
phosphocholine [3.20, 3.23]
glycerophosphocholine [3.23, 3.23]
myo−inositol [3.27, 3.27]
scyllo−inositol [3.35, 3.36]
glucose [3.39, 3.44]
glycine [3.56, 3.56]
phosphoglyceride [4.06, 4.09]
lactate [4.09, 4.13]
triglycerides [4.27, 4.31]
fatty acyl chain −HC=CH− UFA [5.25, 5.38]
tyrosine [6.89, 6.91]
histidine [7.06, 7.08]
phenylalanine [7.31, 7.34]
40%
20%
0%
-20%
-40%
Tube
LH Plasma
Serum
FX Plasma

Figure 4-6 Differences in the metabolome exist by blood collection tube under optimal processing conditions. (A) PCA scores plot showing the effect of different blood tubes on samples under optimal processing conditions. (C, D) Mean NOESY/CPMG spectra of LH plasma (Green), serum (red) and FX Plasma (Grey). (E, F) Heatmap displaying percentage changes in metabolite levels three types of plasma/serum. The numbers in square brackets represent the corresponding spectral region boundaries in parts per million (ppm). Percentage changes calculated from absolute (E) / sum-normalised (F) integral values and compared to LH Plasma. Significant differences in means of metabolites were represented by * ($q < 0.05$).

4.3.4 Evaluation of a Fluoride/Oxalate Additive to Preserve Inter-individual Metabolite Variation using Realistic Timepoints.

Lastly, the potential of a BD Vacutainer containing sodium fluoride and potassium oxalate to mitigate preanalytical variation in the individual blood metabolome was investigated. As expected, 24-hours at either RT or 4 °C resulted in an increase in lactate and a decrease in glucose when stored in either LH plasma or serum tubes (Figure 4-7, Figure 4-8). When LH Plasma samples were centrifuged after a 24-hour delay at 4 °C, the lactate levels increased 34% and the glucose levels decreased 18%. The alterations were similar for the serum samples, and further exacerbated when the samples were left at RT prior to centrifugation. Conversely, FX tubes effectively prevented anaerobic glycolysis for at least 24-hours at RT. Only 7% decrease was observed in glucose levels when FX Plasma samples were centrifuged after a 24-hour delay at 4 °C. It should be noted that as demonstrated previously, glucose levels decreased 6% in FX Plasma (q = 0.096, repeated measure two-way ANOVA, sidak post hoc, FDR correction across metabolites) after 24 hours delay in NMR measurement at 4 °C. Therefore, the decrease of glucose in FX tubes was likely due to general degradation not due to anaerobic glycolysis.

Moreover, the combination of using FX tubes and refrigerating the blood tube during the pre-processing interval effectively prevented metabolite variation between an optimal, 30-minute pre-centrifugation delay and the 24-hour delay (Figure 4-8C). Without refrigeration, glutamate and glutamine levels changed dramatically after 24 hours at RT.

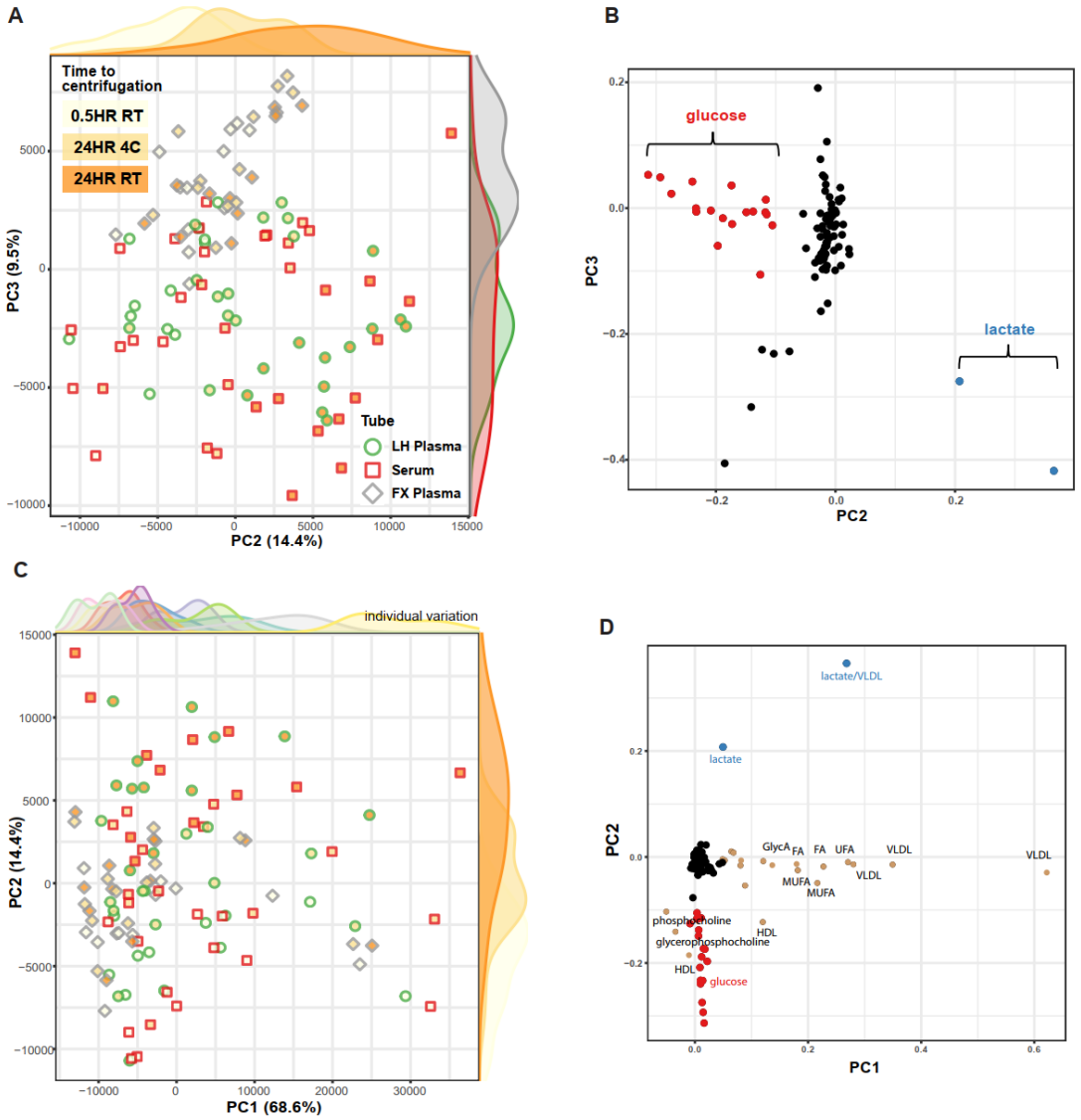

Figure 4-7 Delay in centrifugation led to alteration in glucose and lactate levels. PCA scores plot (A, C) demonstrating the influence of different pre-processing conditions on samples, specifically observed in PC2. Loadings plot (B, D) of the PCA highlighting glucose and lactate as contributors to the variation observed in PC2, while lipoproteins and fatty acids as contributors to individual variation observed in PC1.

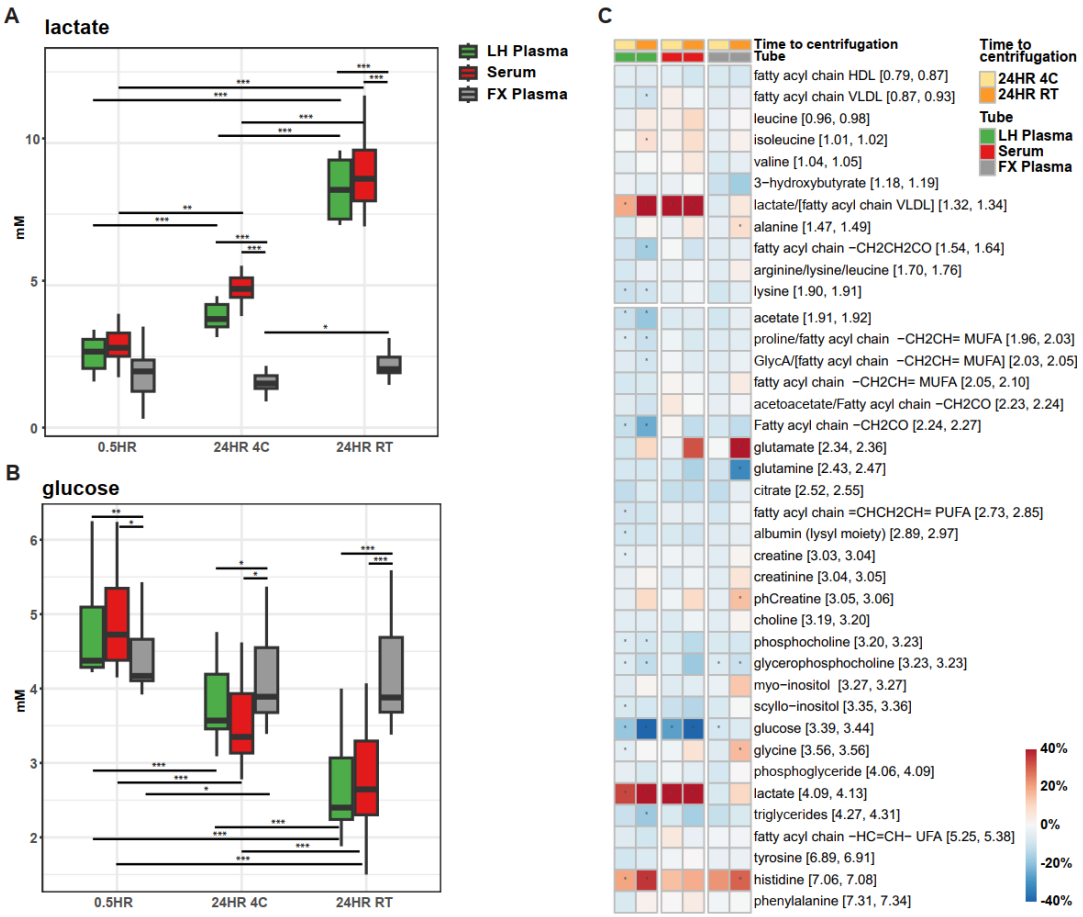

Figure 4-8 Fluoride oxalate blood collection tubes prevent changes to the metabolome for at least 24 hours when stored at 4°C. Boxplots showing increased lactate levels (A) and decreased glucose levels (B) in delayed pre-processing conditions for LH Plasma and Serum, but not in FX Plasma. Heatmap (C) presenting percentage changes in metabolite levels resulting from varied pre-processing conditions across three types of plasma/serum. Percentage changes calculated from absolute integral values and compared to the optimum pre-processing condition. Significant differences in means of metabolites were represented by * ($q < 0.05$).

4.4 Discussion

Blood is the principal biofluid utilised in epidemiological studies utilising metabolomics to predict disease onset, severity, and treatment response. Fluoride oxalate vacutainer blood collection tubes were hypothesised to be a more appropriate blood tube for metabolome studies. To test this, the effect of preanalytical variation in blood sample handling were systematically investigated in lithium heparin, fluoride oxalate, and serum blood tubes. This chapter demonstrates, for the first time, that the use of FX plasma tubes in combination with refrigeration at 4 °C negates metabolome variation

due to preanalytical factors. This is important, as lactate and glucose are established biomarkers for the early diagnosis of cancer (E. Goldberg et al., 2021; Larkin et al., 2022b). Furthermore, they may prove important to the diagnosis and prediction of other diseases when integrated into multivariate blood metabolite algorithms (Buergel et al., 2022). For example, they are also among discriminatory metabolites identified for AE and VGKC/GlyR antibody-mediated psychosis as demonstrated in Chapter 2 and 3. These findings suggest that fluoride oxalate tubes could be beneficial in metabolomic studies where there is variability in blood processing times, pending further validation with a broader range of metabolites and larger sample sizes.

Initial investigations revealed that much of the variation in metabolite levels within and between blood biobank cohorts could be attributed to variations in glycolysis metabolites. This variation is attributed to residual anaerobic glycolysis occurring when erythrocyte separation from serum or plasma is delayed. Delayed sample processing due to a high volume of samples being processed (UK Biobank) or collection methods where the rapid processing of bloods was not prioritised (STORI) led to increased lactate and decreased glucose resonances compared to cohorts where rapid blood processing was prioritised (TwinsUK and SPARE cohorts). As normal lactate levels are < 2 mmol (Foucher & Tubben, n.d.), the absolute concentrations reported in the UK Biobank are not suitable for clinical translation.

Sodium fluoride and potassium oxalate act in concert to inhibit glycolysis in blood samples (Gambino, 2013). Specifically, sodium fluoride inhibits the enzyme enolase, which catalyses the conversion of 2-phosphoglycerate (2-PG) into phosphoenolpyruvate (PEP), the penultimate step in glycolysis. Potassium oxalate precipitates calcium ions to inhibit the clotting cascade. Fluoride oxalate tubes, as expected, showed baseline differences in amino acid levels and glycolytic metabolites compared to serum (Sotelo-Orozco et al., 2021b). Consistent with other studies, the metabolite profile of serum and lithium heparin plasma were comparable (Sotelo-Orozco et al., 2021b), and behaved similarly in response to delayed erythrocyte

separation (Debik, Isaksen, et al., 2022).

Previous studies have documented the effects of delayed erythrocyte separation on metabolite levels as quantified by NMR-based metabolomics techniques (Alexander et al., 2023; Bernini et al., 2011; Brunius et al., 2017; Cruickshank-Quinn et al., 2018; Debik, Isaksen, et al., 2022; Ellervik & Vaught, 2015; Fomenko et al., 2022b; Jobard et al., 2016; Muti et al., 2023; Pinto et al., 2014b; Santos Ferreira et al., 2019b). Consistent with these findings, lactate and glucose are typically most affected. However, in contrast to other reports (Fliniaux et al., 2011b), the chapter also clearly shows in both the UK Biobank and healthy volunteer data that residual glycolytic metabolism does occur (in the absence of an inhibitor of glycolysis) even when blood is stored at 4 °C prior to centrifugation.

After separation of serum or plasma from erythrocytes, metabolite variation is minimal. In the UK Biobank cohort, only histidine showed a significant effect of delay in sample measurement (r = -0.39) compared to interindividual biological variation. Other metabolites, while significantly correlated with measurement delay, showed smaller effect sizes between 0.01 and 0.21 which are less relevant relative to the observed interindividual variation. Similarly, in the healthy volunteer study, a delay in sample measurement over a similar timeframe, for up to 48 hours at 4 °C, resulted in minimal metabolite variation, aligning with findings from the UK Biobank data and early UK Biobank pilot studies that tested delays of up to 24 hours at 4 °C (Barton et al., 2008). Such variation is suitable to be corrected by previously described statistical methods (Ritchie et al., 2023).

These findings provide suggestions for reporting preanalytical variation to aid in the synergy of future metabolomic studies. The proposed reporting guideline consists of key information relating to the individual, the pre-processing variables, and the post-processing variables that may differ between samples in a single study (Table 4-2). The guidelines do not include variables that should be controlled for within a study and ideally between studies, for example, long-term storage temperature of frozen samples,

and NMR spectra acquisition parameters. Analysis of the UK Biobank data also shows that fasting time can strongly influence the concentration of certain metabolites, primarily ketone bodies (Figure 4-9). Recording the time of blood collection, centrifugation, and storage temperatures allows studies to monitor SOP compliance, for which data is sorely lacking in biomarker research, and may also help identify mistreated samples. The UK Biobank has implemented pipelines that allow for automated reporting of key information. For example, barcoded blood tubes were used that, when scanned, allowed for automated logging of sample collection and processing (Downey & Peakman, 2008).

Table 4-2 Key reporting parameters for blood metabolomic profiling by NMR in cohort studies

Variable	Reported by
Time since last meal (hours)	Participant
Time of blood collection	Phlebotomist
Storage temperature pre-centrifugation	Phlebotomist
Time centrifuged	Blood processing technician
Temperature during centrifugation	Blood processing technician
Time frozen	Blood processing technician
Time of NMR sample preparation	NMR technician
Storage temperature pre-data acquisition	NMR technician
Time of data acquisition	NMR technician

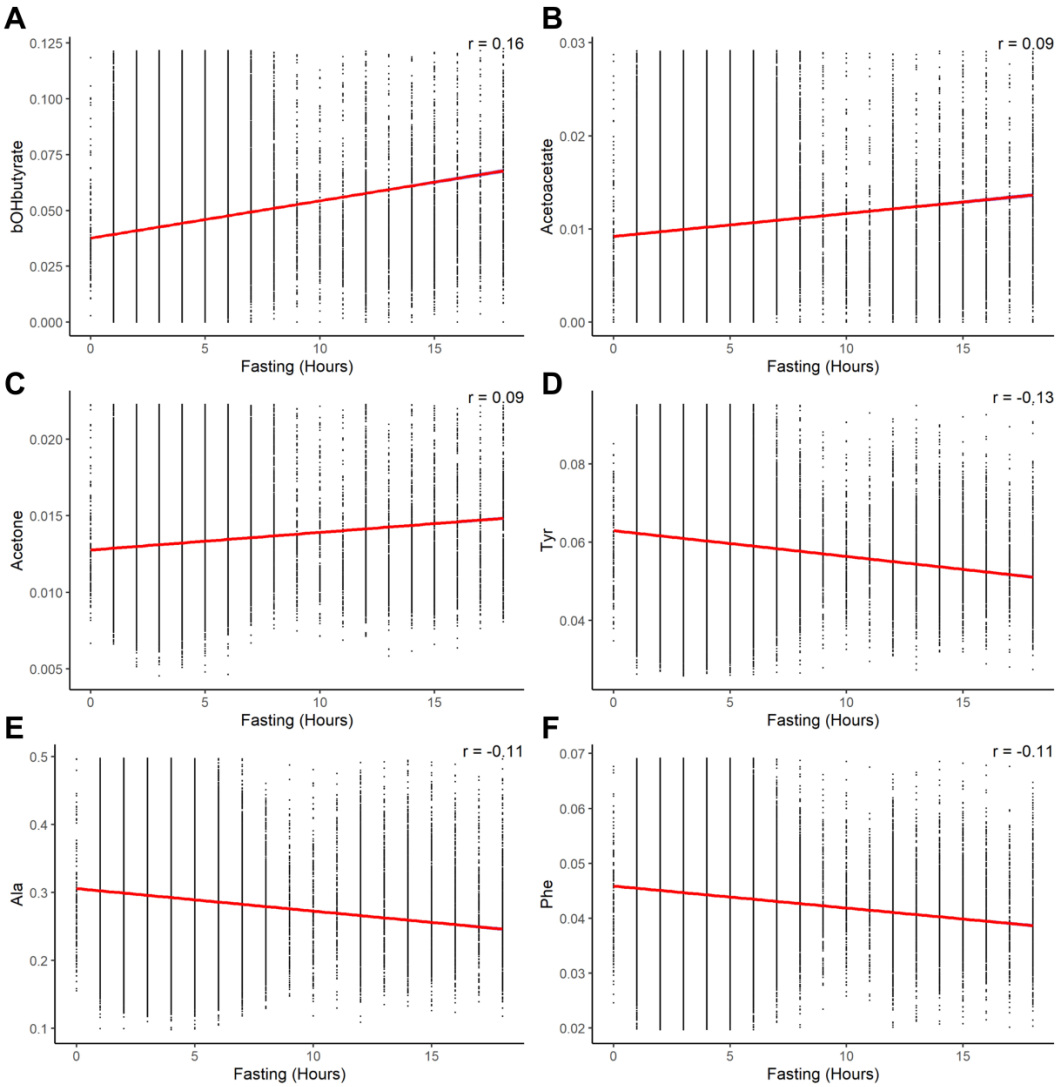

Figure 4-9 Levels of certain metabolites, primarily ketone bodies, were correlated with fasting time.

There are some limitations of this study. The comparison between the UK Biobank and TwinsUK metabolomics datasets was restricted to non-lipid data, such as amino acids and energy metabolites, due to non-overlapping metabolite data and uncertainty in how these values were derived between the two cohorts. While the study provided insights using NMR-based metabolite profiling, which focused on metabolites commonly assayed by this technique, the scope was limited with respect to the range of metabolites analysed. Future research could extend these findings by incorporating a broader spectrum of metabolomic analyses, including mass spectrometry and advanced lipoprotein assays, as well as labile metabolites detectable by NMR such as coenzymes

and antioxidants (Nagana Gowda et al., 2023), to provide a more comprehensive understanding of preanalytical variability across different platforms.

In the healthy control cohort, blood storage in fluoride oxalate tubes resulted in a slight negative bias in glucose levels under optimal processing conditions, which is consistent with previous reports (Waring et al., 2007). This bias did not show variation over time. This relative negative bias may be partly attributed to the dilutional effect of the NaF/KOx additive in the collection tube (Waring et al., 2007). The systematic nature of this difference should not influence metabolome variability when fluoride oxalate tubes are used across and between studies. Studies have also shown that both sodium fluoride (Lippi et al., 2018) and potassium oxalate (Elferink, 1987) have the potential to cause haemolysis after prolonged standing time at room temperature. Alternative methods to inhibit glycolysis, such as citrate-buffered tubes, have been proposed (Lippi et al., 2018). Although these tubes are less prone to haemolysis over time, their additives interfere with NMR spectra and the concentrations of nearby metabolites (Sotelo-Orozco et al., 2021b). In this study, haemolysis was detected only in fluoride oxalate tubes left at room temperature, and not at 4 °C. To address these challenges, the development of novel additives that inhibit major metabolic pathways in blood while preventing haemolysis and maintaining compatibility with metabolomic analysis is encouraged.

4.5 Conclusions

Pre-analytical variation in blood sample collection cause variation within and between biobank biomarker studies. Three blood collection tubes were trialled with the aim of solving technical challenges due to preanalytical variation in blood metabolite levels that are common in cohort studies. This chapter found that a combination of refrigeration at 4 °C and the use of a fluoride/oxalate additive prevented changes in metabolite levels, as compared to optimal processing parameters, for at least 24 hours prior to erythrocyte separation. Additionally, the effect of delayed sample measurement on the stability of quantified metabolites was small, but dependent on the type of blood collection tube used at the pre-processing stage. Based on these findings, a short list of key reporting

guidelines was devised to improve the reproducibility of blood metabolite signatures as biomarkers of health and disease in future cohort studies.

Chapter 5: Extraction Methods for Brain Biopsy NMR Metabolomics: Balancing Metabolite Stability and Protein Precipitation

The data in this chapter has been published as Xiong, W.; Zirpel, F.; Cader, M.Z.; Anthony, D.C.; Probert, F. Extraction Methods for Brain Biopsy NMR Metabolomics: Balancing Metabolite Stability and Protein Precipitation. *Metabolites* **2024**, *14*, 609. https://doi.org/10.3390/metabo14110609.

5.1 Introduction

Chapters 2-4 demonstrated the utility of NMR metabolomics in blood (serum/plasma) analysis as a potential diagnostic tool. Beyond blood, NMR metabolomics also holds significant promise for brain tissue analysis, providing a direct window into metabolic alterations associated with CNS pathologies. This approach could extend to human brain biopsies in clinical settings, where metabolomics offers complementary insights to histological analysis, enhancing diagnostic precision.

However, as with blood metabolomics discussed in Chapter 4, brain metabolomics also faces challenges from pre-analytical variations. Unlike blood analysis, brain metabolomics necessitates the extraction of metabolites from tissues, introducing additional variables such as extraction efficiency, reproducibility, and metabolite stability during and after preparation.

To date, no research has investigated brain metabolite integrity after NMR sample preparation, nor the relationship between metabolite stability and residual protein levels across different extraction methods. This is important yet often neglected because delays between sample preparation and analytical measurement are common in NMR-based metabolomics, especially in studies with large sample sizes. In metabolomic studies, samples are usually prepared in batches and queued for NMR analysis. Insufficient protein denaturation or precipitation could lead to ongoing enzymatic reactions during

this interval, thereby altering the metabolites.

This chapter aims to bridge this gap by evaluating whether such alterations exist with commonly used extraction methods, understanding their impact, and identifying ways to control them. By minimising the effects of preanalytical variability, the measured metabolites can more accurately reflect the *in vivo* state, leading to reliable interpretation. Specifically, this chapter will assess the extraction performance of various solvents on mouse brain tissues, focusing on extraction efficiency, reproducibility, metabolite stability up to eight hours post-NMR sample preparation, and residual protein concentrations (Figure 5-1). The hypothesis is that adequate protein precipitation will preserve metabolite integrity during delays between sample preparation and analytical measurement, thereby providing more reliable NMR-based metabolic profiles.

For the evaluation, 11 extraction methods were included: acetonitrile (MeCN, 50%, 67%, 80%, 100% v/v), methanol (MeOH, 50%, 67%, 80%, 100% v/v), methanol/water/chloroform (MeOH/H_2O/CHCl3, 2:1:2, v/v), 50% MeCN with ultrafiltration, and 50% MeOH with ultrafiltration. Acetonitrile and methanol were selected as the primary extraction solvents due to their ability to precipitate proteins, extract wide ranges of metabolites and their widespread application in metabolomics (Mushtaq et al., 2014). Acetonitrile is relatively less polar than methanol, making it less soluble for proteins (Blanchard, 1981), while methanol is relatively more polar, thereby providing increased solubility for polar metabolites (Nagana Gowda et al., 2015). The ratio of organic solvent to water is important for efficient protein removal (Blanchard, 1981). Varying concentrations of methanol and acetonitrile were included to find a balance between metabolite recovery and sufficient protein precipitation. In this study, 50% MeOH and 50% MeCN were used as negative controls due to an observed instability of key metabolites with their use. These methods provided a baseline for comparison, allowing us to evaluate the performance of more optimised extraction protocols in maintaining metabolite stability. The methanol/water/chloroform method,

widely used in brain extraction since its description by Folch (Folch et al., 1951), was also included. Improved protein precipitation was expected as the decreased polarity of chloroform and the formation of two distinct phases of methanol/chloroform causes proteins to precipitate at the interface. It has been suggested that the addition of chloroform may be required for sufficient lipid removal from lipid-rich tissues such as the brain (Lin et al., 2007). Finally, the use of ultrafiltration with a molecular weight cut-off (MWCO) filter was included as a positive control for protein removal.

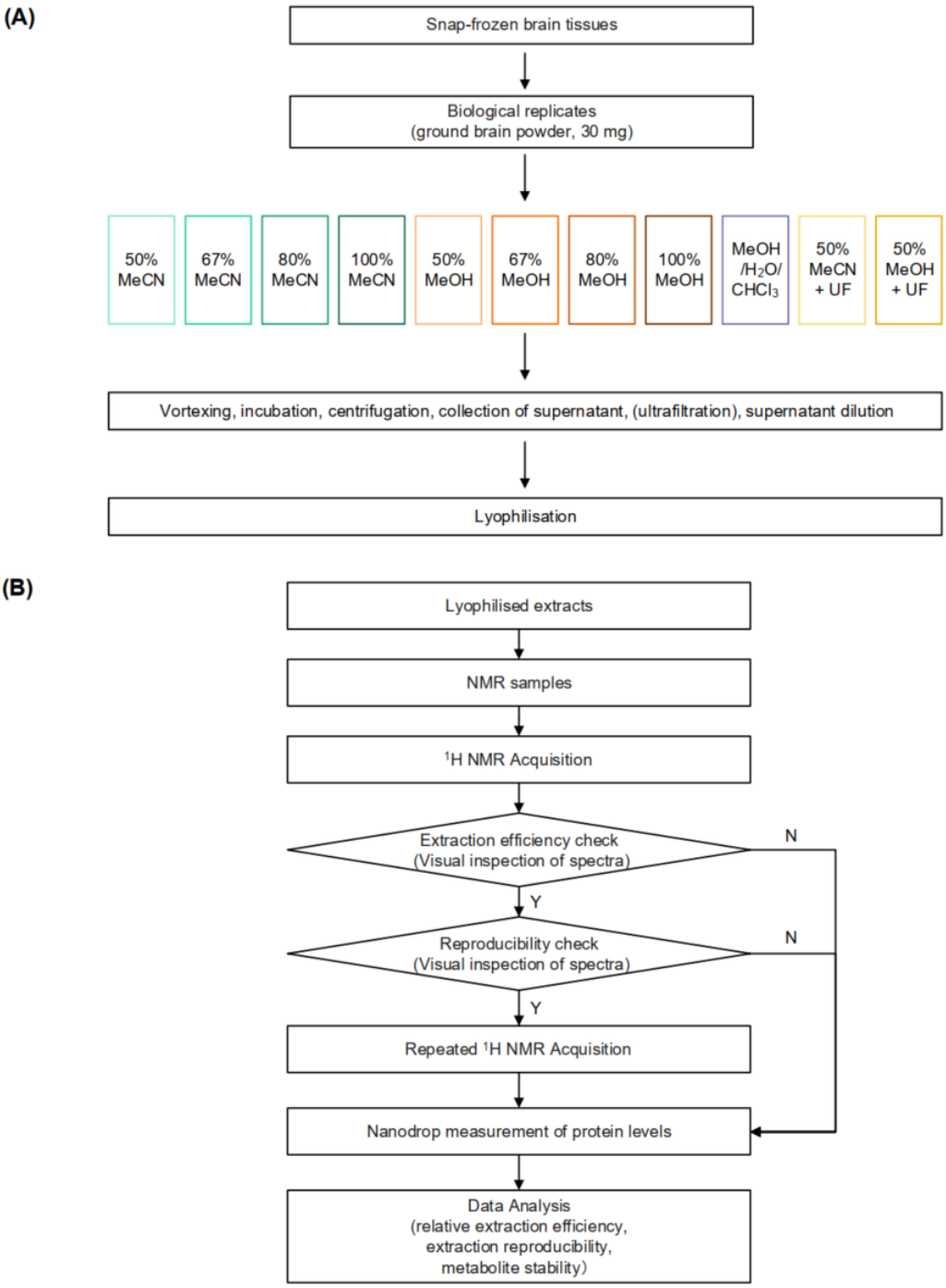

Figure 5-1 Workflow of sample preparation and NMR acquisition for metabolic profiling of brain tissues using various extraction methods. (a) Steps for brain metabolite extraction. (b) Flow of ^{1}H NMR data acquisition and data analysis. The criteria for good extraction efficiency and reproducibility are defined as having a relative extraction efficiency greater than 0.7 and a median relative standard deviation (RSD) of less than 20%. UF, ultrafiltration. N, no. Y, yes.

5.2 Methods

5.2.1 Brain Tissues

Brain tissues were collected from C57BL/6/J mice, after the animals were terminally anesthetised with isoflurane and transcardially perfused with heparinised saline (5,000 USP/L). Samples were stored at -80 °C until they were used for experimental purposes.

Snap-frozen brain tissues were pooled and homogenised using a pestle and mortar on dry ice, a widely recognised method in metabolomics for ensuring consistency across biological replicates (Andresen et al., 2022; Beckonert et al., 2007; Diémé et al., 2017; Fomenko et al., 2022a; Lin et al., 2007). A brain mass of 30 mg (resulting in 42 replicates with a mean of 30.6 ± 0.7 mg) was selected for further extraction based on a balance between metabolite detection sensitivity and tissue conservation (Beckonert et al., 2007).

5.2.2 Brain Metabolite Extraction

Detailed procedures of the 11 extraction protocols used were as follows. The protocols were adapted based on previous experience and the existing literature (Andresen et al., 2022; Beckonert et al., 2007; Diémé et al., 2017; Fomenko et al., 2022a; Lin et al., 2007).

5.2.2.1 MeCN/H_2O Extraction Protocol

For each sample, a ratio of 8-to-1 (in microliters per milligram of sample) of a cold acetonitrile-water mixture was added, with concentrations ranging from 50% to 100% (v/v). This mixture was vigorously shaken using a vortex for 30 seconds to ensure thorough mixing. It was then incubated on ice for 15 minutes, followed by centrifugation at 16,000 x g for 15 minutes at 4 °C. 200 microliters of the clear supernatant from each sample was collected and diluted with H_2O to adjust the final acetonitrile concentration to 40%, enabling it to be freeze-dried effectively. Subsequently, these diluted extracts were then freeze-dried and stored at -80 °C until required for NMR analysis.

5.2.2.2 MeOH/H_2O Extraction Protocol

For each sample, a cold methanol-water mixture with varying concentrations (50%, 67%, 80%, and 100% v/v) was added at a ratio of 8 microliters per milligram of sample. Following addition, the samples were vigorously mixed using a vortex mixer for 30 seconds, incubated on ice for 15 minutes, and then centrifuged at 16,000 x g for 15 minutes at 4 °C. From each sample, 200 microliters of the supernatant were carefully collected. These collected supernatants were further diluted with H_2O to achieve a final methanol concentration of 20%. The resulting extracts were then freeze-dried and stored at -80 °C until required for NMR analysis.

5.2.2.3 MeOH/H_2O/$CHCl_3$ Extraction Protocol

For each sample, a volume of cold 100% methanol (MeOH) was added at a ratio of 5.3 microliters per milligram of sample. The mixture was then subjected to 30 seconds of vigorous mixing using a vortex. Subsequently, a volume of ice-cold H_2O equivalent to 2.7 times the sample mass (µL/mg) and a volume of cold chloroform ($CHCl_3$) equivalent to 5.3 times the sample mass (µL/mg) were added to each sample. The samples were mixed again with a vortex for 30 seconds, then incubated on ice for 15 minutes. Following incubation, the samples were centrifuged at 16,000 x g for 15 minutes at 4 °C to facilitate phase separation. After centrifugation, 200 microliters of the aqueous phase (methanol/water phase) was carefully collected from each sample. This collected phase was then diluted with H_2O to adjust the final methanol concentration to 20%. The diluted extracts were then freeze-dried and stored at -80 °C until required for NMR analysis.

5.2.2.4 MeCN/H_2O and MeOH/H_2O Extraction with Ultrafiltration Protocol

A total of 200 µL of MeCN/H_2O or MeOH/H_2O extract was filtered with 10 kD MWCO filters (Amicon Ultra 0.5mL centrifugal filters UFC501024; 16,000 x g, 15 min, 4 °C). Prior to the use, the filters were washed with 500 µL H_2O (16,000 x g, 30 min, 4 °C) to remove glycerol. Elusion (about 170 µL) was collected and subsequently diluted with

H_2O to create extracts with a final MeCN concentration of 40% or a final MeOH concentration of 20%, lyophilised, and store at -80°C until the day of NMR analysis.

5.2.3 ^{1}H NMR Analysis

Lyophilised extracts were resuspended with 550 µL 75 mM phosphate buffer in D_2O (pH 7.4) containing 32.2 µM sodium salt of 3-(trimethylsilyl) propionic acid-2,2,3,3-d_4 (TSP) and transferred to a 5 mm borosilicate NMR tube (Norell). Deuterated solvents (D_2O) were used exclusively for preparing the NMR buffer to ensure accurate spectral acquisition and minimise water signal interference. For the extraction protocols, regular non-deuterated water (H_2O) was used, as specified in the main text. NMR spectroscopy was performed using a 700-MHz Bruker AVIII spectrometer (Department of Chemistry, University of Oxford) operating at 16.4 T equipped with a ^{1}H [^{13}C/^{15}N] TCI cryoprobe at 298 K. ^{1}H NMR spectra were acquired by using the noesygppr1d pulse sequence (Bruker, a one-dimensional nuclear Overhauser effect spectroscopy [NOESY] presaturation scheme) with the following parameters: td = 32768, d1 = 2 s, p1 = 16.03 µs, ns = 64, aq = 1.46 s, sw = 16 ppm. The total acquisition time for the proposed NOESY spectra was approximately 12 minutes, consisting of 4 minutes for data collection and an additional 8 minutes allocated for sample loading, temperature equilibration, locking, shimming, and tuning. Repeated NMR measurements were conducted for samples that met both the extraction efficiency and reproducibility criteria (defined as extraction efficiency < 0.7 and/or median relative standard deviation [RSD] > 20%), acquiring data at hourly intervals up to an 8-hour delay while stored on the carousel at room temperature (Figure 5-1).

5.2.4 Measurement of Protein Concentrations

The protein concentration of each NMR sample was determined using absorbance measurements at 205 nm with the Thermo Scientific™ NanoDrop™ One instrument.

5.2.5 NMR Data Pre-processing

Resulting free induction decays (FID) were zero-filled by a factor of 2 and multiplied by

an exponential function corresponding to 0.30 Hz line broadening prior to Fourier transformation. All spectra were phased, baseline corrected (using a 3rd degree polynomial), and chemical shifts referenced to the lactate resonance at $\delta = 1.33$ ppm in Topspin 4.1 (Bruker, Germany), and exported to ACD/Labs Spectrus Processor Academic Edition 12.01 (Advanced Chemistry Development, Inc.).

A semi-targeted analysis approach was employed by manually dividing each NMR spectrum into 86 spectral buckets for integration, excluding noise, water signals, in an effort to minimise contributions from varying protein levels across methods (Figure 5-2). For samples prepared using MWCO filters, contaminant signals arising from glycerol were also removed. Metabolite assignment was performed by referencing to literature values (Diémé et al., 2017; Fomenko et al., 2022a; Paskevich et al., 2013; Wishart et al., 2021) , via metabolite spiking and 2D total correlation spectroscopy (TOCSY) experiments. The absolute integral values were subject to the main statistical analysis unless stated otherwise. Integral values were mean centred and scaled to unit variance prior to principal component analysis.

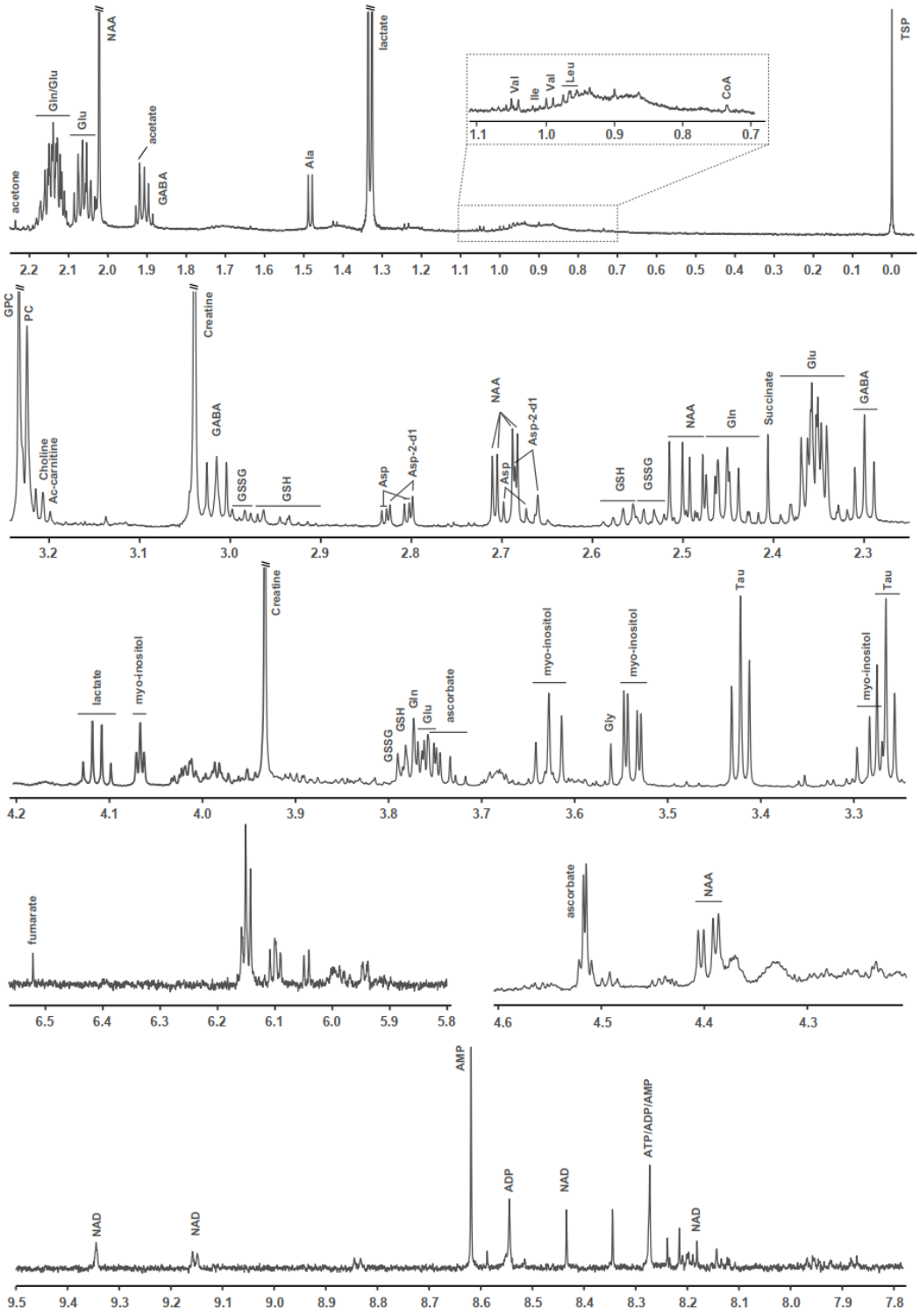

Figure 5-2 Metabolite assignments in a representative NMR spectrum from a brain sample extracted with 50% MeCN.

5.2.6 Data Analysis

Analysis was performed in R software 4.1.2 (R foundation for statistical computing, Vienna, Austria). The ggplot2 (version 3.4.2), pheatmap (version 1.0.12), ropls (version

1.26.4), and metabom8 (version 1.0.0) packages were used for generation of the plots (Kimhofer, 2021; Kolde, 2012; Thévenot et al., 2015b; Villanueva & Chen, 2019). The relative extraction efficiency was determined by calculating the mean total intensity of NMR integrals, normalised to that of the 50% MeCN group. The extraction reproducibility was assessed using the median of the relative standard deviation (RSD) of the replicates for each metabolite resonance. The stability of each spectral bucket was determined by calculating the average percentage change over time up to 8 hours for each bucket across three replicates. The one-way analysis of variance (ANOVA) was used to identify significant differences between the means of groups. Two-tailed *p*-values ≤ 0.05 were considered statistically significant.

5.3 Results and Discussion

5.3.1 Relative Extraction Efficiency

Among the 11 methods examined, 50% MeCN, MeOH/H_2O/$CHCl_3$, 50% MeOH, and 67% MeOH showed comparably high extraction efficiency (defined as the total sum of integrals of the 86 spectral buckets measured, normalised to that of the 50% MeCN group), with mean values and SEM of 1 ± 0.01, 0.96 ± 0.05, 0.88 ± 0.01, and 0.88 ± 0.03, respectively (*p*-value > 0.05, one-way ANOVA) (Figure 5-3A). The remaining nine methods demonstrated lower extraction efficiencies to varying degrees compared to 50% MeCN (*p*-values < 0.05, one-way ANOVA).

The increase in MeCN and MeOH concentrations led to a decrease in extraction efficiency, with MeCN showing a more pronounced decline. This trend was expected since hydrophilic metabolites had limited solubility in organic solvents such as MeCN, and to a lesser extent, MeOH, and in addition, it is supported by a previous serum extraction study (Nagana Gowda et al., 2015). Furthermore, ultrafiltration with MWCO filters resulted in a 27% reduction in extraction efficiency compared to unfiltered 50% MeCN and a 41% reduction compared to unfiltered 50% MeOH (*p*-values < 0.001, one-way ANOVA). In addition, residual glycerol arising from the MWCO filters results in large contaminant signals which obscure metabolite resonances, such as the ones for

glycine and glutamine and myo-inositol (Figure 5-4).

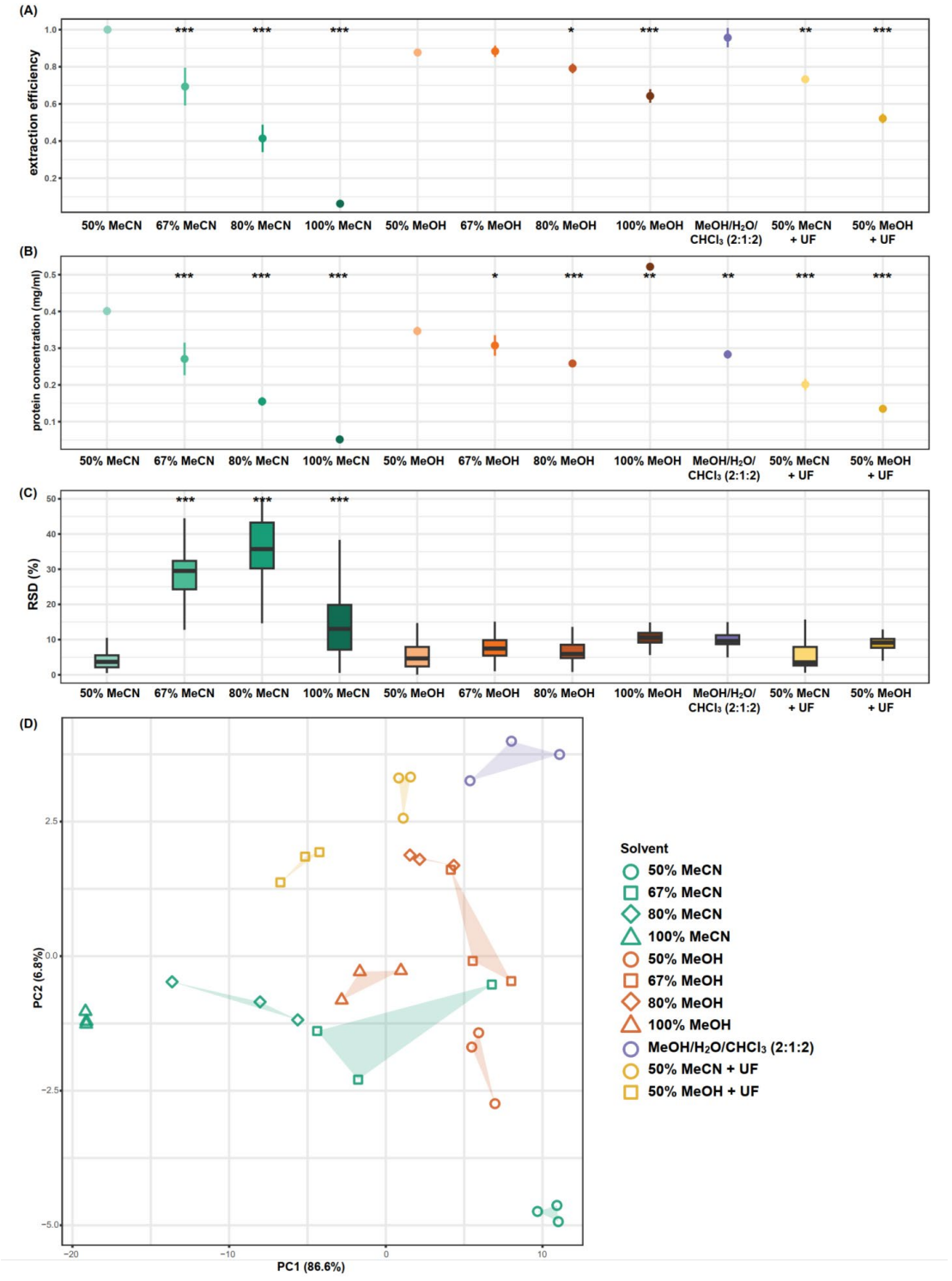

Figure 5-3 Efficiency and reproducibility of the extraction methods tested(A) Relative extraction efficiency, expressed as the mean ± SEM, calculated as the sum of integrals normalised to that of the 50% MeCN group. (B) Protein levels of the NMR samples derived from different brain extracts, expressed as the mean ± SEM. (C) Extraction reproducibility, presented in boxplots, as determined by the relative spectral standard deviation across each of the 86 spectral buckets. (D) PCA scores plot of the brain metabolic profiles from different extraction

methods at 0 h delay in NMR measurement. A smaller spread of the polygon indicates better reproducibility. Results of one-way ANOVA with Dunnett's test for multiple comparisons are reported in reference to the 50% MeCN group. UF, ultrafiltration. * $p < 0.05$, ** $p < 0.01$, *** $p < 0.001$.

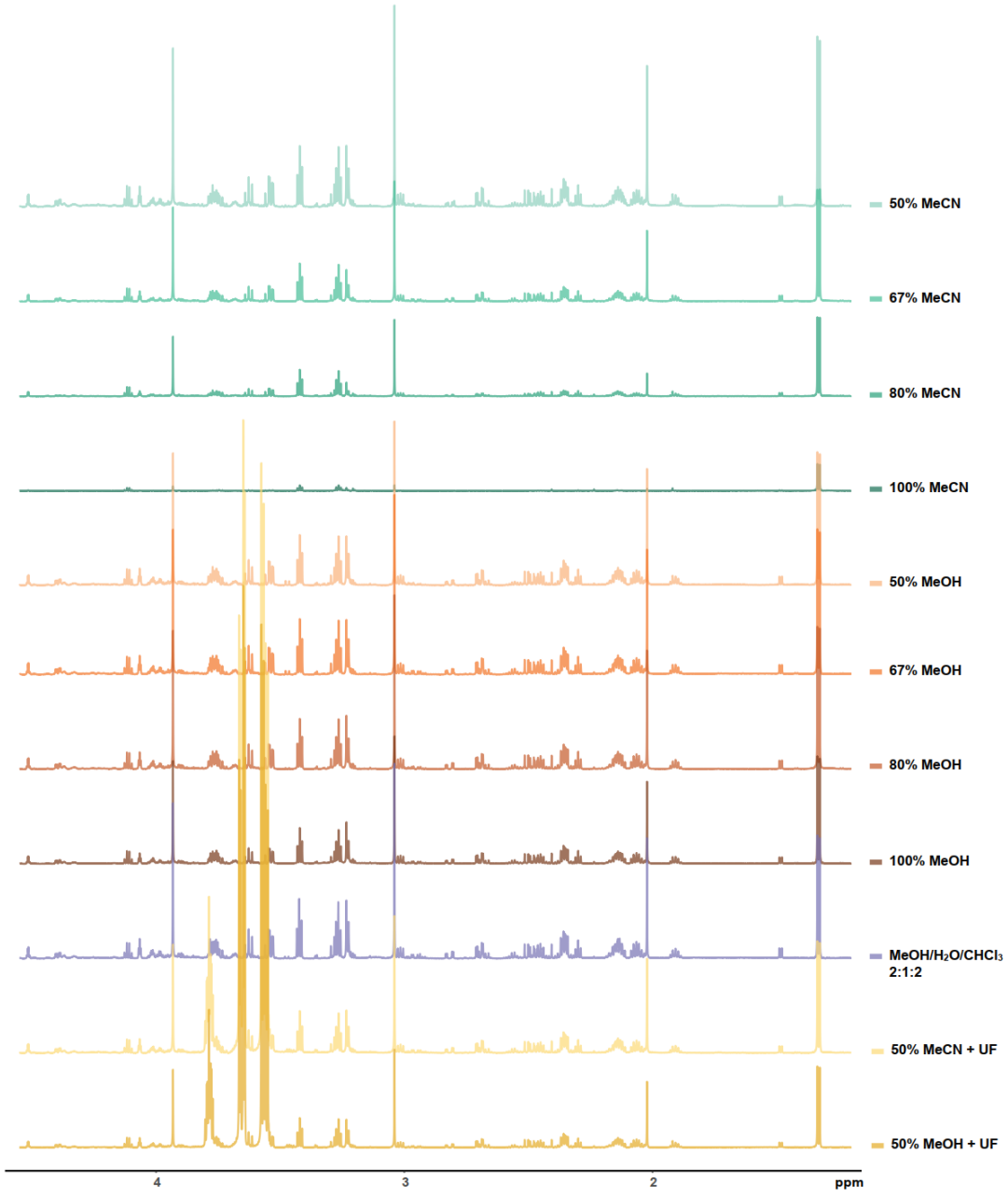

Figure 5-4 Overview of representative NMR spectra for each extraction method.

5.3.2 Protein Levels

No significant difference was observed in the protein levels of samples extracted with 50% MeCN and 50% MeOH (p-value > 0.05, one-way ANOVA, n = 3 per group).

Increasing concentrations of solvent resulted in lower protein concentrations (p-values < 0.001 and < 0.01 for MeCN and MeOH, respectively, one-way ANOVA), with the exception of samples extracted with 100% MeOH which showed higher protein levels (p-value < 0.001, one-way ANOVA). Using MeOH/H_2O/$CHCl_3$ and ultrafiltration also resulted in lower sample protein concentrations compared to 50% MeCN or 50% MeOH (p-value < 0.01, one-way ANOVA), with ultrafiltration yielding the lowest protein concentrations among these three methods (Figure 5-3B).

5.3.3 Extraction Reproducibility

The 67% MeCN, 80% MeCN and 100% MeCN extraction methods demonstrated significantly poorer reproducibility compared to the other extraction methods, as determined by RSD across all 86 spectral buckets measured (p-values < 0.001, one-way ANOVA) (Figure 5-3C). No significant differences were observed between the remaining extraction methods, with median RSD ranging from 3.54% (interquartile range [IQR] 5.55%) to 10.56% (IQR 2.81%). PCA illustrates the clustering and dispersion patterns of each extraction method, revealing the similarities among and within each method (Figure 5-3D). Most methods resulted in distinct clusters in the PCA scores plot, highlighting global metabolite difference across these methods. Methods with lower extraction efficiency tended to cluster towards the left side of the scores plot, indicating lower metabolite yield. For instance, as the concentration of MeCN increased, samples tended to cluster further to the left. Conversely, methods with better protein removal, as identified by lower sample protein concentrations, tended to cluster towards the top of the plot.

Five extraction methods, specifically 67% MeCN, 80% MeCN, 100% MeCN, 100% MeOH, and 50% MeOH with ultrafiltration, demonstrated poor extraction efficiency or reproducibility (as defined by extraction efficiencies < 0.7 and/or median RSD > 20%). As a result, these methods were excluded from further metabolite stability testing.

5.3.4 Metabolite Stability

Metabolite stability was assessed at hourly intervals up to 8 hours following sample preparation for the six extraction methods selected in the previous section. Among the six extraction methods that demonstrated adequate efficiency and reproducibility, only two low-concentration metabolites, CoA and adenosine, were undetectable in the 80% MeOH, MeOH/H_2O/$CHCl_3$, and 50% MeCN + UF methods. The trajectory of each extract over time was visualised using a PCA scores plot (Figure 5-3A). The 50% MeCN, 50% MeOH and 67% MeOH samples displayed significant drift along the second principal component (PC2). Inspection of the loading revealed that multiple aspartate signals (2.65 - 2.84 ppm) and glutamate signals (3.75 - 3.77 ppm) drove the variability of PC2. The changes that occur over time are reproducible in each sample, indicating the alteration in metabolic profile is time-dependent; for example, the 8-hour samples were equivalent to each other in each extraction method. Table 5-1 summarises the stability of the whole spectrum over time for each method. The 50% MeCN, 50% MeOH and 67% MeOH extraction methods resulted in a larger number of metabolite resonances with an RSD greater than 30% after eight hours. A heatmap illustrates the changes in each metabolite resonance over time for the extraction methods (Figure 5-4) with the most variable metabolites (aspartate, glutamate, N-acetyl aspartate [NAA], acetate, glutathione, and ascorbate) summarised in Figure 5-5B.

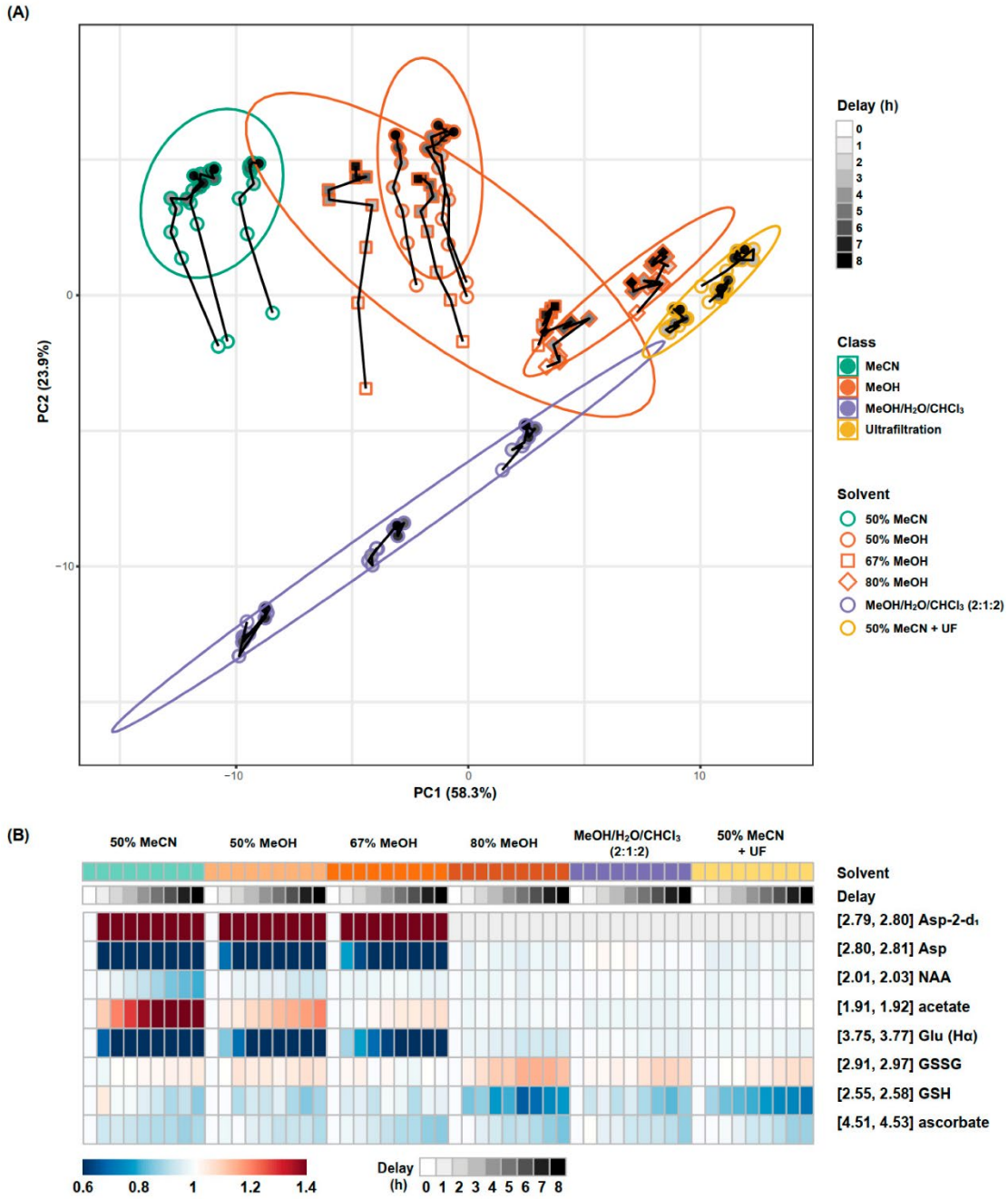

Figure 5-5 Metabolite extract stability assessment for tested methods. (a) PCA scores plot demonstrating temporal metabolome changes after NMR sample preparation. The ellipse indicates the 95% confidence interval for a multivariate distribution for each extraction method. (b) Heatmap depicting percentage changes in unstable metabolites among different extraction methods. Percentage changes for each method are relative to the 0-hour timepoint of each method. No aspartate-2-d1 signals (grey) were observed in the 80% MeOH, MeOH/H2O/CHCl3 (2:1:2), and 50% MeCN with ultrafiltration group. UF, ultrafiltration. Asp, aspartate. Glu, glutamate. NAA, N-acetyl aspartate. GSH and GSSG, reduced form and oxidised form of glutathione, respectively.

Table 5-1 Reproducibility of metabolite resonances over an 8-hour delay for NMR analysis for each extraction method.

RSD (%)	Number of variables (%)					
	50% MeCN	50% MeOH	67% MeOH	80% MeOH	MeOH/H_2O/$CHCl_3$ (2:1:2)	50% MeCN + UF
0-15	70 (82)	68 (81)	60 (71)	73 (90)	76 (94)	77 (95)
15-30	9 (11)	6 (7)	11 (13)	8 (10)	5 (6)	4 (5)
>30	6 (7)	10 (12)	13 (15)	0 (0)	0 (0)	0 (0)

RSD, relative standard deviation. RSD was calculated over nine timepoints (0–8-hour delay) across three replicates for each variable. UF, ultrafiltration.

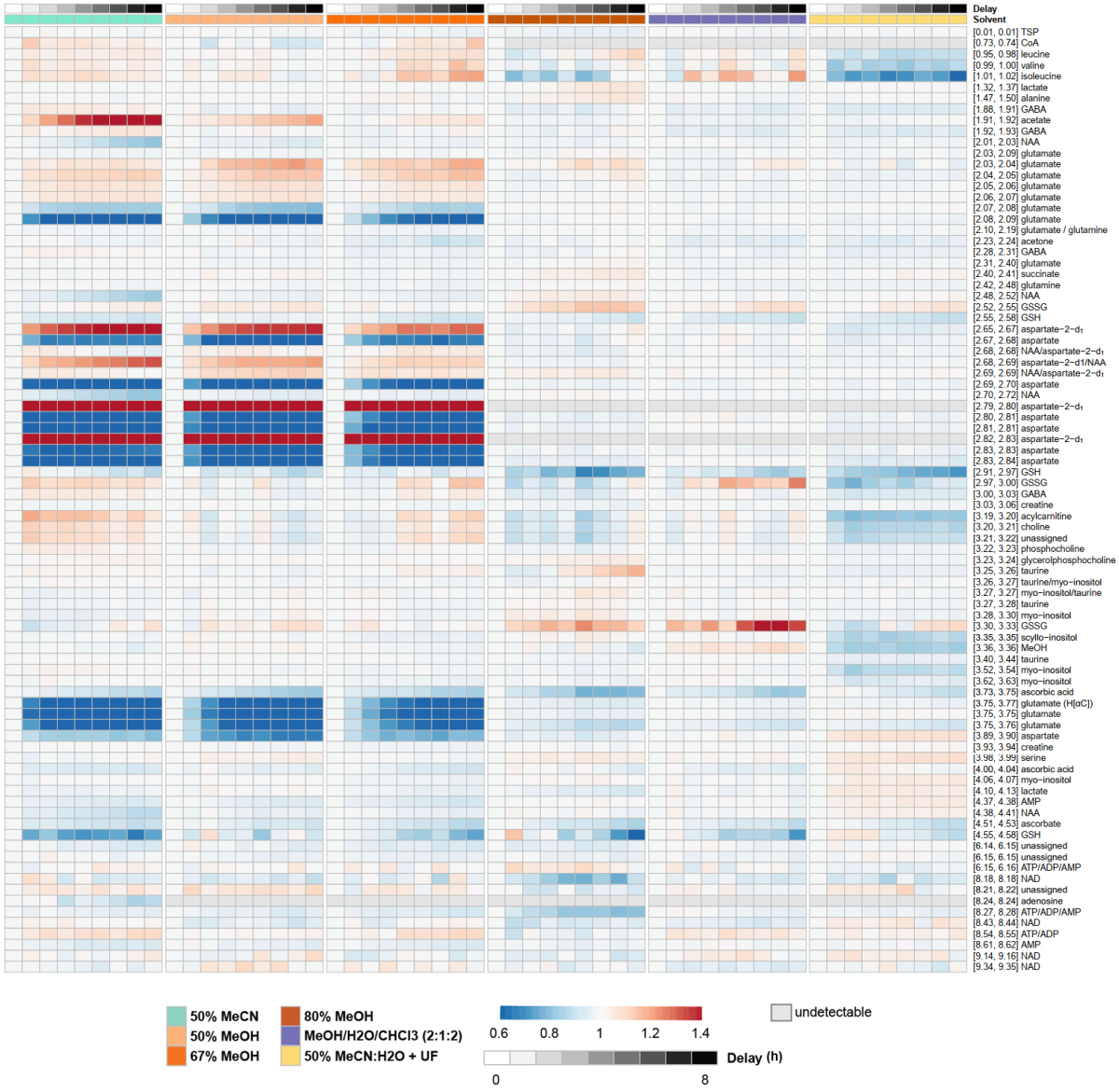

Figure 5-6 Heatmap of NMR resonance percentage changes for metabolites across extraction methods.

5.3.4.1 Aspartate and Glutamate

The instability of aspartate signals was observed in samples extracted with 50% MeCN, 50% MeOH, and 67% MeOH, indicated by a decrease in the doublet of doublet (dd) signals and the generation of nearby doublets signals at 2.82 and 2.68 ppm (p-values < 0.05, one-way ANOVA) (Figure 5-6**,** Figure 5-7). This change was most rapid within the initial hour after NMR sample preparation, with the original aspartate signals disappearing after two hours in samples extracted with 50% MeCN and after four hours in samples extracted with 50% and 67% MeOH (Figure 5-6).

Similarly, the glutamate multiplets, observed at 2.12 ppm and 2.35 ppm, exhibited a reduction in splitting in samples extracted with solvent mixtures of 50% MeCN, 50% MeOH, and 67% MeOH (p-values < 0.05, one-way ANOVA) (Figure 5-4). The overall integrals of these multiplets remained unchanged. Additionally, a considerable reduction was observed in the glutamate dd at 3.76 ppm in samples extracted using these methods (Figure 5-5). The glutamate dd was completely diminished after four hours in samples extracted with 50% MeCN (Figure 5-8).

The observed instability in the resonances of aspartate is attributed to the deuteration of aspartate, a phenomenon previously documented by Paskevich et al (Paskevich et al., 2013). This involves the replacement of the proton at the α-carbon (αH) of aspartate with deuterium, converting aspartate into aspartate-2-d_1. Consequently, it induces a change in the multiplicities of the βCH_2-group in aspartate, transforming the dd from the ABX spin system to AB doublets (Paskevich et al., 2013).

Here, similar to aspartate, deuteration of glutamate was observed. The substitution of the glutamate αH with deuterium would result in the disappearance of the resonance at 3.76 ppm and induce changes in the multiplicities of the βCH_2-group without altering the overall integrals.

The deuteration of aspartate and glutamate may be derived from aspartate transaminase (AST)-mediated metabolism. AST catalyses the interconversion of aspartate and α-

ketoglutarate to oxaloacetate and glutamate, during which the H2 hydrogens of aspartate and glutamate undergo exchange with those of water (D_2O in the NMR buffer) (García-Martín et al., 2002), leading to changes in the observed splitting patterns of NMR resonances. This suggests that AST may have remained active and did not fully precipitate during the extraction process, as supported by the high levels of remaining protein with these methods. While the proposed residual AST activity requires confirmation by independent experiments, current results confirmed that the deuteration is due to residual proteins, as ultrafiltration prevents the detection of any degree of deuteration.

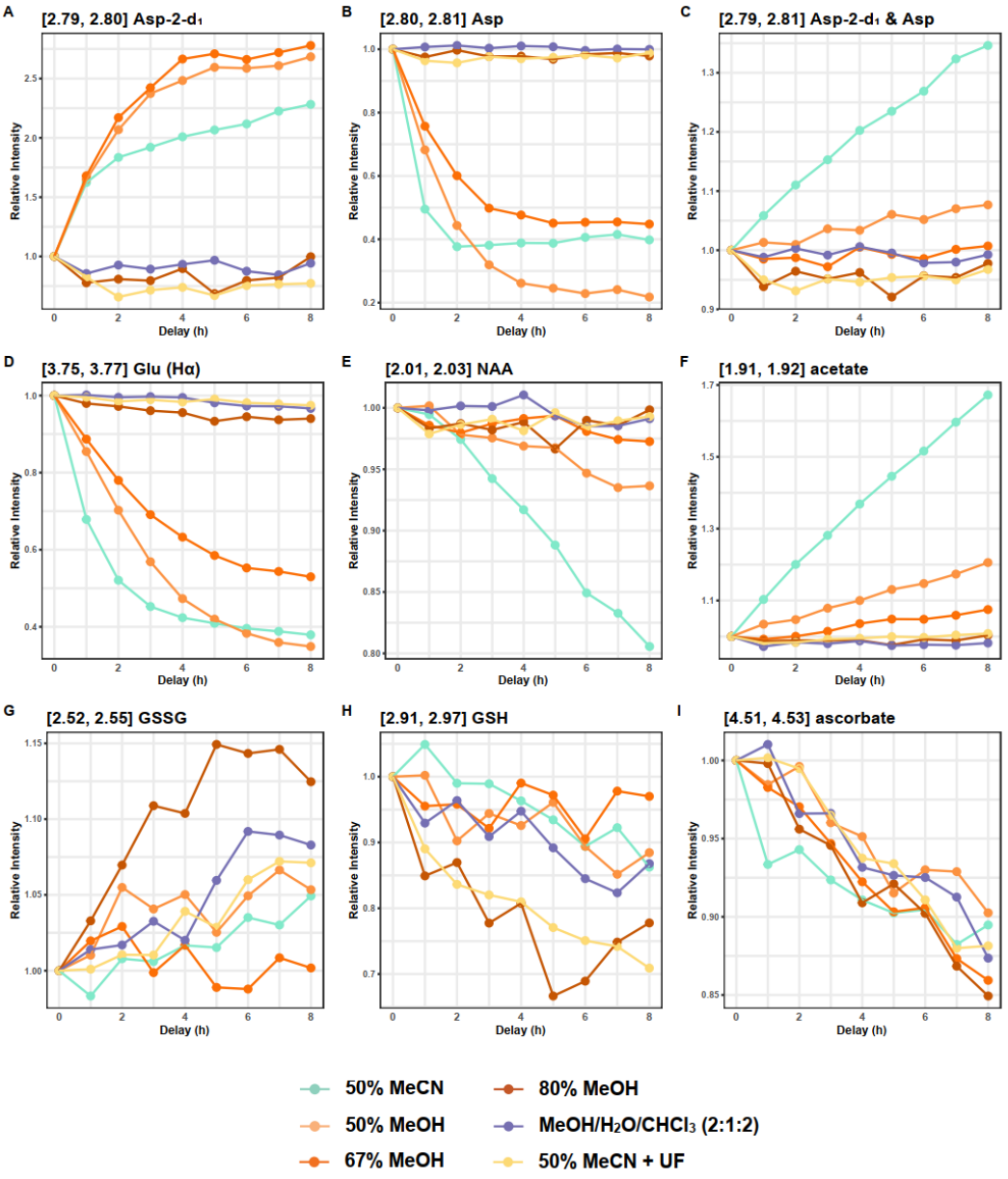

Figure 5-7 Changes in unstable metabolites across different extracts over time post sample preparation. Each data point refers to the mean of three replicates. Values were normalised to the 0-hour delay group within each extraction method. UF, ultrafiltration. Asp, aspartate. Glu, glutamate. NAA, N-acetyl aspartate. GSH and GSSG, reduced form and oxidised form of glutathione, respectively.

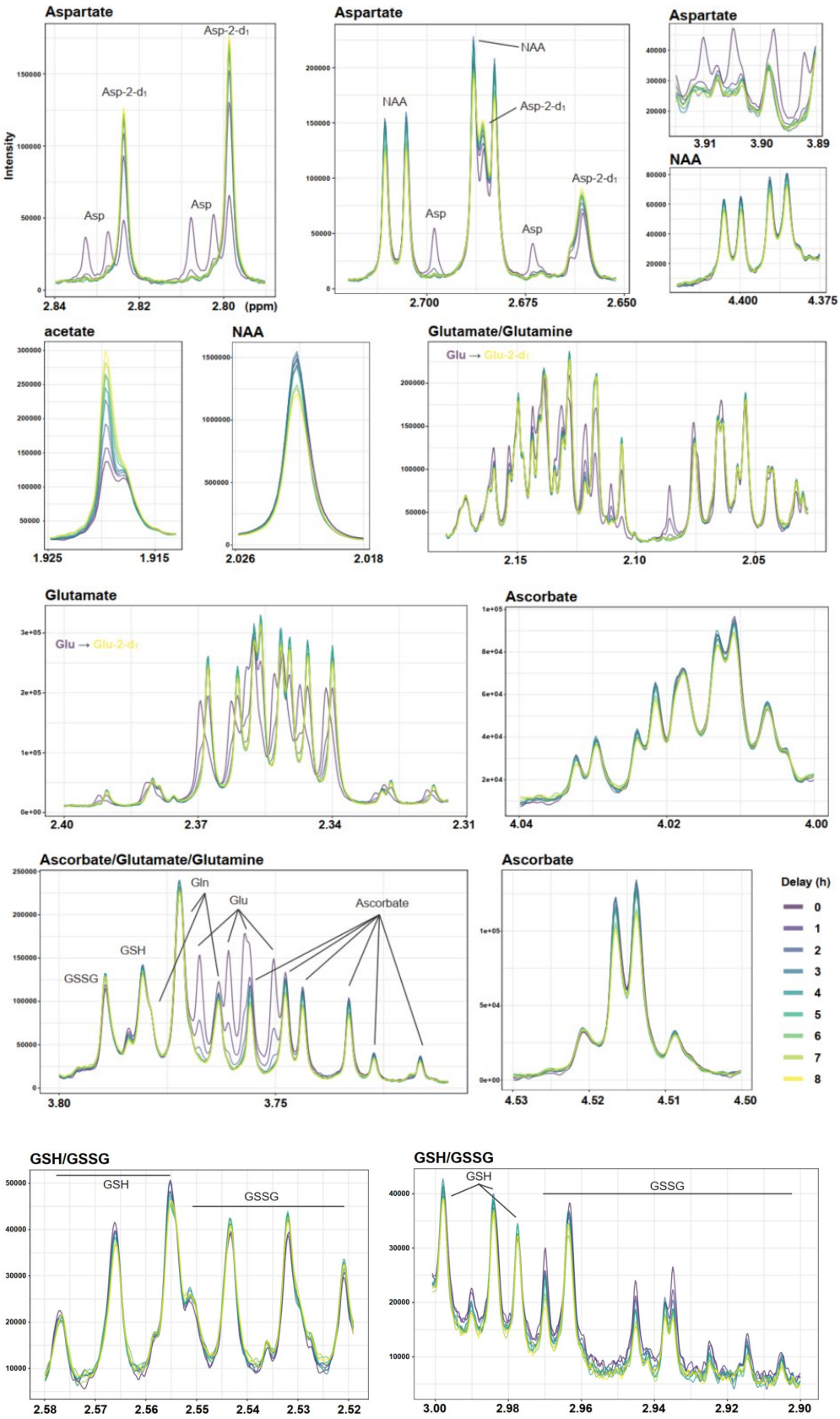

Figure 5-8 NMR spectra illustrating changes in unstable resonances over time delays in NMR measurement in a 50% MeCN brain sample.

5.3.4.2 N-acetyl Aspartate and Acetate

A reduction of N-acetyl aspartate (NAA) was observed in samples extracted with 50% MeCN, and to a lesser extent in those extracted with 50% MeOH (Figure 5-7, *p*-values < 0.05, one-way ANOVA). Concurrently, acetate levels increased (r = -0.94, *p*-value < 0.001, Pearson correlation) and aspartate-2-d_1 levels continued to rise even after the original aspartate signals had vanished (r = -0.82, *p*-value < 0.001, Pearson correlation). These observations suggest a conversion of NAA into aspartate and acetate. This conversion is further evidenced by the negative correlation between aspartate and aspartate-2-d1 at 0-3 hours (r = -0.94, *p*-value < 0.001, Pearson correlation) and their positive correlation at 4-8 hours (r = 0.76, $p < 0.01$, Pearson correlation). Additionally, combining the aspartate resonance and the aspartate-2-d_1 resonance showed a continuous increase over time in the samples extracted with 50% MeCN and 50% MeOH, while this remains unchanged in the 67% MeOH samples. This suggests the deuteration of aspartate and glutamate, and conversion of NAA to acetate and aspartate, represent distinct reactions.

In the brain, aspartoacylase (ASPA) catalyses the hydrolysis of NAA to produce acetate and aspartate (BIRNBAUM et al., 1952). Although independent experiments were not performed to directly confirm the presence of ASPA in the extracts, the observed conversion patterns align with known ASPA activity. Therefore, it is likely that some residual ASPA retained bioactivity in the NMR samples of the brain extracts from 50% MeCN and, to a lesser extent, 50% MeOH, as supported by higher residual protein levels in these samples. The conversion of NAA to acetate and aspartate was reduced and eventually absent as MeOH concentration increased. Despite the presence of residual ASPA remaining speculative, the observed conversion of NAA to aspartate and acetate is protein dependent. The addition of $CHCl_3$ and the use of ultrafiltration further enhanced protein precipitation with these methods and prevented such interconversion.

5.3.4.3 Glutathione

Oxidation of glutathione (GSH) was observed in all samples (p-values < 0.05, one-way ANOVA) with the exception of samples extracted with 67% MeOH (p-value > 0.05, one-way ANOVA). A significant negative correlation was observed between GSH and glutathione disulphide (GSSG) over time (r = -0.83, p-value < 0.001, Pearson correlation) (Figure 5-7, Figure 5-8). This was most evident in samples extracted with 80% MeOH, where a 22% ± 1% reduction in GSH and a 12% ± 6% increase in GSSG was observed after eight hours. GSH oxidation was unrelated to the residual protein content within samples (as these changes still occurred in samples subjected to ultrafiltration) suggesting that spontaneous oxidation outweighs any contribution from glutathione reductase. This aligns with the unstable nature of glutathione and previous findings in NMR-based blood metabolomics, indicating that degassed solvents or derivatising agents are required for accurate GSH measurement (Gowda et al., 2021).

5.3.4.4 Ascorbate

For all extraction methods, ascorbate concentrations showed a gradual decrease over the eight-hour period, resulting in a cumulative reduction of 10-15% across all the methods after eight hours (p-values < 0.05, one-way ANOVA) (Figure 5-7, Figure 5-8). The instability observed in ascorbate did not appear to be related to protein levels, as it still occurred in samples subjected to ultrafiltration. Additionally, a gradual reduction of ascorbic acid was observed in its standard solution in the NMR buffer (Figure 5-9). The spontaneous oxidation of ascorbate aligns with its well-known antioxidant properties and has been reported in previous studies (Bourafai-Aziez et al., 2022).

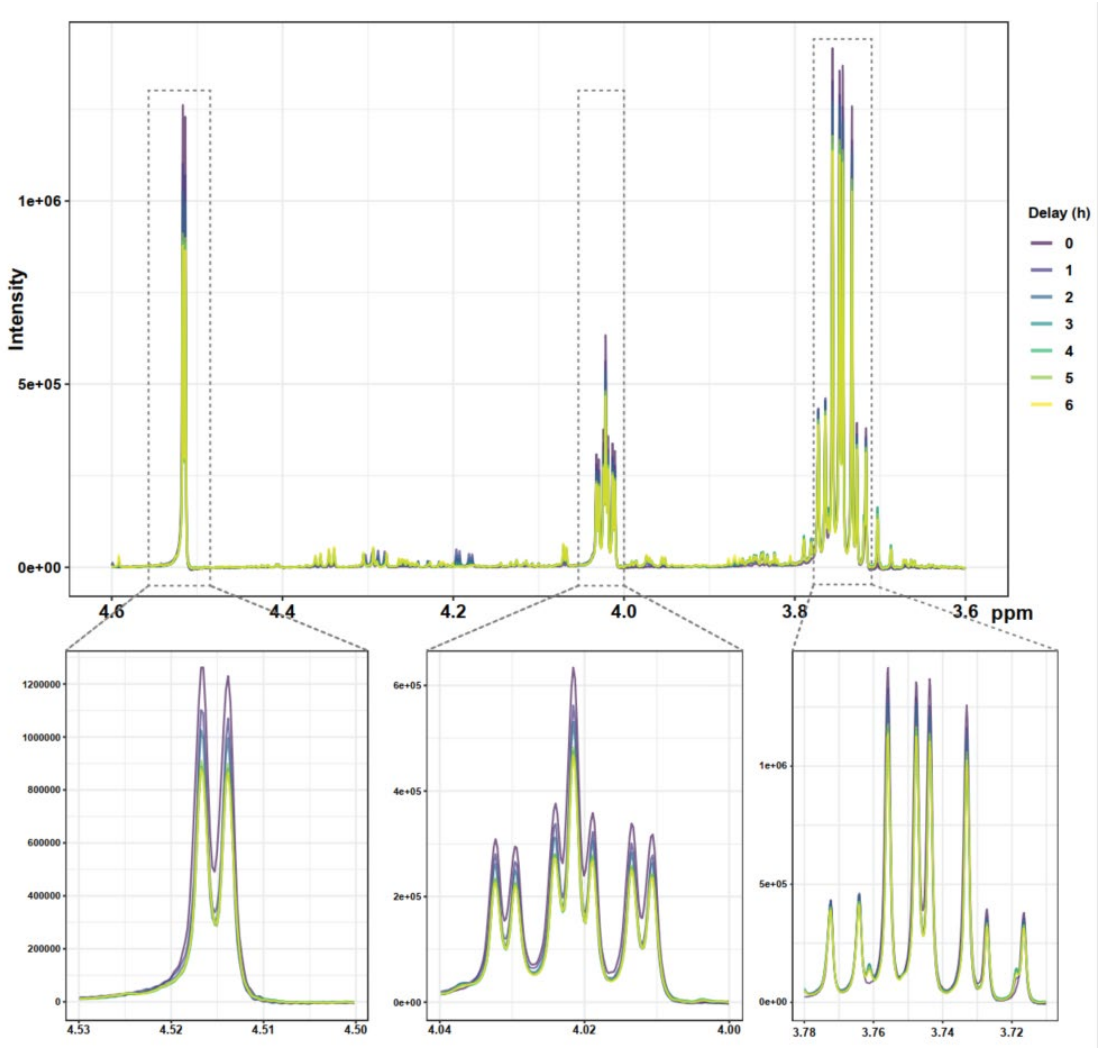

Figure 5-9 NMR spectra illustrating the reduction in ascorbate signals over time in an ascorbic acid standard sample (in phosphate buffer pH = 7.4) during NMR measurement.

5.3.4.5 Macromolecules

In line with the suboptimal deproteinisation of 50% MeCN extracted samples, broad macromolecule resonances were observed within the spectral regions of 0.8 - 1.0 ppm, 1.2 - 1.5 ppm, and 1.6 - 1.8 ppm. In contrast, the other five extraction methods, including 50% MeCN extraction with ultrafiltration, displayed a flat baseline in these regions (Figure 5-10), which is in agreement with previous reports (Gowda & Raftery, 2014; Lin et al., 2007).

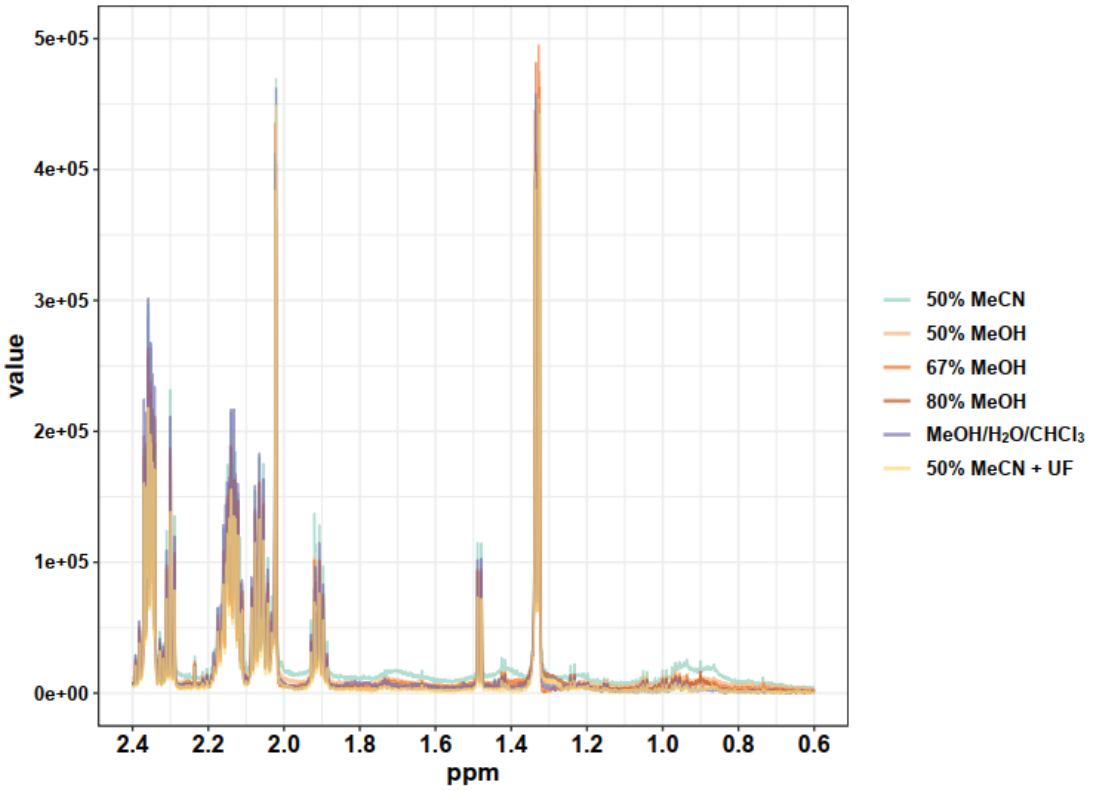

Figure 5-10 Enhanced baseline uniformity at 0.8 – 1.0 ppm, 1.2 – 1.5 ppm, 1.6 – 1.8 ppm in 50% MeCN samples with ultrafiltration (yellow) in contrast to 50% MeCN samples (green).

Interestingly, while no broad macromolecule signals were detectable in samples extracted with 80% MeOH at 0 hours, consistent with improved deproteinisation, two out of three replicates showed the appearance of increasingly broad signals over time at 0.85 - 0.90 ppm and 1.25 - 1.35 ppm (Figure 5-11). This led to increased leucine signals at 0.95-0.98 ppm over time (p-value < 0.001, one-way ANOVA), resulting in a cumulative increase of 13% after eight hours. Moreover, the lactate doublets at 1.33 ppm also had an increase of 9% after eight hours due to the increasing broad signals underneath it (p-value < 0.05, one-way ANOVA). These signals may arise due to the aggregation of residual protein in the sample over time. In contrast, 50% MeCN with ultrafiltration and MeOH/H_2O/$CHCl_3$ extraction resulted in NMR spectra devoid of any broad signals from macromolecules providing optimal baselines for analysis.

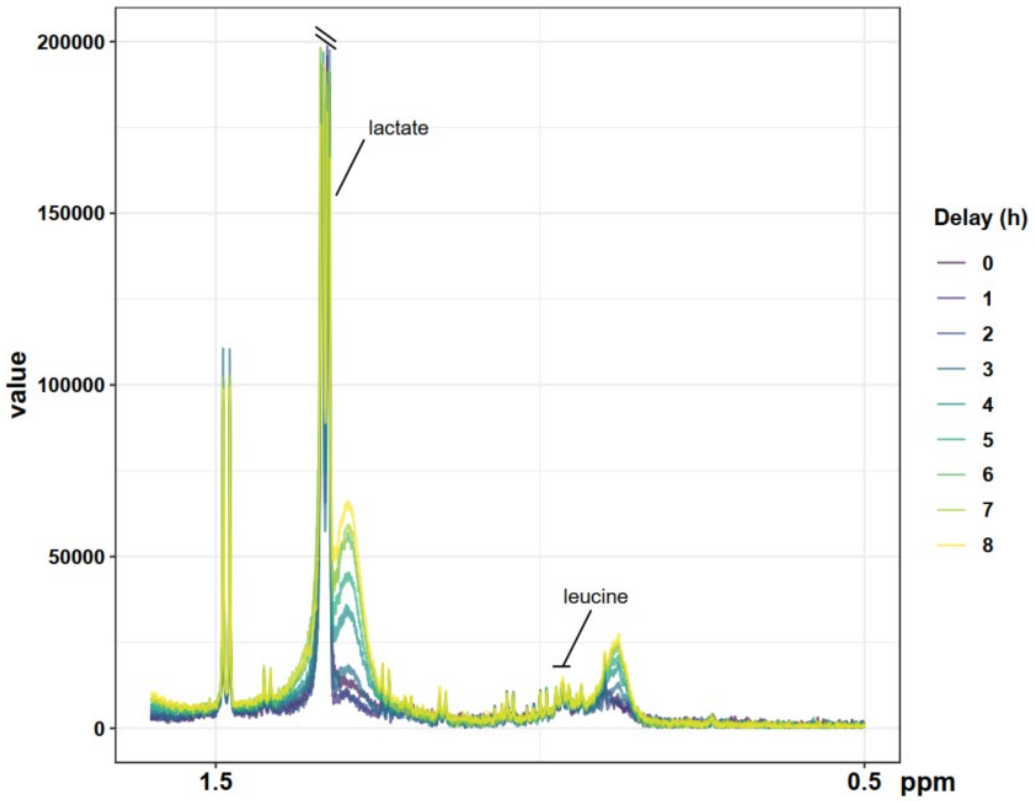

Figure 5-11 NMR spectra illustrating the increasing broad signals over time at 0.85 – 0.90 ppm and 1.25 – 1.35 ppm in an 80% MeOH brain extract during NMR measurement.

5.3.5 Summary and Recommendations

Among the tested methods, five methods (67% MeCN, 80% MeCN, 100% MeCN, 100% MeOH, and 50% MeOH with ultrafiltration) showed inadequate extraction efficiency and/or poor reproducibility, making them unsuitable for NMR brain metabolomics. The performance of the remaining six methods is summarised in Table 5-2, including relative extraction efficiency, reproducibility, protein levels and metabolite stability.

Table 5-2 Summary of the eight brain metabolite extraction methods in terms of extraction efficiency (mean ± SE), reproducibility (median, [IQR]), protein levels (mean ± SE), and metabolite stability.

Extraction method	Relative extraction efficiency (mean ± SE)	Reproducibility, RSD (%, median [IQR])	Protein levels (mg/ml, mean ± SE)	Asp and Glu deuteration	NAA conversion into aspartate and acetate	GSH oxidation to GSSG	Ascorbic acid reduction	Macromolecule signals
50% MeCN	1 ± 0.01	3.68 (3.49)	0.4 ± 0.01	++	++	+	+	+
50% MeOH	0.88 ± 0.01	4.66 (5.67)	0.35 ± 0.01	++	+	+	+	-

Extraction method	Relative extraction efficiency (mean ± SE)	Reproducibility, RSD (%, median [IQR])	Protein levels (mg/ml, mean ± SE)	Asp and Glu deuteration	NAA conversion into aspartate and acetate	GSH oxidation to GSSG	Ascorbic acid reduction	Macromolecule signals
67% MeOH	0.88 ± 0.03	7.48 (4.49)	0.31 ± 0.03	++	-*	-	+	-
80% MeOH	0.79 ± 0.03	5.93 (3.85)	0.26 ± 0.01	-	-	++	+	+
MeOH/H_2O/$CHCl_3$ (2:1:2)	0.96 ± 0.05	9.62 (2.66)	0.3 ± 0.01	-	-	+	+	-
50% MeCN + UF	0.73 ± 0.01	3.54 (5.55)	0.2 ± 0.02	-	-	+	+	-

-: no. -*: marginally. +: yes. ++: yes, and to a greater extent. SE, standard error. RSD, relative standard deviation. IQR, interquartile range. Asp, aspartate. Glu, glutamate. NAA, N-acetyl aspartate. GSH and GSSG, reduced form and oxidised form of glutathione, respectively. UF, ultrafiltration.

Three out of the remaining six methods (50% MeCN, 50% MeOH, and 67% MeOH) demonstrated good extraction efficiency and reproducibility but the deuteration of aspartate and glutamate resonances was observed possibly due to the inadequate denaturation/precipitation of AST. This highlights the importance of considering the effects of deuterated solvents and care should be taken to ensure that the integrals of both the protonated, and deuterated resonances, are combined to avoid spurious results. Furthermore, 50% MeCN and 50% MeOH were found to induce NAA conversion into aspartate and acetate, potentially linked to the insufficient denaturation of ASPA which poses a risk of false discoveries, particularly in the following scenarios: (1) during prolonged room temperature exposure; (2) during lengthy experiments with many samples, leading to long experimental durations; (3) the analysis of tissues where ASPA, potentially responsible for NAA conversion, is known to express; or (4) for the study of systems where the expression of ASPA is essential to the experimental readout. Therefore, these methods are not advised for untargeted metabolomics when these unstable signals are included in the data analysis. The findings highlight the importance of optimising the deproteinisation of tissues where residual enzymes could affect sample stability (including deuteration) or where protein expression levels vary, even when

pulse programs to suppress residual macromolecules are to be used.

Increasing the MeOH ratio to 80% increased protein precipitation ability, which sufficiently denatured residual proteins, but at the expense of decreased extraction efficiency. However, increasing broad signals over time led to an overestimation of lactate and leucine concentrations. This phenomenon was not observed in samples subjected to ultrafiltration or $MeOH/H_2O/CHCl_3$ extraction, likely indicating that the broad signals arise from incomplete protein precipitation. While this method offers simplicity and is well-suited for high-throughput studies, there is a risk of temporal inflation in the resonances of lactate and leucine.

Ultrafiltration, serving as a positive control for protein removal, reduced protein content by half to a 0.2 ± 0.02 mg/mL, as evidenced by the absence of broad macromolecule resonances up to eight hours post sample preparation. Moreover, ultrafiltration preserved the stability of aspartate, glutamate, NAA, and acetate, thus confirming that their instability originated from residual proteins. However, ultrafiltration led to a 27% reduction in overall metabolite abundance compared to the 50% MeCN extraction method. Additionally, glycerol contaminants from the filter masked the detection of glycine, certain myo-inositol, and glutamine resonances in the NMR spectrum. Consequently, ultrafiltration methods do not appear suitable for NMR analysis.

$MeOH/H_2O/CHCl_3$ extraction resulted in improved deproteinisation, while maintaining adequate extraction efficiency and reproducibility in agreement with previous studies (Belle et al., 2002; Diémé et al., 2017; Lin et al., 2007). Therefore, $MeOH/H_2O/CHCl_3$ extraction is recommended for untargeted brain NMR metabolic profiling over other tested methods. One disadvantage of $MeOH/H_2O/CHCl_3$ extraction is that it requires more time and careful handling compared to single-phase extraction methods, particularly during phase transfer, in order to mitigate variability. Moreover, this method does not address the observed decrease in ascorbate and oxidation of GSH. To maintain changes within 10% for glutathione and ascorbate, it is advisable to acquire spectra within 4 hours of sample preparation. For researchers requiring higher accuracy

for these metabolites, further optimisation of extraction methods may be necessary. This could include the addition of antioxidants, or derivatising agents, pH adjustments, the use of degassed solvents, and/or temperature control to reduce the risks of metabolite oxidation (Bourafai-Aziez et al., 2022; Fomenko et al., 2022a; Gowda et al., 2021; X. Yin et al., 2022).

While recommending specific extraction protocols, it is strongly advised to conduct trials of NMR spectroscopy and analysis on biological replicates using the method of choice before progressing to studying valuable samples. Absolute integral values were used in data analysis throughout this chapter to investigate preanalytical impact, while sum normalisation is typically used in metabolomic studies to mitigate the impact of concentration variations resulting from mass differences or pipetting errors (Figure 5-12). This chapter evaluated metabolite integrity at room temperature following NMR sample preparation. Not all NMR spectrometers are equipped with autosamplers that can maintain refrigerated conditions, and preparing and loading samples individually to mitigate enzymatic activity would be labour-intensive and inefficient. This limitation highlights the importance of effective deproteinisation during sample preparation to ensure metabolite stability. When feasible, using autosamplers with refrigeration capabilities is recommended, as this can further mitigate metabolite alterations and enhance the reliability of metabolomics analysis. The focus of this chapter was on the extraction and stability of polar metabolites, as NMR metabolomics is well-suited for aqueous phase extractions. Although the brain is a lipid-rich organ, lipidomics is better addressed using mass spectrometry, and thus, lipid extraction was not within the scope of this NMR-based study. Future studies should consider incorporating lipidomic analyses to obtain a more comprehensive metabolic profile.

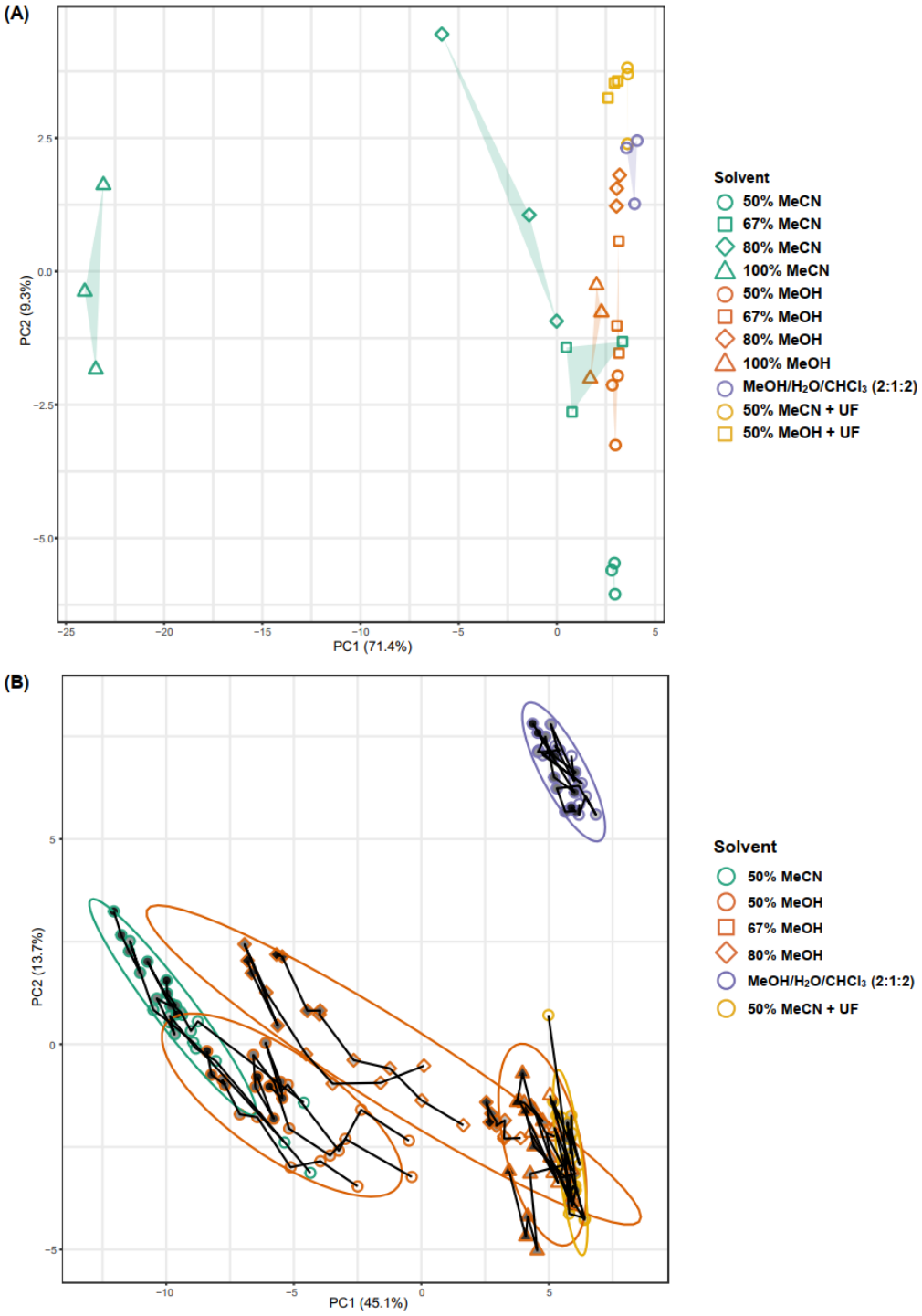

Figure 5-12 Sum normalised method reduced the impact of variations in overall sample concentration. This is compared to **Figure 5-3**D and **Figure 5-5**A, where absolute values were used for PCA. (A) PCA scores plot of the brain metabolic profiles from different extraction methods with no delay in NMR measurement. (B) PCA scores plot of brain metabolic profiles from six extraction methods over a time range from 0 to 8 hours of delay in NMR measurement.

The findings here are specific to brain tissue, which has unique biochemical

characteristics, such as a high lipid content and distinct protein compositions. While the addition of chloroform appears necessary for effective protein precipitation in brain tissue, the requirements may differ for other tissues. The most efficient protein removal method may not always be optimal in terms of time and metabolite recovery. For instance, tissues that lack significant amounts of these enzymes might achieve sufficient protein removal with simpler single-phase extractions, such as 50% MeOH or 50% MeCN. These simpler methods could offer benefits in terms of reproducibility and ease of use, particularly for high-throughput workflows. Future studies would be valuable to explore and optimise extraction protocols tailored to the unique biochemical properties of different tissues.

This chapter highlights the importance of optimising extraction methods for brain NMR metabolomics, particularly in balancing metabolite stability (including that affected by deuteration) and effective protein precipitation. While this chapter used brain tissues from rodent models, these techniques could be similarly applied to human brain biopsies, where the amount of tissue available is also limited. This approach has direct relevance to both animal studies and potential clinical applications in human tissue analysis. Future research should explore the applicability of these protocols to human samples, particularly in clinical settings where precise metabolic profiling is crucial for diagnosis and treatment monitoring. In such cases, while histology alone may not provide a definitive diagnosis, metabolic profiling could offer valuable complementary insights.

5.4 Conclusion

This chapter is the first systematic investigation into the effect of residual protein contamination on metabolite stability following NMR sample preparation in brain tissues. The findings underscore the crucial role of protein precipitation in maintaining metabolite integrity, particularly for key metabolites such as aspartate, glutamate, and N-acetyl aspartate. The results demonstrate that insufficient protein precipitation in commonly used extraction solvents (50% MeCN, 50% MeOH, and 67% MeOH) leads

to metabolite instability (including that affected by deuteration), which can markedly compromise the reliability of NMR-based metabolomics studies. These results highlight the importance of optimising extraction methods for effective deproteinisation to ensure the stability of NMR spectra—a factor often overlooked due to the tolerance of NMR instrumentation to residual protein contamination.

By identifying MeOH/H_2O/$CHCl_3$ extraction as a reproducible method for enhancing metabolite stability, this study provides a valuable tool for brain metabolomics research, which can be readily applied to optimise sample preparation protocols and improve the accuracy of metabolomic profiling. Although MeOH/H_2O/$CHCl_3$ extraction was effective in preventing protein-related instabilities, further optimisation is required to improve the stability of oxidation-sensitive metabolites. Future research should investigate the use of antioxidants, degassed solvents, or other stabilising agents to mitigate oxidation during the extraction process, as this remains a limitation of the present study.

Chapter 6: Discussion

6.1 Principal Findings of the Thesis

The overarching aim of this thesis was to use NMR-based metabolomics for biomarker discovery to improve the diagnostics of antibody-mediated neurological diseases. To achieve this, the thesis addressed four key hypotheses: (1) plasma NMR-based metabolomics can distinguish patients with AE from those with DRE; (2) psychosis patients with NSAb have distinct serum metabolomic profiles compared to those without such antibodies; (3) sodium fluoride/potassium oxalate blood tubes provide better metabolite preservation during preanalytical delays than conventional serum and heparin tubes; and (4) MeOH/H_2O/$CHCl_3$ extraction improves metabolite stability in brain tissue by ensuring more effective protein precipitation.

This thesis demonstrated the utility of NMR-based metabolomics in both blood and brain tissue analyses, offering complementary approaches to address clinical challenges in diagnosing neurological diseases. The principal findings of this thesis are as follows:

1. NMR-based metabolomics successfully distinguished AE from DRE and stratified AE subtypes (NMDAR-, LGI1-, CASPR2-AE). AE-specific plasma metabolic signatures included decreased levels of HDL, phosphatidylcholine, and albumin, while subtype-specific alterations included changes in lactate, glucose, UFA, and GlycA.
2. As the NSAb, causative for AE, have also been detected in some psychosis patients, this thesis extended its approach to investigate serum metabolic profiles in acute psychosis with and without serum NSAb. Contrary to the original hypothesis, no general metabolic signatures were identified for antibody-positive psychosis. However, a metabolically distinct subgroup of patients with psychosis was identified, associated with higher PANSS scores and VGKC/GlyR antibody positivity. Their metabolic signatures indicate a potential inflammatory aetiology, suggestive of an inflammatory subset of psychosis.

3. To facilitate validation and application of blood NMR metabolomics in large cohorts, this thesis explored the impact of pre- and post-processing delays on metabolite variability within and between biobanks. Primary fluctuations observed in glucose and lactate levels were attributed to glycolysis resulting from delayed erythrocyte separation. Fluoride oxalate blood tubes effectively stabilised glucose and lactate levels for 24 hours at both 4 °C and room temperature, making them a viable alternative when rapid processing is not feasible. Furthermore, post-processing delays of 12 hours had negligible effects on the metabolome, indicating the practicality of such workflow.
4. Beyond blood, this thesis investigated NMR metabolomics in brain biopsy tissues to identify metabolic alterations directly associated with brain pathologies. It highlighted the critical role of protein precipitation during metabolite extraction in maintaining metabolite stability. Common extractants like 50% acetonitrile and 50% methanol failed to adequately denature proteins, leading to instability in aspartate, glutamate, NAA, and acetate. The methanol/water/chloroform extraction effectively preserved metabolite stability through robust protein precipitation, demonstrating good efficiency and reproducibility; therefore, it is recommended for untargeted brain NMR metabolomics studies.

In summary, these findings demonstrate the potential of NMR-based metabolomics to advance biomarker discovery and improve diagnostics for neurological diseases by addressing both methodological challenges and clinical applications.

6.2 Limitations and Future Work

6.2.1 AE biomarkers

This finding presents the first non-antibody-based biomarker for differentiating DRE, AE and AE subtypes, offering a promising adjunct to facilitate the diagnosis and

therapeutic decisions. It provides a non-invasive, reliable diagnostic tool that could be used in clinical settings to improve diagnostic accuracy and patient outcomes.

However, there are some limitations to this study. While the diagnostic questions addressed are asked in the context of 'unwell' individuals with specific clinical signs (as would be the case in the clinic), healthy controls or patients with other antibody-mediated diseases were not included, making it challenging to assert whether the identified pattern is specific to AE. Additionally, due to differences in blood collection protocols, it was impossible to integrate NMR metabolomics data from previous research conducted within our lab on antibody-mediated NMOSD (Jurynczyk et al., 2017), or the antibody-mediated psychosis data presented in Chapter 3. Although an ultracentrifugation step of plasma samples prior to NMR analysis was included in accordance with the standard operating procedures used for previous cohorts in the lab, differences in blood collection disallow the integration of these cohorts. Moreover, this procedure depleted VLDL, extracellular vesicles and debris and gave cleaner lipoprotein signals but limits the generalisability of the findings and the broader applications. Future research should aim to determine whether the ultracentrifugation step is essential for achieving the diagnostic performance reported here, as has been the case for other disease cohorts studied in our lab, or if the step can be omitted.

Further research is needed to validate the identified metabolic biomarkers for AE in larger, independent cohorts to confirm their diagnostic utility and generalisability. Additionally, it would be interesting to explore the longitudinal changes in these metabolic profiles during disease progression in the hopes of providing insights into AE pathophysiology and monitor treatment response. Further research should include more AE subtypes, such as AE with other NSAb (e.g., GABAR, GlyR, AMPAR), AE with autoantibodies against intracellular targets, seronegative AE (AE with unidentifiable pathogenic antibodies), and autoimmune psychosis.

Given the observed alterations in lipid and glucose metabolisms, future work should leverage advanced methodologies like NMR lipoprotein profiling (e.g. Bruker iVDR,

Nightingale Health, Numares AXINON), MS-based lipidomics, and MS-based metabolomics to analyse a wider range of related metabolites.

6.2.2 A Metabolically Distinct Subtype of Psychosis Associated with VGKC/GlyR Antibodies

Using NMR metabolomics, this thesis identified a metabolically distinct subtype of acute psychosis associated with VGKC/GlyR antibody and higher PANSS scores. These findings support the hypothesis from previous research that VGKC antibodies may be a non-specific marker of inflammatory brain conditions (Hacohen et al., 2015; Prüss & Lennox, 2016).

In contrast to the findings for AE, no general metabolic signatures were identified for antibody-mediated psychosis, including cases involving NMDAR, LGI1, or CASPR2 antibodies. This divergence may reflect differences in the clinical presentations of these conditions. While these NSAb can be causative in both AE and autoimmune psychosis, the latter is characterised by isolated psychotic symptoms with minimal neurological features and is often considered a mild form of AE (Najjar et al., 2018). One explanation for the absence of distinct metabolic signatures in antibody-mediated psychosis may be the magnitude of the neuroinflammatory response generated by the NSAb in autoimmune psychosis compared to AE. A milder inflammatory response might limit the metabolic changes detectable by NMR, resulting in similar profiles between antibody-positive and antibody-negative psychosis. However, in the psychosis cohort with VGKC/GlyR antibodies, certain metabolic alterations resembling those seen in AE were observed, such as reduced phosphatidylcholine and HDL levels, along with elevated glucose levels. This overlap suggests a shared underlying metabolic dysregulation, potentially linked to inflammation in both conditions.

There are several limitations to the psychosis study. For example, the samples were collected in serum separator tubes and processed after a delay of one to two days. Such extended delays, particularly at room temperature, are known to alter metabolic profiles, especially for metabolites like glucose and lactate (Bervoets et al., 2015; Fliniaux et al.,

2011a; Kamlage et al., 2014, 2018a; Santos Ferreira et al., 2019a). Additionally, the small sample sizes for each group and the absence of other psychiatric or neurological groups limit the ability to assess the specificity of the identified metabolic signatures. Future work should include other autoimmune neurological disorders such as AE and multiple sclerosis. AE shares overlapping symptoms and a similar aetiology with autoimmune psychosis, while multiple sclerosis serves as a neuroinflammatory comparator. Including these groups can help determine whether the observed metabolic changes are unique to psychosis or reflect broader neuroinflammatory processes.

To validate the identified biomarkers and assess their clinical utility, prospective cohorts are important. These allow for standardised sample collection, reduce pre-analytical variability, and enable the observation of how metabolic profiles evolve over time in relation to disease progression or treatment response, helping establish causal relationships. Additionally, measuring routine inflammatory markers such as CRP alongside metabolomics can provide additional insights into the relationship between systemic inflammation and metabolic changes in psychosis. Furthermore, as demonstrated in Chapter 4, preanalytical variations caused by delay in blood preprocessing need to be minimised to improve data quality and reliability. Future sample collection should adopt optimised sample collection protocols, including using fluoride oxalate blood tubes, maintaining blood samples at 4 °C prior to erythrocyte separation, and reducing delays before processing to preserve metabolite integrity.

6.2.3 Preanalytical Variations in Blood Collection

This thesis suggests that fluoride oxalate tubes could be advantageous in metabolomic studies where blood processing times vary, pending further validation with a broader range of metabolites and larger sample sizes. While fluoride oxalate tubes preserve glucose and lactate levels, they also have limitations. Fluoride oxalate tubes are prone to causing haemolysis when left at room temperature for extended periods, consistent with previous studies (Al-Kharusi et al., 2014; Lippi et al., 2018). Haemolysis can significantly impact MS-based metabolic profiles, though it does not impact NMR metabolic profiles

(Bervoets et al., 2015; Kamlage et al., 2014; *P.* Yin et al., 2013). Another point worth noting is that the FX tubes reduce background signals from albumin and lipoproteins, which results in lower integral values compared to serum and LH plasma. If this reduction is limited to proteins without affecting small molecules, it may be a positive outcome, as it could enhance the clarity of metabolite signals by reducing interference from proteins and lipids.

Preanalytical variations, if not addressed properly, can obscure true biological effects or introduce false-positive associations in large-scale metabolomic studies. Recent work has demonstrated the effectiveness of robust regression approaches to remove technical variations in NMR metabolomic data from the UK Biobank (Ritchie et al., 2023). These adjustments accounted for factors such as sample preparation time, shipping plate well, spectrometer batch effects, drift over time within the spectrometer, and outlier shipping plates. Implementing such quality control measures significantly enhances the reproducibility and reliability of metabolomic data across large cohorts and improves the power of genetic and epidemiological studies.

Incorporating computational methods like robust regression into future analyses could complement the development of optimised preanalytical protocols, providing a powerful combined strategy for addressing technical variability in metabolomics. Additionally, extending these findings by incorporating a broader spectrum of metabolomic analyses, including mass spectrometry and advanced lipoprotein assays, would further enhance the understanding of preanalytical variability across different analytical platforms. Discovering novel additives that inhibit major metabolic pathways in blood under anaerobic conditions and prevent haemolysis would greatly improve the reliability of metabolomic studies, particularly in large-scale, multi-site investigations.

6.2.4 Metabolite Extraction Methods for Brain NMR Metabolomics

Among the methods tested, methanol/water/chloroform method was identified as the most suitable brain extraction method for untargeted brain NMR metabolomics. This method effectively preserves metabolite stability by achieving effective protein

precipitation, demonstrating good extraction efficiency and reproducibility. As revealed in this chapter, insufficient protein precipitation can lead to deuteration of Hα in aspartate and glutamate, as well as NAA conversion into aspartate and acetate. Residual enzymatic activities, specifically AST and ASPA, were proposed as the causes of these changes. This conclusion is supported by the observed NMR results (changes in metabolite levels and signal multiplicity), established biochemistry, and existing literature. Future research can perform Western blotting to further substantiate the involvement of AST and ASPA in these processes. Additionally, it would be helpful to investigate the extent that metabolite alteration can be slowed down under conditions that incorporate cooling systems during NMR analysis.

However, the methanol/water/chloroform method does not address the instability of glutathione and ascorbate, likely due to oxidation. To address the limitation, future research could evaluate the use of degassed NMR buffers to minimise oxidative effects during sample preparation. Additionally, derivatising agents such as *N*-ethylmaleimide, which has been successfully applied in NMR-based blood metabolomics (Gowda et al., 2021), can be adapted and assessed or their ability to stabilise labile metabolites like glutathione and ascorbate in brain metabolomics. Further optimisation of methanol/water/chloroform method could involve testing different solvent ratios to improve extraction efficiency and reproducibility while maintaining effective protein precipitation. Additionally, substituting chloroform with less toxic alternatives, such as dichloromethane, can be evaluated to determine if it improves safety without compromising performance.

Despite its advantages, the methanol/water/chloroform method requires more complex processes than single-phase extraction, which may lead to increased variation. The development of single-phase extraction methods that balance adequate protein precipitation with high metabolite recovery could significantly benefit large-scale, high-throughput studies in brain metabolomics. Potential approaches include testing alternative solvents, such as isopropanol, hexane, or methyl tert-butyl ether (MTBE),

and incorporating additives such as salts (e.g., ammonium sulphate) or weak acids (e.g., formic acid) to enhance protein precipitation and stabilise metabolite solubility (Mushtaq et al., 2014).

6.2.5 Change in Bucketing Strategies

Different bucketing strategies were applied across chapters depending on the analysis requirements. Fixed-width bucketing, used in Chapter 4, offers greater reproducibility and is easily automated, although regions with noise or water still require manual exclusion. However, fixed-width bucketing cannot avoid peak splitting or overlapping. To address this, manual bucketing was used in Chapters 3, 5, and 6 to better align bucket boundaries with peak shapes, improving quantification accuracy. While less reproducible across operators, manual bucketing is more effective in resolving complex or overlapping signals. Looking ahead, deconvolution methods with robust reproducibility may offer a more consistent solution to signal overlap.

6.2.6 Multi-omics Integration and Applications of Multiple Machine Learning Methods

This thesis used NMR as analytical technique for metabolomics, which offered several advantages, including minimal sample preparation, fast analytical time, robust instrumentation, non-destructive analysis, detection of biologically important metabolites. However, NMR's sensitivity remains a significant limitation, restricting its ability to detect low-abundance metabolites. Integrating MS with NMR for metabolomics can improve metabolite coverage, increase accuracy of metabolite assignments and provides validation of metabolite changes (Bhinderwala et al., 2018). Such a combined approach not only provides a more holistic understanding of metabolic alterations but also increases the biological interpretability of results and has the potential to boost model performance.

In addition to integrating analytical platforms, integrating metabolomics data from different tissues provides a broader view of an organism's metabolic state and uncovers

tissue-specific metabolic alterations and cross-talk, enriching understanding of systemic metabolic regulation. The value of metabolomics integration further increases when combined with other omics layer, such as genomics, transcriptomics, proteomics and microbiome data. This multi-omics approach provides a more comprehensive understanding of the molecular mechanisms underlying metabolic pathways (C. Chen et al., 2023). For instance, combining transcriptomics with tissue-specific metabolomics can elucidate how gene expression changes influence metabolic processes in distinct tissues, while proteomics can shed light on enzyme activities and protein-metabolite interactions driving these processes.

To enhance the analytical power of integrated omics datasets, additional machine learning methods can be employed alongside OPLS. Algorithms such as random forest (RF), support vector machine (SVM), extreme gradient boosting (XGBoost), and artificial neural networks (ANN) can bring unique strengths in feature selection, classification, and pattern recognition, making them valuable complements to OPLS. RF is valued for its speed, low risk of overfitting, evaluation of feature importance, and good performance on imbalanced or missing data (T. Chen et al., 2013). Similarly, XGBoost is effective for managing high-dimensional sparse data, is robust to missing values, and provides effective tools for evaluating feature importance (Yuan et al., 2024). SVM performs particularly well in scenarios with a large number of features and a small number of training samples (Heinemann et al., 2014). Meanwhile, ANN, particularly deep learning models, are capable of uncovering intricate, non-linear patterns and interactions, making it powerful for analysing large-scale multi-omics datasets (Mendez, Broadhurst, et al., 2019).

Using a combination of machine learning methods can provide a more comprehensive evaluation of the data, enabling cross-validation of findings and reducing biases associated with relying on a single analytical approach. Moreover, advanced interpretability tools, such as Tree-based Shapley Additive Explanations (SHAP), can enhance the analysis by elucidating the contributions of individual features to predictive

models, improving the interpretations of metabolomics data (Bifarin, 2023; J. D. Zhang et al., 2023).

6.3 Concluding Remarks

This thesis has demonstrated the potential of NMR-based blood metabolomics as a diagnostic tool in antibody-mediated neurological diseases, specifically through the identification of biomarkers for AE and VGKC/GlyR-antibody-mediated psychosis. The research highlights the role of metabolic profiling in uncovering disease-specific metabolic signatures, offering promising insights for early diagnosis and personalised treatment strategies. Moreover, the thesis has contributed to the advancements of pre-analytical methods for blood metabolomics and metabolite extraction protocols for brain metabolomics. The use of fluoride oxalate blood tubes effectively minimised pre-analytical variability, paving the way for more robust and reproducible results in clinical studies. For brain tissue metabolomics, the methanol/water/chloroform extraction method emerged as a suitable approach for untargeted metabolomics. This method highlighted the importance of sufficient protein precipitation in preserving metabolite stability and ensuring reliable downstream analyses.

References

Abboud, H., Probasco, J. C., Irani, S., Ances, B., Benavides, D. R., Bradshaw, M., Christo, P. P., Dale, R. C., Fernandez-Fournier, M., Flanagan, E. P., Gadoth, A., George, P., Grebenciucova, E., Jammoul, A., Lee, S.-T., Li, Y., Matiello, M., Morse, A. M., Rae-Grant, A., … Titulaer, M. J. (2021a). Autoimmune encephalitis: Proposed best practice recommendations for diagnosis and acute management. *Journal of Neurology, Neurosurgery & Psychiatry*, *92*(7), 757–768. https://doi.org/10.1136/jnnp-2020-325300

Abboud, H., Probasco, J., Irani, S. R., Ances, B., Benavides, D. R., Bradshaw, M., Christo, P. P., Dale, R. C., Fernandez-Fournier, M., Flanagan, E. P., Gadoth, A., George, P., Grebenciucova, E., Jammoul, A., Lee, S.-T., Li, Y., Matiello, M., Morse, A. M., Rae-Grant, A., … Titulaer, M. (2021b). Autoimmune encephalitis: Proposed recommendations for symptomatic and long-term management. *Journal of Neurology, Neurosurgery & Psychiatry*, *92*(8), 897–907. https://doi.org/10.1136/jnnp-2020-325302

Abboud, T., Rohde, V., & Mielke, D. (2023). Mini review: Current status and perspective of S100B protein as a biomarker in daily clinical practice for diagnosis and prognosticating of clinical outcome in patients with neurological diseases with focus on acute brain injury. *BMC Neuroscience*, *24*(1), 38. https://doi.org/10.1186/s12868-023-00807-2

Abdelhak, A., Foschi, M., Abu-Rumeileh, S., Yue, J. K., D'Anna, L., Huss, A., Oeckl, P., Ludolph, A. C., Kuhle, J., Petzold, A., Manley, G. T., Green, A. J., Otto, M., & Tumani, H. (2022). Blood GFAP as an emerging biomarker in brain and spinal cord disorders. *Nature Reviews Neurology*, *18*(3), Article 3. https://doi.org/10.1038/s41582-021-00616-3

Abdelhak, A., Huss, A., Kassubek, J., Tumani, H., & Otto, M. (2018). Serum GFAP as a biomarker for disease severity in multiple sclerosis. *Scientific Reports*, *8*(1), 14798. https://doi.org/10.1038/s41598-018-33158-8

Abdi, H. (2007). The Bonferonni and Šidák Corrections for Multiple Comparisons. *Encyclopedia of Measurement and Statistics*, *3*.

Aguilar, J. A., Nilsson, M., Bodenhausen, G., & Morris, G. A. (2011). Spin echo NMR spectra without J modulation. *Chemical Communications*, *48*(6), 811–813. https://doi.org/10.1039/C1CC16699A

Alam, A. M., Easton, A., Nicholson, T. R., Irani, S. R., Davies, N. W. S., Solomon, T., & Michael, B. D. (2023). Encephalitis: Diagnosis, management and recent advances in the field of encephalitides. *Postgraduate Medical Journal*, *99*(1174), 815–825. https://doi.org/10.1136/postgradmedj-2022-141812

Al-Diwani, A., Handel, A., Townsend, L., Pollak, T., Leite, M. I., Harrison, P. J., Lennox, B. R., Okai, D., Manohar, S. G., & Irani, S. R. (2019). The psychopathology of NMDAR-antibody encephalitis in adults: A systematic review and phenotypic analysis of individual patient data. *The Lancet Psychiatry*, *6*(3), 235–246. https://doi.org/10.1016/S2215-0366(19)30001-X

Al-Diwani, A., Pollak, T., Langford, A., & Lennox, B. (2017). Synaptic and neuronal autoantibody-associated psychiatric syndromes (SNAps): Controversies and Hypotheses. *Frontiers in Psychiatry*, *8*, 13. https://doi.org/10.3389/fpsyt.2017.00013

Alexander, J. L., Wyatt, N. J., Camuzeaux, S., Chekmeneva, E., Jimenez, B., Sands, C. J., Fuller, H., Takis, P., Ahmad, T., Doyle, J. A., Hart, A., Irving, P. M., Kennedy, N. A., Lees, C. W., Lindsay, J. O., McIntyre, R. E., Parkes, M., Prescott, N. J., Raine, T., … Lamb, C. A. (2023). Considerations for peripheral blood transport and storage during large-scale multicentre metabolome research. *Gut*. https://doi.org/10.1136/gutjnl-2022-329297

Al-Kharusi, A., Al-Lawati, N., Al-Kindi, M., & Mula-Abed, W.-A. (2014). Are Tubes Containing Sodium Fluoride Still Needed for the Measurement of Blood Glucose in Hospital Laboratory Practice? *Oman Medical Journal*, *29*(6), 404–407. https://doi.org/10.5001/omj.2014.109

Allen, N. E., Arnold, M., Parish, S., Hill, M., Sheard, S., Callen, H., Fry, D., Moffat, S., Gordon, M., Welsh, S., Elliott, P., & Collins, R. (2021). Approaches to minimising the epidemiological impact of sources of systematic and random variation that may affect biochemistry assay data in UK Biobank. *Wellcome Open Research*, *5*, 222. https://doi.org/10.12688/wellcomeopenres.16171.2

Álvarez-Sánchez, B., Priego-Capote, F., & Castro, M. D. L. de. (2010). Metabolomics analysis II. Preparation of biological samples prior to detection. *TrAC Trends in Analytical Chemistry*, *29*(2), 120–127. https://doi.org/10.1016/j.trac.2009.12.004

American Diabetes Association. (2011). Diagnosis and Classification of Diabetes Mellitus. *Diabetes Care*, *34*(Suppl 1), S62–S69. https://doi.org/10.2337/dc11-S062

Amorini, A. M., Nociti, V., Petzold, A., Gasperini, C., Quartuccio, E., Lazzarino, G., Di Pietro, V., Belli, A., Signoretti, S., Vagnozzi, R., Lazzarino, G., & Tavazzi, B. (2014). Serum lactate as a novel potential biomarker in multiple sclerosis. *Biochimica et Biophysica Acta (BBA) - Molecular Basis of Disease*, *1842*(7), 1137–1143. https://doi.org/10.1016/j.bbadis.2014.04.005

Anderyas, P., Halliday, A., & Reardon, K. (2022). Anti-LGI1-Associated Myopathy in the Setting of Neuromuscular Hyperexcitability Syndrome. *JAMA Neurology*, *79*(12), 1319–1320. https://doi.org/10.1001/jamaneurol.2022.3479

Andresen, C., Boch, T., Gegner, H. M., Mechtel, N., Narr, A., Birgin, E., Rasbach, E., Rahbari, N., Trumpp, A., Poschet, G., & Hübschmann, D. (2022). Comparison of extraction methods for intracellular metabolomics of human tissues. *Frontiers in Molecular Biosciences*, *9*, 932261. https://doi.org/10.3389/fmolb.2022.932261

Anton, G., Wilson, R., Yu, Z., Prehn, C., Zukunft, S., Adamski, J., Heier, M., Meisinger, C., Römisch-Margl, W., Wang-Sattler, R., Hveem, K., Wolfenbuttel, B., Peters, A., Kastenmüller, G., & Waldenberger, M. (2015a). Pre-Analytical Sample Quality: Metabolite Ratios as an Intrinsic Marker for Prolonged Room Temperature Exposure of Serum Samples. *PLOS ONE*, *10*(3), e0121495. https://doi.org/10.1371/journal.pone.0121495

Anton, G., Wilson, R., Yu, Z., Prehn, C., Zukunft, S., Adamski, J., Heier, M., Meisinger, C., Römisch-Margl, W., Wang-Sattler, R., Hveem, K., Wolfenbuttel, B., Peters, A., Kastenmüller, G., & Waldenberger, M. (2015b). Pre-Analytical Sample Quality: Metabolite Ratios as an Intrinsic Marker for Prolonged Room Temperature Exposure of Serum Samples. *PLOS ONE*, *10*(3), e0121495. https://doi.org/10.1371/journal.pone.0121495

Archie, S. R., Al Shoyaib, A., & Cucullo, L. (2021). Blood-Brain Barrier Dysfunction in CNS Disorders and Putative Therapeutic Targets: An Overview. *Pharmaceutics*, *13*(11), 1779. https://doi.org/10.3390/pharmaceutics13111779

Arciniegas, D. B. (2015). Psychosis. *Continuum : Lifelong Learning in Neurology*, *21*(3 Behavioral Neurology and Neuropsychiatry), 715–736. https://doi.org/10.1212/01.CON.0000466662.89908.e7

Ball, E. G., & Sadusk, J. F. (1936). A STUDY OF THE ESTIMATION OF SODIUM IN BLOOD SERUM. *Journal of Biological Chemistry*, *113*(3), 661–674. https://doi.org/10.1016/S0021-9258(18)74839-4

Balu, R., McCracken, L., Lancaster, E., Graus, F., Dalmau, J., & Titulaer, M. J. (2019). A score that predicts 1-year functional status in patients with anti-NMDA receptor encephalitis. *Neurology*, *92*(3), e244–e252. https://doi.org/10.1212/WNL.0000000000006783

Barber, P. A., Anderson, N. E., & Vincent, A. (2000). Morvan's syndrome associated with voltage-

gated K+ channel antibodies. *Neurology*, *54*(3), 771–772. Scopus. https://doi.org/10.1212/wnl.54.3.771

Barri, T., & Dragsted, L. O. (2013). UPLC-ESI-QTOF/MS and multivariate data analysis for blood plasma and serum metabolomics: Effect of experimental artefacts and anticoagulant. *Analytica Chimica Acta*, *768*, 118–128. https://doi.org/10.1016/j.aca.2013.01.015

Barrios, C., Zierer, J., Würtz, P., Haller, T., Metspalu, A., Gieger, C., Thorand, B., Meisinger, C., Waldenberger, M., Raitakari, O., Lehtimäki, T., Otero, S., Rodríguez, E., Pedro-Botet, J., Kähönen, M., Ala-Korpela, M., Kastenmüller, G., Spector, T. D., Pascual, J., & Menni, C. (2018). Circulating metabolic biomarkers of renal function in diabetic and non-diabetic populations. *Scientific Reports*, *8*(1), Article 1. https://doi.org/10.1038/s41598-018-33507-7

Barton, R. H., Nicholson, J. K., Elliott, P., & Holmes, E. (2008). High-throughput 1H NMR-based metabolic analysis of human serum and urine for large-scale epidemiological studies: Validation study. *International Journal of Epidemiology*, *37*(suppl_1), i31–i40. https://doi.org/10.1093/ije/dym284

Barton, R. H., Waterman, D., Bonner, F. W., Holmes, E., Clarke, R., Consortium, the P., Nicholson, J. K., & Lindon, J. C. (2009). The influence of EDTA and citrateanticoagulant addition to human plasma on information recovery from NMR-based metabolic profiling studies. *Molecular BioSystems*, *6*(1), 215–224. https://doi.org/10.1039/B907021D

Basu, N. N., Ingham, S., Hodson, J., Lalloo, F., Bulman, M., Howell, A., & Evans, D. G. (2015). Risk of contralateral breast cancer in BRCA1 and BRCA2 mutation carriers: A 30-year semi-prospective analysis. *Familial Cancer*, *14*(4), 531–538. https://doi.org/10.1007/s10689-015-9825-9

Beckonert, O., Keun, H. C., Ebbels, T. M. D., Bundy, J., Holmes, E., Lindon, J. C., & Nicholson, J. K. (2007). Metabolic profiling, metabolomic and metabonomic procedures for NMR spectroscopy of urine, plasma, serum and tissue extracts. *Nature Protocols*, *2*(11), Article 11. https://doi.org/10.1038/nprot.2007.376

Belle, J. E. L., Harris, N. G., Williams, S. R., & Bhakoo, K. K. (2002). A comparison of cell and tissue extraction techniques using high-resolution 1H-NMR spectroscopy. *NMR in Biomedicine*, *15*(1), 37–44. https://doi.org/10.1002/nbm.740

Benjamini, Y., & Hochberg, Y. (1995). Controlling the False Discovery Rate: A Practical and Powerful Approach to Multiple Testing. *Journal of the Royal Statistical Society. Series B (Methodological)*, *57*(1), 289–300.

Bennett, M. R., & Devarajan, P. (2011). Chapter 1—Characteristics of an Ideal Biomarker of Kidney Diseases. In C. L. Edelstein (Ed.), *Biomarkers of Kidney Disease* (pp. 1–24). Academic Press. https://doi.org/10.1016/B978-0-12-375672-5.10001-5

Bernini, P., Bertini, I., Luchinat, C., Nincheri, P., Staderini, S., & Turano, P. (2011). Standard operating procedures for pre-analytical handling of blood and urine for metabolomic studies and biobanks. *Journal of Biomolecular NMR*, *49*(3–4), 231–243. https://doi.org/10.1007/s10858-011-9489-1

Bervoets, L., Louis, E., Reekmans, G., Mesotten, L., Thomeer, M., Adriaensens, P., & Linsen, L. (2015). Influence of preanalytical sampling conditions on the 1H NMR metabolic profile of human blood plasma and introduction of the Standard PREanalytical Code used in biobanking. *Metabolomics*, *11*(5), 1197–1207. https://doi.org/10.1007/s11306-015-0774-y

Bharti, S. K., Sinha, N., Joshi, B. S., Mandal, S. K., Roy, R., & Khetrapal, C. L. (2008). Improved quantification from 1H-NMR spectra using reduced repetition times. *Metabolomics*, *4*(4), 367–376. https://doi.org/10.1007/s11306-008-0130-6

Bhinderwala, F., Wase, N., DiRusso, C., & Powers, R. (2018). Combining Mass Spectrometry

and NMR Improves Metabolite Detection and Annotation. *Journal of Proteome Research*, *17*(11), 4017–4022. https://doi.org/10.1021/acs.jproteome.8b00567

Bien, C. G., Vincent, A., Barnett, M. H., Becker, A. J., Blümcke, I., Graus, F., Jellinger, K. A., Reuss, D. E., Ribalta, T., Schlegel, J., Sutton, I., Lassmann, H., & Bauer, J. (2012). Immunopathology of autoantibody-associated encephalitides: Clues for pathogenesis. *Brain*, *135*(5), 1622–1638. https://doi.org/10.1093/brain/aws082

Bifarin, O. O. (2023). Interpretable machine learning with tree-based shapley additive explanations: Application to metabolomics datasets for binary classification. *PLOS ONE*, *18*(5), e0284315. https://doi.org/10.1371/journal.pone.0284315

Biomarkers Definitions Working Group. (2001). Biomarkers and surrogate endpoints: Preferred definitions and conceptual framework. *Clinical Pharmacology & Therapeutics*, *69*(3), 89–95. https://doi.org/10.1067/mcp.2001.113989

BIRNBAUM, S. M., LEVINTOW, L., KINGSLEY, R. B., & GREENSTEIN, J. P. (1952). Specificity of amino acid acylases. *The Journal of Biological Chemistry*, *194*(1), 455–470. Scopus.

Blanchard, J. (1981). Evaluation of the relative efficacy of various techniques for deproteinizing plasma samples prior to high-performance liquid chromatographic analysis. *Journal of Chromatography*, *226*(2), 455–460. https://doi.org/10.1016/s0378-4347(00)86080-6

Blinder, T., & Lewerenz, J. (2019). Cerebrospinal Fluid Findings in Patients With Autoimmune Encephalitis—A Systematic Analysis. *Frontiers in Neurology*, *10*. https://doi.org/10.3389/fneur.2019.00804

Bodaghi, A., Fattahi, N., & Ramazani, A. (2023). Biomarkers: Promising and valuable tools towards diagnosis, prognosis and treatment of Covid-19 and other diseases. *Heliyon*, *9*(2), e13323. https://doi.org/10.1016/j.heliyon.2023.e13323

Bourafai-Aziez, A., Jacob, D., Charpentier, G., Cassin, E., Rousselot, G., Moing, A., & Deborde, C. (2022). Development, Validation, and Use of 1H-NMR Spectroscopy for Evaluating the Quality of Acerola-Based Food Supplements and Quantifying Ascorbic Acid. *Molecules*, *27*(17), 5614. https://doi.org/10.3390/molecules27175614

Brenner, J., Mariotto, S., Bastiaansen, A. E. M., Paunovic, M., Ferrari, S., Alberti, D., de Bruijn, M. A. A. M., Crijnen, Y. S., Schreurs, M. W. J., Neuteboom, R. F., Damoiseaux, J. G. M. C., de Vries, J. M., & Titulaer, M. J. (2023). Predictive Value of Serum Neurofilament Light Chain Levels in Anti-NMDA Receptor Encephalitis. *Neurology*, *100*(21), e2204–e2213. https://doi.org/10.1212/WNL.0000000000207221

Brown, J. A., Codreanu, S. G., Shi, M., Sherrod, S. D., Markov, D. A., Neely, M. D., Britt, C. M., Hoilett, O. S., Reiserer, R. S., Samson, P. C., McCawley, L. J., Webb, D. J., Bowman, A. B., McLean, J. A., & Wikswo, J. P. (2016). Metabolic consequences of inflammatory disruption of the blood-brain barrier in an organ-on-chip model of the human neurovascular unit. *Journal of Neuroinflammation*, *13*(1), 306. https://doi.org/10.1186/s12974-016-0760-y

Brunius, C., Pedersen, A., Malmodin, D., Karlsson, B. G., Andersson, L. I., Tybring, G., & Landberg, R. (2017). Prediction and modeling of pre-analytical sampling errors as a strategy to improve plasma NMR metabolomics data. *Bioinformatics (Oxford, England)*, *33*(22), 3567–3574. https://doi.org/10.1093/bioinformatics/btx442

Buckley, C., Oger, J., Clover, L., Tüzün, E., Carpenter, K., Jackson, M., & Vincent, A. (2001). Potassium channel antibodies in two patients with reversible limbic encephalitis. *Annals of Neurology*, *50*(1), 73–78. https://doi.org/10.1002/ana.1097

Buergel, T., Steinfeldt, J., Ruyoga, G., Pietzner, M., Bizzarri, D., Vojinovic, D., Upmeier Zu Belzen, J., Loock, L., Kittner, P., Christmann, L., Hollmann, N., Strangalies, H., Braunger, J. M., Wild, B., Chiesa, S. T., Spranger, J., Klostermann, F., van den Akker, E. B., Trompet, S., … Landmesser, U.

(2022). Metabolomic profiles predict individual multidisease outcomes. *Nature Medicine*, *28*(11), 2309–2320. https://doi.org/10.1038/s41591-022-01980-3
Cai, X., & Li, R. (2016). Concurrent profiling of polar metabolites and lipids in human plasma using HILIC-FTMS. *Scientific Reports*, *6*(1), 36490. https://doi.org/10.1038/srep36490
Campos, A. M., Maciel, E., Moreira, A. S. P., Sousa, B., Melo, T., Domingues, P., Curado, L., Antunes, B., Domingues, M. R. M., & Santos, F. (2016). Lipidomics of Mesenchymal Stromal Cells: Understanding the Adaptation of Phospholipid Profile in Response to Pro-Inflammatory Cytokines. *Journal of Cellular Physiology*, *231*(5), 1024–1032. https://doi.org/10.1002/jcp.25191
Carstens, G., Verbeek, M. M., Rohlwink, U. K., Figaji, A. A., Brake, L. te, & Laarhoven, A. van. (2024). Metabolite transport across central nervous system barriers. *Journal of Cerebral Blood Flow & Metabolism*, *44*(7), 1063. https://doi.org/10.1177/0271678X241241908
Carvajal-González, A., Leite, M. I., Waters, P., Woodhall, M., Coutinho, E., Balint, B., Lang, B., Pettingill, P., Carr, A., Sheerin, U.-M., Press, R., Press, R., Lunn, M. P., Lim, M., Maddison, P., Meinck, H.-M., Vandenberghe, W., & Vincent, A. (2014). Glycine receptor antibodies in PERM and related syndromes: Characteristics, clinical features and outcomes. *Brain: A Journal of Neurology*, *137*(Pt 8), 2178–2192. https://doi.org/10.1093/brain/awu142
Chandel, N. S. (2021a). Carbohydrate Metabolism. *Cold Spring Harbor Perspectives in Biology*, *13*(1), a040568. https://doi.org/10.1101/cshperspect.a040568
Chandel, N. S. (2021b). Nucleotide Metabolism. *Cold Spring Harbor Perspectives in Biology*, *13*(7), a040592. https://doi.org/10.1101/cshperspect.a040592
Chen, C., Wang, J., Pan, D., Wang, X., Xu, Y., Yan, J., Wang, L., Yang, X., Yang, M., & Liu, G. (2023). Applications of multi-omics analysis in human diseases. *MedComm*, *4*(4), e315. https://doi.org/10.1002/mco2.315
Chen, D., Zhao, S., Li, L., & Li, L. (2023). Controlling pre-analytical process in human serum/plasma metabolomics. *TrAC Trends in Analytical Chemistry*, *169*, 117364. https://doi.org/10.1016/j.trac.2023.117364
Chen, T., Cao, Y., Zhang, Y., Liu, J., Bao, Y., Wang, C., Jia, W., & Zhao, A. (2013). Random Forest in Clinical Metabolomics for Phenotypic Discrimination and Biomarker Selection. *Evidence-Based Complementary and Alternative Medicine*, *2013*(1), 298183. https://doi.org/10.1155/2013/298183
Chen, Y., Li, E.-M., & Xu, L.-Y. (2022). Guide to Metabolomics Analysis: A Bioinformatics Workflow. *Metabolites*, *12*(4), 357. https://doi.org/10.3390/metabo12040357
Cho, E. B., Cho, H.-J., Choi, M., Seok, J. M., Shin, H. Y., Kim, B. J., & Min, J.-H. (2020). Low high-density lipoprotein cholesterol and high triglycerides lipid profile in neuromyelitis optica spectrum disorder: Associations with disease activity and disability. *Multiple Sclerosis and Related Disorders*, *40*, 101981. https://doi.org/10.1016/j.msard.2020.101981
Claridge, T. D. W. (2009). *High-Resolution NMR Techniques in Organic Chemistry*. Newnes.
Committee on Biological Markers of the National Research Council. (1987). Biological markers in environmental health research. *Environmental Health Perspectives*, *74*, 3–9.
Cruickshank-Quinn, C., Zheng, L. K., Quinn, K., Bowler, R., Reisdorph, R., & Reisdorph, N. (2018). Impact of Blood Collection Tubes and Sample Handling Time on Serum and Plasma Metabolome and Lipidome. *Metabolites*, *8*(4), 88. https://doi.org/10.3390/metabo8040088
Cullen, A. E., Palmer-Cooper, E. C., Hardwick, M., Vaggers, S., Crowley, H., Pollak, T. A., & Lennox, B. R. (2021). Influence of methodological and patient factors on serum NMDAR IgG antibody detection in psychotic disorders: A meta-analysis of cross-sectional and case-control studies. *The Lancet Psychiatry*, *8*(2), 109–120. https://doi.org/10.1016/S2215-0366(20)30432-6
Curzon, G. (1979). Relationships between plasma, CSF and brain tryptophan. *Journal of Neural*

Transmission. Supplementum, *15*, 81–92. https://doi.org/10.1007/978-3-7091-2243-3_7
Dai, Y., Zhang, J., Ren, H., Zhou, X., Chen, J., Cui, L., Lang, J., Guan, H., & Sun, D. (2019). Surgical outcomes in patients with anti-N-methyl D-aspartate receptor encephalitis with ovarian teratoma. *American Journal of Obstetrics and Gynecology*, *221*(5), 485.e1-485.e10. https://doi.org/10.1016/j.ajog.2019.05.026
Dalmau, J. (2016). NMDA receptor encephalitis and other antibody-mediated disorders of the synapse. *Neurology*, *87*(23), 2471–2482. https://doi.org/10.1212/WNL.0000000000003414
Dalmau, J., Geis, C., & Graus, F. (2017). Autoantibodies to Synaptic Receptors and Neuronal Cell Surface Proteins in Autoimmune Diseases of the Central Nervous System. *Physiological Reviews*, *97*(2), 839–887. https://doi.org/10.1152/physrev.00010.2016
Dalmau, J., & Graus, F. (2018). Antibody-Mediated Encephalitis. *New England Journal of Medicine*, *378*(9), 840–851. https://doi.org/10.1056/NEJMra1708712
Dalmau, J., Lancaster, E., Martinez-Hernandez, E., Rosenfeld, M. R., & Balice-Gordon, R. (2011). Clinical experience and laboratory investigations in patients with anti-NMDAR encephalitis. *The Lancet. Neurology*, *10*(1), 63–74. https://doi.org/10.1016/S1474-4422(10)70253-2
Dalmau, J., Tüzün, E., Wu, H., Masjuan, J., Rossi, J. E., Voloschin, A., Baehring, J. M., Shimazaki, H., Koide, R., King, D., Mason, W., Sansing, L. H., Dichter, M. A., Rosenfeld, M. R., & Lynch, D. R. (2007). Paraneoplastic anti-N-methyl-D-aspartate receptor encephalitis associated with ovarian teratoma. *Annals of Neurology*, *61*(1), 25–36. https://doi.org/10.1002/ana.21050
Debik, J., Isaksen, S. H., Strømmen, M., Spraul, M., Schäfer, H., Bathen, T. F., & Giskeødegård, G. F. (2022). Effect of Delayed Centrifugation on the Levels of NMR-Measured Lipoproteins and Metabolites in Plasma and Serum Samples. *Analytical Chemistry*, *94*(49), 17003–17010. https://doi.org/10.1021/acs.analchem.2c02167
Debik, J., Sangermani, M., Wang, F., Madssen, T. S., & Giskeødegård, G. F. (2022). Multivariate analysis of NMR-based metabolomic data. *NMR in Biomedicine*, *35*(2), e4638. https://doi.org/10.1002/nbm.4638
Denery, J. R., Nunes, A. A. K., & Dickerson, T. J. (2011). Characterization of differences between blood sample matrices in untargeted metabolomics. *Analytical Chemistry*, *83*(3), 1040–1047. https://doi.org/10.1021/ac102806p
Deng, B., Cai, M., Qiu, Y., Liu, X., Yu, H., Zhang, X., Huang, H., Zhao, X., Yang, W., Dong, S., Jin, L., Chu, S., & Chen, X. (2022). MRI Characteristics of Autoimmune Encephalitis With Autoantibodies to GABAA Receptor. *Neurology Neuroimmunology & Neuroinflammation*, *9*(3), e1158. https://doi.org/10.1212/NXI.0000000000001158
Diamond, B., Honig, G., Mader, S., Brimberg, L., & Volpe, B. T. (2013). Brain-Reactive Antibodies and Disease. *Annual Review of Immunology*, *31*(Volume 31, 2013), 345–385. https://doi.org/10.1146/annurev-immunol-020711-075041
Dibbasey, M., Umukoro, S., & Bojang, A. (2024). Comparative and stability study of glucose concentrations measured in both sodium fluoride and serum separator tubes. *Practical Laboratory Medicine*, *39*, e00360. https://doi.org/10.1016/j.plabm.2024.e00360
Dickens, A. M., Larkin, J. R., Griffin, J. L., Cavey, A., Matthews, L., Turner, M. R., Wilcock, G. K., Davis, B. G., Claridge, T. D. W., Palace, J., Anthony, D. C., & Sibson, N. R. (2014). A type 2 biomarker separates relapsing-remitting from secondary progressive multiple sclerosis. *Neurology*, *83*(17), 1492–1499. https://doi.org/10.1212/WNL.0000000000000905
Diémé, B., Lefèvre, A., Nadal-Desbarats, L., Galineau, L., Madji Hounoum, B., Montigny, F., Blasco, H., Andres, C. R., Emond, P., & Mavel, S. (2017). Workflow methodology for rat brain metabolome exploration using NMR, LC-MS and GC-MS analytical platforms. *Journal of Pharmaceutical and Biomedical Analysis*, *142*, 270–278.

https://doi.org/10.1016/j.jpba.2017.03.068
Dieterle, F., Ross, A., Schlotterbeck, G., & Senn, H. (2006). Probabilistic Quotient Normalization as Robust Method to Account for Dilution of Complex Biological Mixtures. Application in 1H NMR Metabonomics. *Analytical Chemistry*, *78*(13), 4281–4290. https://doi.org/10.1021/ac051632c
Disanto, G., Barro, C., Benkert, P., Naegelin, Y., Schädelin, S., Giardiello, A., Zecca, C., Blennow, K., Zetterberg, H., Leppert, D., Kappos, L., Gobbi, C., Kuhle, J., & Group, the S. M. S. C. S. (2017). Serum Neurofilament light: A biomarker of neuronal damage in multiple sclerosis. *Annals of Neurology*, *81*(6), 857–870. https://doi.org/10.1002/ana.24954
Donatti, A., Canto, A. M., Godoi, A. B., da Rosa, D. C., & Lopes-Cendes, I. (2020). Circulating Metabolites as Potential Biomarkers for Neurological Disorders—Metabolites in Neurological Disorders. *Metabolites*, *10*(10), 389. https://doi.org/10.3390/metabo10100389
Downey, P., & Peakman, T. C. (2008). Design and implementation of a high-throughput biological sample processing facility using modern manufacturing principles. *International Journal of Epidemiology*, *37*(suppl_1), i46–i50. https://doi.org/10.1093/ije/dyn031
Dubey, D., Pittock, S. J., Kelly, C. R., McKeon, A., Lopez-Chiriboga, A. S., Lennon, V. A., Gadoth, A., Smith, C. Y., Bryant, S. C., Klein, C. J., Aksamit, A. J., Toledano, M., Boeve, B. F., Tillema, J.-M., & Flanagan, E. P. (2018). Autoimmune encephalitis epidemiology and a comparison to infectious encephalitis. *Annals of Neurology*, *83*(1), 166–177. https://doi.org/10.1002/ana.25131
Dunn, K. (2023). *Process Improvement Using Data*. https://learnche.org/pid/contents#
Durcan, L., Winegar, D. A., Connelly, M. A., Otvos, J. D., Magder, L. S., & Petri, M. (2016). Longitudinal Evaluation of Lipoprotein Parameters in Systemic Lupus Erythematosus Reveals Adverse Changes with Disease Activity and Prednisone and More Favorable Profiles with Hydroxychloroquine Therapy. *The Journal of Rheumatology*, *43*(4), 745–750. https://doi.org/10.3899/jrheum.150437
Durmowicz, A. G., Witzmann, K. A., Rosebraugh, C. J., & Chowdhury, B. A. (2013). Change in sweat chloride as a clinical end point in cystic fibrosis clinical trials: The ivacaftor experience. *Chest*, *143*(1), 14–18. https://doi.org/10.1378/chest.12-1430
Dürr, M., Nissen, G., Sühs, K.-W., Schwenkenbecher, P., Geis, C., Ringelstein, M., Hartung, H.-P., Friese, M. A., Kaufmann, M., Malter, M. P., Madlener, M., Thaler, F. S., Kümpfel, T., Senel, M., Häusler, M. G., Schneider, H., Bergh, F. T., Kellinghaus, C., Zettl, U. K., … German Network for Research on Autoimmune Encephalitis. (2021). CSF Findings in Acute NMDAR and LGI1 Antibody-Associated Autoimmune Encephalitis. *Neurology(R) Neuroimmunology & Neuroinflammation*, *8*(6), e1086. https://doi.org/10.1212/NXI.0000000000001086
Elferink, J. G. (1987). The mechanism of calcium oxalate crystal-induced haemolysis of human erythrocytes. *British Journal of Experimental Pathology*, *68*(4), 551–557.
Ellervik, C., & Vaught, J. (2015). Preanalytical variables affecting the integrity of human biospecimens in biobanking. *Clinical Chemistry*, *61*(7), 914–934. https://doi.org/10.1373/clinchem.2014.228783
Elliott, P., Peakman, T. C., & on behalf of UK Biobank. (2008). The UK Biobank sample handling and storage protocol for the collection, processing and archiving of human blood and urine. *International Journal of Epidemiology*, *37*(2), 234–244. https://doi.org/10.1093/ije/dym276
Emwas, A.-H. M., Salek, R. M., Griffin, J. L., & Merzaban, J. (2013). NMR-based metabolomics in human disease diagnosis: Applications, limitations, and recommendations. *Metabolomics*, *9*(5), 1048–1072. https://doi.org/10.1007/s11306-013-0524-y
Emwas, A.-H., Roy, R., McKay, R. T., Ryan, D., Brennan, L., Tenori, L., Luchinat, C., Gao, X., Zeri, A. C., Gowda, G. A.Nagana, Raftery, D., Steinbeck, C., Salek, R. M., & Wishart, D. S. (2016).

Recommendations and Standardization of Biomarker Quantification Using NMR-Based Metabolomics with Particular Focus on Urinary Analysis. *Journal of Proteome Research*, *15*(2), 360–373. https://doi.org/10.1021/acs.jproteome.5b00885

Emwas, A.-H., Roy, R., McKay, R. T., Tenori, L., Saccenti, E., Gowda, G. A. N., Raftery, D., Alahmari, F., Jaremko, L., Jaremko, M., & Wishart, D. S. (2019). NMR Spectroscopy for Metabolomics Research. *Metabolites*, *9*(7), 123. https://doi.org/10.3390/metabo9070123

Emwas, A.-H., Saccenti, E., Gao, X., McKay, R. T., dos Santos, V. A. P. M., Roy, R., & Wishart, D. S. (2018). Recommended strategies for spectral processing and post-processing of 1D 1H-NMR data of biofluids with a particular focus on urine. *Metabolomics*, *14*(3), 31. https://doi.org/10.1007/s11306-018-1321-4

Faisal, M., Vedin, T., Edelhamre, M., & Forberg, J. L. (2023). Diagnostic performance of biomarker S100B and guideline adherence in routine care of mild head trauma. *Scandinavian Journal of Trauma, Resuscitation and Emergency Medicine*, *31*(1), 3. https://doi.org/10.1186/s13049-022-01062-w

FDA-NIH Biomarker Working Group. (2016). *BEST (Biomarkers, EndpointS, and other Tools) Resource*. National Institutes of Health (US).

Fehsel, K., & Löffler, S. (2017). First-episode psychosis and abnormal glycaemic control. *The Lancet Psychiatry*, *4*(1), 23–24. https://doi.org/10.1016/S2215-0366(16)30374-1

Feigin, V. L., Nichols, E., Alam, T., Bannick, M. S., Beghi, E., Blake, N., Culpepper, W. J., Dorsey, E. R., Elbaz, A., Ellenbogen, R. G., Fisher, J. L., Fitzmaurice, C., Giussani, G., Glennie, L., James, S. L., Johnson, C. O., Kassebaum, N. J., Logroscino, G., Marin, B., … Vos, T. (2019). Global, regional, and national burden of neurological disorders, 1990–2016: A systematic analysis for the Global Burden of Disease Study 2016. *The Lancet Neurology*, *18*(5), 459–480. https://doi.org/10.1016/S1474-4422(18)30499-X

Feingold, K. R., & Grunfeld, C. (2000). The Effect of Inflammation and Infection on Lipids and Lipoproteins. In K. R. Feingold, B. Anawalt, A. Boyce, G. Chrousos, W. W. de Herder, K. Dhatariya, K. Dungan, J. M. Hershman, J. Hofland, S. Kalra, G. Kaltsas, C. Koch, P. Kopp, M. Korbonits, C. S. Kovacs, W. Kuohung, B. Laferrère, M. Levy, E. A. McGee, … D. P. Wilson (Eds.), *Endotext*. MDText.com, Inc. http://www.ncbi.nlm.nih.gov/books/NBK326741/

Fels, E., Muñiz-Castrillo, S., Vogrig, A., Joubert, B., Honnorat, J., & Pascual, O. (2021). Role of LGI1 protein in synaptic transmission: From physiology to pathology. *Neurobiology of Disease*, *160*, 105537. https://doi.org/10.1016/j.nbd.2021.105537

Fernstrom, J. D. (1981). Dietary precursors and brain neurotransmitter formation. *Annual Review of Medicine*, *32*, 413–425. https://doi.org/10.1146/annurev.me.32.020181.002213

Finke, C., Kopp, U. A., Scheel, M., Pech, L.-M., Soemmer, C., Schlichting, J., Leypoldt, F., Brandt, A. U., Wuerfel, J., Probst, C., Ploner, C. J., Prüss, H., & Paul, F. (2013). Functional and structural brain changes in anti-N-methyl-D-aspartate receptor encephalitis. *Annals of Neurology*, *74*(2), 284–296. https://doi.org/10.1002/ana.23932

Flanagan, E. P., Geschwind, M. D., Lopez-Chiriboga, A. S., Blackburn, K. M., Turaga, S., Binks, S., Zitser, J., Gelfand, J. M., Day, G. S., Dunham, S. R., Rodenbeck, S. J., Clardy, S. L., Solomon, A. J., Pittock, S. J., McKeon, A., Dubey, D., Zekeridou, A., Toledano, M., Turner, L. E., … Irani, S. R. (2023). Autoimmune Encephalitis Misdiagnosis in Adults. *JAMA Neurology*, *80*(1), 30–39. https://doi.org/10.1001/jamaneurol.2022.4251

Fliniaux, O., Gaillard, G., Lion, A., Cailleu, D., Mesnard, F., & Betsou, F. (2011a). Influence of common preanalytical variations on the metabolic profile of serum samples in biobanks. *Journal of Biomolecular NMR*, *51*(4), 457–465. https://doi.org/10.1007/s10858-011-9574-5

Fliniaux, O., Gaillard, G., Lion, A., Cailleu, D., Mesnard, F., & Betsou, F. (2011b). Influence of

common preanalytical variations on the metabolic profile of serum samples in biobanks. *Journal of Biomolecular NMR*, *51*(4), 457–465. https://doi.org/10.1007/s10858-011-9574-5

Florkowski, C. M. (2008). Sensitivity, Specificity, Receiver-Operating Characteristic (ROC) Curves and Likelihood Ratios: Communicating the Performance of Diagnostic Tests. *The Clinical Biochemist Reviews*, *29*(Suppl 1), S83.

Foerch, C., Curdt, I., Yan, B., Dvorak, F., Hermans, M., Berkefeld, J., Raabe, A., Neumann-Haefelin, T., Steinmetz, H., & Sitzer, M. (2006). Serum glial fibrillary acidic protein as a biomarker for intracerebral haemorrhage in patients with acute stroke. *Journal of Neurology, Neurosurgery, and Psychiatry*, *77*(2), 181–184. https://doi.org/10.1136/jnnp.2005.074823

Folch, Jordi., Ascoli, I., Lees, M., Meath, J. A., & LeBaron, F. N. (1951). PREPARATION OF LIPIDE EXTRACTS FROM BRAIN TISSUE. *Journal of Biological Chemistry*, *191*(2), 833–841. https://doi.org/10.1016/S0021-9258(18)55987-1

Fomenko, M. V., Yanshole, L. V., & Tsentalovich, Y. P. (2022a). Stability of Metabolomic Content during Sample Preparation: Blood and Brain Tissues. *Metabolites*, *12*(9), Article 9. https://doi.org/10.3390/metabo12090811

Fomenko, M. V., Yanshole, L. V., & Tsentalovich, Y. P. (2022b). Stability of Metabolomic Content during Sample Preparation: Blood and Brain Tissues. *Metabolites*, *12*(9), 811. https://doi.org/10.3390/metabo12090811

Foucher, C. D., & Tubben, R. E. (n.d.). Lactic Acidosis. In *Lactic Acidosis. [Updated 2022 Jul 18]*. Treasure Island (FL): StatPearls Publishing. https://www.ncbi.nlm.nih.gov/books/NBK470202/

Frank, R., & Hargreaves, R. (2003). Clinical biomarkers in drug discovery and development. *Nature Reviews Drug Discovery*, *2*(7), Article 7. https://doi.org/10.1038/nrd1130

Friedman, J. I., Vrijenhoek, T., Markx, S., Janssen, I. M., van der Vliet, W. A., Faas, B. H. W., Knoers, N. V., Cahn, W., Kahn, R. S., Edelmann, L., Davis, K. L., Silverman, J. M., Brunner, H. G., van Kessel, A. G., Wijmenga, C., Ophoff, R. A., & Veltman, J. A. (2008). CNTNAP2 gene dosage variation is associated with schizophrenia and epilepsy. *Molecular Psychiatry*, *13*(3), 261–266. https://doi.org/10.1038/sj.mp.4002049

Funayama, M., Koreki, A., Takata, T., Kurose, S., Hisamatsu, T., Ono, A., Yagihashi, T., Mizushima, J., Yagi, Y., Ogino, S., Oi, H., Mimura, Y., Shimizu, Y., Kudo, S., Nishi, A., & Mukai, H. (2022). Differentiating autoimmune encephalitis from schizophrenia spectrum disorders among patients with first-episode psychosis. *Journal of Psychiatric Research*, *151*, 419–426. https://doi.org/10.1016/j.jpsychires.2022.05.008

Furukawa, T. A., Levine, S. Z., Tanaka, S., Goldberg, Y., Samara, M., Davis, J. M., Cipriani, A., & Leucht, S. (2015). Initial severity of schizophrenia and efficacy of antipsychotics: Participant-level meta-analysis of 6 placebo-controlled studies. *JAMA Psychiatry*, *72*(1), 14–21. https://doi.org/10.1001/jamapsychiatry.2014.2127

Gable, M. S., Sheriff, H., Dalmau, J., Tilley, D. H., & Glaser, C. A. (2012). The Frequency of Autoimmune N-Methyl-D-Aspartate Receptor Encephalitis Surpasses That of Individual Viral Etiologies in Young Individuals Enrolled in the California Encephalitis Project. *Clinical Infectious Diseases*, *54*(7), 899–904. https://doi.org/10.1093/cid/cir1038

Gaetani, L., Blennow, K., Calabresi, P., Filippo, M. D., Parnetti, L., & Zetterberg, H. (2019). Neurofilament light chain as a biomarker in neurological disorders. *Journal of Neurology, Neurosurgery & Psychiatry*, *90*(8), 870–881. https://doi.org/10.1136/jnnp-2018-320106

Galindo-Prieto, B., Eriksson, L., & Trygg, J. (2015). Variable influence on projection (VIP) for OPLS models and its applicability in multivariate time series analysis. *Chemometrics and Intelligent Laboratory Systems*, *146*, 297–304. https://doi.org/10.1016/j.chemolab.2015.05.001

Gambino, R. (2013). Sodium fluoride: An ineffective inhibitor of glycolysis. *Annals of Clinical Biochemistry*, *50*(Pt 1), 3–5. https://doi.org/10.1258/acb.2012.012135

García-Martín, M. L., García-Espinosa, M. A., Ballesteros, P., Bruix, M., & Cerdán, S. (2002). Hydrogen Turnover and Subcellular Compartmentation of Hepatic [2-13C]Glutamate and [3-13C]Aspartate as Detected by 13C NMR *. *Journal of Biological Chemistry*, *277*(10), 7799–7807. https://doi.org/10.1074/jbc.M107501200

Ghini, V., Abuja, P. M., Polasek, O., Kozera, L., Laiho, P., Anton, G., Zins, M., Klovins, J., Metspalu, A., Wichmann, H.-E., Gieger, C., Luchinat, C., Zatloukal, K., & Turano, P. (2022). Impact of the pre-examination phase on multicenter metabolomic studies. *New Biotechnology*, *68*, 37–47. https://doi.org/10.1016/j.nbt.2022.01.006

Ghini, V., Quaglio, D., Luchinat, C., & Turano, P. (2019). NMR for sample quality assessment in metabolomics. *New Biotechnology*, *52*, 25–34. https://doi.org/10.1016/j.nbt.2019.04.004

Gill, A. J., & Venkatesan, A. (2022). Pathogenic mechanisms in neuronal surface autoantibody-mediated encephalitis. *Journal of Neuroimmunology*, *368*, 577867. https://doi.org/10.1016/j.jneuroim.2022.577867

Golbraikh, A., & Tropsha, A. (2002). Beware of q2! *Journal of Molecular Graphics and Modelling*, *20*(4), 269–276. https://doi.org/10.1016/S1093-3263(01)00123-1

Goldberg, E., Ievari-Shariati, S., Kidane, B., Kim, J., Banerji, S., Qing, G., Srinathan, S., Murphy, L., & Aliani, M. (2021). Comparative metabolomics studies of blood collected in streck and heparin tubes from lung cancer patients. *PLOS ONE*, *16*(4), e0249648. https://doi.org/10.1371/journal.pone.0249648

Goldberg, I., & Rokem, J. S. (2009). Organic and Fatty Acid Production, Microbial. In M. Schaechter (Ed.), *Encyclopedia of Microbiology (Third Edition)* (pp. 421–442). Academic Press. https://doi.org/10.1016/B978-012373944-5.00156-5

Gonzalez-Ortiz, F., Kac, P. R., Brum, W. S., Zetterberg, H., Blennow, K., & Karikari, T. K. (2023). Plasma phospho-tau in Alzheimer's disease: Towards diagnostic and therapeutic trial applications. *Molecular Neurodegeneration*, *18*. https://doi.org/10.1186/s13024-023-00605-8

Gonzalez-Riano, C., Garcia, A., & Barbas, C. (2016). Metabolomics studies in brain tissue: A review. *Journal of Pharmaceutical and Biomedical Analysis*, *130*, 141–168. https://doi.org/10.1016/j.jpba.2016.07.008

Goverman, J. (2009). Autoimmune T cell responses in the central nervous system. *Nature Reviews. Immunology*, *9*(6), 393. https://doi.org/10.1038/nri2550

Gowda, G. A. N., Pascua, V., & Raftery, D. (2021). Extending the Scope of 1H NMR Based Blood Metabolomics for the Analysis of Labile Antioxidants: Reduced and Oxidized Glutathione. *Analytical Chemistry*, *93*(44), 14844–14850. https://doi.org/10.1021/acs.analchem.1c03763

Gowda, G. A. N., & Raftery, D. (2014). Quantitating Metabolites in Protein Precipitated Serum Using NMR Spectroscopy. *Analytical Chemistry*, *86*(11), 5433–5440. https://doi.org/10.1021/ac5005103

Gowda, G. A. N., & Raftery, D. (2021). NMR Based Metabolomics. *Advances in Experimental Medicine and Biology*, *1280*, 19–37. https://doi.org/10.1007/978-3-030-51652-9_2

Granerod, J., Cousens, S., Davies, N. W. S., Crowcroft, N. S., & Thomas, S. L. (2013). New estimates of incidence of encephalitis in England. *Emerging Infectious Diseases*, *19*(9), 1455–1462. https://doi.org/10.3201/eid1909.130064

Graus, F., & Dalmau, J. (2019). Paraneoplastic neurological syndromes in the era of immune-checkpoint inhibitors. *Nature Reviews Clinical Oncology*, *16*(9), 535–548. https://doi.org/10.1038/s41571-019-0194-4

Graus, F., Titulaer, M. J., Balu, R., Benseler, S., Bien, C. G., Cellucci, T., Cortese, I., Dale, R. C.,

Gelfand, J. M., Geschwind, M., Glaser, C. A., Honnorat, J., Höftberger, R., Iizuka, T., Irani, S. R., Lancaster, E., Leypoldt, F., Prüss, H., Rae-Grant, A., … Dalmau, J. (2016). A clinical approach to diagnosis of autoimmune encephalitis. *The Lancet Neurology*, *15*(4), 391–404. https://doi.org/10.1016/S1474-4422(15)00401-9

Gréa, H., Bouchet, D., Rogemond, V., Hamdani, N., Le Guen, E., Tamouza, R., Darrau, E., Passerieux, C., Honnorat, J., Leboyer, M., & Groc, L. (2019). Human Autoantibodies Against N-Methyl-D-Aspartate Receptor Modestly Alter Dopamine D1 Receptor Surface Dynamics. *Frontiers in Psychiatry*, *10*, 670. https://doi.org/10.3389/fpsyt.2019.00670

Gultekin, S. H., Rosenfeld, M. R., Voltz, R., Eichen, J., Posner, J. B., & Dalmau, J. (2000). Paraneoplastic limbic encephalitis: Neurological symptoms, immunological findings and tumour association in 50 patients. *Brain*, *123*(7), 1481–1494. https://doi.org/10.1093/brain/123.7.1481

Haas, M. J., & Mooradian, A. D. (2010). Regulation of high-density lipoprotein by inflammatory cytokines: Establishing links between immune dysfunction and cardiovascular disease. *Diabetes/Metabolism Research and Reviews*, *26*(2), 90–99. https://doi.org/10.1002/dmrr.1057

Hacohen, Y., Singh, R., Rossi, M., Lang, B., Hemingway, C., Lim, M., & Vincent, A. (2015). Clinical relevance of voltage-gated potassium channel–complex antibodies in children. *Neurology*, *85*(11), 967–975. https://doi.org/10.1212/WNL.0000000000001922

Haid, M., Muschet, C., Wahl, S., Römisch-Margl, W., Prehn, C., Möller, G., & Adamski, J. (2018). Long-Term Stability of Human Plasma Metabolites during Storage at −80 °C. *Journal of Proteome Research*, *17*(1), 203–211. https://doi.org/10.1021/acs.jproteome.7b00518

Hébert, J., Day, G. S., Steriade, C., Wennberg, R. A., & Tang-Wai, D. F. (2018). Long-Term Cognitive Outcomes in Patients with Autoimmune Encephalitis. *Canadian Journal of Neurological Sciences*, *45*(5), 540–544. https://doi.org/10.1017/cjn.2018.33

Hébert, J., Muccilli, A., Wennberg, R. A., & Tang-Wai, D. F. (2022). Autoimmune Encephalitis and Autoantibodies: A Review of Clinical Implications. *The Journal of Applied Laboratory Medicine*, *7*(1), 81–98. https://doi.org/10.1093/jalm/jfab102

Heinemann, J., Mazurie, A., Tokmina-Lukaszewska, M., Beilman, G. J., & Bothner, B. (2014). Application of support vector machines to metabolomics experiments with limited replicates. *Metabolomics*, *10*(6), 1121–1128. https://doi.org/10.1007/s11306-014-0651-0

Hoult, D. I. (1976). Solvent peak saturation with single phase and quadrature fourier transformation. *Journal of Magnetic Resonance (1969)*, *21*(2), 337–347. https://doi.org/10.1016/0022-2364(76)90081-0

Hughes, E. G., Peng, X., Gleichman, A. J., Lai, M., Zhou, L., Tsou, R., Parsons, T. D., Lynch, D. R., Dalmau, J., & Balice-Gordon, R. J. (2010). Cellular and synaptic mechanisms of anti-NMDA receptor encephalitis. *The Journal of Neuroscience: The Official Journal of the Society for Neuroscience*, *30*(17), 5866–5875. https://doi.org/10.1523/JNEUROSCI.0167-10.2010

Hutchinson, M., Waters, P., McHugh, J., Gorman, G., O'Riordan, S., Connolly, S., Hager, H., Yu, P., Becker, C.-M., & Vincent, A. (2008). Progressive encephalomyelitis, rigidity, and myoclonus: A novel glycine receptor antibody. *Neurology*, *71*(16), 1291–1292. https://doi.org/10.1212/01.wnl.0000327606.50322.f0

Irani, S. R., Alexander, S., Waters, P., Kleopa, K. A., Pettingill, P., Zuliani, L., Peles, E., Buckley, C., Lang, B., & Vincent, A. (2010a). Antibodies to Kv1 potassium channel-complex proteins leucine-rich, glioma inactivated 1 protein and contactin-associated protein-2 in limbic encephalitis, Morvan's syndrome and acquired neuromyotonia. *Brain*, *133*(9), 2734–2748. Scopus. https://doi.org/10.1093/brain/awq213

Irani, S. R., Alexander, S., Waters, P., Kleopa, K. A., Pettingill, P., Zuliani, L., Peles, E., Buckley,

C., Lang, B., & Vincent, A. (2010b). Antibodies to Kv1 potassium channel-complex proteins leucine-rich, glioma inactivated 1 protein and contactin-associated protein-2 in limbic encephalitis, Morvan's syndrome and acquired neuromyotonia. *Brain*, *133*(9), 2734–2748. https://doi.org/10.1093/brain/awq213

Irani, S. R., Bera, K., Waters, P., Zuliani, L., Maxwell, S., Zandi, M. S., Friese, M. A., Galea, I., Kullmann, D. M., Beeson, D., Lang, B., Bien, C. G., & Vincent, A. (2010). N-methyl-d-aspartate antibody encephalitis: Temporal progression of clinical and paraclinical observations in a predominantly non-paraneoplastic disorder of both sexes. *Brain*, *133*(6), 1655–1667. https://doi.org/10.1093/brain/awq113

Ishida, S., Hashimoto, I., Seike, T., Abe, Y., Nakaya, Y., & Nakanishi, H. (2014). Serum albumin levels correlate with inflammation rather than nutrition supply in burns patients: A retrospective study. *The Journal of Medical Investigation*, *61*(3.4), 361–368. https://doi.org/10.2152/jmi.61.361

Jain, R. W., & Yong, V. W. (2022). B cells in central nervous system disease: Diversity, locations and pathophysiology. *Nature Reviews Immunology*, *22*(8), 513–524. https://doi.org/10.1038/s41577-021-00652-6

James, P. A., Oparil, S., Carter, B. L., Cushman, W. C., Dennison-Himmelfarb, C., Handler, J., Lackland, D. T., LeFevre, M. L., MacKenzie, T. D., Ogedegbe, O., Smith, S. C., Svetkey, L. P., Taler, S. J., Townsend, R. R., Wright, J. T., Narva, A. S., & Ortiz, E. (2014). 2014 evidence-based guideline for the management of high blood pressure in adults: Report from the panel members appointed to the Eighth Joint National Committee (JNC 8). *JAMA*, *311*(5), 507–520. https://doi.org/10.1001/jama.2013.284427

Jang, Y., Lee, S.-T., Kim, T.-J., Jun, J.-S., Moon, J., Jung, K.-H., Park, K.-I., Chu, K., & Lee, S. K. (2018). High albumin level is a predictor of favorable response to immunotherapy in autoimmune encephalitis. *Scientific Reports*, *8*(1), 1012. https://doi.org/10.1038/s41598-018-19490-z

Jiang, W. (2024). *Iris Series: Visualize Math—From Arithmetic Basics to Machine Learning*. GitHub. https://github.com/Visualize-ML

Jiménez, B., Holmes, E., Heude, C., Tolson, R. F., Harvey, N., Lodge, S. L., Chetwynd, A. J., Cannet, C., Fang, F., Pearce, J. T. M., Lewis, M. R., Viant, M. R., Lindon, J. C., Spraul, M., Schäfer, H., & Nicholson, J. K. (2018). Quantitative Lipoprotein Subclass and Low Molecular Weight Metabolite Analysis in Human Serum and Plasma by 1H NMR Spectroscopy in a Multilaboratory Trial. *Analytical Chemistry*, *90*(20), 11962–11971. https://doi.org/10.1021/acs.analchem.8b02412

Jobard, E., Trédan, O., Postoly, D., André, F., Martin, A.-L., Elena-Herrmann, B., & Boyault, S. (2016). A Systematic Evaluation of Blood Serum and Plasma Pre-Analytics for Metabolomics Cohort Studies. *International Journal of Molecular Sciences*, *17*(12), 2035. https://doi.org/10.3390/ijms17122035

Johnson, C. H., Ivanisevic, J., & Siuzdak, G. (2016). Metabolomics: Beyond biomarkers and towards mechanisms. *Nature Reviews. Molecular Cell Biology*, *17*(7), 451–459. https://doi.org/10.1038/nrm.2016.25

Jolliffe, I. (2005). Principal Component Analysis. In *Encyclopedia of Statistics in Behavioral Science*. John Wiley & Sons, Ltd. https://doi.org/10.1002/0470013192.bsa501

Julkunen, H., Cichońska, A., Tiainen, M., Koskela, H., Nybo, K., Mäkelä, V., Nokso-Koivisto, J., Kristiansson, K., Perola, M., Salomaa, V., Jousilahti, P., Lundqvist, A., Kangas, A. J., Soininen, P., Barrett, J. C., & Würtz, P. (2023). Atlas of plasma NMR biomarkers for health and disease in 118,461 individuals from the UK Biobank. *Nature Communications*, *14*(1), Article 1.

https://doi.org/10.1038/s41467-023-36231-7
Jurynczyk, M., Probert, F., Yeo, T., Tackley, G., Claridge, T. D. W., Cavey, A., Woodhall, M. R., Arora, S., Winkler, T., Schiffer, E., Vincent, A., DeLuca, G., Sibson, N. R., Isabel Leite, M., Waters, P., Anthony, D. C., & Palace, J. (2017). Metabolomics reveals distinct, antibody-independent, molecular signatures of MS, AQP4-antibody and MOG-antibody disease. *Acta Neuropathologica Communications*, *5*(1), 95. https://doi.org/10.1186/s40478-017-0495-8
Kalachikov, S., Evgrafov, O., Ross, B., Winawer, M., Barker-Cummings, C., Boneschi, F. M., Choi, C., Morozov, P., Das, K., Teplitskaya, E., Yu, A., Cayanis, E., Penchaszadeh, G., Kottmann, A. H., Pedley, T. A., Hauser, W. A., Ottman, R., & Gilliam, T. C. (2002). Mutations in LGI1 cause autosomal-dominant partial epilepsy with auditory features. *Nature Genetics*, *30*(3), 335–341. https://doi.org/10.1038/ng832
Kamlage, B., Maldonado, S. G., Bethan, B., Peter, E., Schmitz, O., Liebenberg, V., & Schatz, P. (2014). Quality Markers Addressing Preanalytical Variations of Blood and Plasma Processing Identified by Broad and Targeted Metabolite Profiling. *Clinical Chemistry*, *60*(2), 399–412. https://doi.org/10.1373/clinchem.2013.211979
Kamlage, B., Neuber, S., Bethan, B., González Maldonado, S., Wagner-Golbs, A., Peter, E., Schmitz, O., & Schatz, P. (2018a). Impact of Prolonged Blood Incubation and Extended Serum Storage at Room Temperature on the Human Serum Metabolome. *Metabolites*, *8*(1), Article 1. https://doi.org/10.3390/metabo8010006
Kamlage, B., Neuber, S., Bethan, B., González Maldonado, S., Wagner-Golbs, A., Peter, E., Schmitz, O., & Schatz, P. (2018b). Impact of Prolonged Blood Incubation and Extended Serum Storage at Room Temperature on the Human Serum Metabolome. *Metabolites*, *8*(1), 6. https://doi.org/10.3390/metabo8010006
Kanehisa, M., & Goto, S. (2000). KEGG: Kyoto Encyclopedia of Genes and Genomes. *Nucleic Acids Research*, *28*(1), 27–30.
Kang, K. N., Koh, E. Y., Jang, J. Y., & Kim, C. W. (2022). Multiple biomarkers are more accurate than a combination of carbohydrate antigen 125 and human epididymis protein 4 for ovarian cancer screening. *Obstetrics & Gynecology Science*, *65*(4), 346–354. https://doi.org/10.5468/ogs.22017
Karikari, T. K., Pascoal, T. A., Ashton, N. J., Janelidze, S., Benedet, A. L., Rodriguez, J. L., Chamoun, M., Savard, M., Kang, M. S., Therriault, J., Schöll, M., Massarweh, G., Soucy, J.-P., Höglund, K., Brinkmalm, G., Mattsson, N., Palmqvist, S., Gauthier, S., Stomrud, E., … Blennow, K. (2020). Blood phosphorylated tau 181 as a biomarker for Alzheimer's disease: A diagnostic performance and prediction modelling study using data from four prospective cohorts. *The Lancet Neurology*, *19*(5), 422–433. https://doi.org/10.1016/S1474-4422(20)30071-5
Kay, S. R., Fiszbein, A., & Opler, L. A. (1987). The positive and negative syndrome scale (PANSS) for schizophrenia. *Schizophrenia Bulletin*, *13*(2), 261–276. https://doi.org/10.1093/schbul/13.2.261
Kay, S. R., Opler, L. A., & Lindenmayer, J. P. (1988). Reliability and validity of the positive and negative syndrome scale for schizophrenics. *Psychiatry Research*, *23*(1), 99–110. https://doi.org/10.1016/0165-1781(88)90038-8
Kayser, M. S., Titulaer, M. J., Gresa-Arribas, N., & Dalmau, J. (2013). Frequency and characteristics of isolated psychiatric episodes in anti–N-methyl-d-aspartate receptor encephalitis. *JAMA Neurology*, *70*(9), 1133–1139. https://doi.org/10.1001/jamaneurol.2013.3216
Keeler, J. (2016). *Understanding NMR spectroscopy (2004)*. https://www.repository.cam.ac.uk/handle/1810/257364

Kelley, B. P., Patel, S. C., Marin, H. L., Corrigan, J. J., Mitsias, P. D., & Griffith, B. (2017). Autoimmune Encephalitis: Pathophysiology and Imaging Review of an Overlooked Diagnosis. *American Journal of Neuroradiology*, *38*(6), 1070–1078. https://doi.org/10.3174/ajnr.A5086

Kimhofer, T. (2021). *Metabom8* (Version 1.0.0) [Computer software]. Zenodo. https://doi.org/10.5281/zenodo.5487113

Klein, C. J., Lennon, V. A., Aston, P. A., McKeon, A., & Pittock, S. J. (2012). Chronic pain as a manifestation of potassium channel-complex autoimmunity. *Neurology*, *79*(11), 1136–1144. https://doi.org/10.1212/WNL.0b013e3182698cab

Klingenberg, R., Gerdes, N., Badeau, R. M., Gisterå, A., Strodthoff, D., Ketelhuth, D. F. J., Lundberg, A. M., Rudling, M., Nilsson, S. K., Olivecrona, G., Zoller, S., Lohmann, C., Lüscher, T. F., Jauhiainen, M., Sparwasser, T., & Hansson, G. K. (2013). Depletion of FOXP3+ regulatory T cells promotes hypercholesterolemia and atherosclerosis. *The Journal of Clinical Investigation*, *123*(3), 1323–1334. https://doi.org/10.1172/JCI63891

Kolde, R. (2012). Pheatmap: Pretty heatmaps. *R Package Version*, *1*(2), 726.

Koochakpoor, G., Salari-Moghaddam, A., Keshteli, A. H., Afshar, H., Esmaillzadeh, A., & Adibi, P. (2021). Dietary intake of branched-chain amino acids in relation to depression, anxiety and psychological distress. *Nutrition Journal*, *20*(1), 11. https://doi.org/10.1186/s12937-021-00670-z

Korczowska-Łącka, I., Hurła, M., Banaszek, N., Kobylarek, D., Szymanowicz, O., Kozubski, W., & Dorszewska, J. (2023). Selected Biomarkers of Oxidative Stress and Energy Metabolism Disorders in Neurological Diseases. *Molecular Neurobiology*, *60*(7), 4132–4149. https://doi.org/10.1007/s12035-023-03329-4

Kostidis, S., Addie, R. D., Morreau, H., Mayboroda, O. A., & Giera, M. (2017). Quantitative NMR analysis of intra- and extracellular metabolism of mammalian cells: A tutorial. *Analytica Chimica Acta*, *980*, 1–24. https://doi.org/10.1016/j.aca.2017.05.011

Kronenberg, F., Trenkwalder, E., Kronenberg, M. F., König, P., Utermann, G., & Dieplinger, H. (1998). Influence of hematocrit on the measurement of lipoproteins demonstrated by the example of lipoprotein(a). *Kidney International*, *54*(4), 1385–1389. https://doi.org/10.1046/j.1523-1755.1998.00086.x

Krzyściak, W., Bystrowska, B., Karcz, P., Chrzan, R., Bryll, A., Turek, A., Mazur, P., Śmierciak, N., Szwajca, M., Donicz, P., Furman, K., Pilato, F., Kozicz, T., Popiela, T., & Pilecki, M. (2024). Association of Blood Metabolomics Biomarkers with Brain Metabolites and Patient-Reported Outcomes as a New Approach in Individualized Diagnosis of Schizophrenia. *International Journal of Molecular Sciences*, *25*(4), Article 4. https://doi.org/10.3390/ijms25042294

Ladépêche, L., Planagumà, J., Thakur, S., Suárez, I., Hara, M., Borbely, J. S., Sandoval, A., Laparra-Cuervo, L., Dalmau, J., & Lakadamyali, M. (2018). NMDA Receptor Autoantibodies in Autoimmune Encephalitis Cause a Subunit-Specific Nanoscale Redistribution of NMDA Receptors. *Cell Reports*, *23*(13), 3759–3768. https://doi.org/10.1016/j.celrep.2018.05.096

Lai, M., Huijbers, M. G., Lancaster, E., Graus, F., Bataller, L., Balice-Gordon, R., Cowell, J. K., & Dalmau, J. (2010). Investigation of LGI1 as the antigen in limbic encephalitis previously attributed to potassium channels: A case series. *The Lancet Neurology*, *9*(8), 776–785. https://doi.org/10.1016/S1474-4422(10)70137-X

Lai, W., Du, D., & Chen, L. (2022). Metabolomics Provides Novel Insights into Epilepsy Diagnosis and Treatment: A Review. *Neurochemical Research*, *47*(4), 844–859. https://doi.org/10.1007/s11064-021-03510-y

Lancaster, E. (2016). The Diagnosis and Treatment of Autoimmune Encephalitis. *Journal of Clinical Neurology (Seoul, Korea)*, *12*(1), 1–13. https://doi.org/10.3988/jcn.2016.12.1.1

Lane, A. N. (2012). Principles of NMR for Applications in Metabolomics. In T. W.-M. Fan, A. N. Lane, & R. M. Higashi (Eds.), *The Handbook of Metabolomics* (pp. 127–197). Humana Press. https://doi.org/10.1007/978-1-61779-618-0_6

Lang, B., Makuch, M., Moloney, T., Dettmann, I., Mindorf, S., Probst, C., Stoecker, W., Buckley, C., Newton, C. R., Leite, M. I., Maddison, P., Komorowski, L., Adcock, J., Vincent, A., Waters, P., & Irani, S. R. (2017). Intracellular and non-neuronal targets of voltage-gated potassium channel complex antibodies. *Journal of Neurology, Neurosurgery, and Psychiatry*, *88*(4), 353–361. https://doi.org/10.1136/jnnp-2016-314758

Lang, K., & Prüss, H. (2017). Frequencies of neuronal autoantibodies in healthy controls. *Neurology® Neuroimmunology & Neuroinflammation*, *4*(5), e386. https://doi.org/10.1212/NXI.0000000000000386

Larkin, J. R., Anthony, S., Johanssen, V. A., Yeo, T., Sealey, M., Yates, A. G., Smith, C. F., Claridge, T. D. W., Nicholson, B. D., Moreland, J.-A., Gleeson, F., Sibson, N. R., Anthony, D. C., & Probert, F. (2022a). Metabolomic Biomarkers in Blood Samples Identify Cancers in a Mixed Population of Patients with Nonspecific Symptoms. *Clinical Cancer Research*, *28*(8), 1651–1661. https://doi.org/10.1158/1078-0432.CCR-21-2855

Larkin, J. R., Anthony, S., Johanssen, V. A., Yeo, T., Sealey, M., Yates, A. G., Smith, C. F., Claridge, T. D. W., Nicholson, B. D., Moreland, J.-A., Gleeson, F., Sibson, N. R., Anthony, D. C., & Probert, F. (2022b). Metabolomic Biomarkers in Blood Samples Identify Cancers in a Mixed Population of Patients with Nonspecific Symptoms. *Clinical Cancer Research: An Official Journal of the American Association for Cancer Research*, *28*(8), 1651–1661. https://doi.org/10.1158/1078-0432.CCR-21-2855

Laterza, O. F., Hendrickson, R. C., & Wagner, J. A. (2007). Molecular Biomarkers. *Drug Information Journal : DIJ / Drug Information Association*, *41*(5), 573–585. https://doi.org/10.1177/009286150704100504

Ledermann, J., Harter, P., Gourley, C., Friedlander, M., Vergote, I., Rustin, G., Scott, C., Meier, W., Shapira-Frommer, R., Safra, T., Matei, D., Macpherson, E., Watkins, C., Carmichael, J., & Matulonis, U. (2012). Olaparib maintenance therapy in platinum-sensitive relapsed ovarian cancer. *The New England Journal of Medicine*, *366*(15), 1382–1392. https://doi.org/10.1056/NEJMoa1105535

Lee, S. K., & Lee, S.-T. (2016). The Laboratory Diagnosis of Autoimmune Encephalitis. *Journal of Epilepsy Research*, *6*(2), 45–52. https://doi.org/10.14581/jer.16010

Lehmann, R. (2015). Preanalytics: What Can Metabolomics Learn from Clinical Chemistry? *Bioanalysis*, *7*(8), 927–930. https://doi.org/10.4155/bio.15.23

Lennox, B. R., Palmer-Cooper, E. C., Pollak, T., Hainsworth, J., Marks, J., Jacobson, L., Lang, B., Fox, H., Ferry, B., Scoriels, L., Crowley, H., Jones, P. B., Harrison, P. J., Vincent, A., & PPiP study team. (2017). Prevalence and clinical characteristics of serum neuronal cell surface antibodies in first-episode psychosis: A case-control study. *The Lancet. Psychiatry*, *4*(1), 42–48. https://doi.org/10.1016/S2215-0366(16)30375-3

Lennox, B. R., Tomei, G., Vincent, S.-A., Yeeles, K., Pollard, R., Palmer-Cooper, E., Jones, P., Zandi, M. S., & Coles, A. (2019). Study of immunotherapy in antibody positive psychosis: Feasibility and acceptability (SINAPPS1). *Journal of Neurology, Neurosurgery, and Psychiatry*, *90*(3), 365–367. https://doi.org/10.1136/jnnp-2018-318124

Lepoittevin, M., Blancart-Remaury, Q., Kerforne, T., Pellerin, L., Hauet, T., & Thuillier, R. (2023). Comparison between 5 extractions methods in either plasma or serum to determine the optimal extraction and matrix combination for human metabolomics. *Cellular & Molecular Biology Letters*, *28*, 43. https://doi.org/10.1186/s11658-023-00452-x

Levraut, M., Bourg, V., Capet, N., Delourme, A., Honnorat, J., Thomas, P., & Lebrun-Frenay, C. (2021). Cerebrospinal Fluid IL-17A Could Predict Acute Disease Severity in Non-NMDA-Receptor Autoimmune Encephalitis. *Frontiers in Immunology*, *12*, 673021. https://doi.org/10.3389/fimmu.2021.673021

Liao, K. P., Playford, M. P., Frits, M., Coblyn, J. S., Iannaccone, C., Weinblatt, M. E., Shadick, N. S., & Mehta, N. N. (2015). The association between reduction in inflammation and changes in lipoprotein levels and HDL cholesterol efflux capacity in rheumatoid arthritis. *Journal of the American Heart Association*, *4*(2), e001588. https://doi.org/10.1161/JAHA.114.001588

Lin, C. Y., Wu, H., Tjeerdema, R. S., & Viant, M. R. (2007). Evaluation of metabolite extraction strategies from tissue samples using NMR metabolomics. *Metabolomics*, *3*(1), 55–67. https://doi.org/10.1007/s11306-006-0043-1

Lippi, G., Nybo, M., Cadamuro, J., Guimaraes, J. T., van Dongen-Lases, E., & Simundic, A.-M. (2018). Chapter Four - Blood Glucose Determination: Effect of Tube Additives. In G. S. Makowski (Ed.), *Advances in Clinical Chemistry* (Vol. 84, pp. 101–123). Elsevier. https://doi.org/10.1016/bs.acc.2017.12.003

Liu, F., Huang, T., Wang, B., Wang, C., & Guo, S. (2022). Low high-density lipoprotein cholesterol and apolipoprotein A-I levels are associated with poor outcome and relapse in autoimmune encephalitis. *Neuroscience Letters*, *775*, 136546. https://doi.org/10.1016/j.neulet.2022.136546

Liu, F., Wang, B., Wang, C., Zhang, B., & Guo, S. (2021). Lipid profiles and their potential inflammatory effects in anti-N-methyl-D-aspartate receptor encephalitis. *Neurological Sciences: Official Journal of the Italian Neurological Society and of the Italian Society of Clinical Neurophysiology*, *42*(7), 2881–2890. https://doi.org/10.1007/s10072-020-04882-9

Louis, E., Mary, J.-Y., Vernier-Massouille, G., Grimaud, J.-C., Bouhnik, Y., Laharie, D., Dupas, J.-L., Pillant, H., Picon, L., Veyrac, M., Flamant, M., Savoye, G., Jian, R., Devos, M., Porcher, R., Paintaud, G., Piver, E., Colombel, J.-F., Lemann, M., & Groupe D'etudes Thérapeutiques Des Affections Inflammatoires Digestives. (2012). Maintenance of remission among patients with Crohn's disease on antimetabolite therapy after infliximab therapy is stopped. *Gastroenterology*, *142*(1), 63-70.e5; quiz e31. https://doi.org/10.1053/j.gastro.2011.09.034

Louis, E., Resche-Rigon, M., Laharie, D., Satsangi, J., Ding, N., Siegmund, B., D'Haens, G., Picon, L., Bossuyt, P., Vuitton, L., Irving, P., Viennot, S., Lamb, C. A., Pollok, R., Baert, F., Nachury, M., Fumery, M., Gilletta, C., Almer, S., … Hertervig, E. (2023). Withdrawal of infliximab or concomitant immunosuppressant therapy in patients with Crohn's disease on combination therapy (SPARE): A multicentre, open-label, randomised controlled trial. *The Lancet. Gastroenterology & Hepatology*, *8*(3), 215–227. https://doi.org/10.1016/S2468-1253(22)00385-5

Lynch, C. J., & Adams, S. H. (2014). Branched-chain amino acids in metabolic signalling and insulin resistance. *Nature Reviews Endocrinology*, *10*(12), 723–736. https://doi.org/10.1038/nrendo.2014.171

Lyons, O., Whelan, B., Bennett, K., O'Riordan, D., & Silke, B. (2010). Serum albumin as an outcome predictor in hospital emergency medical admissions. *European Journal of Internal Medicine*, *21*(1), 17–20. https://doi.org/10.1016/j.ejim.2009.10.010

Maat, P., Graaff, E. de, Beveren, N. M. van, Hulsenboom, E., Verdijk, R. M., Koorengevel, K., Duijn, M. van, Hooijkaas, H., Hoogenraad, C., & Smitt, P. A. S. (2013). Psychiatric phenomena as initial manifestation of encephalitis by anti-NMDAR antibodies. *Acta Neuropsychiatrica*, *25*(3), 128–136. https://doi.org/10.1111/acn.12013

Maes, P., Monakhova, Y. B., Kuballa, T., Reusch, H., & Lachenmeier, D. W. (2012). Qualitative

and Quantitative Control of Carbonated Cola Beverages Using 1H NMR Spectroscopy. *Journal of Agricultural and Food Chemistry*, *60*(11), 2778–2784. https://doi.org/10.1021/jf204777m

Mallagaray, A., Rudolph, L., Lindloge, M., Mölbitz, J., Thomsen, H., Schmelter, F., Alhabash, M. W., Abdullah, M. R., Saraei, R., Ehlers, M., Graf, T., Sina, C., Petersmann, A., Nauck, M., & Günther, U. L. (2023). Towards a Precise NMR Quantification of Acute Phase Inflammation Proteins from Human Serum. *Angewandte Chemie International Edition*, *62*(35), e202306154. https://doi.org/10.1002/anie.202306154

Manosalva, C., Quiroga, J., Hidalgo, A. I., Alarcón, P., Anseoleaga, N., Hidalgo, M. A., & Burgos, R. A. (2022). Role of Lactate in Inflammatory Processes: Friend or Foe. *Frontiers in Immunology*, *12*. https://www.frontiersin.org/articles/10.3389/fimmu.2021.808799

McClain, K. M., Moore, S. C., Sampson, J. N., Henderson, T. R., Gebauer, S. K., Newman, J. W., Ross, S., Pedersen, T. L., Baer, D. J., & Zanetti, K. A. (2021). Preanalytical Sample Handling Conditions and Their Effects on the Human Serum Metabolome in Epidemiologic Studies. *American Journal of Epidemiology*, *190*(3), 459–467. https://doi.org/10.1093/aje/kwaa202

McCracken, L., Zhang, J., Greene, M., Crivaro, A., Gonzalez, J., Kamoun, M., & Lancaster, E. (2017). Improving the antibody-based evaluation of autoimmune encephalitis. *Neurology® Neuroimmunology & Neuroinflammation*, *4*(6), e404. https://doi.org/10.1212/NXI.0000000000000404

McDermott, J. E., Wang, J., Mitchell, H., Webb-Robertson, B.-J., Hafen, R., Ramey, J., & Rodland, K. D. (2013). Challenges in Biomarker Discovery: Combining Expert Insights with Statistical Analysis of Complex Omics Data. *Expert Opinion on Medical Diagnostics*, *7*(1), 37–51. https://doi.org/10.1517/17530059.2012.718329

McGrath, C. M., & Young, S. P. (2019). Can metabolomic profiling predict response to therapy? *Nature Reviews Rheumatology*, *15*(3), 129–130. https://doi.org/10.1038/s41584-018-0136-z

Mckay, R. T. (2011). How the 1D-NOESY suppresses solvent signal in metabonomics NMR spectroscopy: An examination of the pulse sequence components and evolution. *Concepts in Magnetic Resonance Part A*, *38A*(5), 197–220. https://doi.org/10.1002/cmr.a.20223

Meltzer, H. Y. (1989). Clinical studies on the mechanism of action of clozapine: The dopamine-serotonin hypothesis of schizophrenia. *Psychopharmacology*, *99 Suppl*, S18-27. https://doi.org/10.1007/BF00442554

Mendez, K. M., Broadhurst, D. I., & Reinke, S. N. (2019). The application of artificial neural networks in metabolomics: A historical perspective. *Metabolomics*, *15*(11), 142. https://doi.org/10.1007/s11306-019-1608-0

Mendez, K. M., Reinke, S. N., & Broadhurst, D. I. (2019). A comparative evaluation of the generalised predictive ability of eight machine learning algorithms across ten clinical metabolomics data sets for binary classification. *Metabolomics*, *15*(12), 150. https://doi.org/10.1007/s11306-019-1612-4

Michael, S., Waters, P., & Irani, S. R. (2020). Stop testing for autoantibodies to the VGKC-complex: Only request LGI1 and CASPR2. *Practical Neurology*, *20*(5), 377–384. https://doi.org/10.1136/practneurol-2019-002494

Michetti, F., D'Ambrosi, N., Toesca, A., Puglisi, M. A., Serrano, A., Marchese, E., Corvino, V., & Geloso, M. C. (2019). The S100B story: From biomarker to active factor in neural injury. *Journal of Neurochemistry*, *148*(2), 168–187. https://doi.org/10.1111/jnc.14574

Miller, H. A., Rai, S. N., Yin, X., Zhang, X., Chesney, J. A., van Berkel, V. H., & Frieboes, H. B. (2022). Lung cancer metabolomic data from tumor core biopsies enables risk-score calculation for progression-free and overall survival. *Metabolomics*, *18*(5), 31. https://doi.org/10.1007/s11306-022-01891-x

Miller, W. L., & Auchus, R. J. (2011). The molecular biology, biochemistry, and physiology of human steroidogenesis and its disorders. *Endocrine Reviews*, *32*(1), 81–151. https://doi.org/10.1210/er.2010-0013

Moayyeri, A., Hammond, C. J., Hart, D. J., & Spector, T. D. (2013). The UK Adult Twin Registry (TwinsUK Resource). *Twin Research and Human Genetics*, *16*(1), 144–149. https://doi.org/10.1017/thg.2012.89

Monaghan, T. F., Rahman, S. N., Agudelo, C. W., Wein, A. J., Lazar, J. M., Everaert, K., & Dmochowski, R. R. (2021). Foundational Statistical Principles in Medical Research: Sensitivity, Specificity, Positive Predictive Value, and Negative Predictive Value. *Medicina*, *57*(5), 503. https://doi.org/10.3390/medicina57050503

Moriya, T., Satomi, Y., & Kobayashi, H. (2016). Intensive determination of storage condition effects on human plasma metabolomics. *Metabolomics*, *12*(12), 179. https://doi.org/10.1007/s11306-016-1126-2

Muñiz-Castrillo, S., Haesebaert, J., Thomas, L., Vogrig, A., Pinto, A.-L., Picard, G., Blanc, C., Do, L.-D., Joubert, B., Berzero, G., Psimaras, D., Alentorn, A., Rogemond, V., Dubois, V., Ambati, A., Tamouza, R., Mignot, E., & Honnorat, J. (2021). Clinical and Prognostic Value of Immunogenetic Characteristics in Anti-LGI1 Encephalitis. *Neurology Neuroimmunology & Neuroinflammation*, *8*(3), e974. https://doi.org/10.1212/NXI.0000000000000974

Muranaka, H., Hendifar, A., Osipov, A., Moshayedi, N., Placencio-Hickok, V., Tatonetti, N., Stotland, A., Parker, S., Eyk, J. V., Pandol, S. J., Bhowmick, N. A., & Gong, J. (2023). Plasma Metabolomics Predicts Chemotherapy Response in Advanced Pancreatic Cancer. *Cancers*, *15*(11), 3020. https://doi.org/10.3390/cancers15113020

Mushtaq, M. Y., Choi, Y. H., Verpoorte, R., & Wilson, E. G. (2014). Extraction for metabolomics: Access to the metabolome. *Phytochemical Analysis: PCA*, *25*(4), 291–306. https://doi.org/10.1002/pca.2505

Muti, I. H., Gonzalez Sanchez-Dahl, M., Zhong, A. B., Weng, J., Füzesi, M. V., Kivisäkk, P., Hyman, B. T., Arnold, S. E., Feldman, A. S., Mercaldo, N. D., & Cheng, L. L. (2023). Designing a quality assurance process for quality control of nuclear magnetic resonance metabolomics studies of human blood. *NMR in Biomedicine*, *36*(4), e4868. https://doi.org/10.1002/nbm.4868

Nagana Gowda, G. A., Gowda, Y. N., & Raftery, D. (2015). Expanding the Limits of Human Blood Metabolite Quantitation Using NMR Spectroscopy. *Analytical Chemistry*, *87*(1), 706–715. https://doi.org/10.1021/ac503651e

Nagana Gowda, G. A., Pascua, V., & Raftery, D. (2023). Anomalous Dynamics of Labile Metabolites in Cold Human Blood Detected Using 1H NMR Spectroscopy. *Analytical Chemistry*, *95*(34), 12923–12930. https://doi.org/10.1021/acs.analchem.3c02478

Najjar, S., Steiner, J., Najjar, A., & Bechter, K. (2018). A clinical approach to new-onset psychosis associated with immune dysregulation: The concept of autoimmune psychosis. *Journal of Neuroinflammation*, *15*(1), 40. https://doi.org/10.1186/s12974-018-1067-y

Newgard, C. B. (2012). Interplay between lipids and branched-chain amino acids in development of insulin resistance. *Cell Metabolism*, *15*(5), 606–614. https://doi.org/10.1016/j.cmet.2012.01.024

Ng, S., Masarone, S., Watson, D., & Barnes, M. R. (2023). The benefits and pitfalls of machine learning for biomarker discovery. *Cell and Tissue Research*, *394*(1), 17–31. https://doi.org/10.1007/s00441-023-03816-z

Ngugi, A. K., Bottomley, C., Kleinschmidt, I., Sander, J. W., & Newton, C. R. (2010). Estimation of the burden of active and life-time epilepsy: A meta-analytic approach. *Epilepsia*, *51*(5), 883–890. https://doi.org/10.1111/j.1528-1167.2009.02481.x

Nicholson, J. K., Foxall, P. J., Spraul, M., Farrant, R. D., & Lindon, J. C. (1995). 750 MHz 1H and 1H-13C NMR spectroscopy of human blood plasma. *Analytical Chemistry*, *67*(5), 793–811. https://doi.org/10.1021/ac00101a004

Nishiumi, S., Suzuki, M., Kobayashi, T., & Yoshida, M. (2018). Differences in metabolite profiles caused by pre-analytical blood processing procedures. *Journal of Bioscience and Bioengineering*, *125*(5), 613–618. https://doi.org/10.1016/j.jbiosc.2017.11.011

Norat, P., Soldozy, S., Sokolowski, J. D., Gorick, C. M., Kumar, J. S., Chae, Y., Yağmurlu, K., Prada, F., Walker, M., Levitt, M. R., Price, R. J., Tvrdik, P., & Kalani, M. Y. S. (2020). Mitochondrial dysfunction in neurological disorders: Exploring mitochondrial transplantation. *Npj Regenerative Medicine*, *5*(1), 1–9. https://doi.org/10.1038/s41536-020-00107-x

Nosadini, M., Eyre, M., Molteni, E., Thomas, T., Irani, S. R., Dalmau, J., Dale, R. C., Lim, M., International NMDAR Antibody Encephalitis Consensus Group, Anlar, B., Armangue, T., Benseler, S., Cellucci, T., Deiva, K., Gallentine, W., Gombolay, G., Gorman, M. P., Hacohen, Y., Jiang, Y., … Yeshokumar, A. K. (2021). Use and Safety of Immunotherapeutic Management of N-Methyl-d-Aspartate Receptor Antibody Encephalitis: A Meta-analysis. *JAMA Neurology*, *78*(11), 1333–1344. https://doi.org/10.1001/jamaneurol.2021.3188

Olberg, H., Haugen, M., Storstein, A., & Vedeler, C. A. (2013). Neurological manifestations related to level of voltage-gated potassium channel antibodies. *Journal of Neurology, Neurosurgery & Psychiatry*, *84*(8), 941–943. https://doi.org/10.1136/jnnp-2013-305252

Oldstone, M. B. A. (2014). Molecular Mimicry: Its Evolution from Concept to Mechanism as a Cause of Autoimmune Diseases. *Monoclonal Antibodies in Immunodiagnosis and Immunotherapy*, *33*(3), 158–165. https://doi.org/10.1089/mab.2013.0090

Olsson, B., Portelius, E., Cullen, N. C., Sandelius, Å., Zetterberg, H., Andreasson, U., Höglund, K., Irwin, D. J., Grossman, M., Weintraub, D., Chen-Plotkin, A., Wolk, D., McCluskey, L., Elman, L., Shaw, L. M., Toledo, J. B., McBride, J., Hernandez-Con, P., Lee, V. M.-Y., … Blennow, K. (2019). Association of Cerebrospinal Fluid Neurofilament Light Protein Levels With Cognition in Patients With Dementia, Motor Neuron Disease, and Movement Disorders. *JAMA Neurology*, *76*(3), 318–325. https://doi.org/10.1001/jamaneurol.2018.3746

Oostendorp, M., Engelke, U. F. H., Willemsen, M. A. A. P., & Wevers, R. A. (2006). Diagnosing inborn errors of lipid metabolism with proton nuclear magnetic resonance spectroscopy. *Clinical Chemistry*, *52*(7), 1395–1405. https://doi.org/10.1373/clinchem.2006.069112

Ormseth, M. J., Chung, C. P., Oeser, A. M., Connelly, M. A., Sokka, T., Raggi, P., Solus, J. F., Otvos, J. D., & Stein, C. M. (2015). Utility of a novel inflammatory marker, GlycA, for assessment of rheumatoid arthritis disease activity and coronary atherosclerosis. *Arthritis Research & Therapy*, *17*(1), 117. https://doi.org/10.1186/s13075-015-0646-x

Paglia, G., Del Greco, F. M., Sigurdsson, B. B., Rainer, J., Volani, C., Hicks, A. A., Pramstaller, P. P., & Smarason, S. V. (2018). Influence of collection tubes during quantitative targeted metabolomics studies in human blood samples. *Clinica Chimica Acta*, *486*, 320–328. https://doi.org/10.1016/j.cca.2018.08.014

Pang, Z., Chong, J., Zhou, G., de Lima Morais, D. A., Chang, L., Barrette, M., Gauthier, C., Jacques, P.-É., Li, S., & Xia, J. (2021). MetaboAnalyst 5.0: Narrowing the gap between raw spectra and functional insights. *Nucleic Acids Research*, *49*(W1), W388–W396. https://doi.org/10.1093/nar/gkab382

Pankevich, D. E., Altevogt, B. M., Dunlop, J., Gage, F. H., & Hyman, S. E. (2014). Improving and Accelerating Drug Development for Nervous System Disorders. *Neuron*, *84*(3), 546–553. https://doi.org/10.1016/j.neuron.2014.10.007

Paskevich, S. I., Molchanov, M. V., Timchenko, M. A., & Kutyshenko, V. P. (2013). Sample

pretreatment of brain tissues and cerebrospinal fluid for NMR investigations. *Journal of Analytical Chemistry*, *68*(10), 862–870. https://doi.org/10.1134/S1061934813100092
Patti, G. J., Yanes, O., & Siuzdak, G. (2012). Metabolomics: The apogee of the omics trilogy. *Nature Reviews Molecular Cell Biology*, *13*(4), 263–269. https://doi.org/10.1038/nrm3314
Pavia, D. L., Lampman, G. M., Kriz, G. S., & Vyvyan, J. A. (2014). *Introduction to spectroscopy*. Cengage learning.
Peakman, T. C., & Elliott, P. (2008a). The UK Biobank sample handling and storage validation studies. *International Journal of Epidemiology*, *37*(suppl_1), i2–i6. https://doi.org/10.1093/ije/dyn019
Peakman, T. C., & Elliott, P. (2008b). The UK Biobank sample handling and storage validation studies. *International Journal of Epidemiology*, *37*(suppl_1), i2–i6. https://doi.org/10.1093/ije/dyn019
Pettingill, P., Kramer, H. B., Coebergh, J. A., Pettingill, R., Maxwell, S., Nibber, A., Malaspina, A., Jacob, A., Irani, S. R., Buckley, C., Beeson, D., Lang, B., Waters, P., & Vincent, A. (2015). Antibodies to GABAA receptor α1 and γ2 subunits: Clinical and serologic characterization. *Neurology*, *84*(12), 1233–1241. https://doi.org/10.1212/WNL.0000000000001326
Pignolet, B. S., Gebauer, C. M., & Liblau, R. S. (2013). Immunopathogenesis of paraneoplastic neurological syndromes associated with anti-Hu antibodies. *Oncoimmunology*, *2*(12), e27384. https://doi.org/10.4161/onci.27384
Pinto, J., Domingues, M. R. M., Galhano, E., Pita, C., Almeida, M. do C., Carreira, I. M., & Gil, A. M. (2014a). Human plasma stability during handling and storage: Impact on NMR metabolomics. *Analyst*, *139*(5), 1168–1177. https://doi.org/10.1039/C3AN02188B
Pinto, J., Domingues, M. R. M., Galhano, E., Pita, C., Almeida, M. do C., Carreira, I. M., & Gil, A. M. (2014b). Human plasma stability during handling and storage: Impact on NMR metabolomics. *Analyst*, *139*(5), 1168–1177. https://doi.org/10.1039/C3AN02188B
Pitt, J. J. (2009). Principles and Applications of Liquid Chromatography-Mass Spectrometry in Clinical Biochemistry. *The Clinical Biochemist Reviews*, *30*(1), 19–34.
Pollak, T. A., Lennox, B. R., Müller, S., Benros, M. E., Prüss, H., Tebartz van Elst, L., Klein, H., Steiner, J., Frodl, T., Bogerts, B., Tian, L., Groc, L., Hasan, A., Baune, B. T., Endres, D., Haroon, E., Yolken, R., Benedetti, F., Halaris, A., … Bechter, K. (2020). Autoimmune psychosis: An international consensus on an approach to the diagnosis and management of psychosis of suspected autoimmune origin. *The Lancet Psychiatry*, *7*(1), 93–108. https://doi.org/10.1016/S2215-0366(19)30290-1
Pouget, J. G., Schizophrenia Working Group of the Psychiatric Genomics Consortium, Han, B., Wu, Y., Mignot, E., Ollila, H. M., Barker, J., Spain, S., Dand, N., Trembath, R., Martin, J., Mayes, M. D., Bossini-Castillo, L., López-Isac, E., Jin, Y., Santorico, S. A., Spritz, R. A., Hakonarson, H., Polychronakos, C., … Knight, J. (2019). Cross-disorder analysis of schizophrenia and 19 immune-mediated diseases identifies shared genetic risk. *Human Molecular Genetics*, *28*(20), 3498–3513. https://doi.org/10.1093/hmg/ddz145
Probert, F., Yeo, T., Zhou, Y., Sealey, M., Arora, S., Palace, J., Claridge, T. D. W., Hillenbrand, R., Oechtering, J., Leppert, D., Kuhle, J., & Anthony, D. C. (2021). Integrative biochemical, proteomics and metabolomics cerebrospinal fluid biomarkers predict clinical conversion to multiple sclerosis. *Brain Communications*, *3*(2), fcab084. https://doi.org/10.1093/braincomms/fcab084
Prüss, H. (2021). Autoantibodies in neurological disease. *Nature Reviews Immunology*, *21*(12), 798–813. https://doi.org/10.1038/s41577-021-00543-w
Prüss, H., & Lennox, B. R. (2016). Emerging psychiatric syndromes associated with antivoltage-

gated potassium channel complex antibodies. *Journal of Neurology, Neurosurgery, and Psychiatry*, *87*(11), 1242–1247. https://doi.org/10.1136/jnnp-2015-313000

Qiu, S., Cai, Y., Yao, H., Lin, C., Xie, Y., Tang, S., & Zhang, A. (2023). Small molecule metabolites: Discovery of biomarkers and therapeutic targets. *Signal Transduction and Targeted Therapy*, *8*(1), 1–37. https://doi.org/10.1038/s41392-023-01399-3

Quezada, H., Guzmán-Ortiz, A. L., Díaz-Sánchez, H., Valle-Rios, R., & Aguirre-Hernández, J. (2017). Omics-based biomarkers: Current status and potential use in the clinic. *Boletín Médico Del Hospital Infantil de México (English Edition)*, *74*(3), 219–226. https://doi.org/10.1016/j.bmhime.2017.11.030

Quinones, M. P., & Kaddurah-Daouk, R. (2009). Metabolomics tools for identifying biomarkers for neuropsychiatric diseases. *Neurobiology of Disease*, *35*(2), 165–176. https://doi.org/10.1016/j.nbd.2009.02.019

Ramanathan, S., Al-Diwani, A., Waters, P., & Irani, S. R. (2021). The autoantibody-mediated encephalitides: From clinical observations to molecular pathogenesis. *Journal of Neurology*, *268*(5), 1689–1707. https://doi.org/10.1007/s00415-019-09590-9

Rattray, N. J. W., Deziel, N. C., Wallach, J. D., Khan, S. A., Vasiliou, V., Ioannidis, J. P. A., & Johnson, C. H. (2018). Beyond genomics: Understanding exposotypes through metabolomics. *Human Genomics*, *12*, 4. https://doi.org/10.1186/s40246-018-0134-x

Ren, S., Hinzman, A. A., Kang, E. L., Szczesniak, R. D., & Lu, L. J. (2015). Computational and statistical analysis of metabolomics data. *Metabolomics*, *11*(6), 1492–1513. https://doi.org/10.1007/s11306-015-0823-6

Ripke, S., Neale, B. M., Corvin, A., Walters, J. T. R., Farh, K.-H., Holmans, P. A., Lee, P., Bulik-Sullivan, B., Collier, D. A., Huang, H., Pers, T. H., Agartz, I., Agerbo, E., Albus, M., Alexander, M., Amin, F., Bacanu, S. A., Begemann, M., Belliveau Jr, R. A., … Psychosis Endophenotypes International Consortium. (2014). Biological insights from 108 schizophrenia-associated genetic loci. *Nature*, *511*(7510), 421–427. https://doi.org/10.1038/nature13595

Rispoli, M. G., Valentinuzzi, S., De Luca, G., Del Boccio, P., Federici, L., Di Ioia, M., Digiovanni, A., Grasso, E. A., Pozzilli, V., Villani, A., Chiarelli, A. M., Onofrj, M., Wise, R. G., Pieragostino, D., & Tomassini, V. (2021). Contribution of Metabolomics to Multiple Sclerosis Diagnosis, Prognosis and Treatment. *International Journal of Molecular Sciences*, *22*(20), 11112. https://doi.org/10.3390/ijms222011112

Ritchie, S. C., Surendran, P., Karthikeyan, S., Lambert, S. A., Bolton, T., Pennells, L., Danesh, J., Di Angelantonio, E., Butterworth, A. S., & Inouye, M. (2023). Quality control and removal of technical variation of NMR metabolic biomarker data in ~120,000 UK Biobank participants. *Scientific Data*, *10*(1), Article 1. https://doi.org/10.1038/s41597-023-01949-y

Robertson, J., Porter, D., Sattar, N., Packard, C. J., Caslake, M., McInnes, I., & McCarey, D. (2017). Interleukin-6 blockade raises LDL via reduced catabolism rather than via increased synthesis: A cytokine-specific mechanism for cholesterol changes in rheumatoid arthritis. *Annals of the Rheumatic Diseases*, *76*(11), 1949–1952. https://doi.org/10.1136/annrheumdis-2017-211708

Rogan, A., O'Sullivan, M. B., Holley, A., McQuade, D., & Larsen, P. (2022). Can serum biomarkers be used to rule out significant intracranial pathology in emergency department patients with mild traumatic brain injury? A Systemic Review & Meta-Analysis. *Injury*, *53*(2), 259–271. https://doi.org/10.1016/j.injury.2021.10.015

Ruiz-García, R., Muñoz-Sánchez, G., Naranjo, L., Guasp, M., Sabater, L., Saiz, A., Dalmau, J., Graus, F., & Martinez-Hernandez, E. (2021). Limitations of a Commercial Assay as Diagnostic Test of Autoimmune Encephalitis. *Frontiers in Immunology*, *12*, 691536. https://doi.org/10.3389/fimmu.2021.691536

Rundlöf, T., Mathiasson, M., Bekiroglu, S., Hakkarainen, B., Bowden, T., & Arvidsson, T. (2010). Survey and qualification of internal standards for quantification by 1H NMR spectroscopy. *Journal of Pharmaceutical and Biomedical Analysis*, *52*(5), 645–651. https://doi.org/10.1016/j.jpba.2010.02.007

Saccenti, E., Hoefsloot, H. C. J., Smilde, A. K., Westerhuis, J. A., & Hendriks, M. M. W. B. (2014). Reflections on univariate and multivariate analysis of metabolomics data. *Metabolomics*, *10*(3), 361–374. https://doi.org/10.1007/s11306-013-0598-6

Santos Ferreira, D. L., Maple, H. J., Goodwin, M., Brand, J. S., Yip, V., Min, J. L., Groom, A., Lawlor, D. A., & Ring, S. (2019a). The Effect of Pre-Analytical Conditions on Blood Metabolomics in Epidemiological Studies. *Metabolites*, *9*(4), Article 4. https://doi.org/10.3390/metabo9040064

Santos Ferreira, D. L., Maple, H. J., Goodwin, M., Brand, J. S., Yip, V., Min, J. L., Groom, A., Lawlor, D. A., & Ring, S. (2019b). The Effect of Pre-Analytical Conditions on Blood Metabolomics in Epidemiological Studies. *Metabolites*, *9*(4), 64. https://doi.org/10.3390/metabo9040064

Saoi, M., & Britz-McKibbin, P. (2021). New Advances in Tissue Metabolomics: A Review. *Metabolites*, *11*(10), 672. https://doi.org/10.3390/metabo11100672

Sarkar, A., Ray, D., Shrivastava, A. N., & Sarker, S. (2006). Molecular Biomarkers: Their significance and application in marine pollution monitoring. *Ecotoxicology*, *15*(4), 333–340. https://doi.org/10.1007/s10646-006-0069-1

Sarkis, R. A., Coffey, M. J., Cooper, J. J., Hassan, I., & Lennox, B. (2019). Anti-N-Methyl-D-Aspartate Receptor Encephalitis: A Review of Psychiatric Phenotypes and Management Considerations: A Report of the American Neuropsychiatric Association Committee on Research. *The Journal of Neuropsychiatry and Clinical Neurosciences*, *31*(2), 137–142. https://doi.org/10.1176/appi.neuropsych.18010005

Schmitt, S. E., Pargeon, K., Frechette, E. S., Hirsch, L. J., Dalmau, J., & Friedman, D. (2012). Extreme delta brush. *Neurology*, *79*(11), 1094–1100. https://doi.org/10.1212/WNL.0b013e3182698cd8

Scott, J. G., Gillis, D., Ryan, A. E., Hargovan, H., Gundarpi, N., McKeon, G., Hatherill, S., Newman, M. P., Parry, P., Prain, K., Patterson, S., Wong, R. C. W., Wilson, R. J., & Blum, S. (2018). The prevalence and treatment outcomes of antineuronal antibody-positive patients admitted with first episode of psychosis. *BJPsych Open*, *4*(2), 69–74. https://doi.org/10.1192/bjo.2018.8

Segatto, M., & Pallottini, V. (2020). Facts about Fats: New Insights into the Role of Lipids in Metabolism, Disease and Therapy. *International Journal of Molecular Sciences*, *21*(18), Article 18. https://doi.org/10.3390/ijms21186651

Shillito, P., Molenaar, P. C., Vincent, A., Leys, K., Zheng, W., van den Berg, R. J., Plomp, J. J., Van Kempen, G. Th. H., Chauplannaz, G., Wintzen, A. R., van Dijk, J. G., & Newsom-Davis, J. (1995). Acquired neuromyotonia: Evidence for autoantibodies directed against K+ channels of peripheral nerves. *Annals of Neurology*, *38*(5), 714–722. https://doi.org/10.1002/ana.410380505

Shu, Y., Qin, B., Xu, Y., Sun, X., Chen, Z., Wang, J., Peng, L., Qiu, W., Lu, Z., & Wu, A. (2017). Lipid Metabolism in Patients with Anti-N-Methyl-D-Aspartate Receptor Encephalitis. *Neuroimmunomodulation*, *24*(4–5), 256–263. https://doi.org/10.1159/000485623

Shu, Y., Xu, Y., Chen, C., Li, J., Li, R., Wu, H., Hu, X., Lu, Z., Yu, X., & Qiu, W. (2018). Serum Bilirubin and Albumin in Anti-N-Methyl-D-Aspartate Receptor Encephalitis. *Neuroimmunomodulation*, *25*(4), 206–214. https://doi.org/10.1159/000494801

Silverman, M. G., Ference, B. A., Im, K., Wiviott, S. D., Giugliano, R. P., Grundy, S. M., Braunwald, E., & Sabatine, M. S. (2016). Association Between Lowering LDL-C and

Cardiovascular Risk Reduction Among Different Therapeutic Interventions: A Systematic Review and Meta-analysis. *JAMA*, *316*(12), 1289–1297. https://doi.org/10.1001/jama.2016.13985

Singmann, H., Bolker, B., Westfall, J., Aust, F., & Ben-Shachar, M. S. (2015). afex: Analysis of factorial experiments. *R Package Version 0.13–145*.

Skaper, S. D., Facci, L., Zusso, M., & Giusti, P. (2018). An Inflammation-Centric View of Neurological Disease: Beyond the Neuron. *Frontiers in Cellular Neuroscience*, *12*, 72. https://doi.org/10.3389/fncel.2018.00072

Skene, D. J., Middleton, B., Fraser, C. K., Pennings, J. L. A., Kuchel, T. R., Rudiger, S. R., Bawden, C. S., & Morton, A. J. (2017). Metabolic profiling of presymptomatic Huntington's disease sheep reveals novel biomarkers. *Scientific Reports*, *7*, 43030. https://doi.org/10.1038/srep43030

Smith, K. M., Dubey, D., Liebo, G. B., Flanagan, E. P., & Britton, J. W. (2021). Clinical Course and Features of Seizures Associated With LGI1-Antibody Encephalitis. *Neurology*, *97*(11), e1141–e1149. https://doi.org/10.1212/WNL.0000000000012465

Soininen, P., Kangas, A. J., Würtz, P., Tukiainen, T., Tynkkynen, T., Laatikainen, R., Järvelin, M.-R., Kähönen, M., Lehtimäki, T., Viikari, J., Raitakari, O. T., Savolainen, M. J., & Ala-Korpela, M. (2009). High-throughput serum NMR metabonomics for cost-effective holistic studies on systemic metabolism. *Analyst*, *134*(9), 1781–1785. https://doi.org/10.1039/B910205A

Solleiro-Villavicencio, H., & Rivas-Arancibia, S. (2018). Effect of Chronic Oxidative Stress on Neuroinflammatory Response Mediated by CD4+T Cells in Neurodegenerative Diseases. *Frontiers in Cellular Neuroscience*, *12*, 114. https://doi.org/10.3389/fncel.2018.00114

Sonar, S. A., & Lal, G. (2018). Blood–brain barrier and its function during inflammation and autoimmunity. *Journal of Leukocyte Biology*, *103*(5), 839–853. https://doi.org/10.1002/JLB.1RU1117-428R

Sonderen, A. van, Arends, S., Tavy, D. L. J., Bastiaansen, A. E. M., Bruijn, M. A. A. M. de, Schreurs, M. W. J., Smitt, P. A. E. S., & Titulaer, M. J. (2018). Predictive value of electroencephalography in anti-NMDA receptor encephalitis. *Journal of Neurology, Neurosurgery & Psychiatry*, *89*(10), 1101–1106. https://doi.org/10.1136/jnnp-2018-318376

Sotelo-Orozco, J., Chen, S.-Y., Hertz-Picciotto, I., & Slupsky, C. M. (2021a). A Comparison of Serum and Plasma Blood Collection Tubes for the Integration of Epidemiological and Metabolomics Data. *Frontiers in Molecular Biosciences*, *8*. https://doi.org/10.3389/fmolb.2021.682134

Sotelo-Orozco, J., Chen, S.-Y., Hertz-Picciotto, I., & Slupsky, C. M. (2021b). A Comparison of Serum and Plasma Blood Collection Tubes for the Integration of Epidemiological and Metabolomics Data. *Frontiers in Molecular Biosciences*, *8*. https://www.frontiersin.org/articles/10.3389/fmolb.2021.682134

Spatola, M., Petit-Pedrol, M., Simabukuro, M. M., Armangue, T., Castro, F. J., Barcelo Artigues, M. I., Julià Benique, M. R., Benson, L., Gorman, M., Felipe, A., Caparó Oblitas, R. L., Rosenfeld, M. R., Graus, F., & Dalmau, J. (2017). Investigations in GABAA receptor antibody-associated encephalitis. *Neurology*, *88*(11), 1012–1020. https://doi.org/10.1212/WNL.0000000000003713

Steriade, C., Britton, J., Dale, R. C., Gadoth, A., Irani, S. R., Linnoila, J., McKeon, A., Shao, X.-Q., Venegas, V., & Bien, C. G. (2020a). Acute symptomatic seizures secondary to autoimmune encephalitis and autoimmune-associated epilepsy: Conceptual definitions. *Epilepsia*, *61*(7), 1341–1351. https://doi.org/10.1111/epi.16571

Steriade, C., Britton, J., Dale, R. C., Gadoth, A., Irani, S. R., Linnoila, J., McKeon, A., Shao, X.-Q., Venegas, V., & Bien, C. G. (2020b). Acute symptomatic seizures secondary to autoimmune encephalitis and autoimmune-associated epilepsy: Conceptual definitions. *Epilepsia*, *61*(7),

1341–1351. https://doi.org/10.1111/epi.16571
Steriade, C., Mirsattari, S. M., Murray, B. J., & Wennberg, R. (2016). Subclinical temporal EEG seizure pattern in LGI1-antibody–mediated encephalitis. *Epilepsia*, *57*(8), e155–e160. https://doi.org/10.1111/epi.13436
Sun, B., Ramberger, M., O'Connor, K. C., Bashford-Rogers, R. J. M., & Irani, S. R. (2020). The B cell immunobiology that underlies CNS autoantibody-mediated diseases. *Nature Reviews Neurology*, *16*(9), Article 9. https://doi.org/10.1038/s41582-020-0381-z
Sun, J., & Xia, Y. (2024). Pretreating and normalizing metabolomics data for statistical analysis. *Genes & Diseases*, *11*(3), 100979. https://doi.org/10.1016/j.gendis.2023.04.018
Swayne, A., Tjoa, L., Broadley, S., Dionisio, S., Gillis, D., Jacobson, L., Woodhall, M. R., McNabb, A., Schweitzer, D., Tsang, B., Vincent, A., Irani, S. R., Wong, R., Waters, P., & Blum, S. (2018). Antiglycine receptor antibody related disease: A case series and literature review. *European Journal of Neurology*, *25*(10), 1290–1298. https://doi.org/10.1111/ene.13721
Taylor, J. M. G., Ankerst, D. P., & Andridge, R. R. (2008). Validation of Biomarker-based risk prediction models. *Clinical Cancer Research : An Official Journal of the American Association for Cancer Research*, *14*(19), 5977–5983. https://doi.org/10.1158/1078-0432.CCR-07-4534
Teahan, O., Gamble, S., Holmes, E., Waxman, J., Nicholson, J. K., Bevan, C., & Keun, H. C. (2006). Impact of Analytical Bias in Metabonomic Studies of Human Blood Serum and Plasma. *Analytical Chemistry*, *78*(13), 4307–4318. https://doi.org/10.1021/ac051972y
Teitsma, X. M., Yang, W., Jacobs, J. W. G., Pethö-Schramm, A., Borm, M. E. A., Harms, A. C., Hankemeier, T., van Laar, J. M., Bijlsma, J. W. J., & Lafeber, F. P. J. G. (2018). Baseline metabolic profiles of early rheumatoid arthritis patients achieving sustained drug-free remission after initiating treat-to-target tocilizumab, methotrexate, or the combination: Insights from systems biology. *Arthritis Research & Therapy*, *20*(1), 230. https://doi.org/10.1186/s13075-018-1729-2
Teleanu, R. I., Niculescu, A.-G., Roza, E., Vladâcenco, O., Grumezescu, A. M., & Teleanu, D. M. (2022). Neurotransmitters—Key Factors in Neurological and Neurodegenerative Disorders of the Central Nervous System. *International Journal of Molecular Sciences*, *23*(11), 5954. https://doi.org/10.3390/ijms23115954
Terrault, N. A., Lok, A. S. F., McMahon, B. J., Chang, K.-M., Hwang, J. P., Jonas, M. M., Brown, R. S. J., Bzowej, N. H., & Wong, J. B. (2018). Update on prevention, diagnosis, and treatment of chronic hepatitis B: AASLD 2018 hepatitis B guidance. *Hepatology*, *67*(4), 1560. https://doi.org/10.1002/hep.29800
Tettey, P., Simpson, S., Taylor, B., Blizzard, L., Ponsonby, A.-L., Dwyer, T., Kostner, K., & van der Mei, I. (2014). An adverse lipid profile is associated with disability and progression in disability, in people with MS. *Multiple Sclerosis (Houndmills, Basingstoke, England)*, *20*(13), 1737–1744. https://doi.org/10.1177/1352458514533162
Tettey, P., Simpson, S., Taylor, B., Ponsonby, A.-L., Lucas, R. M., Dwyer, T., Kostner, K., Group, A. investigators, & Mei, I. A. van der. (2017). An adverse lipid profile and increased levels of adiposity significantly predict clinical course after a first demyelinating event. *Journal of Neurology, Neurosurgery & Psychiatry*, *88*(5), 395–401. https://doi.org/10.1136/jnnp-2016-315037
Thévenot, E. A., Roux, A., Xu, Y., Ezan, E., & Junot, C. (2015a). Analysis of the Human Adult Urinary Metabolome Variations with Age, Body Mass Index, and Gender by Implementing a Comprehensive Workflow for Univariate and OPLS Statistical Analyses. *Journal of Proteome Research*, *14*(8), 3322–3335. https://doi.org/10.1021/acs.jproteome.5b00354
Thévenot, E. A., Roux, A., Xu, Y., Ezan, E., & Junot, C. (2015b). Analysis of the Human Adult Urinary Metabolome Variations with Age, Body Mass Index, and Gender by Implementing a

Comprehensive Workflow for Univariate and OPLS Statistical Analyses. *Journal of Proteome Research*, *14*(8), 3322–3335. https://doi.org/10.1021/acs.jproteome.5b00354

Thompson, J., Bi, M., Murchison, A. G., Makuch, M., Bien, C. G., Chu, K., Farooque, P., Gelfand, J. M., Geschwind, M. D., Hirsch, L. J., Somerville, E., Lang, B., Vincent, A., Leite, M. I., Waters, P., Irani, S. R., & Faciobrachial Dystonic Seizures Study Group. (2018). The importance of early immunotherapy in patients with faciobrachial dystonic seizures. *Brain: A Journal of Neurology*, *141*(2), 348–356. https://doi.org/10.1093/brain/awx323

Tilton, W. M., Seaman, C., Carriero, D., & Piomelli, S. (1991). Regulation of glycolysis in the erythrocyte: Role of the lactate/pyruvate and NAD/NADH ratios. *The Journal of Laboratory and Clinical Medicine*, *118*(2), 146–152.

Titulaer, M. J., McCracken, L., Gabilondo, I., Armangué, T., Glaser, C., Iizuka, T., Honig, L. S., Benseler, S. M., Kawachi, I., Martinez-Hernandez, E., Aguilar, E., Gresa-Arribas, N., Ryan-Florance, N., Torrents, A., Saiz, A., Rosenfeld, M. R., Balice-Gordon, R., Graus, F., & Dalmau, J. (2013). Treatment and prognostic factors for long-term outcome in patients with anti-NMDA receptor encephalitis: An observational cohort study. *The Lancet Neurology*, *12*(2), 157–165. https://doi.org/10.1016/S1474-4422(12)70310-1

Trainor, P. J., DeFilippis, A. P., & Rai, S. N. (2017). Evaluation of Classifier Performance for Multiclass Phenotype Discrimination in Untargeted Metabolomics. *Metabolites*, *7*(2), Article 2. https://doi.org/10.3390/metabo7020030

Trevethan, R. (2017). Sensitivity, Specificity, and Predictive Values: Foundations, Pliabilities, and Pitfalls in Research and Practice. *Frontiers in Public Health*, *5*, 307. https://doi.org/10.3389/fpubh.2017.00307

Triba, M. N., Moyec, L. L., Amathieu, R., Goossens, C., Bouchemal, N., Nahon, P., Rutledge, D. N., & Savarin, P. (2014). PLS/OPLS models in metabolomics: The impact of permutation of dataset rows on the K-fold cross-validation quality parameters. *Molecular BioSystems*, *11*(1), 13–19. https://doi.org/10.1039/C4MB00414K

Trygg, J., & Wold, S. (2002). Orthogonal projections to latent structures (O-PLS). *Journal of Chemometrics*, *16*(3), 119–128. https://doi.org/10.1002/cem.695

Tunkel, A. R., Glaser, C. A., Bloch, K. C., Sejvar, J. J., Marra, C. M., Roos, K. L., Hartman, B. J., Kaplan, S. L., Scheld, W. M., & Whitley, R. J. (2008). The Management of Encephalitis: Clinical Practice Guidelines by the Infectious Diseases Society of America. *Clinical Infectious Diseases*, *47*(3), 303–327. https://doi.org/10.1086/589747

Tynkkynen, T., Mursu, J., Nurmi, T., Tuppurainen, K., Laatikainen, R., & Soininen, P. (2012). NMR protocol for determination of oxidation susceptibility of serum lipids and application of the protocol to a chocolate study. *Metabolomics*, *8*(3), 386–398. https://doi.org/10.1007/s11306-011-0323-2

UK Biobank. (2024, May 21). https://www.ukbiobank.ac.uk

Uttara, B., Singh, A. V., Zamboni, P., & Mahajan, R. T. (2009). Oxidative Stress and Neurodegenerative Diseases: A Review of Upstream and Downstream Antioxidant Therapeutic Options. *Current Neuropharmacology*, *7*(1), 65. https://doi.org/10.2174/157015909787602823

Uy, C. E., Binks, S., & Irani, S. R. (2021). Autoimmune encephalitis: Clinical spectrum and management. *Practical Neurology*, *21*(5), 412–423. https://doi.org/10.1136/practneurol-2020-002567

van Coevorden-Hameete, M. H., Titulaer, M. J., Schreurs, M. W. J., de Graaff, E., Sillevis Smitt, P. A. E., & Hoogenraad, C. C. (2016). Detection and Characterization of Autoantibodies to Neuronal Cell-Surface Antigens in the Central Nervous System. *Frontiers in Molecular Neuroscience*, *9*, 37. https://doi.org/10.3389/fnmol.2016.00037

van den Berg, R. A., Hoefsloot, H. C., Westerhuis, J. A., Smilde, A. K., & van der Werf, M. J. (2006). Centering, scaling, and transformations: Improving the biological information content of metabolomics data. *BMC Genomics*, *7*(1), Article 1. https://doi.org/10.1186/1471-2164-7-142

van Sonderen, A., Ariño, H., Petit-Pedrol, M., Leypoldt, F., Körtvélyessy, P., Wandinger, K.-P., Lancaster, E., Wirtz, P. W., Schreurs, M. W. J., Sillevis Smitt, P. A. E., Graus, F., Dalmau, J., & Titulaer, M. J. (2016). The clinical spectrum of Caspr2 antibody–associated disease. *Neurology*, *87*(5), 521–528. https://doi.org/10.1212/WNL.0000000000002917

van Sonderen, A., Schreurs, M. W. J., de Bruijn, M. A. A. M., Boukhrissi, S., Nagtzaam, M. M. P., Hulsenboom, E. S. P., Enting, R. H., Thijs, R. D., Wirtz, P. W., Sillevis Smitt, P. A. E., & Titulaer, M. J. (2016). The relevance of VGKC positivity in the absence of LGI1 and Caspr2 antibodies. *Neurology*, *86*(18), 1692–1699. https://doi.org/10.1212/WNL.0000000000002637

van Sonderen, A., Schreurs, M. W. J., Wirtz, P. W., Sillevis Smitt, P. A. E., & Titulaer, M. J. (2016). From VGKC to LGI1 and Caspr2 encephalitis: The evolution of a disease entity over time. *Autoimmunity Reviews*, *15*(10), 970–974. https://doi.org/10.1016/j.autrev.2016.07.018

Van Steenhoven, R. W., de Vries, J. M., Bruijstens, A. L., Paunovic, M., Nagtzaam, M. M., Franken, S. C., Bastiaansen, A. E., De Bruijn, M. A., Van Sonderen, A., Schreurs, M. W. J., Gardeniers, M., Verdijk, R. M., Balvers, R. K., Sillevis Smitt, P. A., Neuteboom, R. F., & Titulaer, M. J. (2023). Mimics of Autoimmune Encephalitis. *Neurology® Neuroimmunology & Neuroinflammation*, *10*(6), e200148. https://doi.org/10.1212/NXI.0000000000200148

van Veldhuisen, D. J., Ruilope, L. M., Maisel, A. S., & Damman, K. (2016). Biomarkers of renal injury and function: Diagnostic, prognostic and therapeutic implications in heart failure. *European Heart Journal*, *37*(33), 2577–2585. https://doi.org/10.1093/eurheartj/ehv588

Vander Heiden, M. G., Cantley, L. C., & Thompson, C. B. (2009). Understanding the Warburg Effect: The Metabolic Requirements of Cell Proliferation. *Science*, *324*(5930), 1029–1033. https://doi.org/10.1126/science.1160809

Verma, M., Patel, P., & Verma, M. (2011). Biomarkers in Prostate Cancer Epidemiology. *Cancers*, *3*(4), Article 4. https://doi.org/10.3390/cancers3043773

Vignoli, A., Tenori, L., Morsiani, C., Turano, P., Capri, M., & Luchinat, C. (2022). Serum or Plasma (and Which Plasma), That Is the Question. *Journal of Proteome Research*, *21*(4), 1061–1072. https://doi.org/10.1021/acs.jproteome.1c00935

Villanueva, R. A. M., & Chen, Z. J. (2019). ggplot2: Elegant Graphics for Data Analysis (2nd ed.). *Measurement: Interdisciplinary Research and Perspectives*, *17*(3), 160–167. https://doi.org/10.1080/15366367.2019.1565254

Vora, N. M., Holman, R. C., Mehal, J. M., Steiner, C. A., Blanton, J., & Sejvar, J. (2014). Burden of encephalitis-associated hospitalizations in the United States, 1998-2010. *Neurology*, *82*(5), 443–451. https://doi.org/10.1212/WNL.0000000000000086

Vu, T., Siemek, P., Bhinderwala, F., Xu, Y., & Powers, R. (2019). Evaluation of Multivariate Classification Models for Analyzing NMR Metabolomics Data. *Journal of Proteome Research*, *18*(9), 3282–3294. https://doi.org/10.1021/acs.jproteome.9b00227

Wang, F., Debik, J., Andreassen, T., Euceda, L. R., Haukaas, T. H., Cannet, C., Schäfer, H., Bathen, T. F., & Giskeødegård, G. F. (2019). Effect of Repeated Freeze–Thaw Cycles on NMR-Measured Lipoproteins and Metabolites in Biofluids. *Journal of Proteome Research*, *18*(10), 3681–3688. https://doi.org/10.1021/acs.jproteome.9b00343

Wang, H., Zhang, S., Xie, L., Zhong, Z., & Yan, F. (2023). Neuroinflammation and peripheral immunity: Focus on ischemic stroke. *International Immunopharmacology*, *120*, 110332. https://doi.org/10.1016/j.intimp.2023.110332

Want, E. J., O'Maille, G., Smith, C. A., Brandon, T. R., Uritboonthai, W., Qin, C., Trauger, S. A., & Siuzdak, G. (2006). Solvent-Dependent Metabolite Distribution, Clustering, and Protein Extraction for Serum Profiling with Mass Spectrometry. *Analytical Chemistry*, *78*(3), 743–752. https://doi.org/10.1021/ac051312t

Waring, W. S., Evans, L. E., & Kirkpatrick, C. T. (2007). Glycolysis inhibitors negatively bias blood glucose measurements: Potential impact on the reported prevalence of diabetes mellitus. *Journal of Clinical Pathology*, *60*(7), 820–823. https://doi.org/10.1136/jcp.2006.039925

Webb, B. A., Forouhar, F., Szu, F.-E., Seetharaman, J., Tong, L., & Barber, D. L. (2015). Structures of human phosphofructokinase-1 and atomic basis of cancer-associated mutations. *Nature*, *523*(7558), 111–114. https://doi.org/10.1038/nature14405

Wennberg, R., Steriade, C., Chen, R., & Andrade, D. (2018). Frontal infraslow activity marks the motor spasms of anti-LGI1 encephalitis. *Clinical Neurophysiology*, *129*(1), 59–68. https://doi.org/10.1016/j.clinph.2017.10.014

Wesselingh, R., Griffith, S., Broadley, J., Tarlinton, D., Buzzard, K., Seneviratne, U., Butzkueven, H., O'Brien, T. J., & Monif, M. (2023). Peripheral monocytes and soluble biomarkers in autoimmune encephalitis. *Journal of Autoimmunity*, *135*, 103000. https://doi.org/10.1016/j.jaut.2023.103000

Westerhuis, J. A., Hoefsloot, H. C. J., Smit, S., Vis, D. J., Smilde, A. K., van Velzen, E. J. J., van Duijnhoven, J. P. M., & van Dorsten, F. A. (2008). Assessment of PLSDA cross validation. *Metabolomics*, *4*(1), 81–89. https://doi.org/10.1007/s11306-007-0099-6

Wilkins, J. M., & Trushina, E. (2018). Application of Metabolomics in Alzheimer's Disease. *Frontiers in Neurology*, *8*, 719. https://doi.org/10.3389/fneur.2017.00719

Wishart, D. S. (2019). NMR metabolomics: A look ahead. *Journal of Magnetic Resonance*, *306*, 155–161. https://doi.org/10.1016/j.jmr.2019.07.013

Wishart, D. S., Guo, A., Oler, E., Wang, F., Anjum, A., Peters, H., Dizon, R., Sayeeda, Z., Tian, S., Lee, B. L., Berjanskii, M., Mah, R., Yamamoto, M., Jovel, J., Torres-Calzada, C., Hiebert-Giesbrecht, M., Lui, V. W., Varshavi, D., Varshavi, D., … Gautam, V. (2021). HMDB 5.0: The Human Metabolome Database for 2022. *Nucleic Acids Research*, *50*(D1), D622–D631. https://doi.org/10.1093/nar/gkab1062

Wishart, D. S., Rout, M., Lee, B. L., Berjanskii, M., LeVatte, M., & Lipfert, M. (2023). Practical Aspects of NMR-Based Metabolomics. In V. Ghini, K. A. Stringer, & C. Luchinat (Eds.), *Metabolomics and Its Impact on Health and Diseases* (pp. 1–41). Springer International Publishing. https://doi.org/10.1007/164_2022_613

Wishart, D. S., Tzur, D., Knox, C., Eisner, R., Guo, A. C., Young, N., Cheng, D., Jewell, K., Arndt, D., Sawhney, S., Fung, C., Nikolai, L., Lewis, M., Coutouly, M.-A., Forsythe, I., Tang, P., Shrivastava, S., Jeroncic, K., Stothard, P., … Querengesser, L. (2007). HMDB: The Human Metabolome Database. *Nucleic Acids Research*, *35*(Database issue), D521-526. https://doi.org/10.1093/nar/gkl923

Wold, S., Esbensen, K., & Geladi, P. (1987). Principal component analysis. *Chemometrics and Intelligent Laboratory Systems*, *2*(1), 37–52. https://doi.org/10.1016/0169-7439(87)80084-9

Wold, S., Sjöström, M., & Eriksson, L. (2001). PLS-regression: A basic tool of chemometrics. *Chemometrics and Intelligent Laboratory Systems*, *58*(2), 109–130. https://doi.org/10.1016/S0169-7439(01)00155-1

Woodhall, M., Mgbachi, V., Fox, H., Irani, S., & Waters, P. (2022). Utility of Live Cell-Based Assays for Autoimmune Neurology Diagnostics. *The Journal of Applied Laboratory Medicine*, *7*(1), 391–393. https://doi.org/10.1093/jalm/jfab133

World Health Organization. (2019). *Epilepsy: A public health imperative*. World Health

Organization. https://apps.who.int/iris/handle/10665/325293
Worley, B., & Powers, R. (2013). Multivariate Analysis in Metabolomics. *Current Metabolomics*, *1*(1), 92–107. https://doi.org/10.2174/2213235X11301010092
Wu, G. (2009). Amino acids: Metabolism, functions, and nutrition. *Amino Acids*, *37*(1), 1–17. https://doi.org/10.1007/s00726-009-0269-0
Wu, K., Wen, L., Duan, R., Li, Y., Yao, Y., Jing, L., Jia, Y., Teng, J., & He, Q. (2019). Triglyceride Level Is an Independent Risk Factor in First-Attacked Neuromyelitis Optica Spectrum Disorders Patients. *Frontiers in Neurology*, *10*. Scopus. https://doi.org/10.3389/fneur.2019.01230
Wu, L., Cai, F., Zhuo, Z., Wu, D., Zhang, T., Yang, H., Fang, H., & Xiao, Z. (2023). CASPR2 antibody associated neurological syndromes in children. *Scientific Reports*, *13*(1), 2073. https://doi.org/10.1038/s41598-023-28268-x
Xiao, J. F., Zhou, B., & Ressom, H. W. (2012). Metabolite identification and quantitation in LC-MS/MS-based metabolomics. *Trends in Analytical Chemistry : TRAC*, *32*, 1–14. https://doi.org/10.1016/j.trac.2011.08.009
Xu, T.-L., & Gong, N. (2010). Glycine and glycine receptor signaling in hippocampal neurons: Diversity, function and regulation. *Progress in Neurobiology*, *91*(4), 349–361. https://doi.org/10.1016/j.pneurobio.2010.04.008
Yan, J., Kuzhiumparambil, U., Bandodkar, S., Dale, R. C., & Fu, S. (2021). Cerebrospinal fluid metabolomics: Detection of neuroinflammation in human central nervous system disease. *Clinical & Translational Immunology*, *10*(8), e1318. https://doi.org/10.1002/cti2.1318
YAN, K., GAO, L.-N., CUI, Y.-L., ZHANG, Y., & ZHOU, X. (2016). The cyclic AMP signaling pathway: Exploring targets for successful drug discovery (Review). *Molecular Medicine Reports*, *13*(5), 3715–3723. https://doi.org/10.3892/mmr.2016.5005
Yang, J., Zhang, W., Albert, P. S., Liu, A., & Chen, Z. (2024). Combining Biomarkers to Improve Diagnostic Accuracy in Detecting Diseases With Group-Tested Data. *Statistics in Medicine*, *43*(27), 5182–5192. https://doi.org/10.1002/sim.10230
Yang, Q., Wang, G., & Zhang, F. (2020). Role of Peripheral Immune Cells-Mediated Inflammation on the Process of Neurodegenerative Diseases. *Frontiers in Immunology*, *11*, 582825. https://doi.org/10.3389/fimmu.2020.582825
Yeo, T., Probert, F., Jurynczyk, M., Sealey, M., Cavey, A., Claridge, T. D. W., Woodhall, M., Waters, P., Leite, M. I., Anthony, D. C., & Palace, J. (2019). Classifying the antibody-negative NMO syndromes. *Neurology® Neuroimmunology & Neuroinflammation*, *6*(6), e626. https://doi.org/10.1212/NXI.0000000000000626
Yeo, T., Probert, F., Sealey, M., Saldana, L., Geraldes, R., Höeckner, S., Schiffer, E., Claridge, T. D. W., Leppert, D., DeLuca, G., Kuhle, J., Palace, J., & Anthony, D. C. (2021). Objective biomarkers for clinical relapse in multiple sclerosis: A metabolomics approach. *Brain Communications*, *3*(4), fcab240. https://doi.org/10.1093/braincomms/fcab240
Yin, C., Harms, A. C., Hankemeier, T., Kindt, A., & de Lange, E. C. M. (2023). Status of Metabolomic Measurement for Insights in Alzheimer's Disease Progression—What Is Missing? *International Journal of Molecular Sciences*, *24*(5), 4960. https://doi.org/10.3390/ijms24054960
Yin, P., Peter, A., Franken, H., Zhao, X., Neukamm, S. S., Rosenbaum, L., Lucio, M., Zell, A., Häring, H.-U., Xu, G., & Lehmann, R. (2013). Preanalytical aspects and sample quality assessment in metabolomics studies of human blood. *Clinical Chemistry*, *59*(5), 833–845. https://doi.org/10.1373/clinchem.2012.199257
Yin, X., Chen, K., Cheng, H., Chen, X., Feng, S., Song, Y., & Liang, L. (2022). Chemical Stability of Ascorbic Acid Integrated into Commercial Products: A Review on Bioactivity and Delivery

Technology. *Antioxidants*, *11*(1), 153. https://doi.org/10.3390/antiox11010153
Yu, Z., Kastenmüller, G., He, Y., Belcredi, P., Möller, G., Prehn, C., Mendes, J., Wahl, S., Roemisch-Margl, W., Ceglarek, U., Polonikov, A., Dahmen, N., Prokisch, H., Xie, L., Li, Y., Wichmann, H.-E., Peters, A., Kronenberg, F., Suhre, K., … Wang-Sattler, R. (2011). Differences between Human Plasma and Serum Metabolite Profiles. *PLoS ONE*, *6*(7), e21230. https://doi.org/10.1371/journal.pone.0021230
Yu, Z., Zhai, G., Singmann, P., He, Y., Xu, T., Prehn, C., Römisch-Margl, W., Lattka, E., Gieger, C., Soranzo, N., Heinrich, J., Standl, M., Thiering, E., Mittelstraß, K., Wichmann, H.-E., Peters, A., Suhre, K., Li, Y., Adamski, J., … Wang-Sattler, R. (2012). Human serum metabolic profiles are age dependent. *Aging Cell*, *11*(6), 960–967. https://doi.org/10.1111/j.1474-9726.2012.00865.x
Yuan, Y., Du, J., Luo, J., Zhu, Y., Huang, Q., & Zhang, M. (2024). Discrimination of missing data types in metabolomics data based on particle swarm optimization algorithm and XGBoost model. *Scientific Reports*, *14*(1), 152. https://doi.org/10.1038/s41598-023-50646-8
Yue, J. K., Yuh, E. L., Korley, F. K., Winkler, E. A., Sun, X., Puffer, R. C., Deng, H., Choy, W., Chandra, A., Taylor, S. R., Ferguson, A. R., Huie, J. R., Rabinowitz, M., Puccio, A. M., Mukherjee, P., Vassar, M. J., Wang, K. K. W., Diaz-Arrastia, R., Okonkwo, D. O., … TRACK-TBI Investigators. (2019). Association between plasma GFAP concentrations and MRI abnormalities in patients with CT-negative traumatic brain injury in the TRACK-TBI cohort: A prospective multicentre study. *The Lancet. Neurology*, *18*(10), 953–961. https://doi.org/10.1016/S1474-4422(19)30282-0
Zacharias, H. U., Altenbuchinger, M., & Gronwald, W. (2018). Statistical Analysis of NMR Metabolic Fingerprints: Established Methods and Recent Advances. *Metabolites*, *8*(3), Article 3. https://doi.org/10.3390/metabo8030047
Zandi, M. S., Deakin, J. B., Morris, K., Buckley, C., Jacobson, L., Scoriels, L., Cox, A. L., Coles, A. J., Jones, P. B., Vincent, A., & Lennox, B. R. (2014). Immunotherapy for patients with acute psychosis and serum N-Methyl D-Aspartate receptor (NMDAR) antibodies: A description of a treated case series. *Schizophrenia Research*, *160*(1–3), 193–195. https://doi.org/10.1016/j.schres.2014.11.001
Zemans, R. L., Jacobson, S., Keene, J., Kechris, K., Miller, B. E., Tal-Singer, R., & Bowler, R. P. (2017). Multiple biomarkers predict disease severity, progression and mortality in COPD. *Respiratory Research*, *18*(1), 117. https://doi.org/10.1186/s12931-017-0597-7
Zhang, A., Sun, H., Qiu, S., & Wang, X. (2013). NMR-based metabolomics coupled with pattern recognition methods in biomarker discovery and disease diagnosis. *Magnetic Resonance in Chemistry*, *51*(9), 549–556. https://doi.org/10.1002/mrc.3985
Zhang, F., Gao, X., Liu, J., & Zhang, C. (2023). Biomarkers in autoimmune diseases of the central nervous system. *Frontiers in Immunology*, *14*, 1111719. https://doi.org/10.3389/fimmu.2023.1111719
Zhang, J. D., Xue, C., Kolachalama, V. B., & Donald, W. A. (2023). Interpretable Machine Learning on Metabolomics Data Reveals Biomarkers for Parkinson's Disease. *ACS Central Science*, *9*(5), 1035–1045. https://doi.org/10.1021/acscentsci.2c01468
Zheng, L., Hu, F., Huang, L., Lu, J., Yang, X., Xu, J., Wang, S., Shen, Y., Zhong, R., Chu, T., Zhang, W., Li, Y., Zheng, X., Han, B., Zhong, H., Nie, W., & Zhang, X. (2024). Association of metabolomics with PD-1 inhibitor plus chemotherapy outcomes in patients with advanced non-small-cell lung cancer. *Journal for ImmunoTherapy of Cancer*, *12*(4), e008190. https://doi.org/10.1136/jitc-2023-008190

Appendices

The appendices contain the published versions of my four first-author papers relevant to the thesis.

ARTICLE OPEN

Check for updates

The serum metabolomic profile of a distinct, inflammatory subtype of acute psychosis

Belinda Lennox[1,9✉], Wenzheng Xiong[2,3,9], Patrick Waters[4], Alasdair Coles[5], Peter B. Jones[6], Tianrong Yeo[2,7,8], Jeanne Tan May May[7,8], Ksenija Yeeles[1], Daniel Anthony[2] and Fay Probert[3]

A range of studies suggest that a proportion of psychosis may have an autoimmune basis, but this has not translated through into clinical practice—there is no biochemical test able to accurately identify psychosis resulting from an underlying inflammatory cause. Such a test would be an important step towards identifying who might require different treatments and have the potential to improve outcomes for patients. To identify novel subgroups within patients with acute psychosis we measured the serum nuclear magnetic resonance (NMR) metabolite profiles of 75 patients who had identified antibodies (anti-glycine receptor [GlyR], voltage-gated potassium channel [VGKC], Contactin-associated protein-like 2 [CASPR2], leucine-rich glioma inactivated 1 [LGI1], N-methyl-D-aspartate receptor [NMDAR] antibody) and 70 antibody negative patients matched for age, gender, and ethnicity. Clinical symptoms were assessed using the positive and negative syndrome scale (PANSS). Unsupervised principal component analysis identified two distinct biochemical signatures within the cohort. Orthogonal partial least squared discriminatory analysis revealed that the serum metabolomes of NMDAR, LGI1, and CASPR2 antibody psychosis patients were indistinct from the antibody negative control group while VGKC and GlyR antibody patients had significantly decreased lipoprotein fatty acids and increased amino acid concentrations. Furthermore, these patients had more severe presentation with higher PANSS scores than either the antibody negative controls or the NMDAR, LGI1, and CASPR2 antibody groups. These results suggest that a proportion of patients with acute psychosis have a distinct clinical and biochemical phenotype that may indicate an inflammatory subtype.

Molecular Psychiatry (2022) 27:4722–4730; https://doi.org/10.1038/s41380-022-01784-4

INTRODUCTION

There are many lines of evidence to indicate that a proportion of psychosis is linked to increased inflammation and may have an autoimmune basis. Much of this evidence is indirect, such as the association between schizophrenia and genes important for the adaptive immune system [1, 2], and the higher rate of other autoimmune disorders in those with schizophrenia than other people [3, 4]. A more direct clue has come from the identification of antibodies against neuronal cell surface targets in some patients with psychosis [5]. These antibodies, when found in patients with other clinical presentations, in particular autoimmune encephalitis, are considered causative, and removal of the antibodies treats the associated clinical presentation [6–8].

Nuclear magnetic resonance (NMR) metabolomics analysis of biofluid samples is a rapidly growing field which has been shown to identify systemic inflammation and antibody-mediated pathology in a range of diseases [9–11]. Recent studies suggest that the serum metabolome may provide a more sensitive measure of low-grade inflammation than current, clinically used, measures [12, 13]. In addition, the application of unsupervised cluster analysis to metabolomics data can reveal novel metabolic phenotypes within patient cohorts [9, 14], inspection of the small molecules responsible for this clustering can then reveal distinct biochemical pathway changes in these groups. Here we apply NMR serum metabolomics analysis coupled with unsupervised pattern recognition methods to identify novel subgroups within a cohort of psychosis patients and relate the identified metabolic phenotypes to measures of disease severity at presentation, using the positive and negative syndrome scale (PANSS), and the presence of a range of neuronal cell surface antibodies in the serum of these patients.

We have been screening patients with psychosis for neuronal cell surface antibodies for the past nine years. Over this time the range of antibodies that has been recognised has expanded, and the evidence around the pathogenicity of some of these antibodies has grown. For instance, pre-clinical studies support the pathogenicity of the N-methyl-D-aspartate receptor (NMDAR) antibody in patients with autoimmune encephalitis [15], and the nature of the clinical syndrome is well characterised [6, 16]. The clinical relevance of these antibodies in those with psychosis is less certain, even though there are clear overlaps in terms of symptoms seen [17]. Studies that have directly examined NMDAR

[1]Department of Psychiatry, University of Oxford and Oxford Health NHS Foundation Trust, Oxford, UK. [2]Department of Pharmacology, University of Oxford, Oxford, UK. [3]Department of Chemistry, University of Oxford, Oxford, UK. [4]Nuffield Department of Clinical Neurosciences, University of Oxford, Oxford, UK. [5]Department of Clinical Neurosciences, University of Cambridge, Cambridge, UK. [6]Department of Psychiatry, University of Cambridge, Cambridge, UK. [7]Department of Neurology, National Neuroscience Institute, Singapore, Singapore. [8]Duke-NUS Medical School, Singapore, Singapore. [9]These authors jointly supervised this work: Belinda Lennox, Wenzheng Xiong.
✉email: belinda.lennox@psych.ox.ac.uk

Received: 18 January 2022 Revised: 1 September 2022 Accepted: 5 September 2022
Published online: 21 September 2022

antibodies from patients with psychosis also demonstrate their functional effects on synaptic function [18], and small case series of patients with psychosis and NMDAR antibodies demonstrate a comparable treatment response to immunotherapy [19, 20]. By contrast, the evidence around the pathogenicity of antibodies targeting Voltage-Gated Potassium Channel (VGKC) is controversial across all clinical presentations. This was the first neuronal cell surface antibody to be described in association with encephalitis in 2001 [21]. However, more recent studies have specified the particular targets as being components of the VGKC – Leucine-rich glioma-inactivated 1 (LGI1) and Contactin Associated Protein-like 2 (CASPR2) [22], such that the value of testing for generic VGKC antibodies, using radioimmunoassay is now questioned in encephalitis [23], and the clinical recommendation is to only test for LGI1 and CASPR2 [24]. However, the utility of VGKC antibody testing in neurological diseases other than encephalitis remains to be seen. Indeed, other studies indicate that VGKC antibody assays do still have value, indicating an immunotherapy responsive illness in children for instance [25]. There are further antibodies where clinical relevance in CNS disorders is more unclear, such as Glycine receptor (GlyR) antibodies, more associated with progressive encephalomyelitis with rigidity and myoclonus [26], and others that are so rare that there is little to guide clinical practice (GABA-A antibodies) [27].

In order to explore further understand the distinct metabolic phenotypes identified in this psychosis cohort and investigate the possible relevance of these antibodies that we have identified in patients with psychosis, we included a cohort of antibody-positive patients, age and gender matched to patients negative for all antibodies tested, in our cohort. We had the hypothesis that those with defined neuronal cell surface antibodies would have a different metabolomic profile than those without. Furthermore, we explored whether those patients with an inflammatory metabolomic profile had a distinguishing clinical profile, to enable clinicians to detect patients who may need treating in a different way.

MATERIALS/SUBJECTS AND METHODS

Study participants

Serum samples were collected from 1574 patients with acute psychosis across England as part of the Medical Research Council (MRC) Prevalence of Pathogenic Antibodies in Psychosis study (PPiP1 (2013–2014) and PPiP2 2015–2018). The inclusion criteria for the study were ages 16–35, first episode of psychotic illness, antipsychotic medication less than 6 weeks, and at least one moderate or more severe symptom of psychosis. These criteria were then broadened in 2016 to widen the age range 16–70 and extend the length of illness to 24 months and included those at relapse as well as first episode.

Following informed consent, a serum sample was collected, alongside demographic details and a clinician rating of severity of selected positive and negative syndrome scale (PANSS) items at the same time point (P1 Delusions, P2 Conceptual disorganisation, P3 Hallucinatory behaviour, N1 Blunted Affect, N4 Passive/apathetic social withdrawal, N6 Lack of spontaneity and flow of conversation, G5 Mannerisms and posturing and G9 Unusual thought content) [28]. The items mentioned above were rated on a 7-point scale: 1 = absent, 2 = minimal, 3 = mild, 4 = moderate, 5 = moderate severe, 6 = severe, and 7 = extreme [28]. Clinicians were asked to only rate the symptoms that were moderate or more severe (≥4). Absent-mild symptoms did not have ratings by clinicians, and their item score was considered as 1 during statistical analyses. Total and subscales' scores were calculated with the eight items mentioned above.

For the participants in PPiP1 a full PANSS rating was obtained. This therefore includes ratings of specific delusions of suspiciousness or grandiosity (P6 and P7) that were not included in the brief PANSS ratings. We therefore allocated a single P1 rating for these participants taking the highest scoring item from P1, P6 and P7 as the rating for P1 for these participants.

A total of 145 patients with sufficient serum sample volume for both antibody testing and metabolomics analysis were included in this study; 75 patients who were antibody positive along with 70 antibody negative controls matched for age, gender, and ethnicity, and illness course. Two patients were positive for more than one Ab and so were excluded from model training.

Standard protocol approvals, registrations, and patient consents

Written informed consent was obtained from all patients according to the Declaration of Helsinki. Ethical approval was obtained by the local research ethics committee (12/EE/0307 PID 97740).

Serum collection

Serum was collected in a serum separator tube, supplied by the study team, and posted to Oxford. Samples were allowed to clot at room temperature before being centrifuged at 1300 x *g* for 10 min at room temperature. The serum supernatant was immediately stored at −80 °C.

Antibody testing

Antibody testing for NMDAR, GlyR, GABAA, LGI1, CASPR2 IgG antibodies was undertaken in Nuffield Department Clinical Neuroscience, according to published methods [6, 22, 29]. Voltage Gated Potassium Channel (VGKC) Antibodies were measured by radioimmunoassay in a National Health Service (NHS) Clinical laboratory (Oxford University Hospitals NHS Trust). A threshold of 100 pM was taken as the cut-off for a positive result. All samples collected were tested for all antibodies.

Nuclear magnetic resonance (NMR) sample preparation for metabolomics analysis

Serum samples were thawed at room temperature and centrifuged at 100,000 × *g* for 30 min at 4 °C. 150 µL of supernatant was then diluted with 450 µL of 75 mM sodium phosphate buffer prepared in D_2O (pH 7.4). Samples were briefly centrifuged at 3000 × *g* for 5 min before transferring to a 5-mm NMR tube.

All NMR spectra were acquired at 310 K using a 700-MHz Bruker AVIII spectrometer operating at 16.4 T equipped with a ^{1}H [$^{13}C/^{15}N$] TCI cryoprobe (Department of Chemistry, University of Oxford). The Carr-Purcell-Meiboom-Gill (CPMG) pulse sequence was used to suppress large protein resonance. Quality control samples were randomly spread throughout the acquisition to ensure reproducibility. All spectra were preprocessed in Topspin 2.1 (Bruker, Germany); multiplied by a 1D exponential corresponding to a 0.3 Hz line broadening, and zero filled by a factor of 2. All spectra were baseline corrected with a fifth-degree polynomial and referenced to the lactate doublet at 1.33 ppm. Processed spectra were exported to ACD/Labs Spectrus Processor Academic Edition 12.01 (Advanced Chemistry Development, Inc., Toronto, Canada), whereby regions of the spectra between 0.80–8.47, excluding the water resonance (4.13-5.22 ppm), were split into 0.02-ppm-wide bins which were integrated and exported as a.csv file for statistical analysis. Metabolite assignment was performed by referencing to literature values, the Human Metabolome Database [30], and via 2D total correlation spectroscopy (TOCSY) experiments. NMR-detectable serum/plasma metabolites have been previously reported [31–33]. While all metabolite resonances were included in our analysis, most abundant metabolites detectable in serum NMR spectra included 3-hydroxybutyrate, acetoacetate, alanine, arginine, citrate, creatine, creatinine, formate, glucose, glutamate, glutamine, histidine, lactate, lipoproteins (high-density lipoproteins [HDL], low-density lipoproteins [LDL], very low-density lipoproteins [VLDL], and chylomicron), lysine, myo-inositol, N-acetyl

glycoproteins (GlycA, GlycB), phenylalanine, proline, scyllo-inositol, threonine, tyrosine, urea, and valine.

Statistical analysis

Analysis was performed in R software 3.4.3 (R foundation for statistical computing, Vienna, Austria) and GraphPad Prism 9.0.0. Mann-Whitney U test was used for non-normal continuous variables in two-group comparisons. Ordinary one-way ANOVA (with post hoc Tukey's multiple comparisons test) was used for continuous variables in comparisons of more than two groups. When unequal variance present among groups, Brown-Forsythe and Welch ANOVA tests (with Dunnett's T3 multiple comparisons test) were used instead. For variables with non-normal distribution or limited group sample size, Kruskal-Wallis test with Dunn's multiple comparisons test was used in comparisons of more than two groups. Fisher's exact tests were used for categorical variables as appropriate, while a Bonferroni correction was applied throughout to account for multiple comparisons. Two-tailed p-values ≤ 0.05 were considered statistically significant.

A power calculation (PPCA model using the R package MetSizeR) [34–36] confirmed that a sample size of 12 per group (total 24) is sufficient to achieve an FDR cut-off of 0.05 assuming that 20% of the spectral bins measured significantly differ between groups. Thus, the 19 samples collected within the smallest group (VGKC/GlyR) are sufficient to identify metabolite changes while also allowing a 'test' set to be removed.

Multivariate analysis of metabolomics data was carried out using principal component analysis (PCA), an unsupervised analysis showing spontaneous separation of groups, and orthogonal partial least squares discriminant analysis (OPLS-DA), a supervised method to identify significant metabolite changes between groups. All multivariate analysis was using in-house R scripts and the ropls package [37]. OPLS-DA models were validated on independent test data (10%) using an external 10-fold cross-validation strategy with repetition coupled with permutation testing as previously described [12]. A detailed explanation of the cross-validation strategy is included in the supplementary material (Supplementary Fig. 1). All model performance metrics (accuracy, sensitivity, and specificity) are considered significant if they are greater than the corresponding metrics from the random null distribution, determined by the Kolmogorov–Smirnov. Discriminatory variables were identified by calculating the average of the variable importance in projection (VIP) scores of the ensemble of models, which indicated the contribution of a variable to the model. An inflection point was picked manually in the curve of VIP scores and was used as a cut-off for picking discriminatory metabolites in multivariate. Fold changes of discriminatory variables were then calculated and one-way ANOVA with Tukey's post-hoc corrections were conducted to determine group differences. Two-tailed p-values ≤ 0.05 were considered statistically significant in univariate.

RESULTS AND DISCUSSION

Patient demographics and antibody status

The most prevalent serum antibodies detected in those with antibodies were NMDAR antibodies (47%, $n = 35$), followed by VGKC antibodies (19%, $n = 13$). Two double-positive patients were identified, one positive for both CASPR2 and VGKC antibodies and another positive for both CASPR2 and NMDAR antibodies and so these were excluded from model training. The groups were well matched for age, gender, ethnicity, episode type, and illness duration. The VGKC antibody-positive group had higher PANSS total compared to the Control group ($n = 70$, $p < 0.01$, Kruskal-Wallis test), LGI1 antibody positive group ($n = 9$, $p < 0.05$, Kruskal-Wallis test) and NMDAR antibody positive group ($n = 35$, $p < 0.05$, Kruskal-Wallis test) (Table 1).

Two distinct serum biochemical signatures were detected by unsupervised analysis, which correspond to VGKC antibody and GlyR antibody positivity

In an effort to identify novel psychosis subtypes within this cohort, we performed an untargeted analysis of a large panel of serum biochemicals (~100 NMR-detectable small molecules) associated with inflammation, the acute phase response, energy metabolism, amino acid degradation, and fatty acid oxidation. Unsupervised PCA (blinded to antibody status and all other demographic data) of the NMR metabolome alone, spontaneously separated the cohort in to two distinct groups of $n = 18$ and $n = 125$ (Fig. 1a). This suggests, that 18 of the patients in the cohort have distinct serum biochemical signatures when compared to all other samples. When demographic data was superimposed on to the unsupervised scores plot no association between this biochemically distinct group and age, gender, ethnicity, episode type, or disease duration was observed (Supplementary Fig. 2). However, a clear association with antibody status was observed (Fig. 1b). All antibody negative, NMDAR, LGI1 and CASPR2 antibody patients were found to fall with the predominant biochemical signature group while all but two VGKC antibody positive patients (85%, $n = 11$) and all GlyR antibody positive patients (100%, $n = 7$) fell within the 'distinct biochemical signature' group.

This suggests that the serum biochemical signature of NMDAR, LGI1, and CASPR2 antibody psychosis patients is indistinguishable from antibody negative psychosis patients. In contrast, VGKC and GlyR antibody psychosis patients have a shared biochemical signature which is distinct.

Significant metabolic imbalances including decreases in serum lipoproteins along with increased amino acid concentrations were observed in VGKC and GlyR antibody positive psychosis patients

To further understand the biochemical perturbations associated with sub-groups identified above, the cohort was split in to three groups 1. A VGKC and GlyR antibody combined group (VGKC/GlyR, $n = 20$), 2. a group consisting of patients with NMDAR, LGI1, or CASPR2 antibodies (NMDAR/LGI1/CASPR2, $n = 53$), and 3. a control group of patients negative for all antibodies tested (Control, $n = 70$). Supervised OPLS-DA analyses was performed to build predictive models and tested on independent data (data that was not used to train the model).

No separation was observed between the control and NMDAR/LGI1/CASPR2 antibody groups in the OPLS-DA scores plot (Fig. 2a) and the performance of the model, on independent test data, was not significantly better than that expected by random chance (Fig. 2b, p value > 0.05, Kolmogorov-Smirnov test) confirming there are no detectable differences in biochemical signature between these groups in this cohort. In contrast, OPLS-DA was able to predict which patients, in the test data, belonged to the VGKC/GlyR group with 94.78 ± 0.80% accuracy, 99.76 ± 1.21% sensitivity, and 92.75 ± 2.21% specificity (p values all <0.001, Kolmogorov-Smirnov) relative to controls (Fig. 2c, d) and 94.75 ± 0.75% accuracy, 99.60 ± 1.39% sensitivity, and 93.11 ± 2.12% specificity (p values all <0.001, Kolmogorov-Smirnov) relative to NMDAR/LGI1/CASPR2 positive patients (Fig. 2e, f).

The metabolites perturbed in the VGKC and GlyR antibody psychosis patients were identified by inspection of the variable importance of projection (VIP) scores of the significant OPLS-DA models described above. Significant decreases were observed in several fatty acid resonances within serum lipoproteins ($-CH_3$, $(-CH_2-)_n$, $-N(CH_3)_3$, unsaturated fatty acid, $=CH-CH_2-CH_2-$) while several amino acids (leucine, isoleucine, lysine, and valine) were increased in the VGKC and GlyR antibody patients (Fig. 3 and Supplementary Table 1, p values all <0.001, one-way ANOVA with Tukey's post hoc test).

Table 1. Patient information, grouped by different neuronal cell surface antibodies ($n = 143$).

	Ab negative (Ctrl)	Ab positive	GlyR-Ab	VGKC-Ab	CASPR2-Ab	LGI1-Ab	NMDAR-Ab
Number of patients	70	73	7	13	9	9	35
Age (years), median (IQR)	27 (15)	25 (13)	24 (10)	23 (8)	24 (11.5)	25 (15)	32 (18)
Gender, Female, no. (%)	31 (44.3)	30 (41.1)	4 (57.1)	5 (38.5)	3 (33.3)	1 (11.1)	17 (48.6)
Ethnicity (%)							
White	71.4	67.1	100	61.5	55.6	77.8	62.9
Asian	12.9	12.3	0	0	22.2	11.1	17.1
Black (African/ Caribbean)	7.1	9.5	0	23.1	11.1	11.1	5.7
Mixed	4.3	6.8	0	7.7	11.1	0	8.6
Other	4.3	0	0	0	0	0	0
Unknown	0	4.1	0	7.7	0	0	5.7
Disease duration (duration from the episode date to the consent date, days), median (IQR)	86 (258.8)	103 (244.5)	267 (399)	37 (23)	230 (317)	132 (404)	113 (229)
Unknown, no.	0	4	2	1	0	1	0
Episode type, no. (%)							
First episode	45 (64.3)	50 (68.5)	7 (100)	13 (100) (adjusted p value = 0.51)	6 (66.7)	7 (77.8)	17 (48.57)
Relapse	24 (34.3)	22 (30.1)	0 (0)	0 (0)	3 (33.3)	1 (11.1)	18 (51.4)
Unknown	1 (1.4)	1 (1.4)	0 (0)	0 (0)	0 (0)	1 (11.1)	0 (0)
PANSS							
Total score, median (IQR)	12 (6)	14 (8.8)	19 (6)	23 (12.5)**	11 (8.5)	12 (4.5)	13 (7)
Unknown, no.	0	0	1	0	0	0	0

The Kruskal-Wallis test with Dunn's multiple comparisons test was used to identify significant differences of each class compared to Control for numerical variables (age, PANSS scores) while Fisher's exact test was used for categorical variables. Ethnicity data was analysed by comparing White vs Combined Asian/ Black/Mixed/Other ethnic groups in Ctrl, combined VGKC/GlyR Group, combine NMDAR/LGI1/CASPR2 Group, as applicable to Chi-square test/Fisher's exact test. **$p < 0.01$.

Ctrl control, psychosis patients tested negative for the following neuronal cell surface antibodies. *Ab* antibody, psychosis patients tested positive for one of the following neuronal cell surface antibodies. *GlyR* glycine receptor. *VGKC* voltage-gated potassium channel complex. *CASPR2* contactin associated protein-like 2. *LGI1* leucine-rich glioma inactivated 1. *NMDAR* N-methyl-D-aspartate receptor. *PANSS* Positive and Negative Syndrome Scale. *IQR* Interquartile Range.

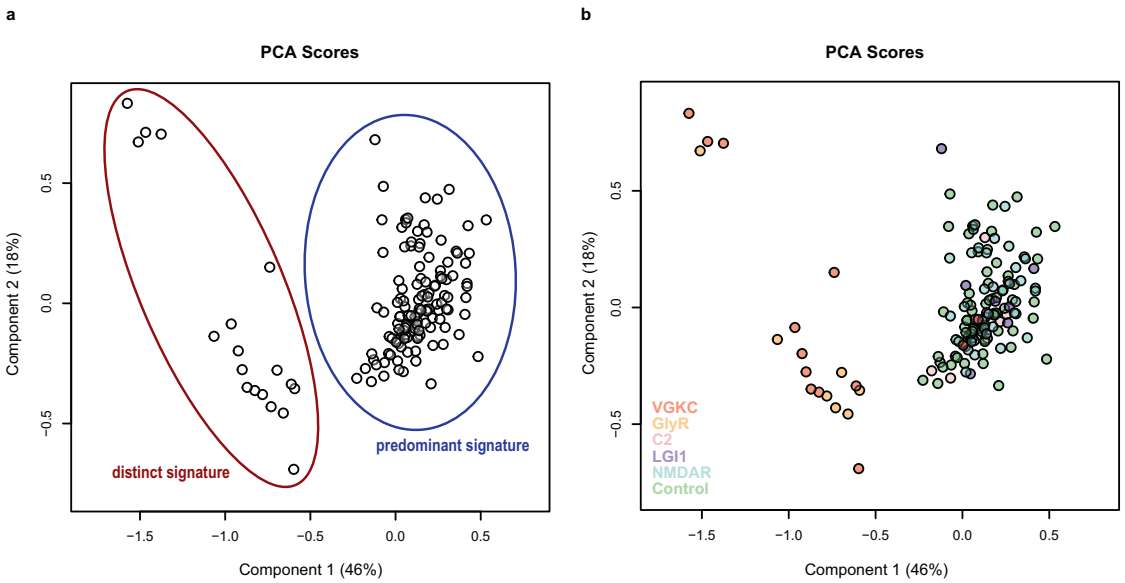

Fig. 1 PCA scores plots of NMR serum metabolomics. a The NMR metabolite signature spontaneously separated the psychosis patient cohort into two groups: the 'predominant biochemical signature group' and the 'distinct biochemical signature group'. **b** Psychosis patients who tested positive for serum antibodies against VGKC (red, $n = 13$) or GlyR (orange, $n = 7$) spontaneously separated from those who tested positive for C2 (pink, $n = 9$), LGI1 (purple, $n = 9$), or NMDAR (blue, $n = 35$) and antibody negative Control (green, $n = 70$) samples.

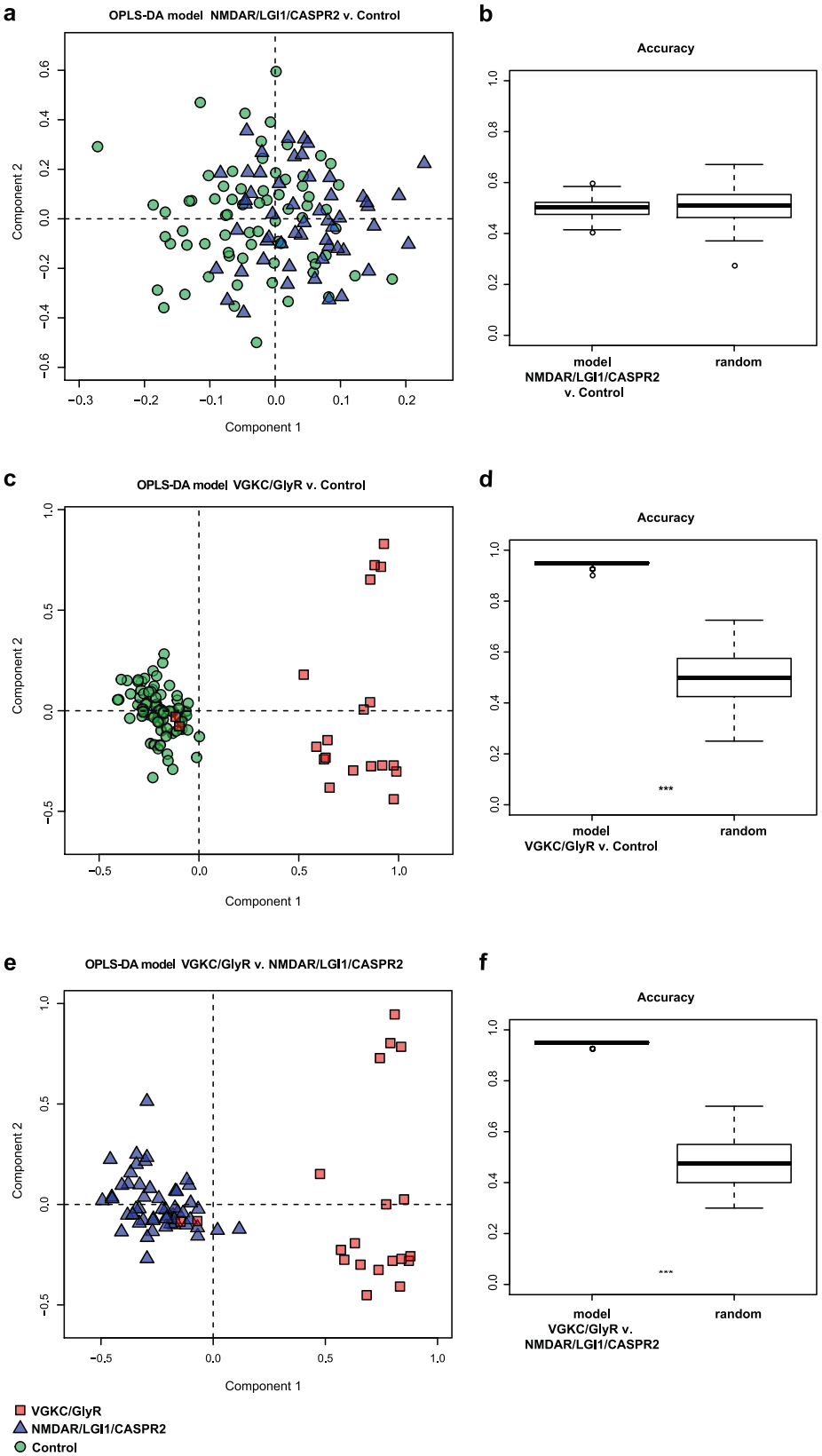

Fig. 2 OPLS-DA models discriminating VGKC/GlyR (red square, $n = 20$) samples from NMDAR/LGI1/CASPR2 (blue triangle, $n = 53$) samples and Control (green circle, $n = 70$) samples using NMR serum metabolomic data. a, **c**, **e** OPLS-DA scores plots of NMDAR/LGI1/CASPR2 v. Control, VGKC&GlyR v. Control, VGKC/GlyR v. NMDAR/LGI1/CASPR2. **b**, **d**, **f** Predictive accuracy of the ensemble of the OPLS-DA models compared with that of the randomly permutated null distribution. Kolmogorov-Smirnov test. ***$p < 0.001$.

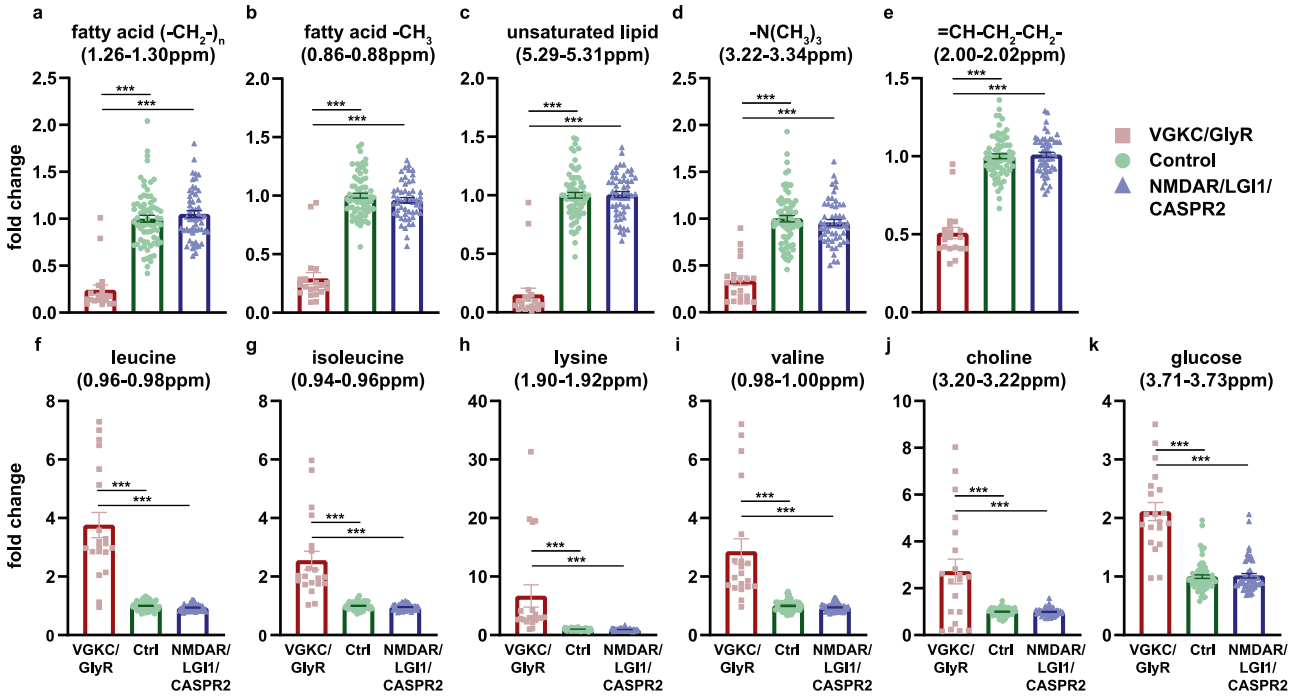

Fig. 3 Levels of discriminatory serum metabolites selected by the OPLS-DA models in VGKC/GlyR (red, $n = 20$), control (green, $n = 70$), and NMDAR/LGI1/CASPR2(blue, $n = 53$) groups. a–e Decreased levels of several fatty acid resonances within serum lipoproteins (−CH3, (−CH2-)n, -N(CH3)3, unsaturated fatty acid, =CH-CH2-CH2−) in the VGKC/GlyR antibody group. **f–k** Increased levels of several amino acids (leucine, isoleucine, lysine, and valine), choline and glucose in the VGKC/GlyR antibody group. Error bars: ±SEM. One-way ANOVA with Tukey's post-hoc corrections. ***$p < 0.001$.

Table 2. Comparison of PANSS scores of patients with VGKC/GlyR antibody, NMDAR/LGI1/CASPR2 antibody test, and antibody negative control groups.

	Ctrl	VGKC/GlyR	NMDAR/LGI1/CASPR2
Number of patients	70	19	53
Age (years), Median (IQR)	27 (15)	23 (8)	28 (15)
Gender, Female, no. (%)	31 (44.3)	8 (42.1)	21 (39.6)
PANSS, Median (IQR)			
Positive symptom score	6 (2.3)	9 (5)*	7 (3)
Negative symptom score	3 (3)	6 (6)*	3 (3)
General symptom score	2 (0)	5 (5)***	2 (0)†††
Total score	12 (6)	19 (8)***	12 (6)†††

The PANSS score for one VGKC/GlyR patient was not available and so was excluded from this table.
The Kruskal-Wallis test with Dunn's multiple comparisons test was used to identify significant differences of each class for numerical variables (age, PANSS scores) while Fisher's exact test was used for categorical variables. *Indicates significant differences of each class compared to Ctrl. †indicates significant differences of each class compared to VGKC/GlyR. *$p < 0.05$, ***$p < 0.001$. $^{\dagger\dagger\dagger}p < 0.001$.
Ctrl control, psychosis patients tested negative for the following neuronal cell surface antibodies. *VGKC/GlyR* voltage-gated potassium channel complex & glycine receptor; psychosis patients tested positive for either antigen. *CASPR2* contactin-associated protein-like 2; LGI1 leucine-rich glioma inactivated 1, *NMDAR* N-methyl-D-aspartate receptor. *NMDAR/LGI1/CASPR2* psychosis patients tested positive for CASPR2/LGI1/NMDAR. *PANSS* Positive and Negative Syndrome Scale. *IQR* Interquartile Range.

Patients with elevated serum VGKC antibody or GlyR antibody have significantly higher PANSS ratings

To determine whether the metabolism disturbances identified in the VGKC and GlyR antibody patients were associated with a distinct clinical phenotype, we investigated the PANSS scores across these groups by comparing the median scores between groups. VGKC and GlyR antibody patients had significantly higher PANSS totals than either the antibody negative or NMDAR, LGI1, CASPR2 antibody patients (both p values < 0.001, Kruskal-Wallis test with Dunn's multiple comparisons test) (Table 2). In exploring the subscale scores, the VGKC/GlyR antibody had higher positive symptoms, negative symptoms, and general symptoms than the control patient groups (p values < 0.05, <0.05, and <0.001, respectively, Kruskal-Wallis test with Dunn's multiple comparisons test) (Table 2). In order to explore the possibility that the biochemical signature identified in the VGKC/GlyR group was a marker of severity of illness, we undertook a separate OPLS-DA model of high PANSS v low PANSS (independent of antibody status). This resulted in lower accuracy, sensitivity, and specificity of model, indicating that this metabolomic profile was not just a marker of illness severity (−30.82%, −28.91%, and −26.51% respectively).

DISCUSSION

Unsupervised and untargeted metabolomics analysis identified a biochemical signature of VGKC and GlyR antibody positive psychosis which consisted of decreased fatty acid lipoprotein levels along with increased leucine, isoleucine, valine, lysine, free choline, and glucose concentrations.

Serum lipoproteins are increasingly recognised to play a role in the immune system and active inflammation is commonly associated with decreased small lipoprotein particles such as high-density lipoproteins (HDL) and low density lipoproteins (LDL) coupled with an increase in triglyceride concentration and the larger, very low-density lipoprotein (VLDL) particles [38]. In addition, pro-inflammatory cytokines have been shown to induce dyslipidaemia [39] and lead to a reduction in HDL cholesterol [40]. Finally, increasing LDL cholesterol concentration and improving HDL cholesterol efflux have been shown to improve C-reactive protein (CRP) associated inflammation in diseases such as rheumatoid arthritis [41, 42]. Thus, the decrease in fatty acid lipoprotein signatures identified here are consistent with increased inflammation in the VGKC and GlyR antibody-positive groups.

Elevated plasma concentrations of branched chain amino acids (BCAA) and lysine have been previously reported in people with schizophrenia [43] and elevated BCAA inhibit transport of dopamine and serotonin precursors (tyrosine and tryptophan, respectively) into the brain, which can lead to anxiety and mood disorders [44, 45] Elevated BCAA may also lead to insulin resistance [46, 47] which is associated with first-episode psychosis [48]. The significant increase in glucose concentration observed here supports this and, along with the increased BCAA levels identified, may be associated with the increased PANSS scores observed in the VGKC and GlyR antibody positive patients.

Taken together, the metabolomics analysis suggests a distinct metabolomic phenotype in VGKC and GlyR antibody positive patients which is associated with increased PANSS scores at presentation, increased inflammation, and potentially decreased neurotransmitter precursors and insulin resistance. Future work, on a larger cohort, will investigate these pathways in more detail.

Our finding of a distinct metabolomic and clinical phenotype associated with VGKC and GlyR antibodies was somewhat against our original hypothesis. The neuronal cell surface antibodies with the strongest evidence for pathogenicity are the NMDAR, LGI1, and CASPR2 antibodies, with substantial case report evidence that they have a direct effect on neuronal function and cause the expression of neuropsychiatric illness. We, therefore, hypothesized that these antibodies would be particularly associated with biochemical markers of inflammation.

However, in spite of the accepted pathogenicity of these antibodies it has also been recognized, paradoxically, that classical measures of neuroinflammation may also be absent in these patients, whether in MRI scans, or in serum or CSF measures of inflammation [49, 50]. The absence of a distinctive metabolomic profile in those with NMDAR/LGI1/CASPR2 serum antibodies in psychosis does not necessarily indicate that these antibodies are not having an effect in the brain in these patients.

VGKC and GlyR antibodies, by contrast do not have such a strong literature to support their direct pathogenicity in neuropsychiatric disorders. A particularly influential paper, reviewing the presence of VGKC antibodies in the absence of LGI1 or CASPR2 antibodies in a clinical cohort at the Mayo clinic, found that the presence of the antibodies was not associated with an immunotherapy responsive illness [51, 52]. However, this clinical sample was of largely older people with a range of other degenerative diagnoses, and not comparable to a younger cohort of people without comorbidity. It is possible therefore, in these cases that the VGKC antibodies were a secondary, non-specific marker of neurodegeneration.

A further clinical study suggests that non-LGI1, non-CASPR2 VGKC antibodies are a non-specific marker of an inflammatory brain condition in children. A series of patients were tested for antibodies, and separately rated according to clinical and paraclinical measures into having a likely inflammatory brain condition, or not. Of 39 patients with these VGKC antibodies, 30 were considered clinically to have an inflammatory condition. The likelihood of an inflammatory condition was raised with a higher titre of the antibody [25]. There are further case reports of those with atypical dementia or pain syndromes and VGKC antibodies that are responsive to immunotherapy, suggesting that these antibodies may indeed be a marker of an inflammatory condition [53]. Further work is now required to investigate the biological function and relevance of titre level of these antibodies in psychosis.

GlyR is a glycine-gated chloride ion channel typically expressed on the surface of motor neurons in the brainstem and spinal cord, regulating neuronal excitability. GlyR is also found in human hippocampus, but its role here is less clear [54]. GlyR antibodies were first described in progressive encephalopathy with rigidity and myoclonus (PERM) [55], and not previously described in association with psychiatric presentations [56].

Taken together, it is likely therefore that these antibodies are acting as non-specific markers of a possible inflammatory aetiology in these patients, rather than indicating a more specific VGKC or GlyR pathology.

The association between the GlyR and VGKC antibodies and higher PANSS ratings overall indicates patients with these antibodies are less responsive to antipsychotic medication. The finding of greater negative symptoms in this group is in keeping with the notion that negative symptoms are the result of neuroinflammation, with inflammatory stimuli decreasing neural activity in the ventral striatum, decreasing connectivity in reward pathways, and resulting in a lack of motivation in patients [34].

There are limitations to this study. As this was a pilot study and a number of different antibodies were included, the numbers in each group were small. There was no significant difference in any of the potential confounders investigated (age, gender, ethnicity, episode type). Nonetheless, we investigated the effect of each potential confounder on the multivariate model and further confirmed that neither age, gender, ethnicity, nor episode type were contributing factors to the models (Supplementary Fig. 2).

Prescribed medication was not recorded in participants recruited after 2016 and it is possible that this could affect the metabolomic profile seen. However, in the samples collected prior to 2017 almost all patients were prescribed atypical antipsychotics, in keeping with usual clinical practice in UK. It is a reasonable assumption that similarly the later patients were also all prescribed an atypical antipsychotic. There would be no reason why those with antibodies would systematically be given a different medication, although we cannot prove this.

The samples were all collected in the same brand of serum separator tube that was supplied by the study team, and the samples were assessed by the same researcher for the presence of antibodies, reducing chance of any systematic bias. The samples were sent at room temperature to the study team. This led to a delay of a day or two before the samples were processed. This delay likely led to a degradation of samples, and a consequent lack of sensitivity to detect some metabolites. We did not measure motor symptoms in the patients to know whether there were any correlates with the GlyR antibodies. Finally, we did not include any other psychiatric or neurological groups, and therefore are unable to say whether this pattern is distinct to psychosis, or not.

These limitations do not detract from the main finding of a biochemically distinct subgroup of patients with first episode psychosis that is associated with higher PANSS scores and VGKC and GyR antibody positivity, which indicates a potential inflammatory aetiology for a proportion of patients, and gives the

potential for different treatment approaches for these patients. Further work is now required to validate the biomarkers identified in a larger, prospective cohort and assess the performance of our multivariate diagnostic model to other inflammatory diseases of the central nervous system and routinely used inflammatory markers.

In conclusion we have demonstrated a distinct biochemical profile of a subgroup of patients with acute psychosis who have a more severe illness. This is particularly exciting, because it is these patients, resistant to current antipsychotic medication, that are in particular need of new therapeutic approaches. If confirmed, these findings could therefore lead to the trial of novel targeted treatments on the basis of individuals' metabolomic profile.

DATA AVAILABILITY

Anonymized data and code will be shared by request from any qualified investigator.

REFERENCES

1. Ripke S, Neale BM, Corvin A, Walters JTR, Farh KH, Holmans PA, et al. Biological insights from 108 schizophrenia-associated genetic loci. Nature 2014;511:421–7.
2. Pouget JG, Schizophrenia Working Group of the Psychiatric Genomics Consortium, Han B, Wu Y, Mignot E, Ollila HM, et al. Cross-disorder analysis of schizophrenia and 19 immune-mediated diseases identifies shared genetic risk. Hum Mol Genet. 2019;28:3498–513.
3. Benros ME, Nielsen PR, Nordentoft M, Eaton WW, Dalton SO, Mortensen PB. Autoimmune diseases and severe infections as risk factors for schizophrenia: a 30-year population-based register study. Am J Psychiatry. 2011;168:1303–10.
4. Chen SJ, Chao YL, Chen CY, Chang CM, Wu ECH, Wu CS, et al. Prevalence of autoimmune diseases in in-patients with schizophrenia: nationwide population-based study. Br J Psychiatry J Ment Sci. 2012;200:374–80.
5. Lennox BR, Palmer-Cooper EC, Pollak T, Hainsworth J, Marks J, Jacobson L, et al. Prevalence and clinical characteristics of serum neuronal cell surface antibodies in first-episode psychosis: a case-control study. Lancet Psychiatry. 2017;4:42–8.
6. Irani SR, Bera K, Waters P, Zuliani L, Maxwell S, Zandi MS, et al. N-methyl-d-aspartate antibody encephalitis: temporal progression of clinical and paraclinical observations in a predominantly non-paraneoplastic disorder of both sexes. Brain 2010;133:1655–67.
7. Vincent A, Buckley C, Schott JM, Baker I, Dewar BK, Detert N, et al. Potassium channel antibody-associated encephalopathy: a potentially immunotherapy-responsive form of limbic encephalitis. Brain J Neurol. 2004;127:701–12.
8. Titulaer MJ, McCracken L, Gabilondo I, Armangué T, Glaser C, Iizuka T, et al. Treatment and prognostic factors for long-term outcome in patients with anti-NMDA receptor encephalitis: an observational cohort study. Lancet Neurol. 2013;12:157–65.
9. Jurynczyk M, Probert F, Yeo T, Tackley G, Claridge TDW, Cavey A, et al. Metabolomics reveals distinct, antibody-independent, molecular signatures of MS, AQP4-antibody and MOG-antibody disease. Acta Neuropathol Commun. 2017;5:95.
10. Radford-Smith DE, Patel PJ, Irvine KM, Russell A, Siskind D, Anthony DC, et al. Depressive symptoms in non-alcoholic fatty liver disease are identified by perturbed lipid and lipoprotein metabolism. PloS One. 2022;17:e0261555.
11. Amigó N, Fuertes-Martín R, Malo AI, Plana N, Ibarretxe D, Girona J, et al. Glycoprotein profile measured by a 1H-nuclear magnetic resonance based on approach in patients with diabetes: a new robust method to assess inflammation. Life Basel Switz. 2021;11:1407.
12. Probert F, Walsh A, Jagielowicz M, Yeo T, Claridge TDW, Simmons A, et al. Plasma nuclear magnetic resonance metabolomics discriminates between high and low endoscopic activity and predicts progression in a prospective cohort of patients with ulcerative colitis. J Crohns Colitis. 2018;12:1326–37.
13. Mokkala K, Houttu N, Koivuniemi E, Sørensen N, Nielsen HB, Laitinen K. GlycA, a novel marker for low grade inflammation, reflects gut microbiome diversity and is more accurate than high sensitive CRP in reflecting metabolomic profile. Metabolomics J Metabolomic Soc. 2020;16:76.
14. Heinemann J. Cluster analysis of untargeted metabolomic experiments. Methods Mol Biol Clifton NJ. 2019;1859:275–85.
15. Hughes EG, Peng X, Gleichman AJ, Lai M, Zhou L, Tsou R, et al. Cellular and synaptic mechanisms of anti-NMDA receptor encephalitis. J Neurosci J Soc Neurosci. 2010;30:5866–75.
16. Dalmau J, Lancaster E, Martinez-Hernandez E, Rosenfeld MR, Balice-Gordon R. Clinical experience and laboratory investigations in patients with anti-NMDAR encephalitis. Lancet Neurol. 2011;10:63–74.
17. Al-Diwani A, Pollak T, Langford A, Lennox B. Synaptic and neuronal autoantibody-associated psychiatric syndromes (SNAps): Controversies and Hypotheses. Front Psychiatry. 2017;8:13.
18. Gréa H, Bouchet D, Rogemond V, Hamdani N, Le Guen E, Tamouza R, et al. Human autoantibodies against N-Methyl-D-Aspartate receptor modestly alter Dopamine D1 receptor surface dynamics. Front Psychiatry. 2019;10:670.
19. Zandi MS, Deakin JB, Morris K, Buckley C, Jacobson L, Scoriels L, et al. Immunotherapy for patients with acute psychosis and serum N-Methyl D-Aspartate receptor (NMDAR) antibodies: a description of a treated case series. Schizophr Res. 2014;160:193–5.
20. Lennox BR, Tomei G, Vincent SA, Yeeles K, Pollard R, Palmer-Cooper E, et al. Study of immunotherapy in antibody positive psychosis: feasibility and acceptability (SINAPPS1). J Neurol Neurosurg Psychiatry. 2019;90:365–7.
21. Buckley C, Oger J, Clover L, Tüzün E, Carpenter K, Jackson M, et al. Potassium channel antibodies in two patients with reversible limbic encephalitis. Ann Neurol. 2001;50:73–8.
22. Irani SR, Alexander S, Waters P, Kleopa KA, Pettingill P, Zuliani L, et al. Antibodies to Kv1 potassium channel-complex proteins leucine-rich, glioma inactivated 1 protein and contactin-associated protein-2 in limbic encephalitis, Morvan's syndrome and acquired neuromyotonia. Brain 2010;133:2734–48.
23. van Sonderen A, Schreurs MWJ, de Bruijn MAAM, Boukhrissi S, Nagtzaam MMP, Hulsenboom ESP, et al. The relevance of VGKC positivity in the absence of LGI1 and Caspr2 antibodies. Neurology 2016;86:1692–9.
24. Lang B, Makuch M, Moloney T, Dettmann I, Mindorf S, Probst C, et al. Intracellular and non-neuronal targets of voltage-gated potassium channel complex antibodies. J Neurol Neurosurg Psychiatry. 2017;88:353–61.
25. Hacohen Y, Singh R, Rossi M, Lang B, Hemingway C, Lim M, et al. Clinical relevance of voltage-gated potassium channel–complex antibodies in children. Neurology 2015;85:967–75.
26. Carvajal-González A, Leite MI, Waters P, Woodhall M, Coutinho E, Balint B, et al. Glycine receptor antibodies in PERM and related syndromes: characteristics, clinical features, and outcomes. Brain J Neurol. 2014;137:2178–92. Pt 8
27. Spatola M, Petit-Pedrol M, Simabukuro MM, Armangue T, Castro FJ, Barcelo Artigues MI, et al. Investigations in GABAA receptor antibody-associated encephalitis. Neurology 2017;88:1012–20.
28. Kay SR, Fiszbein A, Opler LA. The positive and negative syndrome scale (PANSS) for schizophrenia. Schizophr Bull. 1987;13:261–76.
29. Pettingill P, Kramer HB, Coebergh JA, Pettingill R, Maxwell S, Nibber A, et al. Antibodies to GABAA receptor α1 and γ2 subunits: clinical and serologic characterization. Neurology 2015;84:1233–41.
30. Wishart DS, Feunang YD, Marcu A, Guo AC, Liang K, Vázquez-Fresno R, et al. HMDB 4.0: the human metabolome database for 2018. Nucleic Acids Res. 2018;46:D608–17.
31. Foxall PJ, Spraul M, Farrant RD, Lindon LC, Neild GH, Nicholson JK. 750 MHz 1H-NMR spectroscopy of human blood plasma. J Pharm Biomed Anal. 1993;11:267–76.
32. Bell JD, Sadler PJ, Macleod AF, Turner PR, La Ville A. 1H NMR studies of human blood plasma Assignment of resonances for lipoproteins. FEBS Lett. 1987;219:239–43.
33. Tang H, Wang Y, Nicholson JK, Lindon JC. Use of relaxation-edited one-dimensional and two dimensional nuclear magnetic resonance spectroscopy to improve detection of small metabolites in blood plasma. Anal Biochem. 2004;325:260–72.
34. Finucane K, Nyamundanda G, Gormley IC, Fan Y, Gallagher WM, Brennan L, MetSizeR: A Shiny App for Sample Size Estimation in Metabolomic Experiments. 2021 [cited 2022 Feb 1]. Available from: https://CRAN.R-project.org/package=MetSizeR.
35. Nyamundanda G, Gormley IC, Fan Y, Gallagher WM, Brennan L. MetSizeR: selecting the optimal sample size for metabolomic studies using an analysis based approach. BMC Bioinforma. 2013;14:338.
36. Nyamundanda G, Brennan L, Gormley IC. Probabilistic principal component analysis for metabolomic data. BMC Bioinforma. 2010;11:571.
37. Thévenot EA, Roux A, Xu Y, Ezan E, Junot C. Analysis of the human adult urinary metabolome variations with age, body mass index, and gender by implementing a comprehensive workflow for univariate and OPLS statistical analyses. J Proteome Res. 2015;14:3322–35.
38. Feingold KR, Grunfeld C, The effect of inflammation and infection on lipids and lipoproteins. In: Feingold KR, Anawalt B, Boyce A, Chrousos G, de Herder WW, Dhatariya K, et al. editors. Endotext [Internet]. South Dartmouth (MA): MDText.com, Inc.; 2000 [cited 2021 Nov 14]. Available from: http://www.ncbi.nlm.nih.gov/books/NBK326741/.
39. Klingenberg R, Gerdes N, Badeau RM, Gisterå A, Strodthoff D, Ketelhuth DFJ, et al. Depletion of FOXP3+ regulatory T cells promotes hypercholesterolemia and atherosclerosis. J Clin Invest. 2013;123:1323–34.

40. Haas MJ, Mooradian AD. Regulation of high-density lipoprotein by inflammatory cytokines: establishing links between immune dysfunction and cardiovascular disease. Diabetes Metab Res Rev. 2010;26:90–9.
41. Robertson J, Porter D, Sattar N, Packard CJ, Caslake M, McInnes I, et al. Interleukin-6 blockade raises LDL via reduced catabolism rather than via increased synthesis: a cytokine-specific mechanism for cholesterol changes in rheumatoid arthritis. Ann Rheum Dis. 2017;76:1949–52.
42. Liao KP, Playford MP, Frits M, Coblyn JS, Iannaccone C, Weinblatt ME, et al. The association between reduction in inflammation and changes in lipoprotein levels and HDL cholesterol efflux capacity in rheumatoid arthritis. J Am Heart Assoc. 2015;4:e001588.
43. Meltzer HY. Clinical studies on the mechanism of action of clozapine: the dopamine-serotonin hypothesis of schizophrenia. Psychopharmacology. 1989;99:S18–27.
44. Fernstrom JD. Dietary precursors and brain neurotransmitter formation. Annu Rev Med. 1981;32:413–25.
45. Koochakpoor G, Salari-Moghaddam A, Keshteli AH, Afshar H, Esmaillzadeh A, Adibi P. Dietary intake of branched-chain amino acids in relation to depression, anxiety and psychological distress. Nutr J. 2021;20:11.
46. Lynch CJ, Adams SH. Branched-chain amino acids in metabolic signalling and insulin resistance. Nat Rev Endocrinol. 2014;10:723–36.
47. Newgard CB. Interplay between lipids and branched-chain amino acids in development of insulin resistance. Cell Metab. 2012;15:606–14.
48. Fehsel K, Löffler S. First-episode psychosis and abnormal glycaemic control. Lancet Psychiatry. 2017;4:23–4.
49. Finke C, Kopp UA, Scheel M, Pech LM, Soemmer C, Schlichting J, et al. Functional and structural brain changes in anti-N-methyl-D-aspartate receptor encephalitis. Ann Neurol. 2013;74:284–96.
50. Dürr M, Nissen G, Sühs KW, Schwenkenbecher P, Geis C, Ringelstein M, et al. CSF findings in acute NMDAR and LGI1 antibody-associated autoimmune encephalitis. Neurol Neuroimmunol Neuroinflammation. 2021;8:e1086.
51. van Sonderen A, Schreurs MWJ, Wirtz PW, Sillevis Smitt PAE, Titulaer MJ. From VGKC to LGI1 and Caspr2 encephalitis: The evolution of a disease entity over time. Autoimmun Rev. 2016;15:970–4.
52. Klein CJ, Lennon VA, Aston PA, McKeon A, Pittock SJ. Chronic pain as a manifestation of potassium channel-complex autoimmunity. Neurology 2012;79:1136–44.
53. Prüss H, Lennox BR. Emerging psychiatric syndromes associated with antivoltage-gated potassium channel complex antibodies. J Neurol Neurosurg Psychiatry. 2016;87:1242–7.
54. Xu TL, Gong N. Glycine and glycine receptor signaling in hippocampal neurons: diversity, function and regulation. Prog Neurobiol. 2010;91:349–61.
55. Hutchinson M, Waters P, McHugh J, Gorman G, O'Riordan S, Connolly S, et al. Progressive encephalomyelitis, rigidity, and myoclonus: a novel glycine receptor antibody. Neurology 2008;71:1291–2.
56. Swayne A, Tjoa L, Broadley S, Dionisio S, Gillis D, Jacobson L, et al. Antiglycine receptor antibody related disease: a case series and literature review. Eur J Neurol. 2018;25:1290–8.

ACKNOWLEDGEMENTS

This study was funded by NIHR Oxford Health Biomedical Research Centre. The views expressed are those of the authors and not necessarily those of the NHS, the NIHR, or the Department of Health.

AUTHOR CONTRIBUTIONS

The study was designed by BL, DA, and FP. Sample collection and oversight of psychosis screening study from which samples were selected by AC, PJ, KJ, and BL. Metabolomics and antibody testing undertaken by WX, PW, TY, JTMM, and FP. Data analysis and interpretation by BL, WX, PW, AC, PJ, DA, KY, FP. The manuscript was drafted by BL, WX, FP, and edited by PW, AC, PJ, DA, and KY. All authors read and approved the final version of the manuscript.

COMPETING INTERESTS

The authors declare no competing interests.

ADDITIONAL INFORMATION

Supplementary information The online version contains supplementary material available at https://doi.org/10.1038/s41380-022-01784-4.

Correspondence and requests for materials should be addressed to Belinda Lennox.

Reprints and permission information is available at http://www.nature.com/reprints

Publisher's note Springer Nature remains neutral with regard to jurisdictional claims in published maps and institutional affiliations.

ANNALS of Clinical and Translational Neurology
Open Access
AMERICAN NEUROLOGICAL ASSOCIATION

RESEARCH ARTICLE

Distinct plasma metabolomic signatures differentiate autoimmune encephalitis from drug-resistant epilepsy

Wenzheng Xiong[1,2], Tianrong Yeo[2,3,4,5], Jeanne Tan May May[3,4], Tor Demmers[2], Bryan Ceronie[6], Archana Ramesh[6], Ronan N. McGinty[6], Sophia Michael[6], Emma Torzillo[6], Arjune Sen[6], Daniel C. Anthony[2], Sarosh R. Irani[6,7,8] & Fay Probert[1]

[1]Department of Chemistry, University of Oxford, Oxford, UK
[2]Department of Pharmacology, Medical Sciences Division, University of Oxford, Oxford, UK
[3]Department of Neurology, National Neuroscience Institute, Singapore, Singapore
[4]Duke-NUS Medical School, Singapore, Singapore
[5]Lee Kong Chian School of Medicine, Nanyang Technological University, Singapore, Singapore
[6]Nuffield Department of Clinical Neurosciences, University of Oxford, Oxford, UK
[7]Department of Neurology, John Radcliffe Hospital, Oxford University Hospitals, Oxford, UK
[8]Departments of Neurology and Neurosciences, Mayo Clinic, Jacksonville, Florida, USA

Correspondence
Fay Probert, Department of Chemistry, University of Oxford, Oxford, UK.
Tel: +44 1865 275713; E-mail: fay.probert@chem.ox.ac.uk

Sarosh R. Irani, Departments of Neurology and Neurosciences, Mayo Clinic, 4500 San Pablo Road, Jacksonville, FL 32224, USA.
E-mail: irani.sarosh@mayo.edu

Received: 12 January 2024; Revised: 24 April 2024; Accepted: 17 May 2024

***Annals of Clinical and Translational Neurology* 2024; 11(7): 1897–1908**

doi: 10.1002/acn3.52112

Abstract

Objective: Differentiating forms of autoimmune encephalitis (AE) from other causes of seizures helps expedite immunotherapies in AE patients and informs studies regarding their contrasting pathophysiology. We aimed to investigate whether and how Nuclear Magnetic Resonance (NMR)-based metabolomics could differentiate AE from drug-resistant epilepsy (DRE), and stratify AE subtypes. **Methods**: This study recruited 238 patients: 162 with DRE and 76 AE, including 27 with contactin-associated protein-like 2 (CASPR2), 29 with leucine-rich glioma inactivated 1 (LGI1) and 20 with N-methyl-D-aspartate receptor (NMDAR) antibodies. Plasma samples across the groups were analyzed using NMR spectroscopy and compared with multivariate statistical techniques, such as orthogonal partial least squares discriminant analysis (OPLS-DA). **Results**: The OPLS-DA model successfully distinguished AE from DRE patients with a high predictive accuracy of 87.0 ± 3.1% (87.9 ± 3.4% sensitivity and 86.3 ± 3.6% specificity). Further, pairwise OPLS-DA models were able to stratify the three AE subtypes. Plasma metabolomic signatures of AE included decreased high-density lipoprotein (HDL, $-(C\mathbf{H}_2)_n-$, $-C\mathbf{H}_3$), phosphatidylcholine and albumin (lysyl moiety). AE subtype-specific metabolomic signatures were also observed, with increased lactate in CASPR2, increased lactate, glucose, and decreased unsaturated fatty acids (UFA, $-C\mathbf{H}_2CH=$) in LGI1, and increased glycoprotein A (GlycA) in NMDAR-antibody patients. **Interpretation**: This study presents the first non-antibody-based biomarker for differentiating DRE, AE and AE subtypes. These metabolomics signatures underscore the potential relevance of lipid metabolism and glucose regulation in these neurological disorders, offering a promising adjunct to facilitate the diagnosis and therapeutics.

Introduction

Epilepsy is a heterogeneous neurological disorder characterized by recurrent and unpredictable epileptic seizures, affecting approximately 50 million people worldwide.[1] Despite the availability of pharmacological treatments, a significant proportion of people with epilepsy (30%) experience drug-resistant epilepsy (DRE) and do not respond to conventional therapies.[2] Autoimmune encephalitis (AE) describes a group of autoantibody-mediated brain disorders characterized by seizures and neuropsychiatric symptoms with autoantibodies targeting neuroglial cell-surface proteins.[3–5] AE typically gives rise to acute seizures which, like DRE, are often refractory to anti-

seizure medications (ASMs).[4,5] Further, many series in AE patients, especially those with leucine-rich glioma inactivated 1 (LGI1)-antibodies, identify cases originally diagnosed with a non-autoimmune form of epilepsy.[6–8] More rarely, acute AE gives rise to chronic epilepsy.[9,10]

Timely diagnosis and initiation of immunotherapies are crucial for optimal prognosis in AE.[6,11] The diagnosis of AE typically involves a combination of clinical features, laboratory antibody tests and imaging.[6–12] While the detection of neuronal surface antibodies (NSAbs) is a valuable tool, it can be expensive, laborious, and time-sensitive, leading to potential delays in treatment initiation. Moreover, false positive antibody test results are well-recognized to harm patient care[7] and, as there are many seronegative cases, negative test results do not exclude AE.[13] Hence, further adjunctive diagnostics are valuable to AE patients. They may also guide therapy and prognosis. Currently, no robust stratifying biomarkers exist.

Nuclear magnetic resonance (NMR) metabolomics, in combination with multivariate statistical techniques and machine learning, has emerged as a valuable approach for identification of potential biomarkers and disturbed metabolic pathways, as well as the diagnosis and staging of diseases.[14] Recent studies have demonstrated the value of NMR metabolomics in detecting systemic inflammation and autoantibody-mediated pathology in central nervous system (CNS) diseases with overlapping symptoms.[15,16] Previous work has demonstrated ^{1}H NMR metabolomics can successfully discriminate between subsets of autoantibody-mediated psychosis, distinguish multiple sclerosis from autoantibody-mediated neuromyelitis optica spectrum disorder (NMOSD), and differentiate various subtypes of antibody-mediated NMOSD.[15,16] In this study, we hypothesized that NMR metabolomics coupled with robust multivariate analytical methods might distinguish AE from DRE and, further, differentiate three of the commonest subtypes of AE, associated with autoantibodies against LGI1, N-methyl-D-aspartate receptor (NMDAR) and contactin-associated protein-like 2 (CASPR2).

Methods

Human subjects

AE and DRE patients were recruited from John Radcliffe Hospital, Oxford, UK. The study was approved by the Research Ethics Committee (REC16/YH/0013) and all participants gave written informed consent. Matched clinical information was retrieved from the electronic patient record (Cerner Millenium). AE patients were diagnosed based on their clinical syndrome in association with serum and CSF antibody positivity at the peak of their disease determined by fixed and live cell-based assays for CASPR2 and NMDAR-antibodies, and serum positivity alone for LGI1-antibodies, as described previously.[17,18] Inclusion criteria for DRE patients were stipulated such that: (1) DRE patients with known positive antibody results were excluded from the analysis, and (2) Patient records of the DRE patients were reviewed to further exclude cases potentially associated with autoimmune etiologies. Blood was collected in BD™ Vacutainer™ Lithium Heparin tubes (BD 367886) and plasma was isolated by centrifugation at 500 *g* for 10 min at room temperature prior to storage at −80°C.

NMR spectroscopy

On the day of NMR data acquisition, plasma samples were defrosted at room temperature before being centrifuged at 100,000 *g* for 30 min at 4°C. 150 µL of the plasma samples were then mixed with 400 µL NMR buffer (75 mM phosphate buffer in D_2O, pH 7.4) and transferred to a 5 mm borosilicate NMR tube (Norell).

NMR metabolomics analysis of plasma was conducted as previously described.[15] NMR spectroscopy was performed using a 700-MHz Bruker AVIII spectrometer (Department of Chemistry, University of Oxford) operating at 16.4 T equipped with a ^{1}H [^{13}C/^{15}N] TCI cryoprobe at 298 K. ^{1}H spectra of human plasma were acquired using a spin-echo Carr–Purcell–Meiboom–Gill (CPMG) sequence (τ interval of 400 µs, 80 loops, 40 ms total filter time, 32 data collections, 1.5 s acquisition time, relaxation delay of 2 s, fixed receiver gain) to suppress broad signals arising from large molecular weight plasma components. For quality control, pooled samples were spread throughout the run to monitor technical variation.

Resulting free induction decays were zero-filled by a factor of 2 and multiplied by an exponential function corresponding to 0.30 Hz line broadening prior to Fourier transformation. All spectra were phased, baseline corrected, and referenced to the lactate $-CH_3$ doublet resonance at δ = 1.33 ppm, followed by visual inspection for errors and contaminations (Topspin 4.1, Bruker, Germany). Plasma NMR spectra were rationally divided into 122 spectral bins to avoid overlapping signals, integrated and normalized by the sum within each sample, accounting for any variations in sample dilution (ACD/Labs Spectrus Processor Academic Edition 12.01, Advanced Chemistry Development, Inc.). Integral values were pareto scaled prior to multivariate analysis.

Metabolite assignments for NMR signals was performed by referencing to literature values,[19–22] the Human Metabolome Database,[23] and via 2D total correlation spectroscopy (TOCSY) experiments. Approximately 50 metabolites, including a range of lipoprotein and lipid species, amino acids, glucose, organic acids, nucleotides, and amides were identified.

Statistical analysis

Multivariate analyses were performed in R software 4.1.2 (R Foundation for Statistical Computing, Vienna, Austria) using in-house R scripts and the ropls package.[24] Orthogonal partial least squares discriminant analysis (OPLS-DA), a supervised method, was used to generate diagnostic models and identify significant differences in metabolite levels between groups. The number of orthogonal components was optimized through 10 repetitions of the default 7-fold internal cross validation, with the final number determined by the median value obtained from the ten repetitions. OPLS-DA models were validated using a 10-fold external cross validation with 100 repetitions and permutation testing, as previously described.[16] Details of model optimization and cross validation were described in Figure S1. Discriminatory variables were identified by calculating the average of the variable importance in projection (VIP) scores.

Univariate statistical analyses, such as Student's *t* test or one-way ANOVA, were performed to identify significant differences in the mean for each discriminatory metabolite. Benjamini-Hochberg method was used to control the false discovery rate at 0.05. Univariate Receiver Operating Characteristic (ROC) analyses and multivariate ROC analyses on a combination of features using logistic regression were performed using MetaboAnalyst 5.0.[25] For patient demographic and clinical information, normality was tested by Anderson-Darling test. Kruskal-Wallis test with Dunn's multiple comparisons test was used to identify significant differences for non-normal continuous variables. Chi-Square test with Bonferroni correction for multiple comparisons was used for categorical variables. Adjusted two-tailed *p*-values ≤ 0.05 were considered statistically significant.

Results

Clinical features

The patient cohort ($n = 238$) comprised 162 DRE patients, and 76 AE patients including 27 with CASPR2-, 29 with LGI1-, and 20 with NMDAR-antibody encephalitis. Baseline demographic and treatment details are summarized in Table 1. The median age of the DRE patients was 37 years old and 62% were female. As expected, CASPR2 and LGI1 patients were older compared to DRE and more were males (89% and 79%, respectively), whereas NMDAR-antibody encephalitis patients had a median age of 30 and were predominantly female (95%).[6,17,18] While all DRE patients were receiving ASMs (100%), the percentage was lower in AE patients (54%) who frequently received immunotherapies. Again, as expected, more AE patients (19% CASPR2-, 24% LGI1-, 40% NMDAR-antibody patients) had systemic tumors, also focal and generalized seizures contrasted across the cohorts. DRE patients were relatively stable and provided their blood samples during routine outpatient clinics, while AE patients were potentially sampled both during acute in-patient stays and at outpatient clinics.

NMR plasma metabolomics coupled with OPLS-DA models discriminate autoimmune encephalitis patients from those with drug-resistant epilepsy

To compare plasma metabolomic signatures between DRE ($n = 162$) and AE patients ($n = 76$), ^{1}H NMR spectroscopy was performed with predictive models of OPLS-DA using 10-fold external cross validation. Cross validation and permutation testing showed that the model was able to identify AE patients in the test set from DRE patients with 87.0 ± 3.1% accuracy, 87.9 ± 3.4% sensitivity and 86.3 ± 3.6% specificity and the model performed significantly better than random chance (50.0 ± 5.3% accuracy, 50.0 ± 6.9% sensitivity, 49.8 ± 7.4% specificity, $p < 0.001$, Kolmogorov–Smirnov test), indicating it is both robust and not a result of overfitting (Fig. 1A–C, Table S1). In addition, NMR spectra were also obtained for three subjects selected to have post-AE epilepsy who had AE for 2–3 years before being treated as epilepsy with only ASMs (refer to Table S2 for detailed case information). Notably, when applying this OPLS-DA model to predict these three patients using their plasma metabolome, all three patients were classified as epilepsy, clustered with the DRE group (Fig. S2).

Mean spectra from DRE patients and AE patients (Fig. 1D) show discriminatory metabolites derived from the model. Compared to DRE patients, AE patients had increased plasma lactate, glucose and decreased high-density lipoprotein (HDL, fatty acyl chain $-(C\mathbf{H}_2)_n-$, $-C\mathbf{H}_3$ in lipoproteins, the spectral integral predominated by HDL), phosphatidylcholine ($N^+(C\mathbf{H}_3)_3$, choline-containing phospholipids, predominantly phosphatidylcholine), unsaturated fatty acids (UFAs, $-C\mathbf{H}_2CH=$ from the unsaturated fatty acyl components) and albumin (lysyl moiety of albumin)[22] (Table S3).

Univariate ROC analysis was conducted for each of the most discriminatory metabolites, indicating their individual potential to classify AE and DRE patients with an AUC ranging from 0.59 to 0.72 (Fig. 2A–F). Multivariate ROC analysis coupled with logistic regression on all the 11 most discriminatory resonances yielded an AUC of 0.820 (95% CI: 0.744–0.907). Notably, when selecting lactate, HDL ($-C\mathbf{H}_3$), the albumin lysyl moiety, and glucose, four features with lower covariation that are routinely

Table 1. Patient demographic and clinical information.

	DRE (N = 162)	AE-CASPR2 (N = 27)	AE-LGI1 (N = 29)	AE-NMDAR (N = 20)	p value (adjusted p value)
Age, median (IQR)	37 (27, 48)$^{C\ L}$	74 (66, 78)$^{D\ N}$	72 (57, 73)$^{D\ N}$	30 (23, 58)$^{C\ L}$	<0.001 (<0.001)
Sex, *n* (%)					
Female	100 (62%)$^{C\ L\ N}$	3 (11%)$^{D\ N}$	6 (21%)$^{D\ N}$	19 (95%)$^{C\ D\ L}$	<0.001 (<0.001)
BMI, median (IQR)	27 (24, 31)	27 (23, 28)	26 (20, 31)	28 (21, 32)	0.7 (>0.9)
Unknown	60 (37%)	20 (74%)	21 (72%)	10 (50%)	
Use of ASMs, *n* (%)					<0.001 (<0.001)
Yes	162 (100%)$^{C\ L\ N}$	17 (63%)$^{D\ N}$	20 (69%)$^{D\ N}$	4 (20%)$^{C\ D\ L}$	
Unknown	0	3 (11%)	2 (7%)	0	
Use of steroids, *n* (%)					<0.001 (<0.001)
Yes	1 (1%)[e],$^{C\ L\ N}$	6 (22%)$^{D\ L}$	17 (59%)$^{C\ D}$	7 (35%)^{D}	
Unknown	0	1 (4%)	2 (7%)	1 (5%)	
Use of other immunotherapies, *n* (%)					<0.001 (<0.001)
Yes	2 (1%)$^{C\ L\ N}$	9 (33%)^{D}	11 (38%)^{D}	9 (45%)^{D}	
Unknown	0	1 (4%)	2 (7%)	0	
Identified tumor(s), *n* (%)[a]					0.0013 (0.010)
Yes	21 (13%)$^{L\ N}$	5 (19%)	7 (24%)^{D}	8 (40%)^{D}	
Unknown	0	7 (26%)	12 (41%)	0	
Seizure semiology, *n* (%)					<0.001 (<0.001)
Focal seizures	121 (75%)$^{L\ N}$	19 (70%)	24 (83%)^{D}	1 (5%)^{D}	
Focal[b]	65	19	20	1	
Focal + FBTCS[c]	56	0	4	0	
Generalized	39 (24%)$^{L\ N}$	1 (4%)	1 (3%)^{D}	5 (25%)^{D}	
GTCS	36	1	1	5	
Other[d]	3	0	0	0	
Unknown	2 (1%)	7 (26%)	4 (14%)	14 (70%)	
Disease duration (from onset to sampling date, months), median (IQR)	160 (180)$^{C\ L\ N}$	38 (38)^{D}	25 (46)^{D}	16 (24)^{D}	<0.001 (<0.001)
Unknown	1 (1%)	0	0	0	
Seizure-free days (from last seizure to sampling date), median (IQR)	16 (143)$^{C\ L\ N}$	646 (1369)^{D}	272 (726)^{D}	814 (761)^{D}	<0.001 (<0.001)
Never had seizures	0	7 (26%)	2 (7%)	12 (60%)	
Unknown	0	2 (7%)	3 (10%)	2 (10%)	

Kruskal-Wallis test with Dunn's multiple comparisons test was used to identify significant differences of each class in age, BMI, disease duration and seizure-free days. Pairwise Chi-Square test with Bonferroni correction for multiple comparisons were used for categorical variables. Omnibus p-values and adjusted omnibus p-values with Bonferroni correction across demographic variables were reported. D, C, L, and N indicate a significant difference ($p < 0.05$) exists with DRE, CASPR2, LGI1, NMDAR, respectively, in the corresponding post-hoc multiple comparisons.

GTCS, generalized tonic–clonic seizure; IQR, interquartile range.

[a]Identified tumors encompass any tumor (including cancer) detected anywhere in the whole body (including brain), as documented in the electronic patient records at the time of blood sampling.

[b]Includes focal aware seizures and focal impaired awareness seizures.

[c]Focal seizures and focal to bilateral tonic–clonic seizures (FBTCS).

[d]Absence seizures, myoclonus.

[e]The patient was on lifelong hydrocortisone replacement due to childhood-onset hypopituitarism, unrelated to autoimmune pathology.

measurable in the clinical setting, the ROC analysis showed a comparable AUC of 0.820 (95% CI: 0.742–0.892) (Fig. 2G).

Distinct metabolomic signatures identified for each AE subtype

Upon further examination of the discriminatory metabolites, each AE subtype appeared to have its own unique metabolic signature apart from the shared metabolomic perturbation in HDL $-(C\mathbf{H}_2)_n-$, HDL $-C\mathbf{H}_3$, phosphatidylcholine and the albumin lysyl moiety (Fig. 3A). Plasma lactate levels were increased in LGI1-antibody encephalitis patients, and, even more so, in CASPR2-antibody encephalitis patients. Elevated plasma glucose and decreased UFA were only observed in the plasma of LGI1-antibody patients. Individual OPLS-DA models were developed for each AE subtype, compared to the DRE group. These

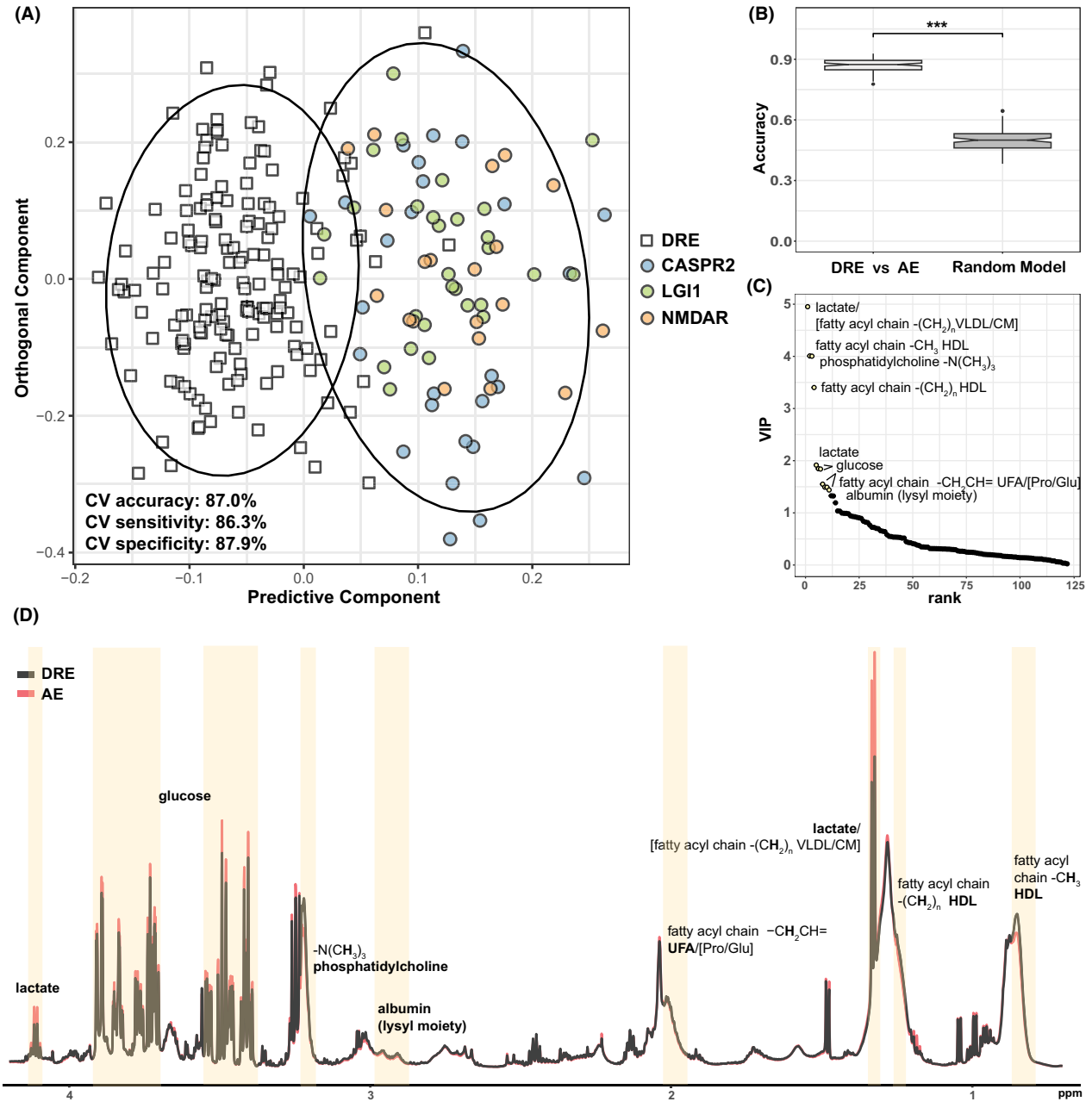

Figure 1. Altered plasma metabolome between AE patients and DRE patients. (A) Representative OPLS-DA scores plot showing separation of AE (circle, $n = 76$) from DRE (square, $n = 162$) patient plasma samples. AE plasma samples are colored according to the subtype (autoantibody specificity, CASPR2/LGI1/NMDAR, blue/green/orange). The ellipses indicate 95% confidence interval. The OPLS-DA model was generated with 1 predictive component and 7 orthogonal components. CV, cross validation. (B) Predictive accuracy of the ensemble of the OPLS-DA models compared with that of the randomly permutated null distribution. Kolmogorov–Smirnov test. ***p <0.001. (C) Discriminatory metabolites driving the separation of the OPLS-DA models, ranked by VIP scores. The top 11 resonances, identified with the inflexion point with a VIP score cutoff of 1.4, were labelled. "/" indicates the mentioned metabolites are overlapped in the spectral region. Metabolite names in square brackets refers to non-dominant overlapping metabolites also found in that spectral region. VLDL, very-low-density lipoproteins. CM, chylomicrons. (D) Mean NMR spectra of plasma samples from AE (red, $n = 76$) and DRE patients (black, $n = 162$) highlighted and labelled with discriminatory metabolites derived from the OPLS-DA models.

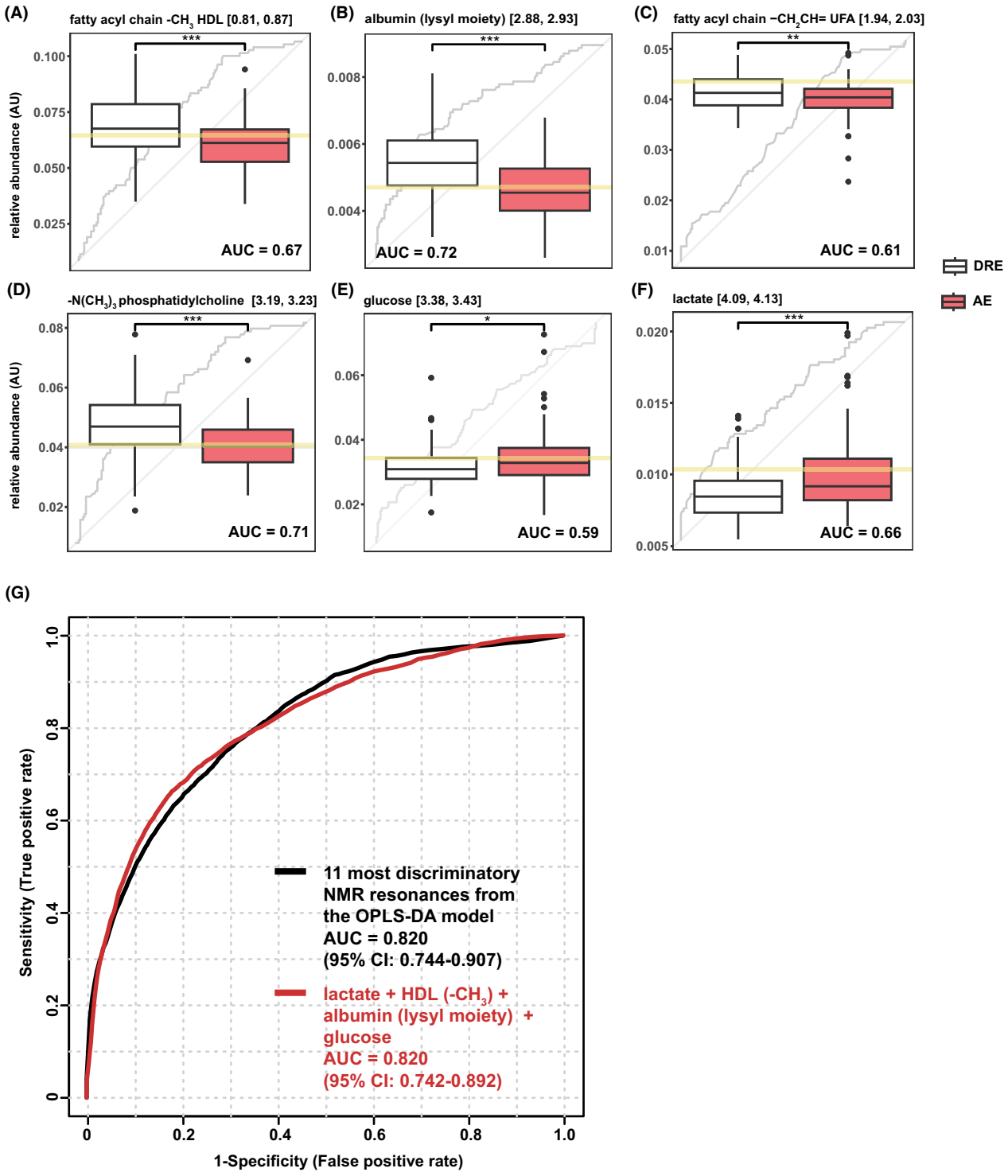

Figure 2. ROC analysis for discriminatory metabolites. (A–F) Boxplots of the highest ranked discriminatory metabolites identified by the OPLS-DA model in AE versus DRE. Gray lines were ROC curves of each metabolite. Yellow lines indicate optimal cutoff (closest to top-left corner) from univariate ROC analyses. (G) Multivariate ROC analysis on a combination of 11 most discriminatory NMR resonances from the OPLS-DA model (black) and on 4 selected features (red).

models achieved cross validation accuracies of 80.0 ± 5.1%, 82.3 ± 5%, and 80.4 ± 7.3% for distinguishing CASPR2-, LGI1- and NMDAR-antibody encephalitis, respectively, from DRE (Table S1). Notably, distinct metabolite signatures were identified for each subtype, including lactate, HDL ($-C\mathbf{H}_3$, $-(C\mathbf{H}_2)_n-$), and phosphatidylcholine for CASPR2; HDL ($-C\mathbf{H}_3$, $-(C\mathbf{H}_2)_n-$), lactate, phosphatidylcholine, glucose and UFA for LGI1; and phosphatidylcholine, HDL ($-C\mathbf{H}_3$, $-(C\mathbf{H}_2)_n-$), and glycoprotein A (GlycA) for NMDAR (Fig. 3A, Fig. S3).

Pairwise OPLS-DA models were built within the three AE subtypes to further study if each subtype can be stratified based on the differences in the metabolomic alteration. The accuracies of the models (CASPR2 vs. LGI1, CASPR2 vs. NMDAR, LGI1 vs. NMDAR) were 69.2 ± 3.0%, 68.9 ± 5.4%, and 77.5 ± 5.0%, respectively (Table S1). The significantly superior performance of the models than random chance (p <0.001, Kolmogorov–Smirnov test) indicated distinct metabolomic alterations exist within the three AE subtypes (Figs. S4 and S5, Table S4). Specific alterations in plasma metabolome in each AE subtype relative to DRE and each other are summarized in the Venn diagram (Fig. 3B).

Potential confounding factors including seizure semiologies

To investigate whether different seizure semiologies or the seizure proximity (Table 1) were reflected in the plasma metabolome, OPLS-DA models were built to compare patients with focal seizures (n = 121) versus patients with generalized seizures (n = 39). However, the 10-fold cross validation demonstrated a mean accuracy of 55.8 ± 5.9%, only marginally superior to random chance. Even when employing a subset of patients with focal aware/impaired awareness seizures (n = 20) matched with patients experiencing generalized tonic–clonic seizures (GTCS) (n = 20) in terms of age, gender, and seizure-free days, the model yielded a mean accuracy of 57.0 ± 4.7%. Similarly, when assessing the impact of seizure proximity by stratifying patients who had seizures in less than 15 days (n = 79) versus those without seizures for more than 300 days (n = 38), the model had a mean accuracy of 58.8 ± 6.0%. These results suggest that the impact of epilepsy on the blood metabolome is independent of the location, the type, and the proximity of seizure.

Other potential confounders lie in the observation that DRE and AE cohorts have multiple differences, as outlined in Table 1. To examine the influence of these potential confounders in our model, scores plots demonstrating the separation of the two groups were colored according to each variable to test for observable correlations (Fig. S6). Among these, age, the use of steroids and other immunotherapies displayed notable correlations. Consequently, we constructed OPLS-DA models based on younger (<25, n = 34) versus older (>50, n = 32) DRE patients, and the model was able to distinguish younger versus older DRE with a 71.9 ± 4.0% cross validation accuracy. Nonetheless, the discriminatory metabolite resonances responsible for the age separation were mainly very-low-density lipoprotein $-(C\mathbf{H}_2)_n-$ (VLDL, 1.26–1.32 ppm) and unsaturated fatty acids $-\mathbf{H}C{=}C\mathbf{H}-$ (5.25–5.38 ppm), different from those driving the separation between DRE and AE (Fig. S7).

A substantial proportion of the AE cohort was undergoing treatment with steroids and/or other immunotherapies. The OPLS-DA model was able to distinguish between AE patients who were using steroids (n = 30) and those who were not (n = 42), with a cross validation accuracy of 65.4 ± 4.1%. AE patients on steroids exhibited elevated glucose and GlycA levels (Fig. S8). However, the OPLS-DA model yielded only a 55.7 ± 4.5% cross validation accuracy to identify AE patients receiving other immunotherapies (n = 44 + 25) (Fig. S9). Therefore, while steroid administration may contribute marginally to the elevation of glucose levels in the AE versus DRE cohorts, the AE pathology remains the primary factor distinguishing their plasma metabolomics.

Discussion

In this study, we demonstrated the ability of metabolomics to differentiate patients with AE from those with DRE, and to separate three common subtypes of autoantibody-mediated AE. To our knowledge, this represents the first biomarker offering these discriminatory properties. While autoantibody assays will likely remain the gold standards, our NMR-based blood test offers a promising adjunct to facilitate the diagnosis of AE given the speed of testing, affordability, and high diagnostic accuracy. Metabolomic testing may be especially valuable when patients present with seizures in the absence of obvious causes such as traumatic brain injury, neoplasms, and infectious disease. Moreover, as autoantibody assays only detect known antibodies, it is conceivable that patients harboring unknown NSAbs may be detected with NMR approaches.[26,27] While prior research has explored non-antibody-based biomarkers such as neurofilament light chain (NfL) and cytokines,[28–31] these have limitations, such as NfL's susceptibility to age and various confounding factors. Hence, the unique advantages offered by our NMR metabolomics methods in AE diagnosis and subtype differentiation may prove valuable for several applications.

In this study, we have found that different AE subtypes (CASPR2, LGI1, NMDAR) have both overlapping and

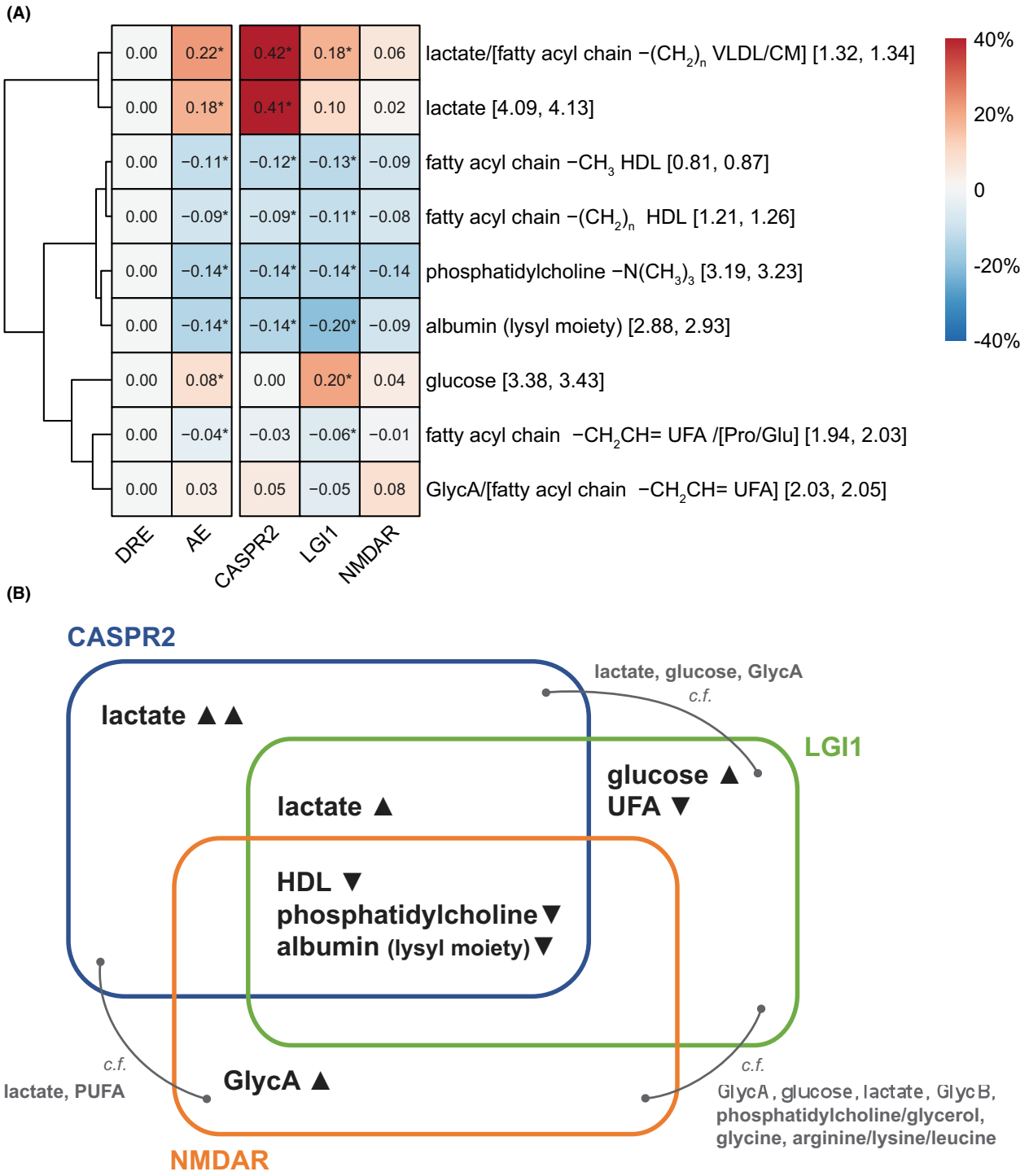

Figure 3. Specific alteration in plasma metabolome in each AE subtype. (A) Heatmap of percentage changes in key metabolites identified by the OPLS-DA models of AE versus DRE, and in each AE subtype relative to the DRE group. Numbers in the square brackets represent the boundary of corresponding spectral region in ppm. "/" indicates the mentioned metabolites are overlapped in the spectral region. Metabolite names in square brackets refers to non-dominant overlapping metabolites also found in that spectral region. * Significance in mean compared to DRE group ($q < 0.05$ in univariate analysis). (B) Venn diagram illustrating metabolic signatures of AE subtypes. Metabolites in black were identified from OPLS-DA models of AE versus DRE, and each AE subtype versus DRE, while metabolites in gray were identified from OPLS-DA models of pairwise AE subtype comparisons. HDL, high-density lipoprotein. UFA, unsaturated fatty acids. PUFA, polyunsaturated fatty acids. GlycA/B, Glycoprotein A/B.

distinct metabolome perturbations, suggesting the existence of both shared and distinct pathogenic mechanisms. Here we show that the common plasma metabolomic signatures shared by AE patients include decreased levels of HDL (fatty acyl chain $-(C\mathbf{H}_2)_n-$, $-CH_3$ resonances), phosphatidylcholine and albumin (lysyl moiety). While the clinical signs in AE are largely associated with the interaction with their respective target antigens in the CNS, there is also some peripheral expression of these proteins (e.g. LGI1), where autoimmune response might have contributed to the altered blood chemistry profiles that we have observed.[32]

Lipid profiles, especially with decreased HDL levels, are implicated in inflammatory and autoimmune diseases. For example, low HDL cholesterol and high triglycerides levels have been associated with higher levels of multiple sclerosis disability, as well as poor recovery and relapse in NMOSD.[33–36] Additionally, several studies have found lower HDL-cholesterol levels in individuals with NMDAR- antibody encephalitis compared to healthy controls, and associated with a poorer prognosis and increased likelihood of relapse.[37–39]

Decreased levels of $-N(CH_3)_3$ resonances from phosphatidylcholine were found in AE plasma in our study, and were highly positively correlated with HDL $-CH_3$ levels ($r = 0.95$, $p < 0.001$, Fig. S10). As phosphatidylcholine is the main phospholipid present in plasma and an integral component of lipoproteins (particularly HDL) the observed decrease in phosphatidylcholine levels may be attributed to the reduced levels of HDL. Additionally, the decreased levels of phosphatidylcholine may occur secondary to AE-induced inflammation, as cellular lipid profiles are modulated following inflammatory stress, including a decrease in phosphatidylcholines.[40]

Consistent with our findings, significantly lower albumin levels have been reported in AE patients, with plasma albumin levels decreased in NMDAR-antibody encephalitis relative to healthy controls, and pre-treatment low plasma albumin associated with worse prognosis in AE.[41,42] Albumin is a negative acute-phase reactant and reduced serum albumin levels have been shown to correlate with systemic and central inflammatory disease, which could be due to increased albumin degradation caused by a high catabolic rate and elevated albumin transudation resulting from increased capillary permeability.[43,44] Thus, taken together, the significant decreases observed in lipoprotein and albumin resonances of AE patients observed here, are consistent with an inflammatory metabolic signature.

Our study has also demonstrated that various subtypes of AE exhibit distinct metabolic changes, aligning with the observation that different NSAbs are often associated with distinct clinical syndromes and prognoses.[12] Elevated lactate levels were observed in both CASPR2- and LGI1-antibody patients, especially for CASPR2-antibody patients, while elevated plasma glucose levels were found in CASPR2-antibody AE only. GlycA levels were higher in NMDAR- and CASPR2-antibody patients but lower in LGI1-antibody patients, while UFA levels were decreased in LGI1-antibody encephalitis only.

Lactate is one of the most enriched by-products of cellular metabolism in tissues with immune cell infiltration. Studies have indicated that the activation of inflammatory immune cells can cause a shift from oxidative phosphorylation to aerobic glycolysis, resulting in an increase in lactate.[45] For example, elevated levels of serum lactate, have been reported in individuals with multiple sclerosis and the increases are positively correlated with increasing disability.[46,47]

GlycA/B, NMR specific biomarkers of systemic inflammation, derive from the glycan moieties of acute-phase proteins.[48] Studies have reported elevated levels of GlycA in patients with autoimmune diseases like rheumatoid arthritis and systemic lupus erythematosus.[49,50] Therefore, the increased GlycA levels observed in NMDAR-antibody patients are potentially indicative of ongoing inflammatory processes in this patient population. However, alone, GlycA is a non-specific marker.[48]

We acknowledge the limitations of our study, as it did not include healthy controls nor patients with other antibody-mediated diseases. Consequently, it is challenging to assert whether the identified pattern is specific to AE. Nonetheless, we conducted a comparative analysis with our prior research, wherein NMR metabolomics enabled successful stratification of antibody-positive NMOSD and relapsing remitting multiple sclerosis patients, along with the identification of an inflammatory subtype of psychosis associated with VGKC/GlyR antibody.[15,16] Notably, we observed some common signatures in the autoantibody-positive NMOSD group, including reduced phosphatidylcholine and lactate levels, along with alterations in lipoprotein profiles.[15] Moreover, a similar profile with reduced phosphatidylcholine and HDL levels, along with elevated glucose levels was observed in the VGKC/GlyR antibody-positive psychosis cohort.[16] The shared metabolic signatures in these cohorts with antibody-mediated diseases underscore the potential relevance of lipid metabolism and glucose regulation in various autoimmune and neurological conditions, warranting further exploration of these metabolic pathways for potential biomarkers or therapeutic targets.

In conclusion, this is the first study to use NMR-based metabolomics in distinguishing AE patients from DRE patients, highlighting the diagnostic potential of the NMR-based blood test for such differentiation. Furthermore, each AE subtype was found to exhibit a distinct

biochemical signature, providing insights into the distinct metabolic impact of the different AE target antigens. Yet, no discriminatory metabolomic signatures were observed for different seizure semiologies or proximity in the DRE cohort. However, it is clear that the blood metabolome of someone experiencing status epilepticus is significantly different from someone with control epilepsy patients.[51] Future work need to validate identified biomarkers externally in an independent cohort. It will also be important to explore the applicability of the NMR blood test in identifying other AE subtypes, seronegative AE patients and whether the AE metabolomic signature might be used to predict the persistence of AE.

Author Contributions

T.Y., D.C.A., S.R.I., F.P. contributed to the conception and design of the study. J.T.M.M., B.C., A.R., R.N.M., S.M., E.T., A.S., S.R.I. contributed to clinical data acquisition and interpretation. T.Y., J.T.M.M., F.P. contributed to the acquisition and analysis of NMR data. W.X., T.D., F.P. contributed to statistical analysis. W.X., D.C.A., S.R.I., F.P. contributed to drafting a significant portion of the manuscript or figures.

Acknowledgements

This study was supported by UCB Pharma. This research was funded in whole or in part by a senior clinical fellowship from the Medical Research Council [MR/V007173/1], Wellcome Trust Fellowship [104079/Z/14/Z], BMA Research Grants- Vera Down grant (2013) and Margaret Temple (2017), Epilepsy Research UK (P1201), the Fulbright UK-US commission (MS-Society research award), the Irish Clinical Academic Training Programme (Wellcome Foundation), the National Institute for Health Research (NIHR) Oxford Biomedical Research Centre (BRC) and Oxford Health BRC. For the purpose of Open Access, the author has applied a CC BY public copyright license to any Author Accepted Manuscript (AAM) version arising from this submission. FP is supported by a Dorothy Hodgkin Early Career Fellowship in Chemistry in association with Somerville College. TY is supported by the Ministry of Health, Singapore through the National Medical Research Council (NMRC/Fellowship/0038/2016 and MOH-TA20nov-002).

Conflict of Interest Statement

SRI has received honoraria/research support from UCB, Immunovant, MedImmun, Roche, Janssen, Cerebral therapeutics, ADC therapeutics, Brain, CSL Behring, and ONO Pharma and receives licensed royalties on patent application WO/2010/046716 entitled "Neurological Autoimmune Disorder," and has filed two other patents entitled "Diagnostic method and therapy" (WO2019211633 and US-2021-0071249-A1; PCT application WO202189788A1) and "Biomarkers" (PCT/GB2022/050614 and WO202189788A1).

Data Availability Statement

Anonymized data and code will be shared by request from any qualified investigator.

References

1. World Health Organization. Epilepsy: A Public Health Imperative. World Health Organization; 2019 [cited 2023 Aug 16]. Available from: https://apps.who.int/iris/handle/10665/325293
2. Ngugi AK, Bottomley C, Kleinschmidt I, Sander JW, Newton CR. Estimation of the burden of active and lifetime epilepsy: a meta-analytic approach. Epilepsia. 2010;51(5):883-890.
3. Dalmau J, Geis C, Graus F. Autoantibodies to synaptic receptors and neuronal cell surface proteins in autoimmune diseases of the central nervous system. Physiol Rev. 2017;97(2):839-887.
4. Ramanathan S, Al-Diwani A, Waters P, Irani SR. The autoantibody-mediated encephalitides: from clinical observations to molecular pathogenesis. J Neurol. 2021;268(5):1689-1707.
5. Sun B, Ramberger M, O'Connor KC, et al. The B cell immunobiology that underlies CNS autoantibody-mediated diseases. Nat Rev Neurol. 2020;16(9):481-492.
6. Thompson J, Bi M, Murchison AG, et al. The importance of early immunotherapy in patients with faciobrachial dystonic seizures. Brain J Neurol. 2018;141(2):348-356.
7. Flanagan EP, Geschwind MD, Lopez-Chiriboga AS, et al. Autoimmune encephalitis misdiagnosis in adults. JAMA Neurol. 2023;80(1):30-39.
8. Van Steenhoven RW, de Vries JM, Bruijstens AL, et al. Mimics of autoimmune encephalitis. Neurol Neuroimmunol Neuroinflamm. 2023;10(6):e200148.
9. Steriade C, Britton J, Dale RC, et al. Acute symptomatic seizures secondary to autoimmune encephalitis and autoimmune-associated epilepsy: conceptual definitions. Epilepsia. 2020;61(7):1341-1351.
10. Smith KM, Dubey D, Liebo GB, Flanagan EP, Britton JW. Clinical course and features of seizures associated with LGI1-antibody encephalitis. Neurology. 2021;97(11):e1141-e1149.
11. Nosadini M, Eyre M, Molteni E, et al. Use and safety of immunotherapeutic management of N-methyl-D-aspartate receptor antibody encephalitis: a meta-analysis. JAMA Neurol. 2021;78(11):1333-1344.

12. Dalmau J, Graus F. Antibody-mediated encephalitis. N Engl J Med. 2018;378(9):840-851.
13. Lee SK, Lee S-T. The laboratory diagnosis of autoimmune encephalitis. J Epilepsy Res. 2016;6(2):45-52.
14. Nagana Gowda GA, Raftery D. Biomarker discovery and translation in metabolomics. Curr Metabolomics. 2013;1 (3):227-240.
15. Jurynczyk M, Probert F, Yeo T, et al. Metabolomics reveals distinct, antibody-independent, molecular signatures of MS, AQP4-antibody and MOG-antibody disease. Acta Neuropathol Commun. 2017;5(1):95.
16. Lennox B, Xiong W, Waters P, et al. The serum metabolomic profile of a distinct, inflammatory subtype of acute psychosis. Mol Psychiatry. 2022;1–9:4722-4730.
17. Irani SR, Bera K, Waters P, et al. N-methyl-D-aspartate antibody encephalitis: temporal progression of clinical and paraclinical observations in a predominantly non-paraneoplastic disorder of both sexes. Brain. 2010;133 (6):1655-1667.
18. Irani SR, Alexander S, Waters P, et al. Antibodies to Kv1 potassium channel-complex proteins leucine-rich, glioma inactivated 1 protein and contactin-associated protein-2 in limbic encephalitis, Morvan's syndrome and acquired neuromyotonia. Brain. 2010;133(9):2734-2748.
19. Soininen P, Kangas AJ, Würtz P, et al. High-throughput serum NMR metabonomics for cost-effective holistic studies on systemic metabolism. Analyst. 2009;134 (9):1781-1785.
20. Tynkkynen T, Mursu J, Nurmi T, Tuppurainen K, Laatikainen R, Soininen P. NMR protocol for determination of oxidation susceptibility of serum lipids and application of the protocol to a chocolate study. Metabolomics. 2012;8(3):386-398.
21. Oostendorp M, Engelke UFH, Willemsen MAAP, Wevers RA. Diagnosing inborn errors of lipid metabolism with proton nuclear magnetic resonance spectroscopy. Clin Chem. 2006;52(7):1395-1405.
22. Nicholson JK, Foxall PJ, Spraul M, et al. 750 MHz ^{1}H and ^{1}H–^{13}C NMR spectroscopy of human blood plasma. Anal Chem. 1995;67(5):793-811.
23. Wishart DS, Tzur D, Knox C, et al. HMDB: the human metabolome database. Nucleic Acids Res. 2007;35:D521-D526.
24. Thévenot EA, Roux A, Xu Y, Ezan E, Junot C. Analysis of the human adult urinary metabolome variations with age, body mass index, and gender by implementing a comprehensive workflow for univariate and OPLS statistical analyses. J Proteome Res. 2015;14(8):3322-3335.
25. Pang Z, Chong J, Zhou G, et al. MetaboAnalyst 5.0: narrowing the gap between raw spectra and functional insights. Nucleic Acids Res. 2021;49(W1):W388-W396.
26. Woodhall M, Mgbachi V, Fox H, Irani S, Waters P. Utility of live cell-based assays for autoimmune neurology diagnostics. J Appl Lab Med. 2022;7(1):391-393.
27. McCracken L, Zhang J, Greene M, et al. Improving the antibody-based evaluation of autoimmune encephalitis. Neurol Neuroimmunol Neuroinflamm. 2017;4(6):e404.
28. Zhang F, Gao X, Liu J, Zhang C. Biomarkers in autoimmune diseases of the central nervous system. Front Immunol. 2023;14:1111719.
29. Wesselingh R, Griffith S, Broadley J, et al. Peripheral monocytes and soluble biomarkers in autoimmune encephalitis. J Autoimmun. 2023;135:103000.
30. Levraut M, Bourg V, Capet N, et al. Cerebrospinal fluid IL-17A could predict acute disease severity in non-NMDA-receptor autoimmune encephalitis. Front Immunol. 2021;12:673021.
31. Brenner J, Mariotto S, Bastiaansen AEM, et al. Predictive value of serum neurofilament light chain levels in anti-NMDA receptor encephalitis. Neurology. 2023;100(21): e2204-e2213.
32. Anderyas P, Halliday A, Reardon K. Anti-LGI1-associated myopathy in the setting of neuromuscular hyperexcitability syndrome. JAMA Neurol. 2022;79 (12):1319-1320.
33. Wu K, Wen L, Duan R, et al. Triglyceride level is an independent risk factor in first-attacked neuromyelitis optica spectrum disorders patients. Front Neurol. 2019;10:1230.
34. Tettey P, Simpson S, Taylor B, et al. An adverse lipid profile is associated with disability and progression in disability, in people with MS. Mult Scler. 2014;20 (13):1737-1744.
35. Tettey P, Simpson S, Taylor B, et al. An adverse lipid profile and increased levels of adiposity significantly predict clinical course after a first demyelinating event. J Neurol Neurosurg Psychiatry. 2017;88(5):395-401.
36. Cho EB, Cho H-J, Choi M, et al. Low high-density lipoprotein cholesterol and high triglycerides lipid profile in neuromyelitis optica spectrum disorder: associations with disease activity and disability. Mult Scler Relat Disord. 2020;40:101981.
37. Liu F, Wang B, Wang C, Zhang B, Guo S. Lipid profiles and their potential inflammatory effects in anti-N-methyl-D-aspartate receptor encephalitis. Neurol Sci. 2021;42 (7):2881-2890.
38. Shu Y, Qin B, Xu Y, et al. Lipid metabolism in patients with anti-N-methyl-D-aspartate receptor encephalitis. Neuroimmunomodulation. 2017;24(4–5):256-263.
39. Liu F, Huang T, Wang B, Wang C, Guo S. Low high-density lipoprotein cholesterol and apolipoprotein A-I levels are associated with poor outcome and relapse in autoimmune encephalitis. Neurosci Lett. 2022;775:136546.
40. Campos AM, Maciel E, Moreira ASP, et al. Lipidomics of mesenchymal stromal cells: understanding the adaptation of phospholipid profile in response to pro-inflammatory cytokines. J Cell Physiol. 2016;231(5):1024-1032.

41. Shu Y, Xu Y, Chen C, et al. Serum bilirubin and albumin in anti-N-methyl-D-aspartate receptor encephalitis. Neuroimmunomodulation. 2018;25(4):206-214.
42. Jang Y, Lee S-T, Kim T-J, et al. High albumin level is a predictor of favorable response to immunotherapy in autoimmune encephalitis. Sci Rep. 2018;8(1):1012.
43. Lyons O, Whelan B, Bennett K, O'Riordan D, Silke B. Serum albumin as an outcome predictor in hospital emergency medical admissions. Eur J Intern Med. 2010;21(1):17-20.
44. Ishida S, Hashimoto I, Seike T, et al. Serum albumin levels correlate with inflammation rather than nutrition supply in burns patients: a retrospective study. J Med Invest. 2014;61(3-4):361-368.
45. Manosalva C, Quiroga J, Hidalgo AI, et al. Role of lactate in inflammatory processes: friend or foe. Front Immunol. 2022;12:808799. doi:10.3389/fimmu.2021.808799
46. Amorini AM, Nociti V, Petzold A, et al. Serum lactate as a novel potential biomarker in multiple sclerosis. Biochim Biophys Acta. 2014;1842(7):1137-1143.
47. Miller WL, Auchus RJ. The molecular biology, biochemistry, and physiology of human steroidogenesis and its disorders. Endocr Rev. 2011;32(1):81-151.
48. Mallagaray A, Rudolph L, Lindloge M, et al. Towards a precise NMR quantification of acute phase inflammation proteins from human serum. Angew Chem Int ed. 2023;62(35):e202306154.
49. Ormseth MJ, Chung CP, Oeser AM, et al. Utility of a novel inflammatory marker, GlycA, for assessment of rheumatoid arthritis disease activity and coronary atherosclerosis. Arthritis Res Ther. 2015;17(1):117.
50. Durcan L, Winegar DA, Connelly MA, Otvos JD, Magder LS, Petri M. Longitudinal evaluation of lipoprotein parameters in systemic lupus erythematosus reveals adverse changes with disease activity and prednisone and more favorable profiles with hydroxychloroquine therapy. J Rheumatol. 2016;43(4):745-750.
51. Hanin A, Chollet C, Demeret S, di Meglio L, Castelli F, Navarro V. Metabolomic changes in adults with status epilepticus: a human case-control study. Epilepsia. 2024;65:929-943.

Supporting Information

Additional supporting information may be found online in the Supporting Information section at the end of the article.

Data S1.

Analyst

ROYAL SOCIETY OF CHEMISTRY

PAPER

View Article Online
View Journal | View Issue

Cite this: *Analyst*, 2024, **149**, 1238

Sodium fluoride preserves blood metabolite integrity for biomarker discovery in large-scale, multi-site metabolomics investigations†

Wenzheng Xiong, [a,b] Daniel C. Anthony,[b] Suzie Anthony,[c] Thi Bao Tien Ho, [b] Edouard Louis,[d] Jack Satsangi[e] and Daniel E. Radford-Smith *[a,b]

Background: Metabolite profiling of blood by nuclear magnetic resonance (NMR) is invaluable to clinical biomarker discovery. To ensure robustness, biomarkers require validation in large cohorts and across multiple centres. However, collection procedures are known to impact on the stability of biofluids that may, in turn, degrade biomarker signals. We trialled three blood collection tubes with the aim of solving technical challenges due to preanalytical variation in blood metabolite levels that are common in cohort studies. *Methods*: We first investigated global NMR-based metabolite variability between biobanks, including the large-scale UK Biobank and TwinsUK biobank of the general UK population, and more targeted biobanks derived from multicentre clinical trials relating to inflammatory bowel disease. We then compared the blood metabolome of 12 healthy adult volunteers when collected into either sodium fluoride/potassium oxalate, lithium heparin, or serum blood tubes using different pre-processing parameters. *Results*: Preanalytical variation in the method of blood collection strongly influences metabolite composition within and between biobanks. This variability can largely be attributed to glucose and lactate. In the healthy control cohort, the fluoride oxalate collection tube prevented fluctuation in glucose and lactate levels for 24 hours at either 4 °C or room temperature (20 °C). *Conclusions*: Blood collection into a fluoride oxalate collection tube appears to preserve the blood metabolome with delayed processing up to 24 hours at 4 °C. This method may be considered as an alternative when rapid processing is not feasible.

Received 7th August 2023,
Accepted 2nd December 2023

DOI: 10.1039/d3an01359f

rsc.li/analyst

Introduction

Metabolite profiling of serum and plasma is emerging as an invaluable tool spanning multiple domains of medical research.[1] Nuclear magnetic resonance (NMR)-based metabolomics techniques involve the simultaneous profiling of many metabolites (small molecular intermediates) in a biofluid or other medium.[2] Inexpensive, high-throughput, and highly reproducible, global metabolite quantification by NMR is now being employed at the frontier of medicine, ranging from population-wide health profiling[3,4] to predicting diagnosis,[5] progression,[6] and response to treatment[7] in a spectrum of diseases.

Clinical biomarkers require validation in large cohorts across multiple centres.[8] NMR-based metabolomics requires minimal sample preparation compared to other metabolomics techniques (*i.e.* mass spectrometry methods).[9] Nevertheless, centrifugation speed and time,[10] incubation temperature,[11–13] storage time at −20 °C and −80 °C,[13,14] the type of collection tube,[15,16] and the number of freeze–thaw cycles[11,14,17,18] are just some of the pre-analytical variables known to strongly influence metabolite composition in blood. While many of these variables may be able to be well-controlled within a given study, the time between blood collection and erythrocyte separation by centrifugation and the time to sample storage at −80 °C present unique challenges due to the pragmatic requirements of large-scale, multi-centre clinical trials from which clinical biomarkers may be robustly identified.[13,19,20] These two factors have been shown to drastically influence the relative abundance of metabolites involved in glycolysis.[10–12,14,18,21–26] To date, it has not been investigated

[a]*Department of Chemistry, University of Oxford, Oxford, UK. E-mail: daniel.radford-smith@some.ox.ac.uk*
[b]*Department of Pharmacology, Medical Sciences Division, University of Oxford, Oxford, UK*
[c]*Department of Radiology, Oxford University Hospitals NHS Foundation Trust, Oxford, UK*
[d]*Department of Gastroenterology, University Hospital CHU of Liège, Liège, Belgium*
[e]*Translational Gastroenterology Unit, Nuffield Department of Experimental Medicine, University of Oxford, Oxford, UK*

† Electronic supplementary information (ESI) available. See DOI: https://doi.org/10.1039/d3an01359f

whether the type of blood collection tube used affects metabolite integrity due to a delay in centrifugation and/or sample measurement. Moreover, conflicting evidence exists as to whether other metabolites not directly involved in glycolysis, such as lipoproteins, are affected by time to centrifugation.[14,21] In this study we aimed to systematically evaluate and compare the relative efficacy of sodium fluoride/potassium oxalate, lithium heparin, and additive-free serum blood tubes in preserving metabolite integrity for up to 24-hours before centrifugation, and up to 48-hours before sample measurement after NMR sample preparation. We expected that sodium fluoride/potassium oxalate blood tubes, which inhibit glycolysis, preserve the metabolic state at the time of blood collection more effectively than the widely used lithium heparin or serum blood vacutainers.

Ideally, standard operating procedures (SOPs) are, prospectively, put in place in advance of longitudinal, multicentre research projects to reduce pre-analytical variability in metabolite levels within and between biobanks. In practice, this may be difficult to achieve depending on the scale and resources of individual collection sites. Previous studies have demonstrated conflicting efficacy of keeping blood tubes refrigerated at 4 °C prior to centrifugation, aliquoting, and freezing on the variability in metabolite levels.[13,18,26] Moreover, a secure cold chain may not be feasible in all sites, and the level of compliance to SOPs is unclear and is often left unreported. Most importantly, all previous studies addressing these pre-analytical variables treated all samples identically when varying time to erythrocyte separation and time at room temperature (RT). Therefore, it is largely unsurprising that, in at least one analytical dimension, inter-individual differences are maintained. In practice, this identical treatment of individual differences does not occur; samples may be processed at any time between, for example, 0 and upwards of 24 hours.

Guidelines on how to prepare samples and observations on the effects of delayed erythrocyte separation are insufficient to advance methods of reducing biomarker variability for NMR. Similarly, *z*-scoring of metabolite concentrations to facilitate comparisons across cohorts[3,27] impedes the discovery of healthy and disease-associated metabolite ranges that may be clinically relevant. Practical solutions to stably preserve blood metabolite levels are required, and clear reporting guidelines are required to explain potential non-biological between-sample variability. In this study, we first investigate global NMR-based metabolite variability between biobanks, including the large-scale UK Biobank and TwinsUK biobank of the general UK population, and more targeted biobanks derived from multicentre clinical trials relating to IBD. We then compared the blood metabolome of 12 healthy adult volunteers when collected into either sodium fluoride/potassium oxalate, lithium heparin, or serum blood tubes using different pre-processing parameters, with the aim of determining the optimal tube type for preserving an individual's blood metabolomic fingerprint with significantly delayed sample processing of up to 24 hours.

Methods

Cohorts

UK Biobank. The UK Biobank is a general population cohort recruited from 22 assessment centres across England, Scotland, and Wales between 2006 and 2010. It comprises 502 411 individuals of middle and old age (mean 56.5 years, range 37–73 years). Written, informed consent was provided by all participants. The UK Biobank has generic ethical approval from the Northwest Multi-centre Research Ethics Committee (ref. 11/NW/03820). The current study is registered under the approved research ID 95409. At the time of this study, NMR metabolomic data was available on ~120 000 participants. Individuals were typically non-fasting prior to blood sampling (median fasting time 3 hours, standard deviation 2.4 hours). Whole blood was collected into spray-coated K_2EDTA tubes and immediately centrifuged at 2500*g* for 10 minutes at 4 °C. Plasma was not aliquoted. Rather, tubes were transported to a central storage facility at 4 °C for aliquoting and archiving at −80 °C (mean time from venepuncture to freezing 24 hours, standard deviation 2.5 hours).[28] Acquisition of NMR metabolite data was performed by Nightingale Health Ltd and is described in detail elsewhere.[4]

TwinsUK. TwinsUK is a volunteer twins cohort in the United Kingdom.[29] Generic ethic approval was obtained from Guys & St Thomas' Trust ethics committee. At the time of this study, NMR metabolomic data was available on ~2000 female individuals across up to three timepoints (total samples 4830) collected between 1996 and 2014. The mean age at blood sampling was 59.4 years (range 34–88 years). Samples were collected after a minimum fast of 6 hours into serum separator blood tubes (BDVacutainer®SST™). The tubes were then allowed to rest after 3× inversions for 40 minutes at 4 °C. Samples were centrifuged for 10 minutes at 1439*g*. Serum was collected immediately and stored at −45 °C.[30] Acquisition of NMR metabolite data was performed by Nightingale Health Ltd and is described elsewhere.[27]

STORI. The STORI trial (2006–2009) investigated the risk of relapse in Crohn's disease after cessation of infliximab in patients who had achieved prolonged remission on combination therapy: infliximab alongside antimetabolites.[31] We included in our study patients with a baseline serum aliquot available for analysis (n = 97).

SPARE. The SPARE trial (2015–2021) sought to evaluate three treatment approaches for Crohn's disease patients in steroid-free remission due to combined infliximab and immunosuppressant therapy: maintaining the combination, continuing only the immunosuppressant, or continuing only infliximab.[32] We include here a subgroup of patients from the SPARE trial who had been randomised to infliximab withdrawal and had a baseline serum aliquot available for analysis (n = 63).

In both STORI and SPARE, biomarkers associated with relapse was a pre-defined secondary endpoint. The standard operating procedure for serum collection and processing is provided in the ESI.† Briefly, blood was collected into BD Vacutainer SST II Advance Tubes (BD 367958), allowed to clot,

and centrifuged at room temperature for 10 minutes at 3000*g*. The target for clotting time at room temperature was between 0.5 and 2 h, and the target time-to-freezing of serum aliquots was within 4 hours of the blood draw. Serum aliquots were then stored at −80 °C. All patients provided informed consent and ethical approval was obtained. All patients had been treated with a combination therapy of infliximab (IFX) and anti-metabolite >8 months and had been in sustained steroid-free remission >6 months. Patients were not fasted prior to blood collection.

Healthy volunteers and controlled variation of pre-analytical parameters. 12 healthy volunteers were recruited from Oxford, UK (mean age 30.3 years, range 23–53 years). Blood was collected under informed written consent. Local ethical approval was obtained from the University of Oxford Medical Sciences Interdivisional Research Ethics Committee.

Blood was collected into BD Vacutainer blood tubes® under the conditions described in Table 1. Vacutainer tubes were centrifuged initially at 300*g* for 10 minutes at 4 °C. After the supernatant (either serum or plasma) was carefully collected into a new tube, the sample was again centrifuged at 5000*g* for 10 minutes at 4 °C and the supernatant collected into a new tube and stored at −80 °C prior to sample preparation.

NMR spectroscopy

NMR spectroscopy and global metabolite quantification from serum and plasma was performed in-house for the SPARE, STORI, and healthy volunteer cohorts. On the day of NMR spectroscopy, serum or plasma samples were thawed at room temperature, mixed by pipetting, and combined with 75 mM sodium phosphate buffer prepared in D_2O (pH 7.4) as a 1 : 5 ratio of serum to buffer (total volume 600 μL) in a 5 mm borosilicate glass NMR tube (Norell 502-7).

^{1}H NMR spectra were acquired at 298 K using a 700 MHz Bruker AVIII spectrometer operating at 16.4 T equipped with a ^{1}H [^{13}C/^{15}N] TCI cryoprobe (Department of Chemistry, University of Oxford). 1D NOESY and CPMG experiments were conducted on each sample, and CPMG spectra were used for downstream analysis. Pooled plasma samples were spread throughout the run of the SPARE and STORI samples to monitor technical variation.

NMR Spectra were phased, baseline corrected (using a fifth-degree polynomial), and referenced to the lactate-CH_3 doublet resonance at δ = 1.33 ppm in Topspin 4.1.4 (Bruker). Spectra were exported to ACD/Labs Spectrus Processor Academic Edition 12.01 (Advanced Chemistry Development, Inc.) for data-preprocessing. The NMR spectra were segmented into 100 integral regions using a manual binning approach, with exclusion of noise and water signals. The integration of metabolite peaks was performed judiciously to minimize overlapping and aligned with literature assignments. Resonances were assigned to metabolites using a combination of literature values and 2D spectra of human plasma and serum, leading to the confident identification of 39 metabolites. Spectral regions with overlapped metabolites were annotated in the assignment using a '/' and '[ ]' notation. The absolute integral values were subject to the main statistical analysis unless stated otherwise. Additional statistical analyses using probabilistic quotient normalisation (PQN)[33] and sum normalisation were included in the ESI.† In the healthy control cohort, lactate and glucose levels were also calculated based on the absolute mmol concentration using a standard curve.

Table 1 Summary of pre-analytical parameters in the healthy volunteer cohort. n = 12 per condition

Tube	Time to centrifugation (hours)	Delay between sample preparation and measurement (hours)
Serum (Red, BD 367837)	0.5 RT	0 (RT), 12 (4 °C), 24 (4 °C), 48 (4 °C)
	24 RT	0 (RT)
	24 4 °C	0 (RT)
Lithium Heparin Plasma (Green, BD 367885)	0.5 RT	0 (RT), 12 (4 °C), 24 (4 °C), 48 (4 °C)
	24 RT	0 (RT)
	24 4 °C	0 (RT)
Fluoride/Oxalate Plasma (Grey, BD 368921)	0.5 RT	0 (RT), 12 (4 °C), 24 (4 °C), 48 (4 °C)
	24 RT	0 (RT)
	24 4 °C	0 (RT)

Statistical analysis

Statistical analysis was performed in R 4.1.2 and GraphPad Prism 9. After pareto scaling of the absolute integral values, multivariate principal component analysis (PCA) was performed using the ropls package to visualise and compare individual metabolite profiles in an unsupervised fashion.[34]

Post-hoc analysis of TwinsUK, STORI, and SPARE NMR data was limited to univariate *t*-testing of glucose and lactate metabolite levels, based on inspection of the corresponding PCA loadings plots. UK Biobank NMR metabolite data were further correlated against time of day of blood collection, fasting time, and delay in sample measurement using Pearson's correlation coefficient. In the healthy control cohort, individual metabolites (39 identified metabolites) were subject to repeated measures two-way ANOVA with Šidák *post hoc* test,[35] and Benjamini–Hochberg method was used for p value adjustment to control the false discovery rate across all metabolites. Adjusted two-tailed p values (q values) ≤ 0.05 were considered statistically significant. * $p \leq 0.05$, ** $p \leq 0.01$, *** $p \leq 0.001$.

Results

Lactate and glucose drive metabolite variation between and within biobanks

NMR metabolite data was collated between the UK Biobank and TwinsUK cohorts. As the TwinsUK cohort is predominately female sex, a female cohort from the UK Biobank (n = 4830) was randomly sampled for comparison. Principal component analysis revealed greater variation in the metabolome within

the UK Biobank cohort compared to the TwinsUK cohort along the first principal component, as well as systematic variation between the two biobanks along the same component (Fig. 1A). Inspection of the corresponding loadings plot revealed the key role of lactate in driving this variation along the first principal component, and glucose in driving within-biobank variation along the second principal component (Fig. 1B).

Lactate levels were increased in the UK Biobank cohort (mean 3.7) relative to the TwinsUK cohort (mean 1.37; mean difference 2.36 [Welch's *t*-test 95%CI 2.33–2.40], Fig. 1C). Glucose levels were decreased in the UK Biobank cohort (mean 3.48) relative to the TwinsUK cohort (mean 3.76; mean difference 0.29 [Welch's *t*-test 95%CI 0.26–0.31], Fig. 1D). Using available metadata pertaining to the UK Biobank, we identified systematic, linear variation in plasma lactate

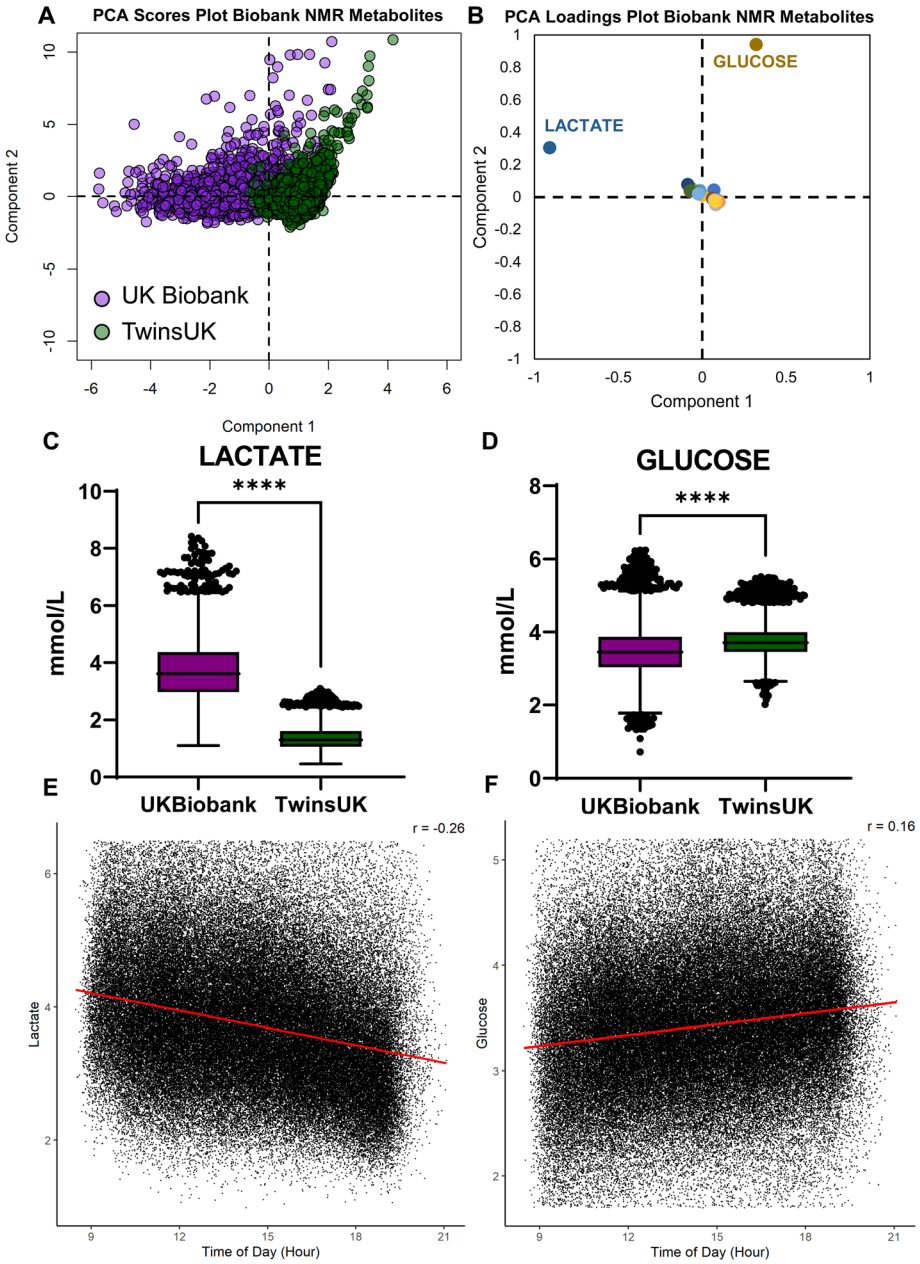

Fig. 1 Lactate and glucose levels drive variation in the blood metabolome within and between biobanks. PCA plot (A) and corresponding loadings plot (B) of TwinsUK and sampled female UK Biobank participants with blood metabolomics data. Boxplots comparing lactate (C) and glucose (D) levels in participants between the UK Biobank and TwinsUK study indicate systematically elevated lactate levels and decreased glucose levels in the UK Biobank, both $p < 0.0001$. Pearson correlation between time of day of sample collection and lactate (E) or glucose (F) concentration in the UK Biobank samples, both $p < 0.0001$. Samples collected earlier in the day likely had a delayed processing time as compared to samples collected later in the day.

(Pearson's r = −0.26, n = 118 021, Fig. 1E) and glucose (Pearson's r = 0.16, n = 118 021, Fig. 1F) levels according to the time of sample collection. This may correspond to a systematic delay between sample collection and centrifugation according to queued collected samples.

As a second example, and on a smaller scale, lactate and glucose were also found to drive serum metabolome variation between clinical biobank data pertaining to the SPARE and STORI cohorts (Fig. 2). Here, data acquisition and relative metabolite quantification were performed in-house. The PCA scores plot (Fig. 2A) and corresponding loadings plot (Fig. 2B) illustrate systematic variation in lactate and glucose levels along the second principal component. Glucose levels were decreased in the STORI cohort (mean 0.0058) relative to the SPARE cohort (mean 0.011; mean difference 0.0055 [Welch's t-test 95%CI 0.0046–0.63]). Lactate levels were increased in the STORI cohort (mean 0.13) relative to the SPARE cohort (mean 0.053; mean difference 0.073 [Welch's t-test 95%CI 0.064–0.082]). These differences are visualised in the median NMR spectrum of each cohort (Fig. 2E).

Effects of delayed sample measurement on absolute plasma and serum metabolite concentrations

UK Biobank metabolomic metadata was used to determine the effect of time between sample preparation and measurement on plasma metabolite levels. Approximately 25% of samples were run within 12 hours of sample preparation, 63% within 24 hours, and 97% within 48 hours (Fig. 3A). The top six metabolites had a Pearson correlation coefficient >0.1 (p < 0.0001) and are shown in Fig. 3B–G. Plasma histidine concentration showed a strong negative correlation with time to sample preparation (Pearson's r = −0.36, Fig. 3B). Glycine (r =

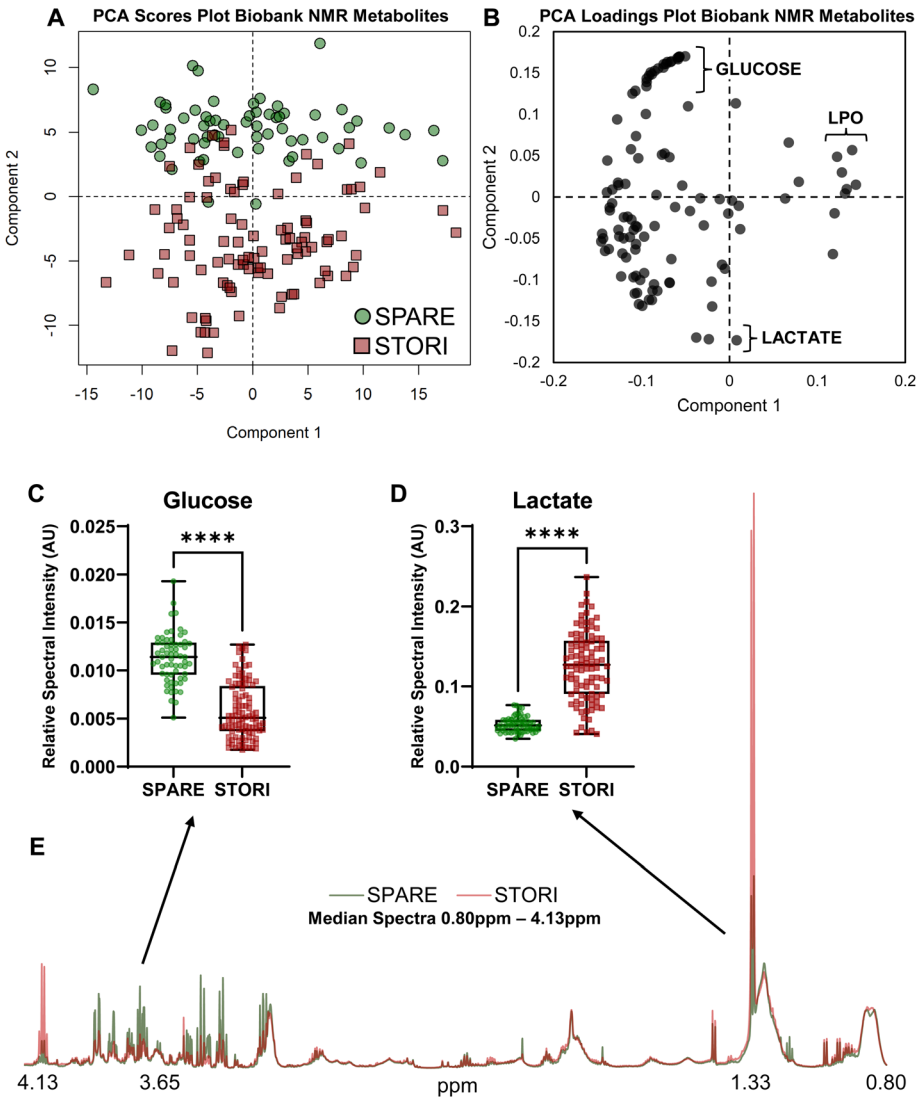

Fig. 2 Lactate and glucose levels contribute to blood metabolite variation between discovery and validation cohorts in clinical trials. PCA plot (A) and corresponding loadings plot (B) of the SPARE and STORI participant baseline serum metabolomics data. Variation between cohorts is driven by serum glucose (C) and lactate (D) resonances, both p < 0.0001. Median NMR spectrum of SPARE and STORI samples (E).

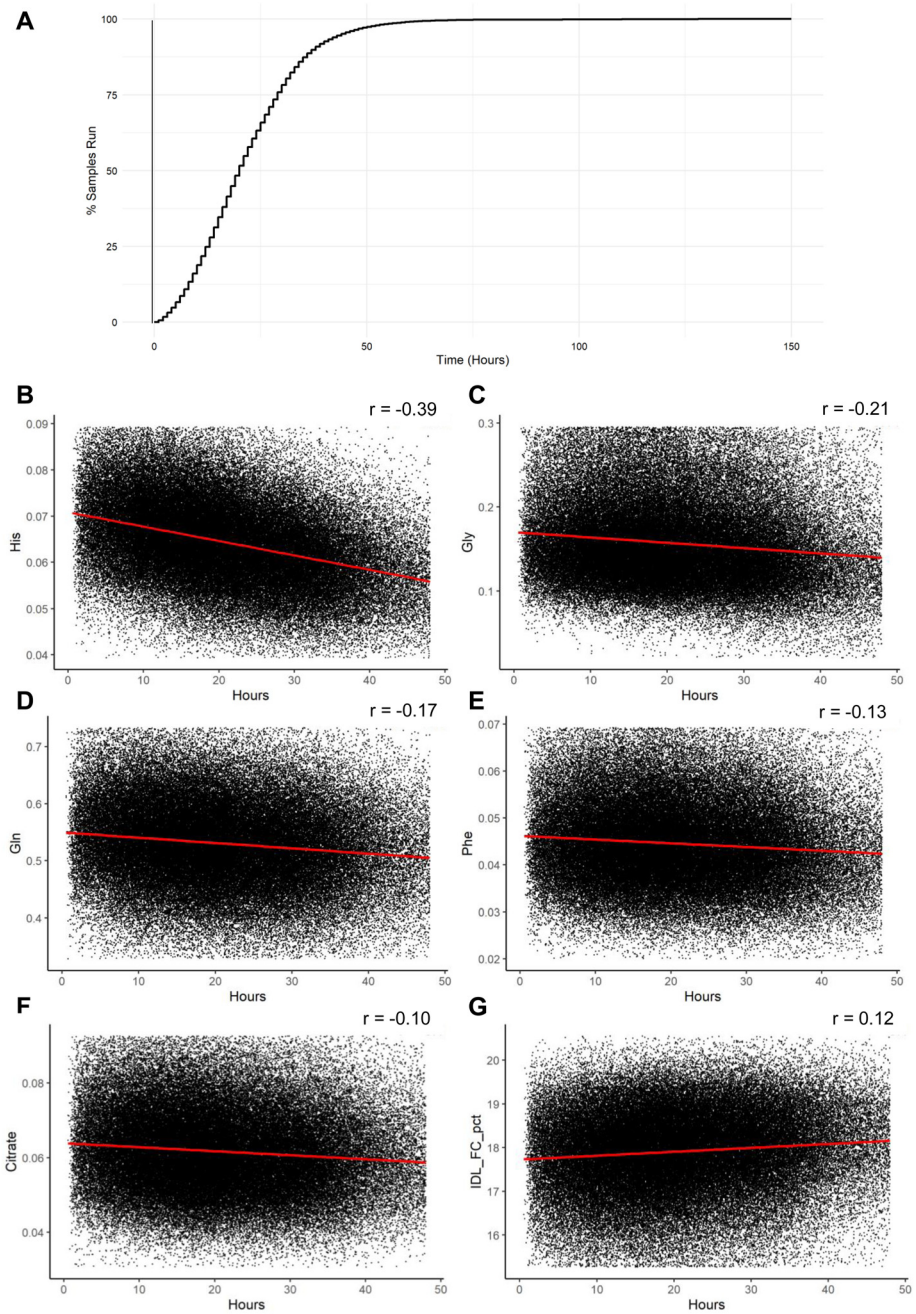

Fig. 3 Histidine is the metabolite predominately affected by delayed sample measurement in the UK Biobank. Line graph indicating the percentage of plasma samples analysed by NMR once prepared for analysis, within a given timeframe (A). Pearson correlation between time to sample measurement by NMR and histidine (B), glycine (C), glutamine (D), phenylalanine (E), citrate (F), and IDL_FC_pct (G), all $p < 0.0001$.

−0.14), glutamine ($r = -0.13$), phenylalanine ($r = -0.09$), citrate ($r = -0.10$) were also negative correlated with time to sample preparation, while free cholesterol in intermediate density lipoprotein ($r = 0.10$) was positive correlated (Fig. 3C–G, respectively).

In the healthy control cohort ($n = 12$ per condition), we found changes in the metabolome as a result of delayed sample measurement (Fig. 4). Consistent with data from the UK Biobank, the effect of delayed sample measurement was small relative to interindividual variation (Fig. 4A, B, and S1†). Most samples shifted in the second component in the PCA scores plot, driving by decreased levels of glucose, high-density lipoprotein (HDL) and glycerophosocholine (Fig. 4C and D). The stability of the serum/plasma metabolome was maintained even after a 12-hour delay in NMR measurement, as demonstrated by minimal changes in metabolite levels (Fig. 4C). However, when LH Plasma samples were subjected to a 24-hour delay in measurement, a significant decrease was

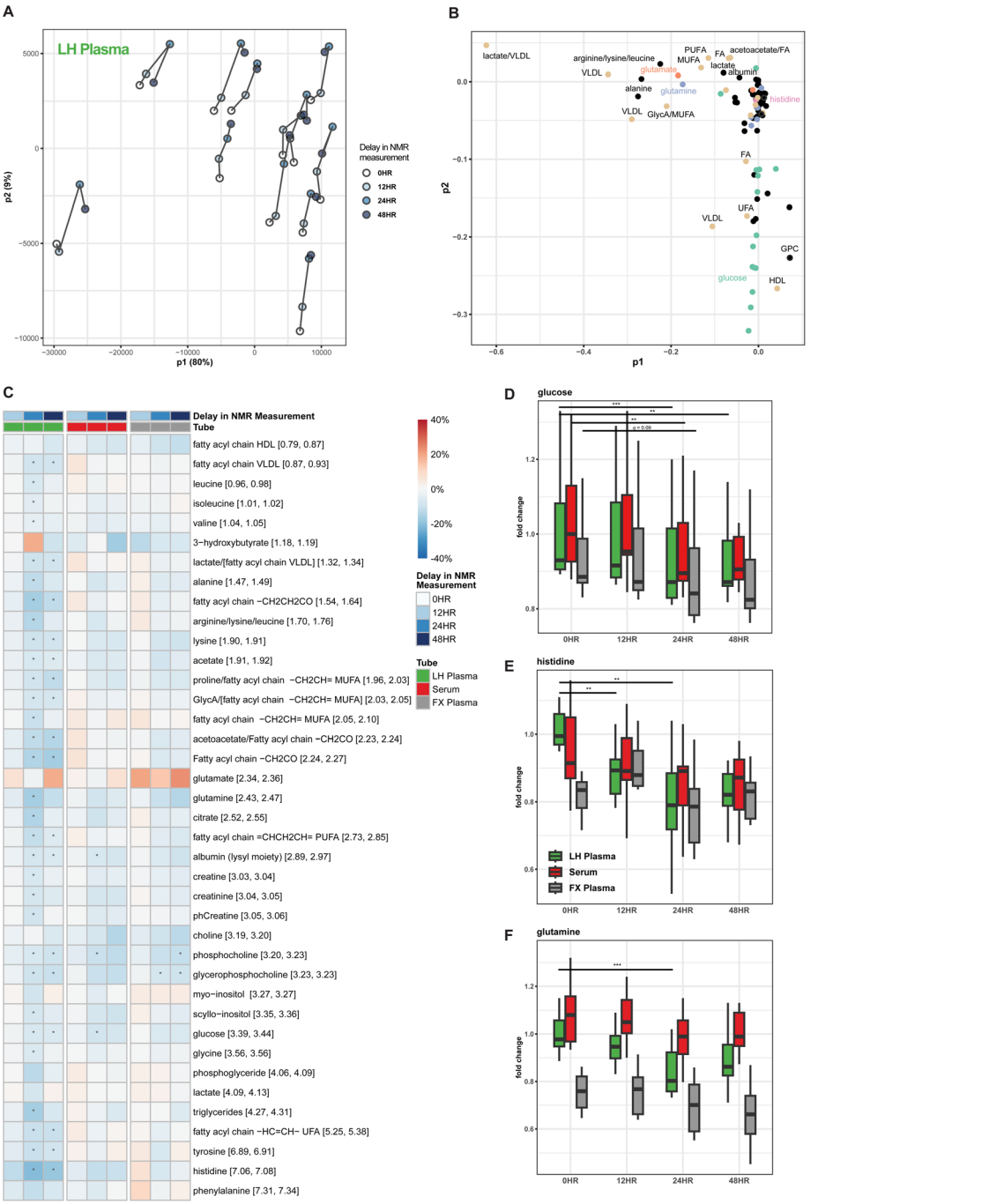

Fig. 4 Variation in the metabolome due to delayed sample measurement is small compared to interindividual variation in the healthy control cohort. PCA scores plot (A) demonstrating the effect of delayed NMR measurement on LH plasma samples. Each line connects samples from the same individual. Loadings plot (B) illustrating the metabolites that contribute to the variation observed in principal component 1 and 2. Heatmap (C) displaying percentage changes in metabolite levels resulting from varied delays in NMR measurement across three types of plasma/serum. The numbers in square brackets represent the corresponding spectral region boundaries in parts per million (ppm). Percentage changes calculated from absolute integral values and compared to the optimum processing condition. Significant differences in means of metabolites were represented by * (q < 0.05). Boxplots presenting the effect of delayed NMR measurement on levels of histidine (D), glutamine (E), and glutamate (F). "/" indicates the mentioned metabolites are overlapped in the spectral region. Metabolite names in square brackets refers to non-dominant overlapping metabolites also found in that spectral region.

observed in 31 out of 39 metabolites. Notably, it was observed that LH Plasma samples started forming precipitates after 12 hours, and all samples exhibited precipitates after 24 hours. In contrast, serum and FX plasma demonstrated better stability than LH Plasma after a 24-hour and even 48-hour delay in measurement as indicated by changes in per-

centages of most metabolites below 10% and significant alterations observed in only a few metabolites (Table S1†). The majority of metabolites showed a decreasing trend resulting from the delay in measurement, except for glutamate, which tended to increase over time, particularly in FX plasma (Fig. 4C). Albumin, phosphocholine, glycerophosphocholine and glucose levels significantly decrease after 24 hours in at least two types of plasma/serum samples. Aligning with our observations in the UK Biobank dataset, histidine and glutamine levels tend to decrease over time, especially after 24 hours in LH Plasma (Fig. 4E and F, and Table S1†).

Metabolite differences by tube type using optimal processing parameters in the healthy control cohort

We next investigated how abundances of metabolites differed between BD Vacutainers under optimal processing conditions. Absolute metabolite concentrations of LH plasma (green) and serum (red) tubes were comparable (Fig. S2, and Table S2†). In contrast, the total integral of the spectra (spectral intensity) from FX plasma (grey) was reduced in both the NOESY and CPMG experiments due to the decline in albumin and lipoprotein levels in FX plasma (Fig. S2†). When using a PQN or sum-normalised approach to adjust for the total integral between samples and make FX plasma comparable, few differences remained between tube types (Table S2†). Branched chain amino acids (BCAAs, including leucine, isoleucine, valine) were increased in FX tubes relative to LH plasma and serum. And 3-hydroxybutyrate levels increased in FX plasma compared to LH plasma and serum, potentially influenced by variations in the lipoprotein line shape (Fig. S2†).

Evaluation of a fluoride/oxalate additive to preserve inter-individual metabolite variation using realistic timepoints

Lastly, we investigated whether the combination of sodium fluoride and potassium oxalate in a BD Vacutainer could mitigate against preanalytical variation in the individual blood metabolome. As expected, 24-hours at either RT or 4 °C resulted in an increase in lactate and a decrease in glucose when stored in either LH plasma or serum tubes (Fig. 5A–D, and Fig. S3†). When LH plasma samples were centrifuged after a 24-hour delay at 4 °C, the lactate levels increased 34% and the glucose levels decreased 18% (Table S2†). The alterations were similar for the serum samples, and further exacerbated when the samples were left at RT prior to centrifugation. Conversely, FX tubes effectively prevented anaerobic glycolysis for at least 24-hours at RT. Only 7% decrease was observed in glucose levels when FX plasma samples were centrifuged after a 24-hour delay at 4 °C. It should be noted that as demonstrated previously, glucose levels decreased 6% in FX plasma (q = 0.096, two-way ANOVA, sidak *post hoc*, FDR correction across metabolites, Table S1†) after 24 hours delay in NMR measurement at 4 °C. Therefore, the decrease of glucose in FX tubes was likely due to general degradation not due to anaerobic glycolysis.

Moreover, the combination of using FX tubes and refrigerating the blood tube during the pre-processing interval effectively prevented metabolite variation between an optimal, 30-minute pre-centrifugation delay and the 24-hour delay (Fig. 5A and E). Without refrigeration, glutamate and glutamine levels changed dramatically after 24 hours at RT (Table S2†).

Discussion

Blood is the main biofluid utilised in epidemiological studies utilising metabolomics to predict disease onset, severity, and treatment response. We hypothesised that fluoride oxalate vacutainer blood collection tubes would thus be a more appropriate blood tube for metabolome studies. To test this hypothesis, we systematically investigated the effect of preanalytical variation in blood sample handling in lithium heparin, fluoride oxalate, and serum blood tubes. To our knowledge, we demonstrate for the first time that the use of FX plasma tubes in combination with refrigeration at 4 °C negates metabolome variation due to preanalytical factors. This is important, as lactate and glucose are established biomarkers for the early diagnosis of cancer,[36,37] and may prove important to the diagnosis and prediction of other diseases when integrated into multivariate blood metabolite algorithms.[3] Our findings suggest that fluoride oxalate tubes could be beneficial in metabolomic studies where there is variability in blood processing times, pending further validation with a broader range of metabolites and larger sample sizes.

Our initial investigations revealed that much of the variation in metabolite levels within and between blood biobank cohorts could be attributed to variations in glycolysis metabolites. This variation is attributed to residual anaerobic glycolysis occurring when erythrocyte separation from serum or plasma is delayed. Delayed sample processing due to a high volume of samples being processed (UK Biobank) or collection methods where the rapid processing of bloods was not prioritised (STORI) led to increased lactate and decreased glucose resonances compared to cohorts where rapid blood processing was prioritised (TwinsUK and SPARE cohorts). As normal lactate levels are <2 mmol,[38] the absolute concentrations reported in the UK Biobank are not suitable for clinical translation.

Sodium fluoride and potassium oxalate act in concert to inhibit glycolysis in blood samples.[39] Specifically, sodium fluoride inhibits the enzyme enolase, which catalyses the conversion of 2-phosphoglycerate (2-PG) into phosphoenolpyruvate (PEP), the penultimate step in glycolysis. Potassium oxalate precipitates calcium ions to inhibit the clotting cascade. Fluoride oxalate tubes, as expected, showed baseline differences in amino acid levels and glycolytic metabolites compared to serum.[15] Consistent with other studies, the metabolite profile of serum and lithium heparin plasma were comparable,[15] and behaved similarly in response to delayed erythrocyte separation.[21]

Previous studies have documented the effects of delayed erythrocyte separation on metabolite levels as quantified by

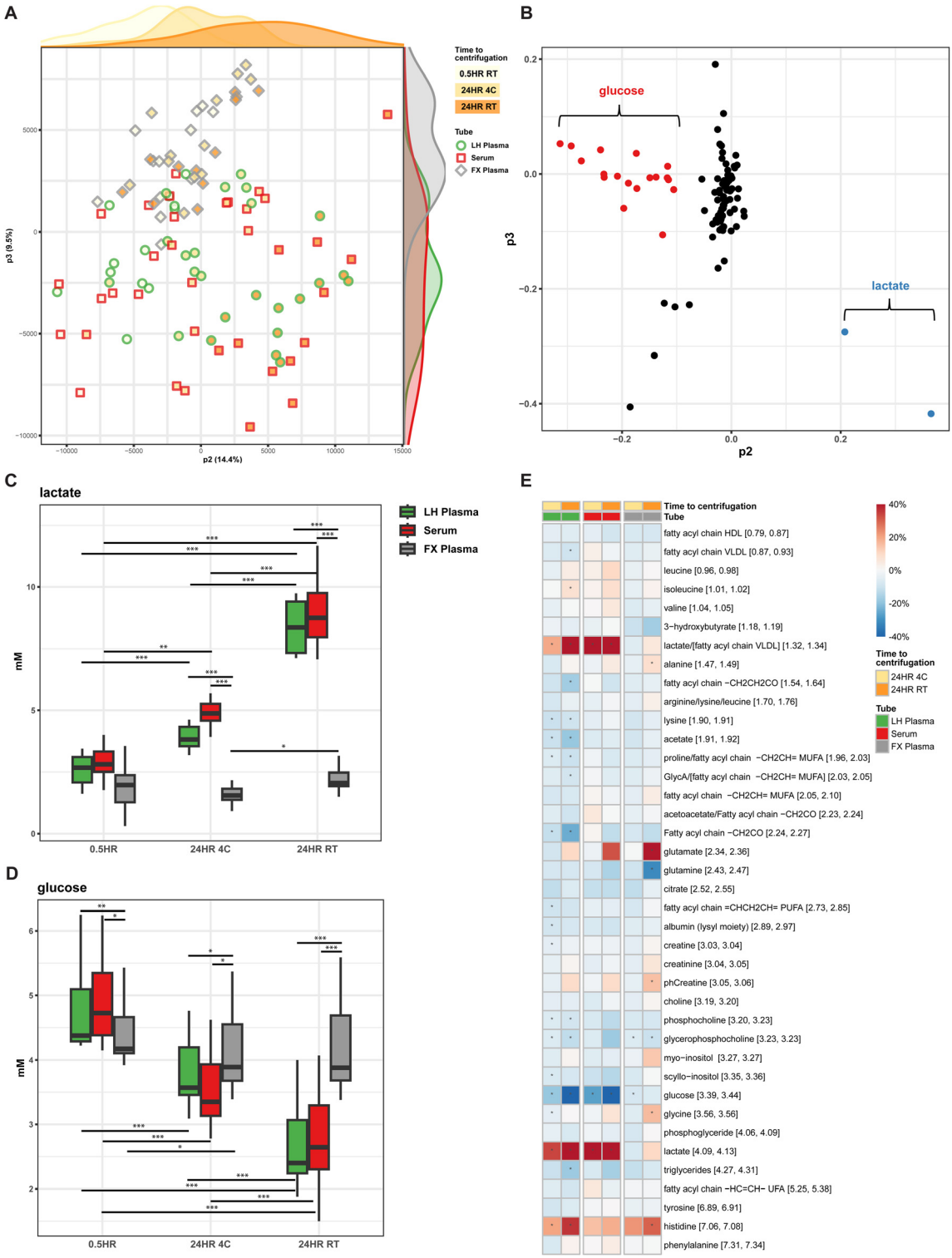

Fig. 5 Fluoride oxalate blood collection tubes prevent changes to the metabolome for at least 24 hours when stored at 4 °C. PCA scores plot (A) demonstrating the influence of different pre-processing conditions on samples, specifically observed in PC2. Loadings plot (B) of the PCA highlighting glucose and lactate as contributors to the variation observed in PC2. Boxplots showing increased lactate levels (C) and decreased glucose levels (D) in delayed pre-processing conditions for LH plasma and serum, but not in FX plasma. Heatmap (E) presenting percentage changes in metabolite levels resulting from varied pre-processing conditions across three types of plasma/serum. The numbers in square brackets represent the corresponding spectral region boundaries in parts per million (ppm). Percentage changes calculated from absolute integral values and compared to the optimum pre-processing condition. Significant differences in means of metabolites were represented by * ($q < 0.05$). "/" indicates the mentioned metabolites are overlapped in the spectral region. Metabolite names in square brackets refers to non-dominant overlapping metabolites also found in that spectral region.

NMR-based metabolomics techniques.[10,12–14,17,19,21–24,40] Consistent with our own study, lactate and glucose are typically most affected. However, in contrast to other reports,[18] we also clearly show in both the UK Biobank and healthy volunteer data that residual glycolytic metabolism does occur (in the absence of an inhibitor of glycolysis) even when blood is stored at 4 °C prior to centrifugation.

After separation of serum or plasma from erythrocytes, metabolite variation is minimal. In the UK Biobank cohort, only histidine showed a significant effect of delay in sample measurement ($r = -0.39$) compared to interindividual biological variation. Other metabolites, while significantly correlated with measurement delay, showed smaller effect sizes between 0.01 and 0.21 which are less relevant relative to the observed interindividual variation. In our healthy volunteer study, we also investigated a delay in sample measurement over a similar timeframe, for up to 48 hours at 4 °C. Again, we found minimal variation in metabolite levels, consistent with the UK Biobank data and early UK Biobank pilot studies that tested delays of up to 24 hours at 4 °C.[41] Such variation is suitable to be corrected by previously described statistical techniques.[42]

We also provide suggestions for reporting preanalytical variation to aid in the synergy of future metabolomic studies. The reporting guideline consists of key information relating to the individual, the pre-processing variables, and the post-processing variables that may differ between samples in a single study (Table 2). The guidelines do not include variables that should be controlled for within a study and ideally between studies, for example, long-term storage temperature of frozen samples, and NMR spectra acquisition parameters. We have shown that fasting time can strongly influence the concentration of certain metabolites, primarily ketone bodies (Fig. S4†). Recording the time of blood collection, centrifugation, and storage temperatures allows studies to record SOP compliance, for which data is sorely lacking in biomarker research, and may also help identify mistreated samples. The UK Biobank has implemented pipelines that allow for automated reporting of key information. For example, barcoded blood tubes were used that, when scanned, allowed for automated logging of sample collection and processing.[43]

We recognise the limitations of this study. When comparing the UK Biobank and TwinsUK metabolomics datasets, we limited the comparison to non-lipid data (amino acids and energy metabolites) due to non-overlapping metabolite data and uncertainty in how these values were derived between the two cohorts. While our study provided insights using NMR-based metabolite profiling, which focused on metabolites commonly assayed by this technique, we acknowledge that the scope was limited with respect to the range of metabolites analysed. Future research could extend these findings by incorporating a broader spectrum of metabolomic analyses, including mass spectrometry and advanced lipoprotein assays, as well as labile metabolites detectable by NMR such as coenzymes and antioxidants,[44] to provide a more comprehensive understanding of preanalytical variability across different platforms.

In the healthy control cohort, blood storage in fluoride oxalate tubes resulted in a slight negative bias in glucose levels under optimal processing conditions, which is consistent with previous reports.[45] This bias did not show variation over time. As we suggest that the fluoride oxalate tube type should be implemented between and across studies, this small, systematic difference will not affect metabolome variability. However, the presence of this negative bias may affect the reported prevalence of fasting hyperglycaemia, which may be relevant for the screening of diabetes mellitus in the general population. Studies have also shown that both sodium fluoride[46] and potassium oxalate[47] have the potential to cause haemolysis after prolonged standing time at room temperature. We considered other, more effective methods of inhibiting glycolysis, such as citrate-buffered tubes,[46] which are also less prone to haemolysing samples over time. However, these additives are known to interfere with the NMR spectrum and the concentrations of neighbouring metabolites.[15] In our study, haemolysis was detected only in fluoride oxalate tubes left at room temperature, and not at 4 °C. Nevertheless, we encourage the discovery of novel additives that inhibit major metabolic pathways in blood under anaerobic conditions and in the absence of haemolysis.

Table 2 Key reporting parameters for blood metabolomic profiling by NMR in cohort studies

Variable	Reported by
Time since last meal (hours)	Participant
Time of blood collection	Phlebotomist
Storage temperature pre-centrifugation	
Time centrifuged	Blood processing technician
Temperature during centrifugation	
Time frozen	
Time of NMR sample preparation	NMR technician
Storage temperature pre-data acquisition	
Time of data acquisition	

Conclusions

Pre-analytical variation in blood sample collection cause variation within and between biobank biomarker studies. We trialled three blood collection tubes with the aim of solving technical challenges due to preanalytical variation in blood metabolite levels that are common in cohort studies. We found that a combination of refrigeration at 4 °C and the use of a fluoride/oxalate additive prevented changes in metabolite levels, as compared to optimal processing parameters, for at least 24 hours prior to erythrocyte separation. We also showed that the effect of delayed sample measurement on the stability of quantified metabolites was small, but dependent on the type of blood collection tube used at the pre-processing stage. Using this information, we devised a short list of key reporting guidelines that could be implemented in future cohort studies to improve the reproducibility of blood metabolite signatures as biomarkers of health and disease.

Data availability

Metabolomics data have been deposited to the EMBL-EBI MetaboLights database[48] (**https://doi.org/10.1093/nar/gkz1019**, with the identifier MTBLS8861).

Author contributions

Conceptualisation – DCA & DRS; data curation – WX & DRS; formal analysis – WX & DRS; investigation – JS, EL, SA, & DRS; methodology – DRS, SA, WX, & HTBT; supervision – DCA & DRS; writing draft – WX & DRS; writing review and editing – WX, DCA, SA, HTBT, EL, JS, & DRS.

Conflicts of interest

There are no conflicts to declare.

References

1 D. S. Wishart, Emerging applications of metabolomics in drug discovery and precision medicine, *Nat. Rev. Drug Discovery*, 2016, **15**(7), 473–484.
2 O. Beckonert, H. C. Keun, T. M. D. Ebbels, *et al.*, Metabolic profiling, metabolomic and metabonomic procedures for NMR spectroscopy of urine, plasma, serum and tissue extracts, *Nat. Protoc.*, 2007, **2**(11), 2692–2703.
3 T. Buergel, J. Steinfeldt, G. Ruyoga, *et al.*, Metabolomic profiles predict individual multidisease outcomes, *Nat. Med.*, 2022, **28**(11), 2309–2320.
4 H. Julkunen, A. Cichońska, M. Tiainen, *et al.*, Atlas of plasma NMR biomarkers for health and disease in 118,461 individuals from the UK Biobank, *Nat. Commun.*, 2023, **14**(1), 604.
5 D. E. Radford-Smith, E. A. Selvaraj, R. Peters, *et al.*, A novel serum metabolomic panel distinguishes IgG4-related sclerosing cholangitis from primary sclerosing cholangitis, *Liver Int.*, 2022, **42**(6), 1344–1354.
6 F. Probert, A. Walsh, M. Jagielowicz, *et al.*, Plasma Nuclear Magnetic Resonance Metabolomics Discriminates Between High and Low Endoscopic Activity and Predicts Progression in a Prospective Cohort of Patients With Ulcerative Colitis, *J. Crohns Colitis*, 2018, **12**(11), 1326–1337.
7 G. Caspani, G. Turecki, R. W. Lam, *et al.*, Metabolomic signatures associated with depression and predictors of antidepressant response in humans: A CAN-BIND-1 report, *Commun. Biol.*, 2021, **4**(1), 903.
8 D. Vuckovic, Current trends and challenges in sample preparation for global metabolomics using liquid chromatography–mass spectrometry, *Anal. Bioanal. Chem.*, 2012, **403**(6), 1523–1548.
9 M. Jacob, A. L. Lopata and M. Dasouki, Abdel Rahman AM. Metabolomics toward personalized medicine, *Mass Spectrom. Rev.*, 2019, **38**(3), 221–238.
10 E. Jobard, O. Trédan, D. Postoly, *et al.*, A Systematic Evaluation of Blood Serum and Plasma Pre-Analytics for Metabolomics Cohort Studies, *Int. J. Mol. Sci.*, 2016, **17**(12), 2035.
11 P. Yin, A. Peter, H. Franken, *et al.*, Preanalytical aspects and sample quality assessment in metabolomics studies of human blood, *Clin. Chem.*, 2013, **59**(5), 833–845.
12 D. L. Santos Ferreira, H. J. Maple, M. Goodwin, *et al.*, The Effect of Pre-Analytical Conditions on Blood Metabolomics in Epidemiological Studies, *Metabolites*, 2019, **9**(4), 64.
13 J. L. Alexander, N. J. Wyatt, S. Camuzeaux, *et al.*, Considerations for peripheral blood transport and storage during large-scale multicentre metabolome research, *Gut*, 2024, **73**, 379–383, [cited 2023 May 23]; available from: **https://gut.bmj.com/content/early/2023/02/07/gutjnl-2022-329297**.
14 J. Pinto, M. R. M. Domingues, E. Galhano, *et al.*, Human plasma stability during handling and storage: impact on NMR metabolomics, *Analyst*, 2014, **139**(5), 1168–1177.
15 J. Sotelo-Orozco, S.-Y. Chen, I. Hertz-Picciotto and C. M. Slupsky, A Comparison of Serum and Plasma Blood Collection Tubes for the Integration of Epidemiological and Metabolomics Data, *Front. Mol. Biosci.*, 2021, **8**, 682134, [cited 2023 May 24]. Available from: **https://www.frontiersin.org/articles/10.3389/fmolb.2021.682134**.
16 A. Vignoli, L. Tenori, C. Morsiani, P. Turano, M. Capri and C. Luchinat, Serum or Plasma (and Which Plasma), That Is the Question, *J. Proteome Res.*, 2022, **21**(4), 1061–1072.
17 I. H. Muti, M. Gonzalez Sanchez-Dahl, A. B. Zhong, *et al.*, Designing a quality assurance process for quality control of nuclear magnetic resonance metabolomics studies of human blood, *NMR Biomed.*, 2023, **36**(4), e4868.
18 O. Fliniaux, G. Gaillard, A. Lion, D. Cailleu, F. Mesnard and F. Betsou, Influence of common preanalytical variations on the metabolic profile of serum samples in biobanks, *J. Biomol. NMR.*, 2011, **51**(4), 457–465.
19 C. Ellervik and J. Vaught, Preanalytical variables affecting the integrity of human biospecimens in biobanking, *Clin. Chem.*, 2015, **61**(7), 914–934.
20 G. Anton, R. Wilson, Z. Yu, *et al.*, Pre-Analytical Sample Quality: Metabolite Ratios as an Intrinsic Marker for Prolonged Room Temperature Exposure of Serum Samples, *PLoS One*, 2015, **10**(3), e0121495.
21 J. Debik, S. H. Isaksen, M. Strømmen, *et al.*, Effect of Delayed Centrifugation on the Levels of NMR-Measured Lipoproteins and Metabolites in Plasma and Serum Samples, *Anal. Chem.*, 2022, **94**(49), 17003–17010.
22 M. V. Fomenko, L. V. Yanshole and Y. P. Tsentalovich, Stability of Metabolomic Content during Sample Preparation: Blood and Brain Tissues, *Metabolites*, 2022, **12**(9), 811.
23 P. Bernini, I. Bertini, C. Luchinat, P. Nincheri, S. Staderini and P. Turano, Standard operating procedures for pre-analytical handling of blood and urine for metabolomic studies and biobanks, *J. Biomol. NMR.*, 2011, **49**(3–4), 231–243.

24 C. Brunius, A. Pedersen, D. Malmodin, *et al.*, Prediction and modeling of pre-analytical sampling errors as a strategy to improve plasma NMR metabolomics data, *Bioinformatics*, 2017, **33**(22), 3567–3574.
25 K. M. McClain, S. C. Moore, J. N. Sampson, *et al.*, Preanalytical Sample Handling Conditions and Their Effects on the Human Serum Metabolome in Epidemiologic Studies, *Am. J. Epidemiol.*, 2021, **190**(3), 459–467.
26 T. C. Peakman and P. Elliott, The UK Biobank sample handling and storage validation studies, *Int. J. Epidemiol.*, 2008, **37**(suppl_1), i2–i6.
27 C. Barrios, J. Zierer, P. Würtz, *et al.*, Circulating metabolic biomarkers of renal function in diabetic and non-diabetic populations, *Sci. Rep.*, 2018, **8**(1), 15249.
28 N. E. Allen, M. Arnold, S. Parish, *et al.*, Approaches to minimising the epidemiological impact of sources of systematic and random variation that may affect biochemistry assay data in UK Biobank, *Wellcome Open Res.*, 2021, **5**, 222.
29 A. Moayyeri, C. J. Hammond, D. J. Hart and T. D. Spector, The UK Adult Twin Registry (TwinsUK Resource), in *Twin Research and Human Genetics*, Cambridge University Press, 2013, vol. 16((1)), pp. 144–149.
30 Z. Yu, G. Zhai, P. Singmann, *et al.*, Human serum metabolic profiles are age dependent, *Aging Cell*, 2012, **11**(6), 960–967.
31 E. Louis, J.-Y. Mary, G. Vernier-Massouille, *et al.*, Maintenance of remission among patients with Crohn's disease on antimetabolite therapy after infliximab therapy is stopped, *Gastroenterology*, 2012, **142**(1), 63–70. e5; quiz e31.
32 E. Louis, M. Resche-Rigon, D. Laharie, *et al.*, Withdrawal of infliximab or concomitant immunosuppressant therapy in patients with Crohn's disease on combination therapy (SPARE): a multicentre, open-label, randomised controlled trial, *Lancet Gastroenterol. Hepatol.*, 2023, **8**(3), 215–227.
33 S. Cacciatore, L. Tenori, C. Luchinat, P. R. Bennett and D. A. MacIntyre, KODAMA: an R package for knowledge discovery and data mining, *Bioinformatics*, 2017, **33**(4), 621–623.
34 E. A. Thévenot, A. Roux, Y. Xu, E. Ezan and C. Junot, Analysis of the Human Adult Urinary Metabolome Variations with Age, Body Mass Index, and Gender by Implementing a Comprehensive Workflow for Univariate and OPLS Statistical Analyses, *J. Proteome Res.*, 2015, **14**(8), 3322–3335.
35 H. Singmann, B. Bolker, J. Westfall, F. Aust and M. S. Ben-Shachar, afex: Analysis of factorial experiments. *R package version 013–145*. 2015.
36 J. R. Larkin, S. Anthony, V. A. Johanssen, *et al.*, Metabolomic Biomarkers in Blood Samples Identify Cancers in a Mixed Population of Patients with Nonspecific Symptoms, *Clin. Cancer Res.*, 2022, **28**(8), 1651–1661.
37 E. Goldberg, S. Ievari-Shariati, B. Kidane, *et al.*, Comparative metabolomics studies of blood collected in streck and heparin tubes from lung cancer patients, *PLoS One*, 2021, **16**(4), e0249648.
38 C. D. Foucher and R. E. Tubben Lactic Acidosis, in *Lactic Acidosis [Updated 2022 Jul 18]*, StatPearls Publishing, Treasure Island (FL), Available from: **https://www.ncbi.nlm.nih.gov/books/NBK470202/**.
39 R. Gambino, Sodium fluoride: an ineffective inhibitor of glycolysis, *Ann. Clin. Biochem.*, 2013, **50**(Pt 1), 3–5.
40 C. Cruickshank-Quinn, L. K. Zheng, K. Quinn, R. Bowler, R. Reisdorph and N. Reisdorph, Impact of Blood Collection Tubes and Sample Handling Time on Serum and Plasma Metabolome and Lipidome, *Metabolites*, 2018, **8**(4), 88.
41 R. H. Barton, J. K. Nicholson, P. Elliott and E. Holmes, High-throughput ^{1}H NMR-based metabolic analysis of human serum and urine for large-scale epidemiological studies: validation study, *Int. J. Epidemiol.*, 2008, **37**(suppl_1), i31–i40.
42 S. C. Ritchie, P. Surendran, S. Karthikeyan, *et al.*, Quality control and removal of technical variation of NMR metabolic biomarker data in ~120,000 UK Biobank participants, *Sci. Data*, 2023, **10**(1), 64.
43 P. Downey and T. C. Peakman, Design and implementation of a high-throughput biological sample processing facility using modern manufacturing principles, *Int. J. Epidemiol.*, 2008, **37**(suppl_1), i46–i50.
44 G. A. Nagana Gowda, V. Pascua and D. Raftery, Anomalous Dynamics of Labile Metabolites in Cold Human Blood Detected Using ^{1}H NMR Spectroscopy, *Anal. Chem.*, 2023, **95**(34), 12923–12930.
45 W. S. Waring, L. E. Evans and C. T. Kirkpatrick, Glycolysis inhibitors negatively bias blood glucose measurements: potential impact on the reported prevalence of diabetes mellitus, *J. Clin. Pathol.*, 2007, **60**(7), 820–823.
46 G. Lippi, M. Nybo, J. Cadamuro, J. T. Guimaraes, E. van Dongen-Lases and A.-M. Simundic, Chapter Four - Blood Glucose Determination: Effect of Tube Additives, in *Advances in Clinical Chemistry*, ed. G. S. Makowski, Elsevier, 2018. pp. 101–123 [cited 2023 May 24]. Available from: **https://www.sciencedirect.com/science/article/pii/S0065242317300689**.
47 J. G. Elferink, The mechanism of calcium oxalate crystal-induced haemolysis of human erythrocytes, *Br. J. Exp. Pathol.*, 1987, **68**(4), 551–557.
48 K. Haug, K. Cochrane, V. C. Nainala, *et al.*, MetaboLights: a resource evolving in response to the needs of its scientific community, *Nucleic Acids Res.*, 2020, **48**(D1), D440–D444.

metabolites

MDPI

Article

Extraction Methods for Brain Biopsy NMR Metabolomics: Balancing Metabolite Stability and Protein Precipitation

Wenzheng Xiong [1,2], Florian Zirpel [3], M. Zameel Cader [3], Daniel C. Anthony [2] and Fay Probert [1,*]

[1] Department of Chemistry, University of Oxford, Oxford OX1 3TA, UK; wenzheng.xiong@some.ox.ac.uk
[2] Department of Pharmacology, Medical Sciences Division, University of Oxford, Oxford OX1 3QT, UK; daniel.anthony@pharm.ox.ac.uk
[3] Nuffield Department of Clinical Neurosciences, University of Oxford, Oxford OX3 9DU, UK; florian.zirpel@ndcn.ox.ac.uk (F.Z.); zameel.cader@ndcn.ox.ac.uk (M.Z.C.)
* Correspondence: fay.probert@chem.ox.ac.uk

Abstract: Background/Objectives: Metabolic profiling of tissue samples via liquid-state nuclear magnetic resonance (NMR) requires the extraction of polar metabolites in a suitable deuterated solvent. Such methods often prioritise metabolite recovery over protein removal due to the relatively low sensitivity of NMR metabolomics and the routine use of methods able to supress residual protein signals. However, residual protein may impact metabolite integrity and the metabolite stability after NMR sample preparation is often overlooked. This study aimed to investigate the effect of residual protein contamination in rodent brain extracts and identify a reproducible extraction method that optimises metabolite recovery while ensuring sample stability. **Methods**: The performance of acetonitrile/water (50–100% MeCN), methanol/water (50–100% MeOH), and methanol/water/chloroform ($MeOH/H_2O/CHCl_3$) were assessed for extraction efficiency, reproducibility, residual protein contamination, and metabolite stability up to eight hours post NMR sample preparation. **Results**: Aspartate and glutamate deuteration were observed in 50% MeCN, 50% MeOH, and 67% MeOH extractions along with the conversion of N-acetyl aspartate to aspartate and acetate in 50% MeCN and 50% MeOH extractions. Both observations correlated with residual protein contamination and, thus, are a result of inadequate protein precipitation, as confirmed by ultrafiltration. $MeOH/H_2O/CHCl_3$ extraction preserved the stability of these metabolites while maintaining good extraction efficiency and reproducibility. **Conclusions**: Thus, we recommend $MeOH/H_2O/CHCl_3$ extraction for untargeted brain NMR metabolic profiling due to its effective protein precipitation and reliable performance. Nonetheless, the performance of detecting metabolites prone to oxidation such as ascorbate and glutathione is not improved by this method.

Keywords: metabolomics; extraction; brain; NMR; metabolites

Citation: Xiong, W.; Zirpel, F.; Cader, M.Z.; Anthony, D.C.; Probert, F. Extraction Methods for Brain Biopsy NMR Metabolomics: Balancing Metabolite Stability and Protein Precipitation. *Metabolites* **2024**, *14*, 609. https://doi.org/10.3390/metabo14110609

Academic Editor: Andreas Stadlbauer

Received: 30 September 2024
Revised: 1 November 2024
Accepted: 6 November 2024
Published: 10 November 2024

1. Introduction

Metabolic profiling aims to measure the full complement of low-molecular-weight metabolites within biological samples, offering a biochemical snapshot that mirrors the current physiological condition of an organism [1]. The field of metabolomics, particularly in examining brain tissues, has evolved, allowing researchers to interrogate the biochemical shifts associated with varying physiological states and to understand better the downstream molecular mechanisms that contribute to the outcome of individual disease pathologies [2].

Nuclear magnetic resonance (NMR) and mass spectrometry (MS) are the primary analytical techniques in metabolomics research. Although NMR has limitations in sensitivity, detecting metabolites above micromolar levels, its advantages are significant. These include high reproducibility, intrinsic quantification capabilities, and a non-destructive analytical process, meaning the sample remains intact after data acquisition. Additionally, pulse programmes can be used to suppress chemical shifts arising from macromolecules,

which greatly simplifies sample preparation [3]. Notably, NMR accounts for about 20% of all brain metabolomics research, as indicated by PubMed data showing 383 references for "metabolomics AND brain AND nuclear magnetic resonance NOT MRI NOT HRMAS" compared to 1600 for "metabolomics AND brain AND mass spectrometry NOT MSI" over the last two decades.

Metabolic profiling via liquid-state NMR requires the extraction of biological tissue samples, the concentration of metabolites to levels compatible with NMR detection, and the simultaneous removal of macromolecules in a manner that preserves metabolite stability. The selection of the extraction method, including the choice of extraction solvent, depends on factors such as the type of biological sample studied and the molecules of interest. Methanol/water and acetonitrile/water are commonly favoured for their efficient extraction of polar metabolites, precipitation of proteins, analytical compatibility, and ease of handling [4]. Additionally, methanol/water/chloroform is commonly used for simultaneous biphasic extraction of polar and non-polar metabolites and for improved protein precipitation, despite being more time-consuming [5].

The choice of extraction solvent can significantly impact reproducibility, metabolite recovery, and protein removal. For instance, methanol has emerged as the preferred extractant for plasma samples due to its superior performance in these areas compared to acetonitrile [6–10]. Similarly, different extraction methods have been evaluated in liver tissues, where acetonitrile/water demonstrated the highest metabolite yield but also recovered some macromolecules and lipids, whereas methanol/water/chloroform provides excellent deproteinisation while maintaining high yield and reproducibility [5]. In NMR analysis of brain extracts, acetonitrile/water also showed better yield compared to methanol/water and methanol/dichloromethane/water, while methanol/water showed lower reproducibility [11].

Due to the reduced sensitivity of NMR relative to MS along with the routine use of pulse programs, such as the Carr–Purcell–Meiboom–Gill sequence, which filter out macromolecule signals, extraction methods which prioritise metabolite recovery over deproteinisation are often favoured in NMR metabolomics studies. However, residual proteins in samples may still alter metabolic profiles either through enzymatic activity or binding to free metabolites. Indeed, it has been shown that brain homogenates, containing residual protein, undergo significant metabolic changes with prolonged incubation, whereas minimal changes occur in the aqueous phase of brain extracts subjected to the methanol/chloroform/water method after incubation [12]. Furthermore, Paskevich et al. discovered that after NMR sample preparation, the alpha-hydrogen (αH) of aspartate was replaced by deuterium from the NMR buffer, whereas deproteinated samples extracted with a methanol/water/chloroform mixture could prevent this replacement [13].

This observation gives rise to the hypothesis that residual proteins in brain NMR samples can continue to alter the metabolome. While residual enzymatic activity is a well-documented issue in metabolomics, particularly for biofluids such as serum, plasma, and urine, where it has been extensively studied [14–17], these biofluids can often be analysed directly by NMR after being mixed with an appropriate buffer, without the need for an extraction step. In contrast, brain tissue samples require a more complex preparation process, including an extraction step, to obtain a liquid-state NMR spectrum. Prior to NMR analysis, mixing the lyophilised brain tissue extracts with the NMR buffer (e.g., deuterated phosphate buffer, pH 7.4) can potentially reactivate residual enzymes, leading to metabolite conversions. Despite the critical role of extraction in preparing brain tissues for NMR analysis, no research has systematically investigated the relationship between metabolite stability and residual protein levels across different extraction methods in rodent brain extracts. The study at hand aims to bridge this gap in knowledge by evaluating whether such alterations exist with commonly used extraction methods, understanding their impact, and identifying ways to control them. By minimising the effects of preanalytical variability, we can ensure that the measured metabolites accurately reflect the in vivo state, leading to improved interpretation. Specifically, we will assess the extraction performance of various solvents on

mouse brain tissues, focusing on extraction efficiency, reproducibility, metabolite stability up to eight hours post NMR sample preparation, and residual protein concentrations (Figure 1). We hypothesise that adequate protein precipitation will preserve metabolite integrity during delays between sample preparation and analytical measurement, thereby providing more reliable NMR-based metabolic profiles.

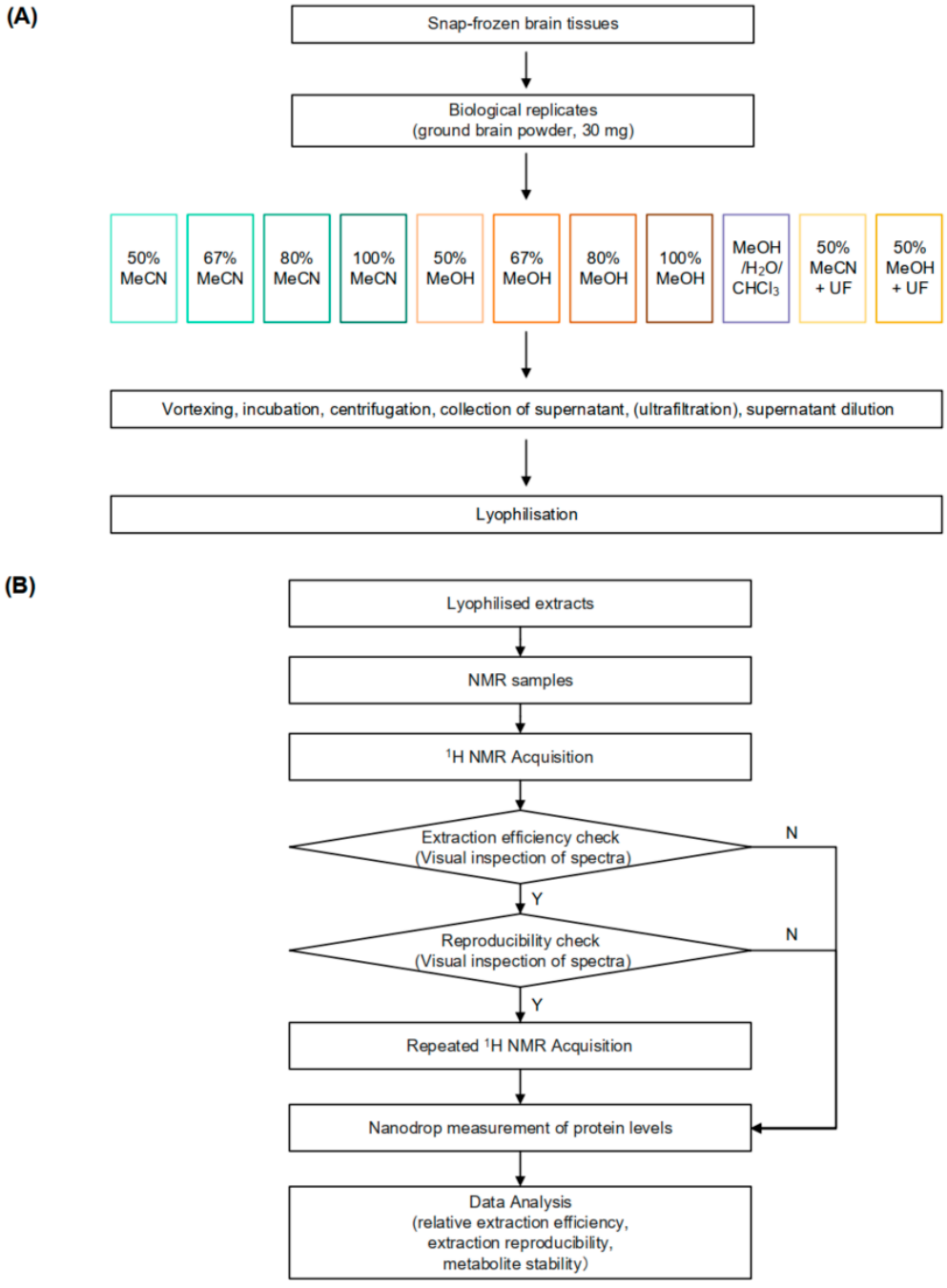

Figure 1. Workflow of sample preparation and NMR acquisition for metabolic profiling of brain tissues using various extraction methods. (**A**) Steps for brain metabolite extraction. (**B**) Flow of ^{1}H NMR data acquisition and data analysis. The criteria for good extraction efficiency and reproducibility are defined as having a relative extraction efficiency greater than 0.7 and a median relative standard deviation (RSD) of less than 20%. UF, ultrafiltration. N, no. Y, yes.

For our evaluation, we included 11 extraction methods: acetonitrile (MeCN, 50%, 67%, 80%, 100%, v/v), methanol (MeOH, 50%, 67%, 80%, 100%, v/v), methanol/water/chloroform ($MeOH/H_2O/CHCl_3$, 2:1:2, v/v), 50% MeCN with ultrafiltration, and 50% MeOH with ultrafiltration. Acetonitrile and methanol were selected as the primary extraction solvents due to their ability to precipitate proteins, extract wide ranges of metabolites, and their widespread application in metabolomics [18]. Acetonitrile is relatively less polar than methanol, making it less soluble for proteins [19], while methanol is relatively more polar, thereby increasing solubility for polar metabolites [8]. The ratio of organic solvent to water is important for efficient protein removal [19]. We included varying concentrations of methanol and acetonitrile to identify a balanced ratio optimising both metabolite recovery and sufficient protein precipitation. In this study, 50% MeOH and 50% MeCN were used as negative controls due to their observed instability of the key metabolites. These methods provided a baseline for comparison, allowing us to evaluate the performance of more optimised extraction protocols in maintaining metabolite stability. The methanol/water/chloroform method, widely used in brain extraction since its description by Folch [20], was also included. Improved protein precipitation was expected as the decreased polarity of chloroform and the formation of two distinct phases of methanol/chloroform caused proteins to precipitate at the interface. It has been suggested that the addition of chloroform may be required for sufficient lipid removal from lipid-rich tissues such as the brain [5]. Finally, we included the use of ultrafiltration with a molecular weight cut-off (MWCO) filter as a positive control for protein removal.

2. Materials and Methods

2.1. Brain Tissues

Brain tissues were collected from C57BL/6/J mice, after the animals were terminally anesthetised with isoflurane and transcardially perfused with heparinised saline (5000 USP/L). Samples were stored at −80 °C until they were used for experimental purposes.

Snap-frozen brain tissues were pooled and homogenised using a pestle and mortar on dry ice, a widely recognised method in metabolomics for ensuring consistency across biological replicates [5,11,12,21,22]. A brain mass of 30 mg (resulting in 42 replicates with a mean of 30.6 ± 0.7 mg) was selected for further extraction based on a balance between metabolite detection sensitivity and tissue conservation [21].

2.2. Brain Metabolite Extraction

Detailed procedures of the 11 extraction protocols used were as follows. The protocols were adapted based on our previous experience and the existing literature [5,11,12,21,22].

2.2.1. MeCN/H_2O Extraction Protocol

For each sample, we added an ice-cold acetonitrile–water mixture, at a ratio of 8-to-1 (in microliters per milligram of sample), with concentrations ranging from 50% to 100% (v/v). This mixture was vortexed vigorously for 30 s to ensure thorough mixing. It was then incubated on ice for 15 min, followed by centrifugation at 16,000× g for 15 min at 4 °C. We collected 200 microliters of the clear supernatant from each sample and diluted it with H_2O to adjust the final acetonitrile concentration to 40%, enabling it to be freeze-dried effectively. Subsequently, these diluted extracts were freeze-dried and stored at −80 °C until use in NMR spectroscopy.

2.2.2. MeOH/H_2O Extraction Protocol

For each sample, an ice-cold methanol–water mixture with varying concentrations (50%, 67%, 80%, and 100% v/v) was added at a ratio of 8 microliters per milligram of sample. Following the addition, the samples were vigorously mixed using a vortex mixer for 30 s, incubated on ice for 15 min, and then centrifuged at 16,000× g for 15 min at 4 °C. From each sample, 200 microliters of the supernatant were collected. The collected supernatants were further diluted with H_2O to achieve a final methanol concentration

of 20%. The resulting extracts were then freeze-dried and stored at −80 °C until use in NMR spectroscopy.

2.2.3. MeOH/H_2O/$CHCl_3$ Extraction Protocol

For each sample, a volume of ice-cold 100% methanol (MeOH) was added at a ratio of 5.3 microliters per milligram of sample. The mixture was then subjected to 30 s of vigorous vortexing. Subsequently, a volume of ice-cold H_2O equivalent to 2.7 times the sample mass (μL/mg) and a volume of ice-cold chloroform ($CHCl_3$) equivalent to 5.3 times the sample mass (μL/mg) were added to each sample. The samples were mixed with a vortex for 30 s, then incubated on ice for 15 min. Following the incubation, the samples were centrifuged at 16,000× *g* for 15 min at 4 °C to facilitate phase separation. After centrifugation, 200 microliters of the aqueous phase (methanol/water phase) was collected from each sample. This collected phase was then diluted with H_2O to adjust the final methanol concentration to 20%. The diluted extracts were freeze-dried and stored at −80 °C until use in NMR spectroscopy.

2.2.4. MeCN/H_2O and MeOH/H_2O Extraction with Ultrafiltration Protocol

A total of 200 μL of MeCN/H_2O or MeOH/H_2O extract was filtered with 10 kD MWCO filters (Amicon® Ultra 0.5mL centrifugal filters UFC501024, Merck KGaA, Darmstadt, Germany; 16,000× *g*, 15 min, 4 °C). Prior to the use, the filters were washed with 500 μL H_2O (16,000× *g*, 30 min, 4 °C) to remove glycerol. Despite the wash, glycerol contamination persisted in ultrafiltration samples. Elusion (about 170 μL) was collected and subsequently diluted with H_2O to create extracts with a final MeCN concentration of 40% or a final MeOH concentration of 20%, lyophilised, and stored at −80 °C until use in NMR spectroscopy.

2.3. H NMR Analysis

Lyophilised extracts were resuspended with 550 μL 75 mM phosphate buffer D_2O (pH 7.4) containing 32.2 μM sodium salt of 3-(trimethylsilyl) propionic acid-2,2,3,3-d_4 (TSP) and transferred to a 5 mm borosilicate NMR tube (NORELL®, Inc., Morganton, NC, USA). Deuterated solvents (D_2O) were used exclusively for preparing the NMR buffer to ensure accurate spectral acquisition and minimise water signal interference. For the extraction protocols, regular non-deuterated water (H_2O) was used, as specified in the main text. NMR spectroscopy was performed using a 700-MHz Bruker AVIII spectrometer (Department of Chemistry, University of Oxford) operating at 16.4 T equipped with a ^1H [$^{13}C/^{15}N$] TCI cryoprobe at 298 K. ^1H NMR spectra were acquired by using the noesygppr1d pulse sequence (Bruker Corporation, Billerica, MA, USA, a one-dimensional nuclear Overhauser effect spectroscopy [NOESY] presaturation scheme) with the following parameters: td = 32,768, d1 = 2 s, p1 = 16.03 μs, ns = 64, aq = 1.46 s, sw = 16 ppm. The total acquisition time for the proposed NOESY spectra was approximately 12 min, consisting of 4 min for data collection and an additional 8 min allocated for sample loading, temperature equilibration, locking, shimming, and tuning. Repeated NMR measurements were conducted for samples that met both the extraction efficiency and reproducibility criteria (defined as extraction efficiency < 0.7 and/or median RSD > 20%), acquiring data at hourly intervals up to an 8-h delay while stored on the carousel at room temperature (Figure 1B).

2.4. Measurement of Protein Concentrations

The protein concentration of each NMR sample was determined using absorbance measurements at 205 nm with the NanoDrop™ One instrument (Thermo Fisher Scientific, Waltham, MA, USA).

2.5. NMR Data Pre-Processing

Resulting free induction decays (FIDs) were zero-filled by a factor of 2 and multiplied by an exponential function corresponding to 0.30 Hz line broadening prior to Fourier trans-

formation. All spectra were phased, baseline corrected (using a 3rd degree polynomial), and chemical shifts referenced to the lactate resonance at δ 1.33 ppm in Topspin 4.1 (Bruker Corporation, Billerica, MA, USA) and exported to ACD/Labs Spectrus Processor Academic Edition 12.01 (Advanced Chemistry Development, Inc., Toronto, ON, Canada).

A semi-targeted analysis approach was employed by manually dividing each NMR spectrum into 86 spectral buckets for integration, excluding noise and water signals, to minimise contributions from varying protein levels across different methods. For samples prepared using MWCO filters, contaminant signals arising from glycerol were also removed. NMR buckets and corresponding assignments are listed in Table S1 (Figure S1, Table S1). Metabolite assignment was performed in reference to the literature values [11–13,23] via metabolite spiking and 2D total correlation spectroscopy (TOCSY) experiments. The absolute integral values were subject to the main statistical analysis unless stated otherwise. Integral values were mean centred and scaled to unit variance prior to principal component analysis.

2.6. Data Analysis

Analysis was performed in the R software 4.1.2 (R foundation for statistical computing, Vienna, Austria). The ggplot2 (version 3.4.2), pheatmap (version 1.0.12), ropls (version 1.26.4), and metabom8 (version 1.0.0) packages were used for the generation of the plots [24–27]. The relative extraction efficiency was determined by calculating the mean total intensity of NMR integrals, normalised to that of the 50% MeCN group. The extraction reproducibility was assessed using the median of the relative standard deviation (RSD) of the replicates for each metabolite resonance. The stability of each spectral bucket was determined by calculating the average percentage change over time up to 8 h for each bucket across three replicates. The one-way analysis of variance (ANOVA) was used to identify significant differences between the means of groups. Two-tailed p-values ≤ 0.05 were considered statistically significant.

3. Results and Discussion

3.1. Relative Extraction Efficiency

Among the 11 methods examined, 50% MeCN, MeOH/H_2O/$CHCl_3$, 50% MeOH, and 67% MeOH showed comparably high extraction efficiency (defined as the total sum of integrals of the 86 spectral buckets measured, normalised to that of the 50% MeCN group), with mean values of 1 ± 0.01, 0.96 ± 0.05, 0.88 ± 0.01, and 0.88 ± 0.03, respectively (p-value > 0.05, one-way ANOVA) (Figure 2A). The remaining nine methods demonstrated lower extraction efficiencies to varying degrees compared to 50% MeCN (p-values < 0.05, one-way ANOVA).

The increase in MeCN and MeOH concentrations led to a decrease in extraction efficiency, with MeCN showing a more pronounced decline. This trend was expected since hydrophilic metabolites had limited solubility in organic solvents such as MeCN, and to a lesser extent, MeOH, and in addition, it is supported by a previous serum extraction study [8]. Furthermore, ultrafiltration with MWCO filters resulted in a 27% reduction in extraction efficiency compared to unfiltered 50% MeCN and a 41% reduction compared to unfiltered 50% MeOH (p-values < 0.001, one-way ANOVA). In addition, residual glycerol arising from the MWCO filters results in large contaminant signals which obscure metabolite resonances, such as the ones for glycine and glutamine and myo-inositol. Representative NMR spectra for each extraction method are shown in Figure S2.

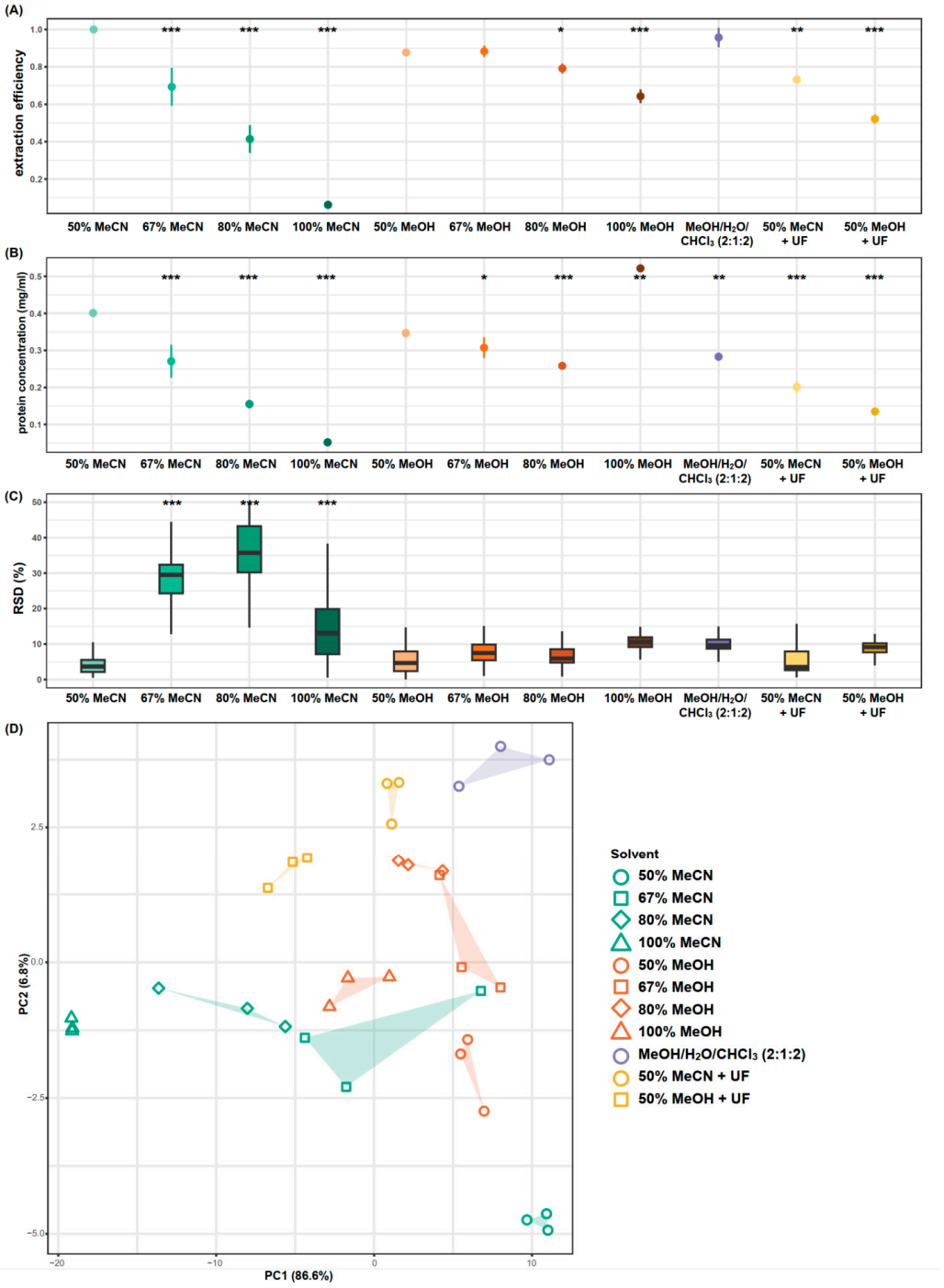

Figure 2. Efficiency and reproducibility of the extraction methods tested. (**A**) Relative extraction efficiency, expressed as the mean ± SEM, calculated as the sum of integrals normalised to that of the 50% MeCN group. (**B**) Protein levels of the NMR samples derived from different brain extracts, expressed as the mean ± SEM. (**C**) Extraction reproducibility, presented in boxplots, as determined by the relative spectral standard deviation across each of the 86 spectral buckets. (**D**) PCA scores plot of the brain metabolic profiles from different extraction methods at 0 h delay in NMR measurement. A smaller spread of the polygon indicates better reproducibility. Results of one-way ANOVA with Dunnett's test for multiple comparisons are reported in reference to the 50% MeCN group. UF, ultrafiltration. * $p < 0.05$, ** $p < 0.01$, *** $p < 0.001$.

3.2. Protein Levels

No significant difference was observed in the protein levels of samples extracted with 50% MeCN and 50% MeOH (p-value > 0.05, one-way ANOVA, n = 3 per group). Increasing concentrations of solvent resulted in lower protein concentrations (p-values < 0.001 and <0.01 for MeCN and MeOH, respectively, one-way ANOVA), with the exception of samples extracted with 100% MeOH which showed higher protein levels (p-value < 0.001, one-way ANOVA). Using MeOH/H_2O/$CHCl_3$ and ultrafiltration also resulted in lower sample protein concentrations compared to 50% MeCN or 50% MeOH (p-value < 0.01, one-way ANOVA), with ultrafiltration yielding the lowest protein concentrations among these three methods (Figure 2B).

3.3. Extraction Reproducibility

The 67% MeCN, 80% MeCN and 100% MeCN extraction methods demonstrated significantly poorer reproducibility compared to the other extraction methods, as determined by RSD across all 86 spectral buckets measured (p-values < 0.001, one-way ANOVA) (Figure 2C). No significant differences were observed between the remaining extraction methods, with median RSDs ranging from 3.54% (interquartile range [IQR] 5.55%) to 10.56% (IQR 2.81%). PCA illustrates the clustering and dispersion patterns of each extraction method, revealing the similarities among and within each method (Figure 2D). Most methods resulted in distinct clusters in the PCA scores plot, highlighting global metabolite differences across these methods. Methods with lower extraction efficiency tended to cluster towards the left side of the scores plot, indicating lower metabolite yield. For instance, as the concentration of MeCN increased, samples tended to cluster further to the left. Conversely, methods with better protein removal, as identified by lower sample protein concentrations, tended to cluster towards the top of the plot.

Five extraction methods, specifically 67% MeCN, 80% MeCN, 100% MeCN, 100% MeOH, and 50% MeOH with ultrafiltration, demonstrated poor extraction efficiency or reproducibility (as defined by extraction efficiencies < 0.7 and/or median RSD > 20%). As a result, these methods were excluded from further metabolite stability testing.

3.4. Metabolite Stability

Metabolite stability was assessed at hourly intervals up to 8 h following sample preparation for the six extraction methods selected in the previous section. Among the six extraction methods that demonstrated adequate efficiency and reproducibility, only two low-concentration metabolites, CoA and adenosine, were undetectable in the 80% MeOH, MeOH/H_2O/$CHCl_3$, and 50% MeCN + UF methods (Figure S3). The trajectory of each extract over time was visualised using a PCA scores plot (Figure 3A). The 50% MeCN, 50% MeOH, and 67% MeOH samples displayed significant drift along the second principal component (PC2). Inspection of the loadings revealed that multiple aspartate signals (2.65–2.84 ppm) and glutamate signals (3.75–3.77 ppm) drove the variability of PC2 (Figure S4). The changes that occur over time are reproducible in each sample, indicating the alteration in metabolic profile is time-dependent; for example, the 8 h samples were equivalent to each other in each extraction method. Table 1 summarises the stability of the whole spectrum over time for each method. The 50% MeCN, 50% MeOH, and 67% MeOH extraction methods resulted in a larger number of metabolite resonances with an RSD greater than 30% after eight hours. A heatmap illustrates the changes in each metabolite resonance over time for the extraction methods (Figure S3), with the most variable metabolites (aspartate, glutamate, N-acetyl aspartate [NAA], acetate, glutathione, and ascorbate) summarised in Figure 3B.

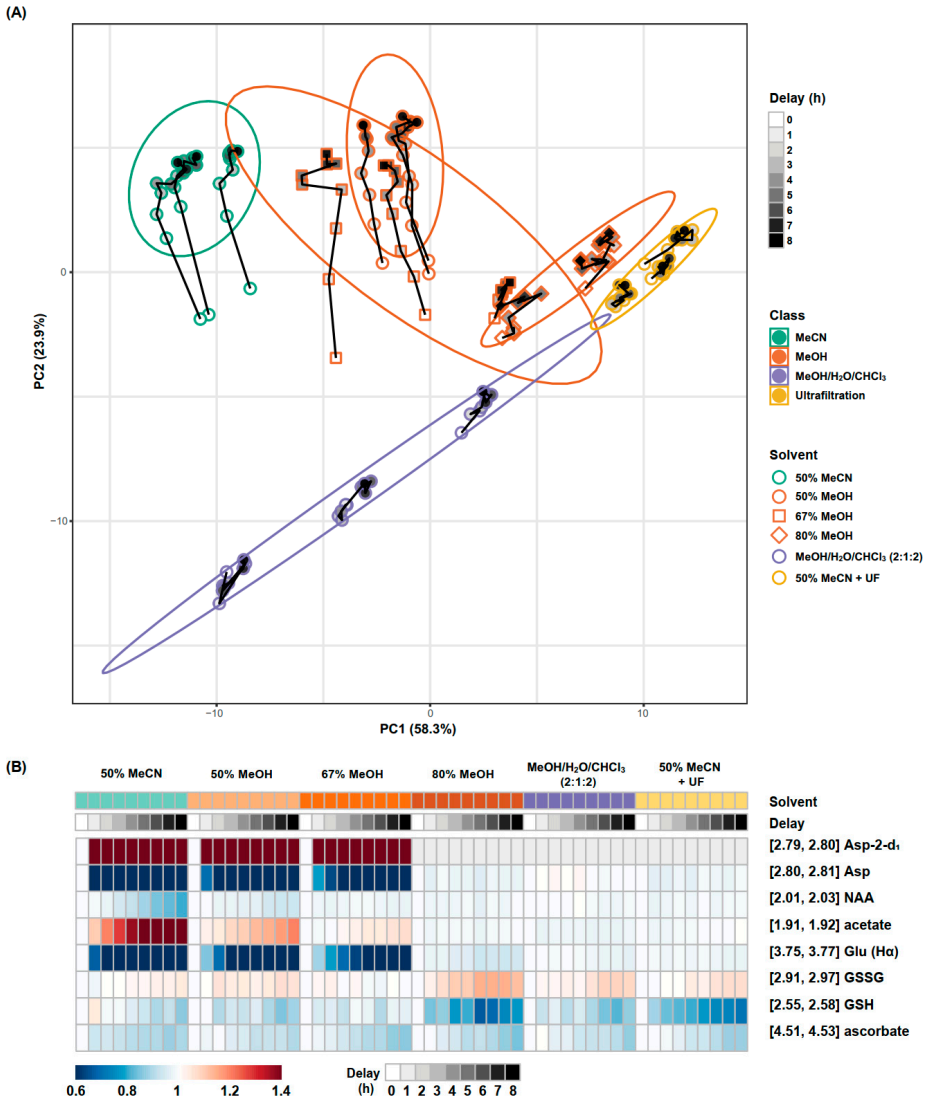

Figure 3. Metabolite extract stability assessment for tested methods. (**A**) PCA scores plot demonstrating the temporal metabolome changes after NMR sample preparation. The ellipse indicates the 95% confidence interval for a multivariate distribution for each extraction method. The trajectory lines connect data points at different delay times from the same sample. (**B**) Heatmap depicting percentage changes, relative to the 0 h timepoint, in unstable metabolites for each extraction method. No aspartate-2-d_1 signals (grey) were observed in the 80% MeOH, MeOH/H_2O/$CHCl_3$ (2:1:2), and 50% MeCN with ultrafiltration groups. UF, ultrafiltration. Asp, aspartate. Glu, glutamate. NAA, N-acetyl aspartate. GSH and GSSG, reduced form and oxidised form of glutathione, respectively.

Table 1. Reproducibility of metabolite resonances over an 8 h delay for NMR analysis for each extraction method.

RSD (%)	Number of Variables (%)					
	50% MeCN	50% MeOH	67% MeOH	80% MeOH	MeOH/ H_2O/$CHCl_3$ (2:1:2)	50% MeCN + UF
0–15	70 (82)	68 (81)	60 (71)	73 (90)	76 (94)	77 (95)
15–30	9 (11)	6 (7)	11 (13)	8 (10)	5 (6)	4 (5)
>30	6 (7)	10 (12)	13 (15)	0 (0)	0 (0)	0 (0)

RSD, relative standard deviation. RSD was calculated over nine timepoints (0–8 h delay) across three replicates for each variable. UF, ultrafiltration.

3.4.1. Aspartate and Glutamate

The instability of aspartate signals was observed in samples extracted with 50% MeCN, 50% MeOH, and 67% MeOH, indicated by a decrease in the doublet of doublet (dd) signals and the generation of nearby doublets signals at 2.82 and 2.68 ppm (p-values < 0.05, one-way ANOVA) (Figures 4 and S3, Table S1). This change was most rapid within the initial hour after NMR sample preparation, with the original aspartate signals disappearing after two hours in samples extracted with 50% MeCN and after four hours in samples extracted with 50% and 67% MeOH (Figure S5).

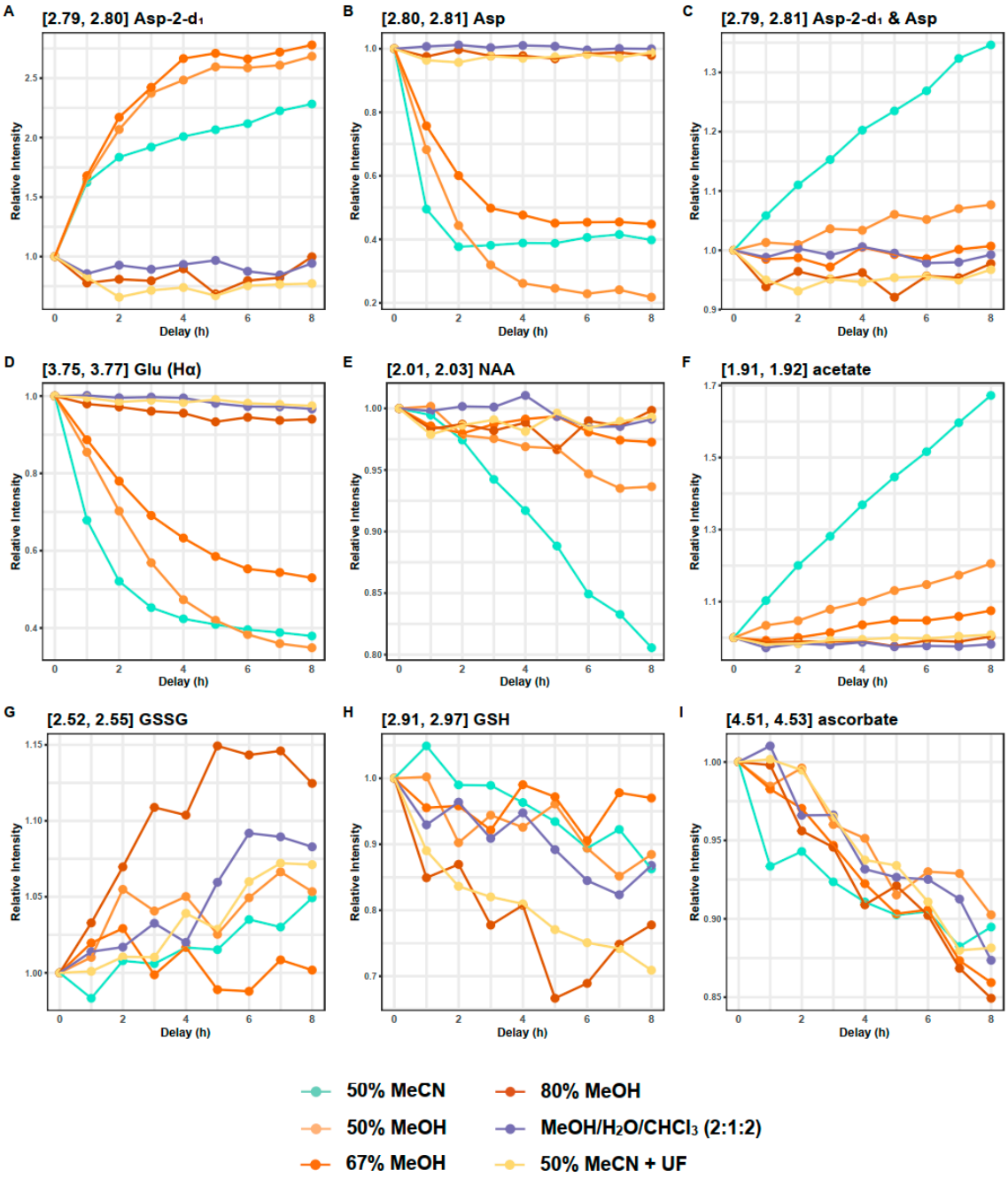

Figure 4. Changes in unstable metabolites across different extracts over time post sample preparation. Each data point refers to the mean of three replicates. Values were normalised to the 0 h delay group within each extraction method. UF, ultrafiltration. Asp, aspartate. Glu, glutamate. NAA, N-acetyl aspartate. GSH and GSSG, reduced form and oxidised form of glutathione, respectively.

Similarly, the glutamate multiplets, observed at 2.12 ppm and 2.35 ppm, exhibited a reduction in splitting in samples extracted with solvent mixtures of 50% MeCN, 50% MeOH, and 67% MeOH (p-values < 0.05, one-way ANOVA) (Figure S3). The overall integrals of these multiplets remained unchanged. Additionally, a considerable reduction was observed in the glutamate dd at 3.76 ppm in samples extracted using these methods (Figure 4). The glutamate dd was completely diminished after four hours in samples extracted with 50% MeCN (Figure S5).

The observed instability in the resonances of aspartate is attributed to the deuteration of aspartate, a phenomenon previously documented by Paskevich et al. [13]. This involves the replacement of the proton at the α-carbon (αH) of aspartate with deuterium, converting aspartate into aspartate-2-d_1. Consequently, it induces a change in the multiplicities of the βCH_2-group in aspartate, transforming the dd from the ABX spin system to AB doublets [13].

Here, similar to aspartate, we observed deuteration of glutamate. Substitution of the glutamate αH with deuterium would result in the disappearance of the resonance at 3.76 ppm and induce changes in the multiplicities of the βCH_2-group without altering the overall integrals.

The deuteration of aspartate and glutamate may be derived from aspartate transaminase (AST)-mediated metabolism. AST catalyses the interconversion of aspartate and α-ketoglutarate to oxaloacetate and glutamate, during which the H2 hydrogens of aspartate and glutamate undergo exchange with those of water (D_2O in the NMR buffer) [28], leading to changes in the observed splitting patterns of NMR resonances. This suggests that AST may have remained active and did not fully precipitate during the extraction process, as supported by the high levels of remaining protein with these methods. While the proposed residual AST activity requires confirmation by independent experiments, our results confirmed that the deuteration is due to residual proteins, as ultrafiltration prevents the detection of any degree of deuteration.

3.4.2. N-Acetyl Aspartate and Acetate

A reduction of N-acetyl aspartate (NAA) was observed in samples extracted with 50% MeCN, and to a lesser extent in those extracted with 50% MeOH (Figures 4 and S3, Table S1, p-values < 0.05, one-way ANOVA). Concurrently, acetate levels increased ($r = -0.94$, p-value < 0.001, Pearson correlation, Figure S6) and aspartate-2-d_1 levels continued to rise even after the original aspartate signals had vanished ($r = -0.82$, p-value < 0.001, Pearson correlation, Figure S6). These observations suggest a conversion of NAA into aspartate and acetate. This conversion is further evidenced by the negative correlation between aspartate and aspartate-2-d_1 at 0–3 h ($r = -0.94$, p-value < 0.001, Pearson correlation) and their positive correlation at 4–8 h ($r = 0.76$, p-value < 0.01, Pearson correlation). Additionally, combining the aspartate resonance and the aspartate-2-d_1 resonance showed a continuous increase over time in the samples extracted with 50% MeCN and 50% MeOH, while this remains unchanged in the 67% MeOH samples. This suggests the deuteration of aspartate and glutamate, and conversion of NAA to acetate and aspartate, represent distinct reactions.

In the brain, aspartoacylase (ASPA) catalyses the hydrolysis of NAA to produce acetate and aspartate [29]. Although we did not perform independent experiments to directly confirm the presence of ASPA in the extracts, the observed conversion patterns align with known ASPA activity. Therefore, it is likely that some residual ASPA retained bioactivity in the NMR samples of the brain extracts from 50% MeCN and, to a lesser extent, 50% MeOH, as supported by higher residual protein levels in these samples. The conversion of NAA to acetate and aspartate was reduced and eventually absent as MeOH concentration increased. Despite the presence of residual ASPA remaining speculative, the observed conversion of NAA to aspartate and acetate is protein dependent. The addition of $CHCl_3$ and the use of ultrafiltration further enhanced protein precipitation with these methods and prevented such interconversion.

3.4.3. Glutathione

Oxidation of glutathione (GSH) was observed in all samples (p-values < 0.05, one-way ANOVA) with the exception of samples extracted with 67% MeOH (p-value > 0.05, one-way ANOVA). A significant negative correlation was observed between GSH and glutathione disulphide (GSSG) over time ($r = -0.83$, p-value < 0.001, Pearson correlation) (Figure 4, Figures S3 and S5). This was most evident in samples extracted with 80% MeOH, where a 22% ± 1% reduction in GSH and a 12% ± 6% increase in GSSG was observed after eight hours. GSH oxidation was unrelated to the residual protein content within samples (as these changes still occurred in samples subjected to ultrafiltration) suggesting that spontaneous oxidation outweighs any contribution from glutathione reductase. This aligns with the unstable nature of glutathione and previous findings in NMR-based blood metabolomics, indicating that degassed solvents or derivatising agents are required for accurate GSH measurement [30].

3.4.4. Ascorbate

For all extraction methods, ascorbate concentrations showed a gradual decrease over the eight-hour period, resulting in a cumulative reduction of 10–15% across all the methods after eight hours (p-values < 0.05, one-way ANOVA) (Figures 4 and S5). The instability observed in ascorbate did not appear to be related to protein levels, as it still occurred in samples subjected to ultrafiltration. Additionally, a gradual reduction of ascorbic acid was observed in its standard solution in the NMR buffer (Figure S7). The spontaneous oxidation of ascorbate aligns with its well-known antioxidant properties and has been reported in previous studies [31].

3.4.5. Macromolecules

In line with the suboptimal deproteinisation of 50% MeCN-extracted samples, broad macromolecule resonances were observed within the spectral regions of 0.8–1.0 ppm, 1.2–1.5 ppm, and 1.6–1.8 ppm. In contrast, the other five extraction methods, including 50% MeCN extraction with ultrafiltration, displayed a flat baseline in these regions (Figure S8), which is in agreement with previous reports [5,10].

Interestingly, while no broad macromolecule signals were detectable in samples extracted with 80% MeOH at 0 h, consistent with improved deproteinisation, two out of three replicates showed the appearance of increasingly broad signals over time at 0.85–0.90 ppm and 1.25–1.35 ppm (Figure S9). This led to increased leucine signals at 0.95–0.98 ppm over time (p-value < 0.001, one-way ANOVA), resulting in a cumulative increase of 13% after eight hours. Moreover, the lactate doublets at 1.33 ppm also had an increase of 9% after eight hours due to the increasing broad signals underneath it (p-value < 0.05, one-way ANOVA). These signals may arise due to the aggregation of residual protein in the sample over time. In contrast, 50% MeCN with ultrafiltration and MeOH/H_2O/$CHCl_3$ extraction resulted in NMR spectra devoid of any broad signals from macromolecules, providing optimal baselines for analysis.

3.5. Summary and Recommendations

Among the tested methods, five methods (67% MeCN, 80% MeCN, 100% MeCN, 100% MeOH, and 50% MeOH with ultrafiltration) showed inadequate extraction efficiency and/or poor reproducibility, making them unsuitable for NMR brain metabolomics. The performance of the remaining six methods is summarised in Table 2, including relative extraction efficiency, reproducibility, protein levels, and metabolite stability.

Table 2. Summary of the six brain metabolite extraction methods in terms of extraction efficiency (mean ± SE), reproducibility (median, [IQR]), protein levels (mean ± SE), and metabolite stability.

Extraction Method	Relative Extraction Efficiency (Mean ± SE)	Reproducibility, RSD (%, Median [IQR])	Protein Levels (mg/mL, Mean ± SE)	Asp and Glu Deuteration	NAA Conversion into Aspartate and Acetate	GSH Oxidation to GSSG	Ascorbic Acid Reduction	Macromolecule Signals
50% MeCN	1 ± 0.01	3.68 (3.49)	0.4 ± 0.01	++	++	+	+	+
50% MeOH	0.88 ± 0.01	4.66 (5.67)	0.35 ± 0.01	++	+	+	+	-
67% MeOH	0.88 ± 0.03	7.48 (4.49)	0.31 ± 0.03	++	-*	-	+	-
80% MeOH	0.79 ± 0.03	5.93 (3.85)	0.26 ± 0.01	-	-	++	+	+
MeOH/H_2O/$CHCl_3$ (2:1:2)	0.96 ± 0.05	9.62 (2.66)	0.3 ± 0.01	-	-	+	+	-
50% MeCN + UF	0.73 ± 0.01	3.54 (5.55)	0.2 ± 0.02	-	-	+	+	-

-: no. -*: marginally. +: yes. ++: yes, and to a greater extent. SE, standard error. RSD, relative standard deviation. IQR, interquartile range. Asp, aspartate. Glu, glutamate. NAA, N-acetyl aspartate. GSH and GSSG, reduced form and oxidised form of glutathione, respectively. UF, ultrafiltration.

Three out of the remaining six methods (50% MeCN, 50% MeOH, and 67% MeOH) demonstrated good extraction efficiency and reproducibility, but the deuteration of aspartate and glutamate resonances was observed, possibly due to the inadequate denaturation/precipitation of AST. This highlights the importance of considering the effects of deuterated solvents and care should be taken to ensure that the integrals of both the protonated and deuterated resonances are combined to avoid spurious results. Furthermore, 50% MeCN and 50% MeOH were found to induce NAA conversion into aspartate and acetate, potentially linked to the insufficient denaturation of ASPA which poses a risk of false discoveries, particularly in the following scenarios: (1) during prolonged room temperature exposure; (2) during lengthy experiments with many samples, leading to long experimental durations; (3) the analysis of tissues where ASPA, potentially responsible for NAA conversion, is known to express; or (4) for the study of systems where the expression of ASPA is essential to the experimental readout. Therefore, these methods are not advised for untargeted metabolomics when these unstable signals are included in the data analysis. Our results highlight the importance of optimising the deproteinisation of tissues where residual enzymes could affect sample stability (including deuteration) or where protein expression levels vary, even when pulse programs to suppress residual macromolecules are to be used.

Increasing the MeOH ratio to 80% increased protein precipitation ability, which sufficiently denatured residual proteins, but at the expense of decreased extraction efficiency. However, increasing broad signals over time led to an overestimation of lactate and leucine concentrations. This phenomenon was not observed in samples subjected to ultrafiltration or MeOH/H_2O/$CHCl_3$ extraction, likely indicating that the broad signals arise from incomplete protein precipitation. While this method offers simplicity and is well-suited for high-throughput studies, there is a risk of temporal inflation in the resonances of lactate and leucine.

Ultrafiltration, serving as a positive control for protein removal, reduced protein content by half to a 0.2 ± 0.02 mg/mL, as evidenced by the absence of broad macromolecule resonances up to eight hours post sample preparation. Moreover, ultrafiltration preserved the stability of aspartate, glutamate, NAA, and acetate, thus confirming that their instability originated from residual proteins. However, ultrafiltration led to a 27% reduction in overall metabolite abundance compared to the 50% MeCN extraction method. Additionally, glycerol contaminants from the filter masked the detection of glycine, certain myo-inositol, and glutamine resonances in the NMR spectrum. Consequently, ultrafiltration methods do not appear suitable for NMR analysis.

MeOH/H_2O/$CHCl_3$ extraction resulted in improved deproteinisation, while maintaining adequate extraction efficiency and reproducibility in agreement with previous studies [5,11,32]. Therefore, MeOH/H_2O/$CHCl_3$ extraction is recommended for untargeted brain NMR metabolic profiling over other tested methods. One disadvantage of MeOH/H_2O/$CHCl_3$ extraction is that it requires more time and careful handling compared to single-phase extraction methods, particularly during phase transfer, in order to mitigate

variability. Moreover, this method does not address the observed decrease in ascorbate and oxidation of GSH. To maintain changes within 10% for glutathione and ascorbate, it is advisable to acquire spectra within 4 h of sample preparation. For researchers requiring higher accuracy for these metabolites, further optimisation of extraction methods may be necessary. This could include the addition of antioxidants, or derivatising agents, pH adjustments, the use of degassed solvents, and/or temperature control to reduce the risks of metabolite oxidation [12,30,31,33].

While recommending specific extraction protocols, we strongly advise conducting trials of NMR spectroscopy and analysis on biological replicates using the method of choice before progressing to studying valuable samples. Absolute integral values were used in data analysis throughout this study to investigate preanalytical impact, while sum normalization is typically used in metabolomic studies to mitigate the impact of concentration variations resulting from mass differences or pipetting errors (Figure S10). This study evaluated metabolite integrity at room temperature following NMR sample preparation. Not all NMR spectrometers are equipped with autosamplers that can maintain refrigerated conditions, and preparing and loading samples individually to mitigate enzymatic activity would be labour-intensive and inefficient. This limitation highlights the importance of effective deproteinisation during sample preparation to ensure metabolite stability. When feasible, using autosamplers with refrigeration capabilities is recommended, as this can further mitigate metabolite alterations and enhance the reliability of metabolomics analysis. The focus of this study was on the extraction and stability of polar metabolites, as NMR metabolomics is well-suited for aqueous phase extractions. Although the brain is a lipid-rich organ, lipidomics is better addressed using mass spectrometry, and thus, lipid extraction was not within the scope of this NMR-based study. We recommend that future studies incorporate lipidomic analyses for a more comprehensive metabolic profile.

Our findings are specific to brain tissue, which has unique biochemical characteristics, such as a high lipid content and distinct protein compositions. While the addition of chloroform appears necessary for effective protein precipitation in brain tissue, the requirements may differ for other tissues. The most efficient protein removal method may not always be optimal in terms of time and metabolite recovery. For instance, tissues that lack significant amounts of these enzymes might achieve sufficient protein removal with simpler single-phase extractions, such as 50% MeOH or 50% MeCN. These simpler methods could offer benefits in terms of reproducibility and ease of use, particularly for high-throughput workflows. Future studies would be valuable to explore and optimise extraction protocols tailored to the unique biochemical properties of different tissues.

Our study highlights the importance of optimising extraction methods for brain NMR metabolomics, particularly in balancing metabolite stability (including that affected by deuteration) and effective protein precipitation. While this study used brain tissues from rodent models, these techniques could be similarly applied to human brain biopsies, where the amount of tissue available is also limited. This approach has direct relevance to both animal studies and potential clinical applications in human tissue analysis. Future research should explore the applicability of these protocols to human samples, particularly in clinical settings where precise metabolic profiling is crucial for diagnosis and treatment monitoring. In such cases, while histology alone may not provide a definitive diagnosis, metabolic profiling could offer valuable complementary insights.

4. Conclusions

This study is the first systematic investigation into the effect of residual protein contamination on metabolite stability following NMR sample preparation in brain tissues. The findings underscore the crucial role of protein precipitation in maintaining metabolite integrity, particularly for key metabolites such as aspartate, glutamate, and N-acetyl aspartate. Our results demonstrate that insufficient protein precipitation in commonly used extraction solvents (50% MeCN, 50% MeOH, and 67% MeOH) leads to metabolite instability (including that affected by deuteration), which can markedly compromise the

reliability of NMR-based metabolomics studies. These results highlight the importance of optimising extraction methods for effective deproteinisation to ensure the stability of NMR spectra—a factor often overlooked due to the tolerance of NMR instrumentation to residual protein contamination.

By identifying MeOH/H_2O/$CHCl_3$ extraction as a reproducible method for enhancing metabolite stability, we provide a valuable tool for brain metabolomics research, which can be readily applied to optimise sample preparation protocols and improve the accuracy of metabolomic profiling. Although MeOH/H_2O/$CHCl_3$ extraction was effective in preventing protein-related instabilities, further optimisation is required to improve the stability of oxidation-sensitive metabolites. Future research should investigate the use of antioxidants, degassed solvents, or other stabilising agents to mitigate oxidation during the extraction process, as this remains a limitation of the present study.

Supplementary Materials: The following supporting information can be downloaded at: https://www.mdpi.com/article/10.3390/metabo14110609/s1, Figure S1: Metabolite assignments in a representative NMR spectrum from a brain Sample Extracted with 50% MeCN. Figure S2: Overview of representative NMR spectra for each extraction method. Figure S3: Heatmap of NMR resonance percentage changes for metabolites across extraction methods. Figure S4: Loadings plot of PCA (corresponding to scores plot on Figure 2D) highlighting the contributions of Asp-2-d1, Asp, and Glu to variation in PC2. Figure S5: NMR spectra illustrating changes in unstable resonances over time delays in NMR measurement in a 50% MeCN brain sample. Figure S6: Pearson correlation of unstable metabolites in 50% MeCN samples. Pearson correlation coefficient r is visualised with different sized circles in the upper triangular of the correlation matrix, and the r values are shown in the lower triangular. *p* values were adjusted with the false discovery rate. The plot includes only significant correlations. (A) 0–8-h samples. (B) 0–3-h samples (C) 4–8-h samples. Figure S7: NMR spectra illustrating the reduction in ascorbate signals over time in an ascorbic acid standard sample (in phosphate buffer pH = 7.4) during NMR Measurement. Figure S8: Enhanced baseline uniformity at 0.8–1.0 ppm, 1.2–1.5 ppm, 1.6–1.8 ppm in 50% MeCN samples with ultrafiltration (yellow) in contrast to 50% MeCN samples (green). Figure S9: NMR spectra illustrating the increasing broad signals over time at 0.85–0.90 ppm and 1.25–1.35 ppm in an 80%MeOH brain extract during NMR measurement. Figure S10: Sum normalised method reduced the impact of variations in overall sample concentration. This is compared to Figures 2D and 3A, where absolute values were used for PCA. (A) PCA scores plot of the brain metabolic profiles from different extraction methods with no delay in NMR measurement. (B) PCA scores plot of brain metabolic profiles from six extraction methods over a time range from 0 to 8 h of delay in NMR measurement. Table S1: Mean ± standard error of metabolite resonance integrals across groups at different NMR measurement delays. One-way ANOVA was performed to assess significant differences between group means.

Author Contributions: Conceptualisation, W.X., D.C.A. and F.P.; methodology, W.X., F.Z. and F.P.; formal analysis, W.X.; visualisation, W.X.; resources, M.Z.C., D.C.A. and F.P.; supervision, D.C.A. and F.P.; writing—original draft preparation, W.X.; writing—review and editing, W.X., F.Z., M.Z.C., D.C.A. and F.P.; funding acquisition, M.Z.C., D.C.A. and F.P. All authors have read and agreed to the published version of the manuscript.

Funding: This research was funded in part by PhytoAPP EU framework (2021–2025, to D.C.A. and W.X.) and a Dorothy Hodgkin Early Career Fellowship in Chemistry in association with Somerville College, University of Oxford (to F.P.).

Institutional Review Board Statement: The animal study protocol was approved by UK Home Office (license code P23FF9052, date of approval 4 March 2019).

Data Availability Statement: The original data presented in this study are openly available in the Oxford University Research Archive at http://dx.doi.org/10.5287/ora-degojb2kw.

Conflicts of Interest: The authors declare no conflicts of interest.

References

1. Hollywood, K.; Brison, D.R.; Goodacre, R. Metabolomics: Current Technologies and Future Trends. *Proteomics* **2006**, *6*, 4716–4723. [CrossRef] [PubMed]
2. Gonzalez-Riano, C.; Garcia, A.; Barbas, C. Metabolomics Studies in Brain Tissue: A Review. *J. Pharm. Biomed. Anal.* **2016**, *130*, 141–168. [CrossRef] [PubMed]
3. Letertre, M.P.M.; Giraudeau, P.; de Tullio, P. Nuclear Magnetic Resonance Spectroscopy in Clinical Metabolomics and Personalized Medicine: Current Challenges and Perspectives. *Front. Mol. Biosci.* **2021**, *8*, 698337. [CrossRef] [PubMed]
4. Álvarez-Sánchez, B.; Priego-Capote, F.; de Castro, M.L. Metabolomics Analysis II. Preparation of Biological Samples Prior to Detection. *TrAC Trends Anal. Chem.* **2010**, *29*, 120–127. [CrossRef]
5. Lin, C.Y.; Wu, H.; Tjeerdema, R.S.; Viant, M.R. Evaluation of Metabolite Extraction Strategies from Tissue Samples Using NMR Metabolomics. *Metabolomics* **2007**, *3*, 55–67. [CrossRef]
6. Want, E.J.; O'Maille, G.; Smith, C.A.; Brandon, T.R.; Uritboonthai, W.; Qin, C.; Trauger, S.A.; Siuzdak, G. Solvent-Dependent Metabolite Distribution, Clustering, and Protein Extraction for Serum Profiling with Mass Spectrometry. *Anal. Chem.* **2006**, *78*, 743–752. [CrossRef]
7. Cai, X.; Li, R. Concurrent Profiling of Polar Metabolites and Lipids in Human Plasma Using HILIC-FTMS. *Sci. Rep.* **2016**, *6*, 36490. [CrossRef]
8. Nagana Gowda, G.A.; Gowda, Y.N.; Raftery, D. Expanding the Limits of Human Blood Metabolite Quantitation Using NMR Spectroscopy. *Anal. Chem.* **2015**, *87*, 706–715. [CrossRef]
9. Lepoittevin, M.; Blancart-Remaury, Q.; Kerforne, T.; Pellerin, L.; Hauet, T.; Thuillier, R. Comparison between 5 Extractions Methods in Either Plasma or Serum to Determine the Optimal Extraction and Matrix Combination for Human Metabolomics. *Cell Mol. Biol. Lett.* **2023**, *28*, 43. [CrossRef]
10. Gowda, G.A.N.; Raftery, D. Quantitating Metabolites in Protein Precipitated Serum Using NMR Spectroscopy. *Anal. Chem.* **2014**, *86*, 5433–5440. [CrossRef]
11. Diémé, B.; Lefèvre, A.; Nadal-Desbarats, L.; Galineau, L.; Madji Hounoum, B.; Montigny, F.; Blasco, H.; Andres, C.R.; Emond, P.; Mavel, S. Workflow Methodology for Rat Brain Metabolome Exploration Using NMR, LC-MS and GC-MS Analytical Platforms. *J. Pharm. Biomed. Anal.* **2017**, *142*, 270–278. [CrossRef] [PubMed]
12. Fomenko, M.V.; Yanshole, L.V.; Tsentalovich, Y.P. Stability of Metabolomic Content during Sample Preparation: Blood and Brain Tissues. *Metabolites* **2022**, *12*, 811. [CrossRef] [PubMed]
13. Paskevich, S.I.; Molchanov, M.V.; Timchenko, M.A.; Kutyshenko, V.P. Sample Pretreatment of Brain Tissues and Cerebrospinal Fluid for NMR Investigations. *J. Anal. Chem.* **2013**, *68*, 862–870. [CrossRef]
14. Kamlage, B.; Maldonado, S.G.; Bethan, B.; Peter, E.; Schmitz, O.; Liebenberg, V.; Schatz, P. Quality Markers Addressing Preanalytical Variations of Blood and Plasma Processing Identified by Broad and Targeted Metabolite Profiling. *Clin. Chem.* **2014**, *60*, 399–412. [CrossRef] [PubMed]
15. Ghini, V.; Quaglio, D.; Luchinat, C.; Turano, P. NMR for Sample Quality Assessment in Metabolomics. *New Biotechnol.* **2019**, *52*, 25–34. [CrossRef]
16. Ghini, V.; Abuja, P.M.; Polasek, O.; Kozera, L.; Laiho, P.; Anton, G.; Zins, M.; Klovins, J.; Metspalu, A.; Wichmann, H.-E.; et al. Impact of the Pre-Examination Phase on Multicenter Metabolomic Studies. *New Biotechnol.* **2022**, *68*, 37–47. [CrossRef]
17. Kamlage, B.; Neuber, S.; Bethan, B.; González Maldonado, S.; Wagner-Golbs, A.; Peter, E.; Schmitz, O.; Schatz, P. Impact of Prolonged Blood Incubation and Extended Serum Storage at Room Temperature on the Human Serum Metabolome. *Metabolites* **2018**, *8*, 6. [CrossRef]
18. Mushtaq, M.Y.; Choi, Y.H.; Verpoorte, R.; Wilson, E.G. Extraction for Metabolomics: Access to the Metabolome. *Phytochem. Anal.* **2014**, *25*, 291–306. [CrossRef]
19. Blanchard, J. Evaluation of the Relative Efficacy of Various Techniques for Deproteinizing Plasma Samples Prior to High-Performance Liquid Chromatographic Analysis. *J. Chromatogr.* **1981**, *226*, 455–460. [CrossRef]
20. Folch, J.; Ascoli, I.; Lees, M.; Meath, J.A.; LeBaron, F.N. Preparation of lipide extracts from brain tissue. *J. Biol. Chem.* **1951**, *191*, 833–841. [CrossRef]
21. Beckonert, O.; Keun, H.C.; Ebbels, T.M.D.; Bundy, J.; Holmes, E.; Lindon, J.C.; Nicholson, J.K. Metabolic Profiling, Metabolomic and Metabonomic Procedures for NMR Spectroscopy of Urine, Plasma, Serum and Tissue Extracts. *Nat. Protoc.* **2007**, *2*, 2692–2703. [CrossRef] [PubMed]
22. Andresen, C.; Boch, T.; Gegner, H.M.; Mechtel, N.; Narr, A.; Birgin, E.; Rasbach, E.; Rahbari, N.; Trumpp, A.; Poschet, G.; et al. Comparison of Extraction Methods for Intracellular Metabolomics of Human Tissues. *Front. Mol. Biosci.* **2022**, *9*, 932261. [CrossRef] [PubMed]
23. Wishart, D.S.; Guo, A.; Oler, E.; Wang, F.; Anjum, A.; Peters, H.; Dizon, R.; Sayeeda, Z.; Tian, S.; Lee, B.L.; et al. HMDB 5.0: The Human Metabolome Database for 2022. *Nucleic Acids Res.* **2021**, *50*, D622–D631. [CrossRef] [PubMed]
24. Villanueva, R.A.M.; Chen, Z.J. Ggplot2: Elegant Graphics for Data Analysis (2nd Ed.). *Meas. Interdiscip. Res. Perspect.* **2019**, *17*, 160–167. [CrossRef]
25. Kolde, R. Pheatmap: Pretty Heatmaps. *R Package Version* **2012**, *1*, 726.

26. Thévenot, E.A.; Roux, A.; Xu, Y.; Ezan, E.; Junot, C. Analysis of the Human Adult Urinary Metabolome Variations with Age, Body Mass Index, and Gender by Implementing a Comprehensive Workflow for Univariate and OPLS Statistical Analyses. *J. Proteome Res.* **2015**, *14*, 3322–3335. [CrossRef]
27. Kimhofer, T. Metabom8. 2021. Available online: https://github.com/tkimhofer/metabom8 (accessed on 5 November 2024).
28. García-Martín, M.L.; García-Espinosa, M.A.; Ballesteros, P.; Bruix, M.; Cerdán, S. Hydrogen Turnover and Subcellular Compartmentation of Hepatic [2-13C]Glutamate and [3-13C]Aspartate as Detected by 13C NMR*. *J. Biol. Chem.* **2002**, *277*, 7799–7807. [CrossRef]
29. BIRNBAUM, S.M.; LEVINTOW, L.; KINGSLEY, R.B.; GREENSTEIN, J.P. Specificity of Amino Acid Acylases. *J. Biol. Chem.* **1952**, *194*, 455–470. [CrossRef]
30. Gowda, G.A.N.; Pascua, V.; Raftery, D. Extending the Scope of 1H NMR Based Blood Metabolomics for the Analysis of Labile Antioxidants: Reduced and Oxidized Glutathione. *Anal. Chem.* **2021**, *93*, 14844–14850. [CrossRef]
31. Bourafai-Aziez, A.; Jacob, D.; Charpentier, G.; Cassin, E.; Rousselot, G.; Moing, A.; Deborde, C. Development, Validation, and Use of 1H-NMR Spectroscopy for Evaluating the Quality of Acerola-Based Food figure ments and Quantifying Ascorbic Acid. *Molecules* **2022**, *27*, 5614. [CrossRef]
32. Belle, J.E.L.; Harris, N.G.; Williams, S.R.; Bhakoo, K.K. A Comparison of Cell and Tissue Extraction Techniques Using High-Resolution 1H-NMR Spectroscopy. *NMR Biomed.* **2002**, *15*, 37–44. [CrossRef] [PubMed]
33. Yin, X.; Chen, K.; Cheng, H.; Chen, X.; Feng, S.; Song, Y.; Liang, L. Chemical Stability of Ascorbic Acid Integrated into Commercial Products: A Review on Bioactivity and Delivery Technology. *Antioxidants* **2022**, *11*, 153. [CrossRef] [PubMed]